QUANTUM CHEMICAL AND SPECTROSCOPIC INVESTIGATIONS OF SUBSTITUTED QUINOLINE, AZATRICYCLO AND PYRAZINE CARBOXAMIDE DERIVATIVES

Thesis Submitted to the

University of Calicut

For the award of the degree of

DOCTOR OF PHILOSOPHY

IN

PHYSICS

By

RANJITH P K

POST GRADUATE AND RESEARCH

DEPARTMENT OF PHYSICS

CHRIST COLLEGE (AUTONOMOUS)

IRINJALAKUDA, THRISSUR

MARCH 2019

CERTIFICATE

This is to certify that the work embodied in the thesis entitled **"QUANTUM CHEMICAL AND SPECTROSCOPIC INVESTIGATIONS OF SUBSTITUTED QUINOLINE, AZATRICYCLO AND PYRAZINE CARBOXAMIDE DERIVATIVES"** has been carried out by RANJITH P K under my supervision and Guidance.

Supervising Teacher

Dr. P. L. Anto
Research Guide
Department of physics
Christ College, (Autonomous),
Irinjalakuda

DECLARATION

I hereby declare that the Ph.D thesis entitled **"QUANTUM CHEMICAL AND SPECTROSCOPIC INVESTIGATIONS OF SUBSTITUTED QUINOLINE, AZATRICYCLO AND PYRAZINE CARBOXAMIDE DERIVATIVES"** is an independent work carried out by me and it has not been submitted anywhere else for any other degree, diploma or title.

IRINJALAKUDA **RANJITH P K**

ACKNOWLEDGEMENTS

My thesis titled “Quantum Chemical and Spectroscopic Investigations of Substituted Quinoline, Azatricyclo and Pyrazine Carboxamide Derivatives” brings a great sense of satisfaction in the process of completion.

I am very thankful to almighty for his grace upon me. I can express my happiness in this moment only by acknowledging the help and guidance that I have received every step of the way to create my thesis.

Primarily, it is my privilege to express my gratitude to my supervisor, Dr. P. L Anto for giving me an opportunity to pursue PhD under his expert supervision. He has guided me in every step of the research process and is an inspiring advisor that I can ever imagine. Dr. P. L Anto’s enlightening guidance and compassionate nature helped me throughout the work.

My gratitude also extends to Dr. C. Yohannan Panicker, research supervisor who deserves a special thanks, as this thesis would not have been possible without his kind support and encouragement. His understanding, encouraging suggestions and personal guidance have provided a good basis for my current work.

I am very grateful to Dr. Mathew Paul Ukken, the Principal, Christ College (Autonomous), Irinjalakuda, Dr. Joseph V. P, Research Coordinator, Christ College (Autonomous), Irinjalakuda, and Faculty members of Department of Physics, Christ College (Autonomous), Irinjalakuda, for providing necessary facilities to carry out the necessary investigation. I take this moment to reminisce the Late Rev. Fr. Dr. Jose T.M, C M I, Former Principal, Christ College (Autonomous), Irinjalakuda granted permission to ensure my PhD course and Dr. Balu Kuzuvely, former research coordinator, Christ College (Autonomous), Irinjalakuda for his valuable advice.

I would also like to thank the Principal and the faculty members of the Department of Physics, M.P.M.M.S.N. Trusts College, Shoranur for constant encouragement throughout the work.

A special thanks to Dr. Parameswaran P. Head of Department and Associate Professor, Department of Chemistry, NIT Calicut and the research scholars of computational lab for extending timeless support for making calculations theoretically.

I am extremely thankful to my parents and other relatives for their encouragement and support. My wife Sreevidya and my loving son Ahan Krishnan have shown indefinable patience, love and support during the long and demanding years of hectic research work. Their committed affection and encouragement have helped me in many difficult situations during my research work.

My expression of gratitude to my beloved wife and son, go beyond my words. Lastly, I thank each and every one sincerely from the bottom of my heart.

RANJITH P K

PREFACE

QUANTUM CHEMICAL AND SPECTROSCOPIC INVESTIGATIONS OF SUBSTITUTED QUINOLINE, AZATRICYCLO AND PYRAZINE CARBOXAMIDE DERIVATIVES

The thesis is a detailed investigation of spectroscopic, computational DFT studies and molecular docking of two quinoline, two pyrazine carboxamide and one azatricyclo organic compound.

Chapter 1 gives a general introduction related to FT-IR, FT-Raman theory and their instrumentation. Also a brief introduction about theories used such as density functional theory, HOMO – LUMO analysis, natural bond orbital analysis, Fukui function, average local ionisation energies, molecular docking, etc.

In **chapter 2** we have reported spectroscopic characterisation and reactivity study of Ethyl 4-hydroxy-2-oxo-1,2-dihydroquinoline-3-carboxylate by DFT and MD approaches. The hyper polarizability of the title compound is calculated. Global reactivity parameters were predicted. With the help of MEP map the relative reactivity towards electrophilic and nucleophilic attacks were predicted.

In chapter 3 a detailed interpretation of FT-IR and FT-Raman, reactive properties of N-(3-iodo-4-methylphenyl) pyrazine-2-carboxamide by molecular dynamics simulation and DFT calculation. Using NBO analysis charge delocalisation and stability of has been analysed. The electrophilic attacking site of the molecule is calculated using ALIE method. Reactive site of the molecule find out using Fukui function.

Combined spectroscopic and computational study of 3-[(4-Carboxyphenyl) carbamoyl]-4-hydroxy-2-oxo-1,2-dihydroquinoline-6-carboxylic acid has been performed in order to conduct detailed characterisation and evaluation of their reactive properties and reported in **chapter 4**. Spectroscopic properties have also been obtained with DFT calculation and the obtained results have been mutually compared. The docked ligand form stable complexes with ubiquinol- cytochrome reductase which give binding affinity value -9.1 Kcal/mol. The docking results suggest that the title compound might exhibit inhibitory activity against anti- malarial diseases.

In chapter 5 spectroscopic characterisation of 6-Chloro-N-(3-iodo-4-methylphenyl)-pyrazine-2-carboxamide have been obtained theoretically and experimentally. MEP study revealed the electrophilic and nucleophilic sites. Experimental investigation encompassed spectroscopic characterisation by FT-IR and FT-Raman techniques while computational studies includes DFT calculation. The molecular docking studies reveal that the ligand bind active site of the macromolecule and could have inhibitory activity against the anti-inflammatory receptor.

A theoretical study on molecular structure, chemical reactivity and molecular docking study of 1,7,8,9-tetrachloro-10,10-dimethoxy-4-[3-(4-benzylpiperazin-1-yl)propyl]-4-azatricyclo[5.2.1.02,6] dec-8-ene-3, 5-dione presented in **chapter 6**. MEP analysis given the title molecule. The HOMO-LUMO analysis predicted the molecular energetic parameters and NBO analysis give the strong interaction with in the molecule. The docked title compound form a stable complex with factor Xa inhibitor and can be lead compound for developing new anti-coagulant drug.

LIST OF ABBREVIATIONS

ALIE	Average Local Ionization Energy
aug-cc	Augmented Correlation Consistent
BDE	Bond Dissociation Energy
B3LYP	Becke 3-Parameter (Exchange), Lee, Yang and Parr (correlation; density functional theory)
cc-pVDZ	Correlation Consistent Polarized Valance Double Zeta
DFT	Density Functional Theory
ED	Electron Density
FT	Fourier Transform
GAR2PED	Gaussian archive record 2 potential energy distribution
GTO	Gaussian Type Orbitals
HF	Hartree-Fock
HOMO	Highest Occupied Molecular Orbital
ICT	Intramolecular Charge Transfer
IR	Infra-Red
LUMO	Lowest Unoccupied Molecular Orbital
MD	Molecular Dynamics
MEP	Molecular Electrostatic Potential
NBO	Natural Bond Orbital
NdYAG	Neodymium Yttrium Aluminium Garnet
NLO	Nonlinear Optical
NMR	Nuclear Magnetic Resonance
PAS	Prediction of Activity Spectra
PDB	Protein Data Bank
PED	Potential Energy Distribution
PES	Potential Energy Surface
QZVPP	Quadruple Zeta Valance Plus Polarization

RDF	Radial Distribution Function
SCF	Self-Consistent Field
SDD	Stuttgart/Dresden
SEM	Scanning electron microscope
SERS	Surface Enhanced Raman Spectrum
STO	Slater-Type Orbital
UV	Ultraviolet
Vis	Visible
XRD	X-ray Diffraction
$\bar{\nu}$	Wavenumber
ε_i	Orbital energy
$\rho_i(\vec{r})$	Electronic density of i^{th} molecular orbital at the point $\vec{r}$
$\rho(\vec{r})$	Total electronic density function
δ	Fraction of electrons
g(r)	Probability of finding a particle at distance r
ν	Frequency
δ	In-plane deformation
γ	Out-of-plane deformation
ρ	Rocking mode
τ	Tortional

CONTENTS

LIST OF TABLES

LIST OF FIGURES

CHAPTER I

INTRODUCTION

1.1 General Introduction

Quantum chemical calculations are good tool used for predicting the properties of molecules even those which are not synthesized in the laboratory. The main objective of this technique is to find the information regarding geometrical structure and various chemical and physical properties of the molecule. It uses the most modern computational calculations to perform the quantum chemical methods to obtain molecular properties such as optimized geometry, geometrical parameters, vibrational wave number assignments, Frontier Molecular Orbital Analysis, Non-linear Optical Properties, Molecular Electrostatic Potential, Natural Bond Analysis, Fukui Functions, Average Local Ionization Energy, Bond Dissociation Energy, Degradation properties by autoxidation and hydrolysis and Molecular Docking. To support the theoretical investigations, FT-IR, FT-Raman spectra are experimentally recorded.

1.2 Infrared Spectroscopy

Spectroscopy is the study of the quantized interaction of electromagnetic energy with matter. In Organic molecules, we deal with molecular spectroscopy. In general, any spectral feature, *i.e.* a band or group of bands, is due not to the whole molecule, but to an identifiable part of the molecule, which we loosely call a chromophore [1]. A chromophore may correspond to a functional group *(e.g.* a hydroxyl group, carbonyl group). However, it may equally well correspond to a single atom within a molecule or to a group of atoms *(e.g.* a methyl group) which is not normally associated with chemical functionality. The detection of a chromophore permits us to deduce the presence of a structural fragment or a structural element in the molecule. Infrared spectroscopy deals with vibrational energy levels of the molecule and interaction of infrared radiation. An infrared spectrum is the fingerprint of the compound with absorption peaks corresponding to the frequencies with which a group vibrates. Since no two compound can produce the exactly the same IR spectrum there for IR spectroscopy can be used in the qualitative analysis of every kind of material. To analyse all the frequencies of vibration at a time FT-IR spectrometer is used. It improves the scanning speed of the ordinary IR

spectrometers. The problem was resolved by the production of interferogram in FT-IR spectrometer. The decoding of each individual frequency from the interferogram is done by the method of Fourier transform using computer.

1.21 FT-IR Instrumentation

There are three elementary modules in an FT-IR system; radiation source, interferometer and detector. The identical types of radiation sources are used for both dispersive and Fourier Transform Spectrometers. However, the source is periodically water-cooled in FT-IR instruments to provide better power and stability. In contrast, a totally different method is taken in an FT-IR spectrometer to measure the absorption at component frequencies.The monochromator is replaced by an interferometer, which splits radiant beams, produces an optical path difference between the beams, and then recombines them in order to produce interference signals measured as a function of optical path difference. The interferometer generates interference signals, which gives infrared spectral information generated after passing through a sample. The ordinarily used interferometer is a Michelson interferometer. The source is the typical glower operated at high temperatures. The Michelson interferometer contains of a source, a beam splitter B and two plane mirrors M_1 and M_2. The two mirrors are vertical to each other. The beam splitter is a partially reflecting device and is often made by depositing a thin film of germanium onto a flat KBr substrate. One mirror is fixed (M_1) and other is capable of movements (M_2). The beam splitter allows half of the radiation to fixed mirror and the remaining half to other mirror. The two beams are reflected back to beam splitter where they recombines. The recombined beam if focused through a sample, the sample absorption will bring to light as gaps in the frequency distribution which on transformation gives a typical absorption spectrum. In the experiment, the detector signal is given to a multichannel computer

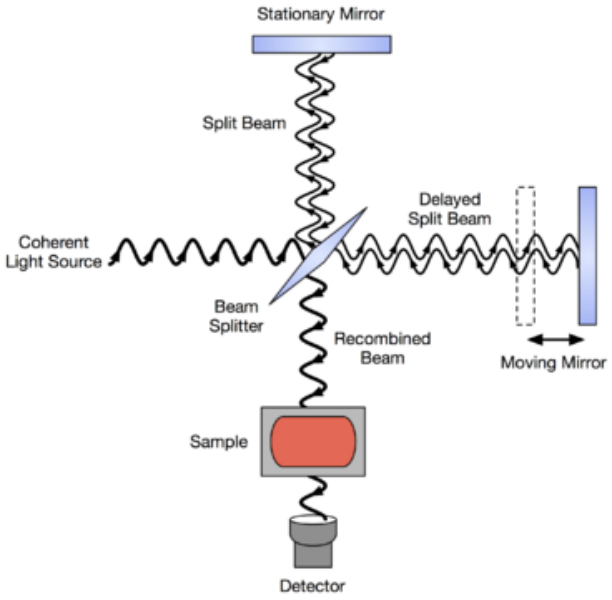

while mirror M_2 is moved. The computer then compute the Fourier transform of the collected data and plots it on the paper.

1.3 FT-Raman Spectroscopy

The interaction of electromagnetic radiation with matter sometimes produces inelastic scattering and due to that appearance in the altered frequency in the resultant radiation is called Raman scattering. To occur Raman scattering there will be a change in the polarizability of the molecule. Using this technique we can study the molecular normal mode vibration which are both IR active or IR inactive is the key idea of Raman spectroscopy. Raman scattering is a very feeble effect accompanied with Rayleigh scattering with intensity usually 3 to 5 orders of magnitude greater [2]. Generally the range of Raman shift from 4000 to 0 cm^{-1} with the upper and lower limit depends on the instrument used. The advantage of Raman spectroscopy is that it can be used to study solid, liquid as well as gaseous samples. The FT-Raman spectroscopy has made possible the study of materials that was earlier impossible because of fluorescence. The information about the energies and molecular vibrations and rotations are contained in the scattered radiation produced by the Raman effect and these in turn are depended on the atoms or ions that constitute the molecule, the chemical bonds between them, the symmetry of the structure and the physicochemical environment.

1.31 Instrumentation

The problem facing the event of Raman qualitative analysis instrumentation is the inherent weakness of the inelastic scattering. Therefore to provide a detectable Raman signal an energetic light is needed. In recent years, microelectronics revolution has further improved the technique with the developments of stepper motor drives, photon counting devices, digital data acquisition techniques and computer data processing and provided the chemists and physicists a way that is additional helpful and versatile than infrared qualitative analysis. Some of the benefits of Raman over infrared technique are: Raman qualitative analysis could be a scattering method, so samples of any size or shape can be examined.

FT-Raman spectrometers are designed to eliminate the fluorescence problem encountered in conventional Raman spectroscopy. The FT-Raman instrument has the following components: (1) A near IR Laser excitation source, generally an Nd:YAG laser working at 1.06 μm. (2) An interferometer equipped with an appropriate beam splitter, made of glass, and a detector for the

near IR region. The detector is usually In GaAs or Ge semiconductor detector. (3) A sample chamber with scattering optics that match the input port of the Fourier transform instrument. (4) An optical filter rejection of the Raleigh scattered light. A schematic representation of such FT-Raman instrument is shown in fig.

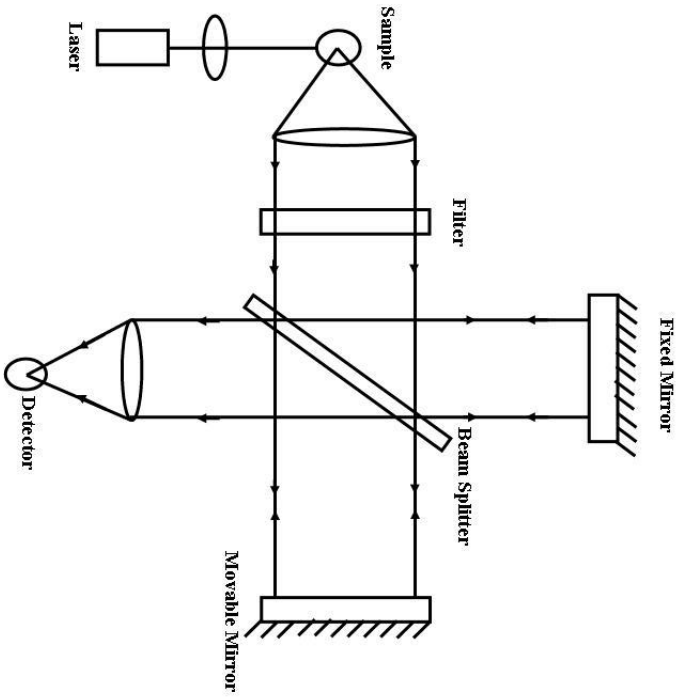

To eliminate fluorescence threshold frequency of excitation is tuned in the Nd:YAG laser beam. Another method of optical alignment can be realized by using fiber optics. With fiber-optic components, optical alignment is virtually eliminated which allows rapid switching from one sample to another. One of the benefits of Fourier transform instrument is that it will collect all the scattered radiation over the whole vary of frequencies at the same time throughout the entire amount of the detection and it is called multiplexing. This becomes an obstacle, as the intense Rayleigh line is the primary source of noise. Multiplexing redistributes the 48 noise associated with Rayleigh line across the entire spectrum by the FT process and this is called as multiplex disadvantage. Interferometer can be combined with Rayleigh line filters (notch filters) so as forestall the results of the multiplex disadvantage. The Rayleigh line filters minimizes the amount of Rayleigh scattered light entering the interferometer and is essential for FT-Raman spectroscopy.

1.4 Mutual Exclusion Principle

It is seen that molecule having centre of symmetry shows IR active vibrations are Raman inactive and vice-versa. This complimentary nature is because of the electrical characteristic of the vibration. If a bond is powerfully polarised, a small change in its length such as that occurs during a vibration, will have only a small additional effect on polarisation. Vibrations involving polar bonds (C-O, N-O, and O-H) are therefore, comparatively weak Raman scatterers. Such polarised bonds, however, carry their charges during the vibrational motion, (unless neutralised by symmetry factors), which results in a large net dipole moment

change and produce strong IR absorption band. Conversely, comparatively neutral bonds (C-C, C-H, C=C) suffer large changes in polarisability during a vibration, though this is less easy to visualise. But the dipole moment is not similarly affected and vibrations that involve this type of bond are strong Raman scatterers but weak in the IR.

1.5 Quantum Chemical Calculations

The fundamental tool for quantum calculations is Schrodinger equation. Using fundamental laws of Physics computational chemistry simulates chemical structure and reactions numerically. Electronic structure theory and Molecular mechanics are the two broad areas within the computational chemistry to perform the basic types of calculations.

1.5.1 Molecular Mechanics

Classical mechanics is the key idea behind the prediction of molecular structure and other properties in Molecular mechanics. Depending upon the set of equations defining how the potential energy of a molecule varies with the atomic position (Force field) there are different types of molecular mechanics methods are available.

1.5.2 Electronic Structure Method

In this method laws of quantum mechanics are used for the computational calculations. The exact solution for the Schrodinger equation is possible only for smallest systems hence various approximation methods are needed to solve problem using electronic structure method. The electronic structure method can be classified in to two major classes.

1. **Semi-Empirical Methods**:- Using some parameters available for the type of chemical system, we can solve the approximate form of the Schrodinger equation. Depending on these parameter sets there are different Semi-empirical methods available for computation.
2. **Ab initio Methods: -** In this method experimental parameters are not used for the computation. Ab initio technique uses rigorous mathematical approximations to solve the Schrodinger equation. Ab initio methods results good quality quantitative predictions for wide range of systems. Now, a third class of electronic structure theory have come in to wide use called Density functional theory which disused in the later sections.

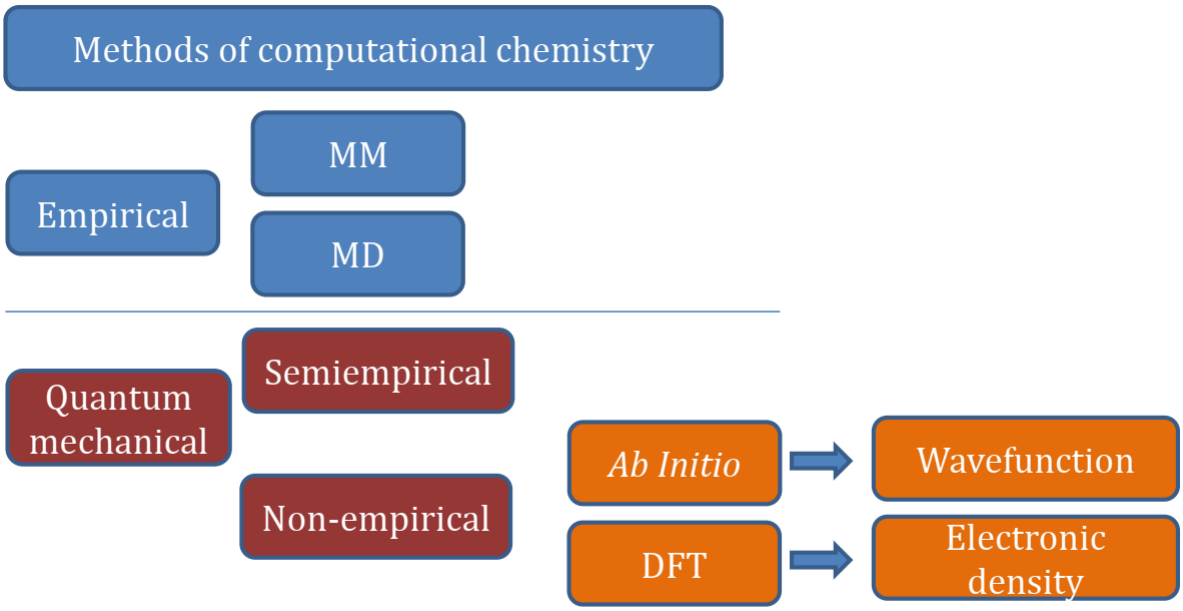

1.6 Gaussian-Software for Computations

Gaussian [3] is a famous ab initio electronic structure package that is able to compute energies, geometries, vibrational frequencies, transition states, reaction paths, excited states and a range of properties based on many uncorrelated and correlated wave functions. Gaussian is employed by chemists, chemical engineers, biochemists, physicists and others for research in established and emerging areas of chemical interest. It was initially released in 1970 by John Pople and his research group at Carnegie-Mellon University. Pople uses Gaussian orbitals in the place of ordinary slater type orbitals to speed up calculation. Beginning from the basic laws of quantum mechanics, Gaussian calculates the energies, molecular structures, and vibrational frequencies of molecular systems, together with numerous molecular properties. Theoretical calculations by Gaussian are used for analysing chemical bonding as well. The present version of the software is Gaussian 16.

1.7 Density Functional Theory (DFT)

Density functional theory is a quantum mechanical theory in which using the ground state electronic density directly investigate the electronic structure of the many body systems. The mapping of ground state electronic density to ground state electronic wave function is the key idea of this theory. In the Hatree-Fock theory the many electron wave function contains 3n variables but the electron density is a function of 3 variables only this leads the fast quantum calculations in density functional theory. The theoretical origin of DFT was from Thomas-

Fermi model and Hohenberg-Kohn (H-K) theorems [4]. The first H-K theorem establishes the ground state energy is a functional of the electron density and the second H-K theorem demonstrate that ground state density minimises the total electronic energy of the system.

The main problem of DFT is that to find out exact functional that maps the electron density to the electronic wave function. The basic functional used in the DFT are local density functional (LDA) and the generalised gradient approximation (GGA). In LDA functional only depends upon the value of density at the coordinate where the functional is evaluated. LDA is a good approximation for solid state physics and is inadequate for molecular calculations. In GGA the gradient of the electron density at the coordinate where the functional is evaluated and it gives good results for ground state geometries and energies. In order to increase the accuracy some advanced functional like exchange and correlation functional, Hybrid functional etc. are used. BLYP functional is a correlation exchange functional in which B stands for Becke is the exchange functional and LYP for Lee, Yang and Paar is the correlation functional [5].

The deficiencies of pure DFT exchange functional are overcome by the use of hybrid functional which mixes the component of exact exchange energy component from the HF theory. B3LYP is the widely used hybrid functional in molecular calculations. Where the parameter 3 controlling the amount of exact HF exchange energy mixed in.

1.8 Basis Sets

All electronic structure calculations on molecules make the assumption that molecular wave functions can be represented as the linear combination of atomic orbitals (LCAO). The atomic orbital functions could be assumed to be the solutions of the Schrödinger equation for the hydrogen atom, which have an exp(-r) dependence, where r is the distance from the nucleus. Nevertheless, integration involving these functions can be difficult and it was shown in 1950 (4) that these could be replaced by Gaussian functions, which have the form $\exp(-r^2)$, and for which there exist analytical solutions for the integrals. The combination of several Gaussian functions with different bandwidths does give a closer match to real atomic functions. A linear combination of several Gaussian functions with different α values (half-bandwidths) can look like the atomic functions 1s and so forth but many are needed in any LCAO-MO. They are usually combined together so as to make them look like the usual atomic functions; that is, a single basis function is composed of one or more Gaussian functions. The quality of final results will depends on the basis set used in the quantum chemical calculations. Slater-Type orbital (STO) is the simplest Gaussian basis set. STO can be approximated as linear combination of N primitive Gaussian function. By increasing the number of basis function per

atom we can improve the basis set. Polarised functions are used to incorporate different bonding situation. The 6-31G* is an example for polarised basis set that adds D polarisation functions to each non-hydrogen atom [6]. Larger basis set are also available which add multiple polarisation function per atom for the triple zeta basis set [7] or additional function for the valance shell electrons.

1.9 Applications of Quantum Chemical Methods

1.91 Natural Bond Orbital (NBO) Analysis

An NBO analysis describes the Lewis like molecular bonding pattern of electron pairs (or of individual electrons in the open-shell case) in the optimally compact form of the molecule. More specifically, NBOs are orthonormal sets of localized orbitals with maximum occupancy whose leading N/2 members (or N members in the open-shell case) give the Lewis-like description of the total N-electron density. NBO analysis is a supportive tool for understanding the delocalization of the electron density, hyper conjugation effects and is useful to measure an intermolecular or intramolecular interaction.

In quantum theory, NBO is a calculated bonding orbital with maximum electron density. Natural bond orbital (NBO) analysis [8] was originated as a technique for studying Hybridization and covalence effects in polyatomic wave functions. The work of Foster and Weinhold was extended by Reed, who employed NBO analysis that exhibited by Hydrogen-bonded complexes [9] .The Second order perturbation analysis is carried out by examining all possible interactions between "filled" (donor) Lewis-type NBOs and "empty" (acceptor) non-Lewis NBOs, and estimating their energetic importance by second order perturbation theory. Since these interactions lead to donation of occupancy from the localized NBOs of the idealized Lewis structure into the empty non-Lewis orbitals, they are referred to as "delocalization" corrections to the zeroth-order natural Lewis structure. For each donor NBO and acceptor NBO, the stabilization energy E_2 associated with delocalization is calculated as

$$E(2) = \Delta E_{ij} = q_i \frac{F(i,j)^2}{\varepsilon_j - \varepsilon_i}$$

Where q_i is the donor orbital occupancy, ε_i and ε_j are diagonal elements (orbital energies) and F_{ij} is the off-diagonal NBO Fock matrix element.

1.92 Molecular Electrostatic Potential

The idea of molecular electrostatic mapping is to find out electrostatic potential V(r) that is created in the space around a molecule by its nuclei and electrons (treated as static distributions of charge) using this we can analysing and predicting molecular reactive behaviour [10]. MEP shows the three dimensional charge distribution with in the molecule. It allow us to visualize molecules shape and size [11]. In order to understand this three dimensional map a colour spectrum is given to it with red as the lowest electrostatic potential energy and blue as the highest energy (Potential increases in the order red < orange < yellow < green < blue). Since these charged regions are normal reactive part of the molecule it enable us to predict how molecule interact with other molecule [12]. The importance of MEP lies within the incontrovertible fact that it at the same time displays molecular size, shape as well as positive, negative and neutral electrostatic potential regions in terms of colour spectrum and is very useful in research of molecular structure with its physiochemical property relationship [13, 14].

1.93 Molecular Docking

The molecular docking approach is the molecular modelling method in which interaction between a small molecule and a protein at the atomic level, which allow us to characterize the behaviour of small molecules in the binding site of target proteins along with we can explain fundamental biochemical processes [15]. The docking process involves two basic steps: prediction of the ligand conformation as well as its position and orientation within these sites and assessment of the binding affinity. Using different quantum chemical method we can identify the location of the binding site in the protein before docking processes which considerably increases the efficiency of the docking. In several cases, the binding site is indeed known before docking ligands into it. Also, one can obtain information about the sites by evaluating the target protein with a family of proteins sharing a comparable function or with proteins co-crystallized with other ligands. Molecular docking designs were executed using AutoDock Vina software package.

1.94 Average Local Ionization Energy

The ionization energy, I of an N electron molecule or atom is defined by the equation

$I = E(N-1) - E(N)$, where E is the energy of the system. Using experimental methods ionization energy can be measured with high precision [16]. For molecules there are two types of ionization energies.

(1) Adiabatic ionization energy: -corresponds to neutral molecules/ ions in ground state. It does not affect the specific equilibrium geometry.

(2) Vertical ionization energy: -change in geometry due to vibrational excitation. Molecule does not in the vibrational ground state.

The average local ionization energy is the energy necessary to remove an electron from the point r in the space of a system.

$$I(r) = \sum_i \frac{\rho_i(r)|\varepsilon_i|}{\rho(r)}$$

$\rho(r)$ is the total electronic density a, $\rho_i(r)$ is that of the i^{th} occupied orbital and ε_i is the energy of i^{th} orbital. The lowest values of $I(r)$ reveal the locations of the least tightly-held electrons, and thus the favoured sites for reaction with electrophiles or radicals. Chemical reactivity is local. It varies from one site in a molecule to another. In seeking to understand and predict reactive behaviour, it is therefore important to be able to identify and rank the sites with the least strongly held, most available electrons as well as those where the electrons are tightly bound. This requires focusing not upon particular electronic orbitals, which are usually delocalized to some extent, but rather upon specific points in the space of the molecule, even though electrons from several different orbitals may have a significant probability of being at each such point. It is for these reasons that the concept of an average local ionization energy, was introduced [17].

1.95 Fukui Function

Fukui function (FF) offers information on the reactivity sites (electrophilic and nucleophilic) within the molecule and also it gives a scheme for understanding of chemical reactions. The functional derivative of the chemical potential respect to electronic potential due to nuclei at constant electron number is the one of the definition of Fukui function. Using finite difference approximation we can define Fukui function as

$f^+(r) = \rho_{N+1}(r) - \rho_N(r)$

$f^-(r) = \rho_N(r) - \rho_{N-1}(r)$

N – Electron density at a point in space around the molecule.

N+1 – Anion with an electron added to the LUMO of the neutral molecule

N-1 – Cation with an electron removed from the HOMO of the neutral molecule

Using Jaguar software package we can calculate the f^- and f^+. Fukui functions and its maximum value on the molecular surface indicates the most reactive sites. For electrophilic atom f^+ are large and positive and for nucleophilic f^- are large negative value [18]. These values correspond to the qualitative descriptors of reactivity of different atoms in the molecule. A study by Ayers and Parr [19] has shown that FF is larger when attacked by soft reagents and in places where the FF is smaller when attacked by hard reagents.

1.96 Bond Dissociation Energy

Bond dissociation energy (BDE) is defined as the enthalpy change at 298 K and 101.3 kPa for the gas-phase reaction. A sound knowledge of BDE is fundamental to understanding many chemical and biochemical processes. From BDE we can possible to understand which chemical bond are strongest and which are weakest [20]. Therefore, considerable efforts have been devoted to the determination of BDEs of various molecules. Nonetheless, because of the experimental difficulties in dealing with highly reactive radical species, it remains notoriously difficult to accurately measure the BDEs of many important compounds. An alternative approach to get BDE is to use quantum chemistry theories. This approach has proven to be useful and important in many fields because it is relatively simple, fast and cheap. Nevertheless, because open-shell radical systems are involved in the computation, one should be very careful to choose theoretical methods for the BDE calculations. Generally speaking, unrestricted Hartree-Fock and perturbation methods were not recommended for BDE calculations due to their spin-contamination problems. More sophisticated ab initio methods such as QCISD and CCSD certainly performed better than HF and MP2 for the BDE calculations, but recent studies showed that these advanced methods might also seriously underestimate some BDEs [20]. A more popular theoretical method for BDE calculations is the density functional theory (DFT). This method usually does not show serious spin-contamination and therefore, is believed to be desirable for open-shell systems. The relatively low CPU-cost of the DFT method is also advantageous.

1.97 Frontier Molecular Orbitals

The lowest unoccupied molecular orbital (LUMO) and highest occupied molecular orbital (HOMO) of a molecule sometimes referred to as frontier molecular orbitals. The role of HOMO and LUMO in a chemical reaction was first noticed by Fukui [21]. In the HOMO-LUMO picture of the molecule red colour indicates positive phase and the green colour for negative phase. The charge transfer with in the molecule can be predicted using the HOMO-LUMO energy gap. A large gap indicates high stability and least reactivity and small gap indicates low stability and high reactivity of the molecule [22]. The chemical reactions between molecules are largely governed by HOMO-LUMO interactions (the highest-energy electrons (HOMO) of one molecule "looking for" the lowest-energy unfilled space (LUMO) in the other molecule). The electron-rich component's (nucleophile) HOMO will interact strongly with the electron-deficient component's (electrophile) LUMO. The strength of interaction between orbitals is proportional to their overlap and inversely proportional to their

energy separation. HOMOB–LUMOA interaction will control the reactivity between A (Lewis acid or electrophile) and B (Lewis base or nucleophile).

1.98 Non Linear Optical (NLO) Studies

The response of the dielectric materials at the atomic level towards electric component of the high intense electromagnetic wave is the key idea of analysing NLO effects [23, 24]. NLO materials has many application in the field of information technology and industrial applications. Many organic molecules shows high polarizability and thus are good candidates for NLO studies. Materials for second order NLO must be non-Centro symmetric structural characteristics because it can be shown that the odd order polarizability are orientation independent and even term vanishes in Centro-symmetric environment. Chromophores containing donor and acceptor substituent linked through π-backbone shows larger NLO response [25]. The perturbation of external electric field give rise to a pathway for the conjugated π electrons. By adding strong electron dominating and withdrawing entities and tuning the distance between donor and acceptor atoms we can enhance the optical non linearity of organic molecules.

1.10 References

[1] L. D. Field, S. Sternhell, J. R. Kalman, Organic Structures from Spectra Fourth Edition John Wiley & Sons Ltd 2008.

[2] Hand book of vibrational spectroscopy John Wiley & Sons Ltd 2006.

[3] M. J. Frisch, G. W. Trucks, H. B. Schlegel, G. E. Scuseria, M. A. Robb, J. R. Cheeseman, G. Scalmani, V. Barone, B. Mennucci, G. A. Petersson, H. Nakatsuji, M. Caricato, X. Li, H. P. Hratchian, A. F. Izmaylov, J. Bloino, G. Zheng, J. L. Sonnenberg, M. Hada, M. Ehara, K. Toyota, R. Fukuda, J. Hasegawa, M. Ishida, T. Nakajima, Y. Honda, O. Kitao, H. Nakai, T. Vreven, J. A. Montgomery Jr., J. E. Peralta, F. Ogliaro, M. Bearpark, J. J. Heyd, E. Brothers, K. N. Kudin, V. N. Staroverov, R. Kobayashi, J. Normand, K.Raghavachari, A. Rendell, J. C. Burant, S. S. Iyengar, J. Tomasi, M. Cossi, N. Rega, J. M. Millam, M. Klene, J. E. Knox, J. B. Cross, V. Bakken, C. Adamo, J. Jaramillo, R. Gomperts, R. E. Stratmann, O. Yazyev, A. J. Austin, R. Cammi, C. Pomelli, J. W. Ochterski, R. L. Martin, K. Morokuma, V. G. Zakrzewski, G. A. Voth, P. Salvador, J. J. Dannenberg, S. Dapprich, A. D. Daniels, Ö. Farkas, J. B. Foresman, J. V. Ortiz, J. Cioslowski, D. J. Fox, Gaussian 09, Revision A.1, Gaussian, Inc., Wallingford CT (2009).

[4] S. T. Epstein, C. M. Rosenthal, The Hohenberg-Kohn theorem, J. Chem. Phys. 64 (1976) 247-249.

[5] C. Lee, W. Yang and R. G. Parr, Development of the Colic-Salvetti correlation-energy formula into a functional of the electron density Phys. Rev. B 37 (1988) 785-789.

[6] I. N. Levine, Quantum chemistry, Prentice-Hall, Inc., New Jersey 4th Ed. (1991).

[7] J. B. Foresman, A. Frisch, Exploring chemistry with electronic structure methods, Gaussian Inc, Pittsburgh, (1993).

[8] A. E. Reed, F. Weinhold, Natural bond orbital analysis of near-Hartree-Fock water dimer, J. Chem. Phys. 78 (1983) 4066-4073.

[9] L. Pauling, The nature of the chemical bond. iii. The transition from one extreme bond type to another J. Am. Chem. Soc. 54 (3) (1932) 988-1003.

[10] E. Scrocco, J. Tomasi, The electrostatic molecular potential as a tool for the interpretation of molecular properties, Top. Curr. Chem. 42 (1973) 95-170.

[11] I. G. Csizmadia, Theory and Practice of MO Calculations on Organic Molecules, Elsevier, Amsterdam, 1976.

[12] D. W. Oxtoby, H. P. Gillis, A. Campion, Principles of Modern Chemistry. 6th Ed. Belmont, CA: Thomson Brooks/Cole.2008.

[13] J. S. Murray, K. Sen, Molecular Electrostatic Potential concepts and application, 1st Ed. Elsevier Science (1996).

[14] I. Alkorta, J. J. Perez, H. O. Villar, Molecular polarization maps as a tool for studies of intermolecular interactions and chemical reactivity, J. Mol. Graph. 12 (1994) 3-13.

[15] B. J. McConkey, V. Sobolev, M. Edelman, The performance of current methods in ligand-protein docking. Current Science, 83 (2002) 845–855.

[16] D. R. Lide (ed.), Handbook of Chemistry and Physics, 78th ed., CRC, New York, 1997.

[17] P. Sjoberg, T. Brinck, J. S. Murray, P. Politzer, Average local ionization energies on the molecular surfaces of aromatic systems as guides to chemical reactivity, Can. J. Chem. 68 (1990) 1440–1443.

[18] F. Mendez, J. L. Gazquez, Chemical Reactivity of Enolate Ions: The Local Hard and Soft Acids and Bases Principle Viewpoint, J. Am. Chem. Soc. 116 (1994) 9298-9301.

[19] P. W. Ayers, R. G. Parr, Variational principles for describing chemical reactions: the Fukui function and chemical hardness revisited, J. Am. Chem. Soc. 122 (2000) 2010-2018.

[20] S. J. Blanksby, G. B Ellison, Bond dissociation energies of organic molecules, *Acc. Chem. Res.* 36 (2003) 255-63.

[21] T. Karthick, V. Balachandran, S. Perumal, Rotational isomers, vibrational assignments HOMO-LUMO, NLO properties and molecular electrostatic potential surface of N-(2 bromoethyl Phthalimide, J mol. Struct. 1005 (2011) 202-213.

[22] K. Rajalakshmi, S. Gunasekaran, S.Kumaresan, vibrational spectra electronic and quantum mechanical investigations on ciprofloxacin, Indian Journal of Physics, 88 (2014) 733.

[23] J. Zyss, Molecular Nonlinear Optics: Materials, Physics and Devices. Academic Press, New York. 1994.

[24] D. S. Chemla, J. Zyss, Nonlinear Optical Properties of Organic Molecules and Crystals. Vols. 1 and 2. Academic Press, FL, USA. 1987.

[25] R. L. Sutherland, D. G. McLean, S. Kirkpatrick, Handbook of Nonlinear Optics, 2nd Edition, Marcel Dekker, New York, 2003.

CHAPTER II
NEW QUINOLINE DERIVATIVE: SPECTROSCOPIC CHARACTERIZATION AND REACTIVITY STUDY BY DFT AND MD APPROACHES

2.1. Introduction

Quinoline derivatives have wide range of applications as anti-bacterial, anti-fungal [1-4], anti-mycobacterial [5], anti-malarial [6-11], anti-filarial [12], local anaesthetic [13] and anti-inflammatory [14] agents. They are also used as metallic organic coordination polymers [15] and in the field of organic light emitting devices [16, 17]. Quinoline derivatives are inhibitors in vivo experiments and block the replication of HIV-1 cells (in vitro study) [18-20]. There are several highly active anti-cancer quinolines described recently [21-23]. For this wide spectrum biological activity quinoline has been claimed privileged structure [24, 25]. Thus it can be assumed that more quinoline based compounds will appear in the literature and industry. Organic molecules with potentially significant biological activities represent great threat to environment due to their high stability. They accumulate, especially in water resources since natural conditions are far from being enough to decompose them [26]. Unfortunately, in the case of pharmaceutical organic pollutants conventional water purification methods are also not efficient [27, 28]. Advanced oxidation processes are seen as useful tool in order to force degradation of these molecules [27, 29-34]. DFT calculations and MD simulations are frequently employed in order to predict reactive properties of pharmaceutical molecules [35-38], which is also of great importance for improvement of existing and development of new methodologies based on advanced oxidation processes.

2.2 Experimental Details

Ethyl 4-hydroxy-2-oxo-1,2-dihydroquinoline-3-carboxylate was obtained in neat microwave assisted synthesis (scheme) as reported in literature [39]. All reagents were purchased from Aldrich. Kieselgel 60, 0.040-0.063 mm (Merck, Darmstadt, Germany) was used for column chromatography. TLC experiments were performed on alumina-backed silica gel 40 F254 plates (Merck, Darmstadt, Germany). The plates were illuminated under UV (254 nm) and evaluated in iodine vapour. The melting points were determined on Boetius PHMK 05 (VEB Kombinat Nagema, Radebeul, Germany) and are uncorrected. Elemental analyses were carried out on an automatic Perkin-Elmer 240 microanalyser (Boston, USA). The purity of the final compounds was checked by the HPLC separation module Waters Alliance 2695 XE (Waters Corp., Milford, MA, U.S.A.). The detection wavelength 210 nm was chosen. The peaks in the chromatogram of the solvent (blank) were deducted from the peaks in the

chromatogram of the sample solution. The purity of individual compounds was determined from the area peaks in the chromatogram of the sample solution. UV spectra (λ, nm) were determined on a Waters Photodiode Array Detector 2996 (Waters Corp., Milford, MA, USA) in ca 6×10^{-4} M methanolic solution and log ε (the logarithm of molar absorption coefficient ε) was calculated for the absolute maximum λ_{max} of individual target compounds. ^{1}H NMR spectrum was recorded on a Bruker AM-500 (499.95 MHz for ^{1}H), Bruker BioSpin Corp., Germany. Chemicals shifts are reported in ppm (δ) to internal $Si(CH_3)_4$, when diffused easily exchangeable signals are omitted.

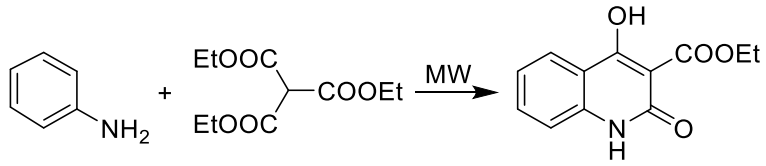

Ethyl 4-hydroxy-2-oxo-1,2-dihydroquinoline-3-carboxylate: Aniline (0.46 mL, 0.005 mol) and triethylmethanetricarboxylate (2.12 mL, 0.01 mol) were heated in microwave reactor for 8 min at 60% power level. The mixture was then cooled to room temperature and 7 mL of Et_2O was added. The crude product was crystallized from MeOH. A white crystalline compound was obtained. Yield 50%.Mp 116-120 °C. Anal. Calc. for $C_{12}H_{11}NO_4$ (233.22): C 61.80%, H 4.75%; found: C 61.65%, H 4.39%. HPLC purity 95.01%. UV (nm), λ_{max}/log ε: 244.2/3.59. ^{1}H NMR (DMSO-*d*$_6$, 500 MHz) δ: 1.19 (t, 3H), 4.17 (q, 2H), 4.70 (s, 1H), 7.09 (t, 2H), 7.32 (t, 1H), 7.52 (d, *J*=8.5 Hz, 1H), 10.30 (t, 1H).

The FT-IR spectrum (Fig.1) was recorded using KBr pellets on a DR/Jasco FT-IR 6300 spectrometer. The FT-Raman spectrum (Fig. 2) was obtained on a Bruker RFS 100/s, Germany. For excitation of the spectrum the emission of Nd:YAG laser was used, excitation wavelength 1064 nm, maximal power 150 mW, measurement on solid sample.

2.3 Computational Details

Calculations of the wavenumbers, molecular geometry, polarizability values, frontier molecular orbital analysis were carried out with Gaussian 09 program [40] using the B3LYP/6-311++G(d,p) quantum chemical calculation method. A scaling factor of 0.9613 is used to scale the theoretically obtained wavenumbers [41] and the assignments of the vibrational wavenumbers are done by using Gauss View [42] and GAR2PED software [43]. Parameters corresponding to optimized geometry of the title compound (Fig. 3) are given in Table 1. In this work Schrödinger Materials Science Suite 2015-4 was used for the investigation of reactivity of the title molecule. Concretely, Jaguar 9.0 [44] program was used for DFT calculations, while Desmond [45-48] program was used for MD simulations. DFT calculations

with Jaguar have been performed by B3LYP exchange-correlation functional [49] with 6-311++G(d,p), 6-31+G(d,p) and 6-311G(d,p) basis sets for the calculations of ALIE, Fukui functions and BDEs, respectively. MD simulations with Desmond program have been performed by OPLS 2005 force field [50], with simulation time set to 10 ns. Temperature was set to 300 K, while pressure was to 1.0325 bar. Also, cut off radius was set to 12 Å, while modelled system was of isothermal-isobaric (NPT) ensemble class. For the solvent a simple point charge (SPC) model [51] was used. One EHODQC molecule was placed into the cubic box with ~3000 water molecules, in order to model the system. A method for the analysis of electron density developed by Johnson et al. [52, 53] and implemented in Jaguar program was used for the determination of non-covalent interactions. Maestro GUI [54] was used for the preparation of input files and analysis of results when Schrödinger Materials Science Suite 2015-4 was used.

2.4 Results and Discussions

2.4.1 Optimized Geometrical Parameters

For the title compound the bond lengths of C_1-C_2 = 1.4065 Å, C_2-C_3 = 1.4121 Å and C_3-C_4 = 1.4079 Å and these values are greater than that of C_1-C_6 (1.3865 Å) and C_4-C_5 (1.3851 Å) due to adjacent quinoline ring and the reported values are C_1-C_2 = 1.4020 Å, C_2-C_3 = 1.4171 Å, C_4-C_3 = 1.4043 Å [55]. The values of bond lengths C_{13}-C_{15} (1.4711 Å) and C_{15}-C_{19} (1.4686 Å) are high which is due to the adjacent C=O and carboxylate groups. The bond angles C_1-C_2-C_3 (119.7°) and C_2-C_3-C_4 (119.5°) are lesser than 120° because of the presence of quinoline ring. The angles C_3-C_{14}-C_{15} and C_2-N_{11}-C_{13} are 121.6° and 127.0° respectively, which can be assumed as due to the presence of OH group which is electropositive. According to literature the corresponding reported bond angles are C_1-C_2-C_3 (119.6°), C_2-C_3-C_4 (119.4°), C_2-N_{14}-C_{20} (125.8°), C_3-C_{15}-C_{18} (121.3°) and N_{14}-C_{20}-C_{118} (114.2°) respectively [56]. The presence of higher electro negative group C=O would be the reason for the lesser bond angle of N_{11}-C_{13}-C_{15} (114.3°). The ethyl group is tilted almost perpendicular from the quinoline ring as evident from the dihedral angle C_{19}-C_{21}-C_{22}-C_{25} = 85.3º.

2.4.2 IR and Raman Spectra

The observed IR and Raman bands and calculated (scaled) wavenumbers and assignments are given in Table 2. The C_{13}=O_{16} and C_{14}=C_{15} stretching vibrations are assigned at 1718 cm^{-1} (DFT), 1752 cm^{-1} (IR), 1745 cm^{-1} (Raman) and at 1557 cm^{-1} (DFT), 1558 cm^{-1} (IR), 1556 cm^{-1} (Raman) respectively. The C=O and C=C stretching modes have high IR intensities and PEDs of 68 and 45%. The C=O stretching vibration in the spectra of carboxylate give rise to a strong band in the region 1600-1700 cm^{-1} [57]. The bands observed at 1668 cm^{-}

^{1} in IR spectrum,1669 cm^{-1} in Raman spectrum and at 1632 cm^{-1} (DFT) with IR intensity 157.87, Raman activity 131.63 and with a PED of 56% are assigned as C_{19}=O_{20} stretching mode of the title compound. The C-O-C stretching modes are observed at 1279 cm^{-1} and at 1085 cm^{-1} theoretically and the mode at 1279 cm^{-1} has high IR intensity of 213.56 while the other mode at 1085 cm^{-1} has a moderate IR intensity of 62.74 with PEDs around 40%. Ulahannan et al. [58] reported the C-O stretching mode for a similar derivative at 1298 cm^{-1} (IR), 1319 cm^{-1} (Raman) and 1313 cm^{-1} (DFT). The stretching band of C_{14}-O_{17} is expected in the region 1220 ± 40 cm^{-1} [56, 59, 60] and the band at 1229 cm^{-1} (DFT) is assigned as C-O stretching vibration with IR intensity of 77.81, Raman activity of 11.83 and a PED of 44% of the title compound while the reported value is 1206 cm^{-1}(DFT) [58].

The O-H stretching vibration gives rise to a band at 3050 ± 150 cm^{-1} [57]. The band observed at 2930 cm^{-1} experimentally and 2925 cm^{-1} in DFT calculation is assigned as the O-H stretching vibration. The downshift of the OH stretching mode is due to the strong hydrogen bonded system present in the title compound as reported in literature [61, 62]. The OH in-plane and out-of-plane deformation modes are expected at 1395 ± 55 cm^{-1} and at 905 ± 70 cm^{-1} respectively [57]. For the title compound the band at 1354 cm^{-1} (DFT) is assigned as the in-plane O-H deformation band. Similarly the bands at 864 cm^{-1} (IR), 866 cm^{-1} (Raman) and 876 cm^{-1} (DFT) are assigned as the O-H out-of-plane deformation bands of the title compound. The in-plane OH bending mode has a high IR intensity and Raman activity of 201.95 and 246.61 and a band of 1348 cm^{-1} is observed experimentally in both spectra. Rajeev et al. [58] reported a band at 1412 cm^{-1} as the in-plane O-H deformation.

The N-H stretching vibrations are expected [63] in the range 3500-3300 cm^{-1}. In the present study the bands observed at 3458, 3313 cm^{-1} in the IR spectrum and 3455 cm^{-1} theoretically is assigned as N-H stretching vibrational mode which has a PED of 100% and IR intensity 41.77 and Raman activity 93.15. In the present case the N-H stretching mode splits into a doublet and downshifted from the computed value which indicates the weakening of the N-H bond [64, 65]. N-H group shows bands at 1510-1500, 1350-1250 and 740-730 cm^{-1} [66]. According to literature if N-H is a part of a closed ring [66] the N-H deformation band is absent in the region 1510-1500 cm^{-1}. In the present case the N-H in-plane deformation band is observed at 1499 cm^{-1} in IR spectrum, 1503 cm^{-1} in the Raman spectrum and at 1484 cm^{-1} theoretically and this mode has IR intensity 44.68, Raman activity 35.14 with a PED 33%.The out-of-plane deformation bands of N-H are expected in the range 650 ± 50 cm^{-1} and the bands observed at 602 cm^{-1} (IR), 619 cm^{-1} (Raman), 595 cm^{-1} (DFT) assigned as γNH mode of the

title compound. This mode has 82% PED with 71.31 as IR intensity and a low Raman activity less than 10.00.

The vibrations of CH_2 group (stretching, deformation mode vibrations) appear in the range 2960-2930, 2835-2835 and 1475-775 cm^{-1} respectively. These bands are observed at 2990, 1311, 1167, 808 cm^{-1} in IR spectrum, 2971, 1305, 1164 cm^{-1} in Raman spectrum and 3009, 2980,1464, 1459, 1293, 1165, 790, 748 cm^{-1} theoretically for the title compound [57]. For the methyl group, stretching vibrations are expected in the region 3050-2800 cm^{-1} [57]. The DFT calculations give these modes at 3040, 3019 and 2943 cm^{-1} respectively, while the observed values are, 3033, 2940 cm^{-1} (IR), 2940 cm^{-1} (Raman). The deformation modes of the methyl group are expected in the region 1460-1080 cm^{-1} [57, 58] and the bands at 1478, 1457, 1386, 1165, 1085 cm^{-1} (DFT), at 1473, 1447, 1167 cm^{-1} (IR) and at 1455, 1164, 1082 cm^{-1} (Raman) are assigned as the bending modes of the methyl group of the title compound.

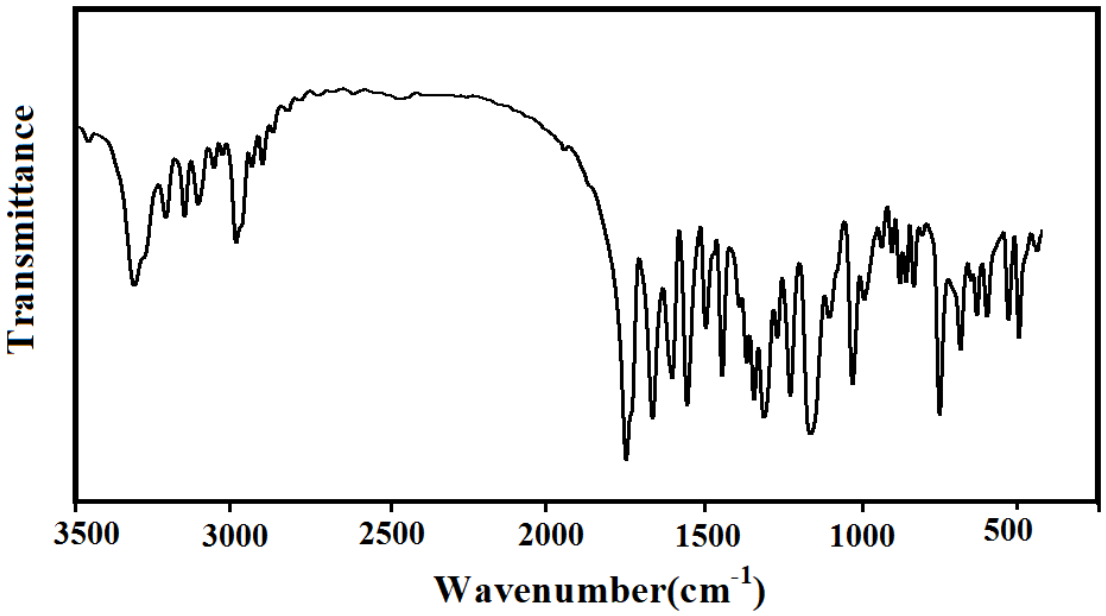

Fig. 1 FT-IR spectrum of ethyl-4-hydroxy- 2-oxo-1,2-dihydroquinoline-3-carboxylate

In the present case, the quinoline C-C stretching ring modes are observed at 1558 cm^{-1} in the IR spectrum, 1556 cm^{-1} in the Raman spectrum, 1557, 1067 cm^{-1} theoretically with high IR intensities and the C-N stretching modes are at 1271, 1182 cm^{-1} in the Raman spectrum, 1267, 1226 cm^{-1} theoretically with PEDs 55 and 42%. Both the modes possess moderate IR intensities. Rajeev et al. reported the quinoline stretching modes at 1610, 1445, 1020 cm^{-1} (C-C), 1262 cm^{-1} (C-N) in the IR spectrum, 1609, 1051, 1022 cm^{-1} (C-C), 1202 cm^{-1}

[1] (C-N) in the Raman spectrum, 1607, 1433, 1045, 1035cm^{-1} (C-C), 1270, 1230 cm^{-1} (C-N) theoretically [58].

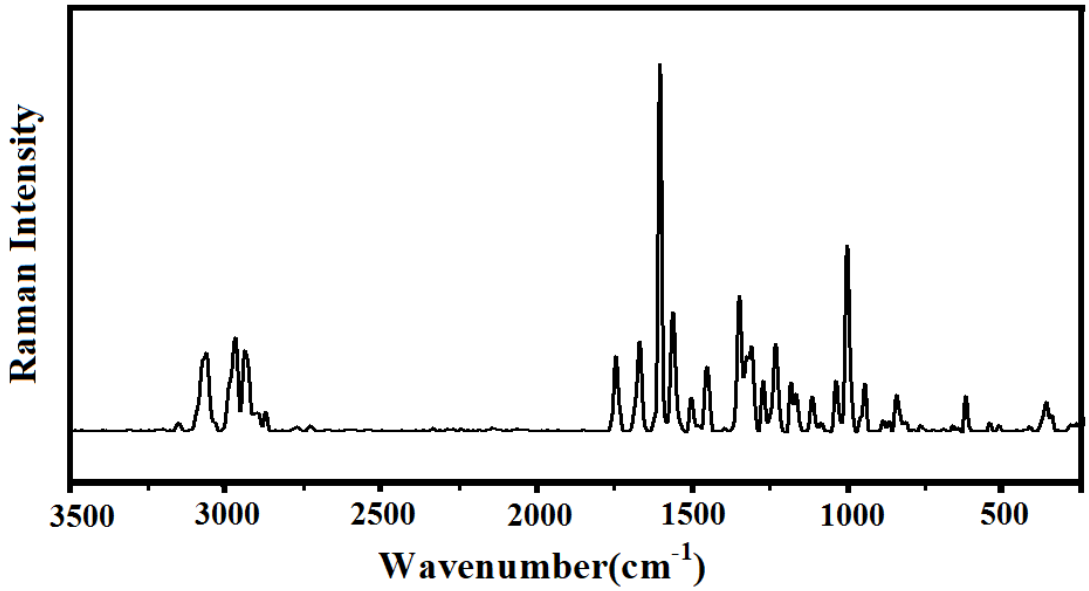

Fig. 2 FT-Raman spectrum of ethyl-4-hydroxy-2-oxo-1,2-dihydroquinoline-3-carboxylate

The DFT calculations give the C-H stretching modes of the phenyl ring of the title compound at 3111, 3090, 3078, 3064 cm^{-1}. The bands observed at 3153, 3110, 3060 cm^{-1} in the IR spectrum and at 3141, 3064 cm^{-1} in the Raman spectrum are assigned as C-H stretching modes of the phenyl ring [57]. The bands observed at 1607,1499 cm^{-1} in IR spectrum, 1603, 1503 cm^{-1} in Raman spectrum and at 1618,1586, 1484, 1464, 1336 cm^{-1} theoretically are assigned as phenyl ring stretching modes of the title compound which are expected in the region 1620-1250 cm^{-1} [57]. In the present case, the band observed at 1031 cm^{-1} in IR spectrum,1033 cm^{-1} in Raman spectrum and 1023 cm^{-1} theoretically with a PED contribution of 59% and average IR intensity and Raman activity is assigned as the ring breathing mode of the phenyl ring which is expected in region 1020-1070cm^{-1} [56]. Panicker et al. [67] reported the ring breathing mode of di-substituted benzene at 1018 cm^{-1} (IR), 1034 cm^{-1} (Raman) and 1019 cm^{-1} (DFT). For the title compound, the bands observed at 1227, 1102 cm^{-1} (IR), 1271, 1230, 1107 cm^{-1} (Raman) and 1267, 1229, 1155, 1143, 1096 cm^{-1} (DFT) are assigned as the C-H in-plane bending modes of the phenyl ring. The C-H out-of-plane deformations are expected below 1000 cm^{-1} [57] and for the title compound the theoretical calculations give bands at 950, 925, 834 and 745 cm^{-1} as γCH modes of the phenyl ring. Experimentally these bands are observed at 941 cm^{-1} in the IR spectrum and at 944 cm^{-1} in the Raman spectrum.

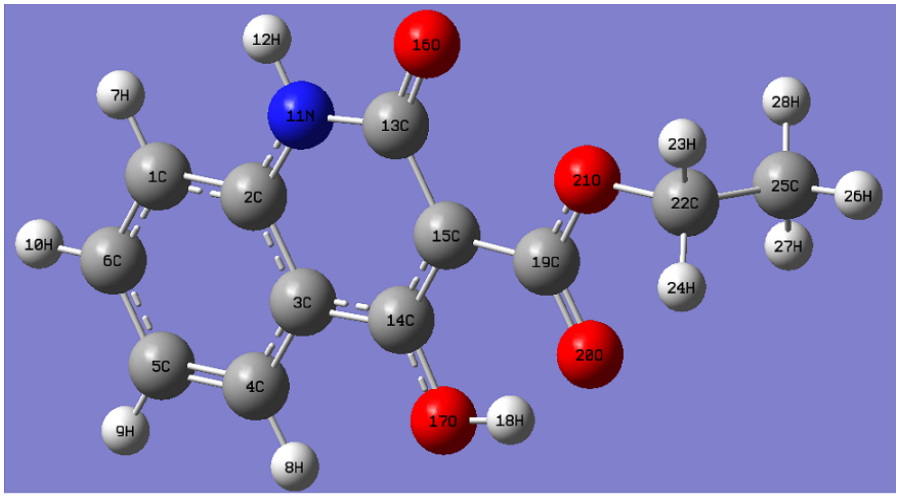

Fig. 3 Optimized geometry of ethyl-4-hydroxy-2-oxo-1,2-dihydroquinoline-3-carboxylate

2.4.3 Frontier Molecular Orbitals

Frontier molecular orbital study is used to explain the chemical behaviour and stability of the molecular system. The atomic orbital components of the frontier molecular orbitals are shown in Fig. 4. The delocalization of HOMO and LUMO over the molecular system shows the charge transfer within the molecular system. The HOMO-LUMO gap is found to be 3.073 eV.

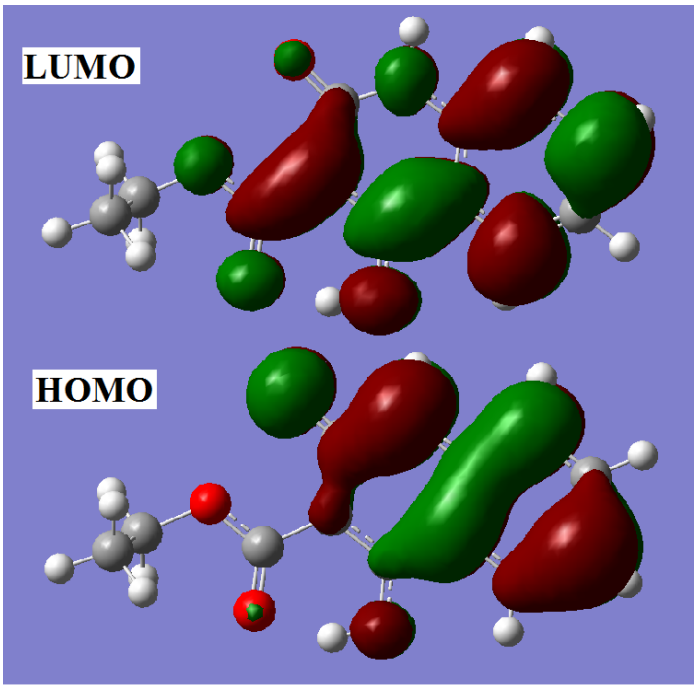

Fig. 4 HOMO-LUMO plots of ethyl-4-hydroxy-2-oxo-1,2-dihydroquinoline-3-carboxylate

2.4.4 Molecular Electrostatic Potential

Molecular electrostatic potential and electron density are related to each other to find the reactive sites for electrophilic and nucleophilic sites [68, 69].The negative (red and yellow) regions of MEP map (Fig.5) were related to electrophilic reactivity while the positive (blue) regions to nucleophilic reactivity.

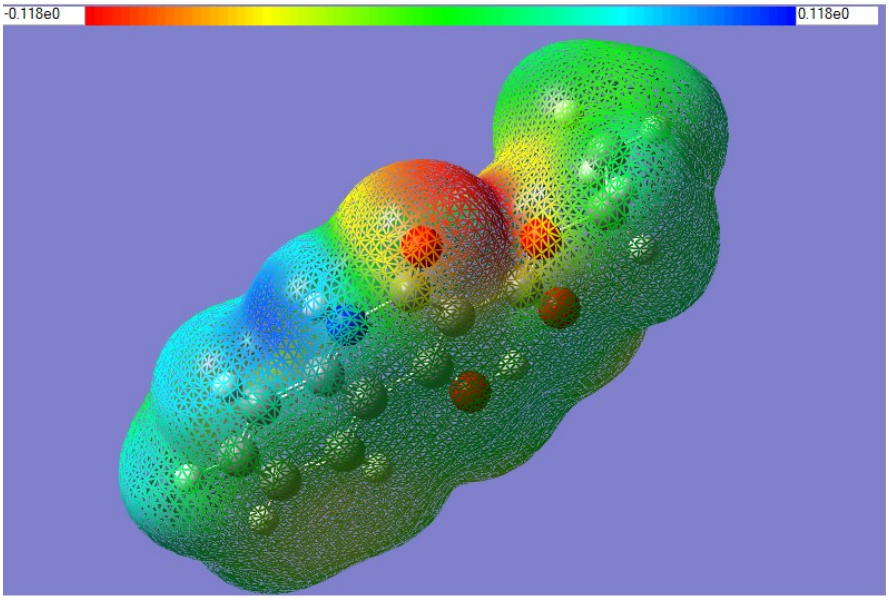

Fig. 5 MEP plot of ethyl-4-hydroxy-2-oxo-1,2-dihydroquinoline-3-carboxylate

2.4.5 ALIE Surface, Fukui Functions, Fukui Indices and Non Covalent Interactions

Average local ionization energy (ALIE) is very important quantity that reflects the local reactivity properties of some molecular system. This quantum molecular descriptor indicates what amount of energy is required for the removal of electron from molecule. In this regard, molecule sites where ALIE values are the lowest are the ones that are the most sensitive towards electrophilic attacks. Sjoberg et al. [70, 71] defined ALIE as a sum of orbital energies weighted by the orbital densities according to the following equation:

$$I(r)=\sum_i \frac{\rho_i(\vec{r})|\varepsilon_i|}{\rho(\vec{r})}. \qquad (1)$$

where $\rho_i(\vec{r})$ denotes electronic density of the i-th molecular orbital at the point $\vec{r}$, ε_i denotes orbital energy, while $\rho(\vec{r})$ denotes total electronic density function [72, 73]. In order to detect molecule sites that are mostly prone to electrophilic attacks in this work we have mapped ALIE values to the electron density surface, Fig.6.

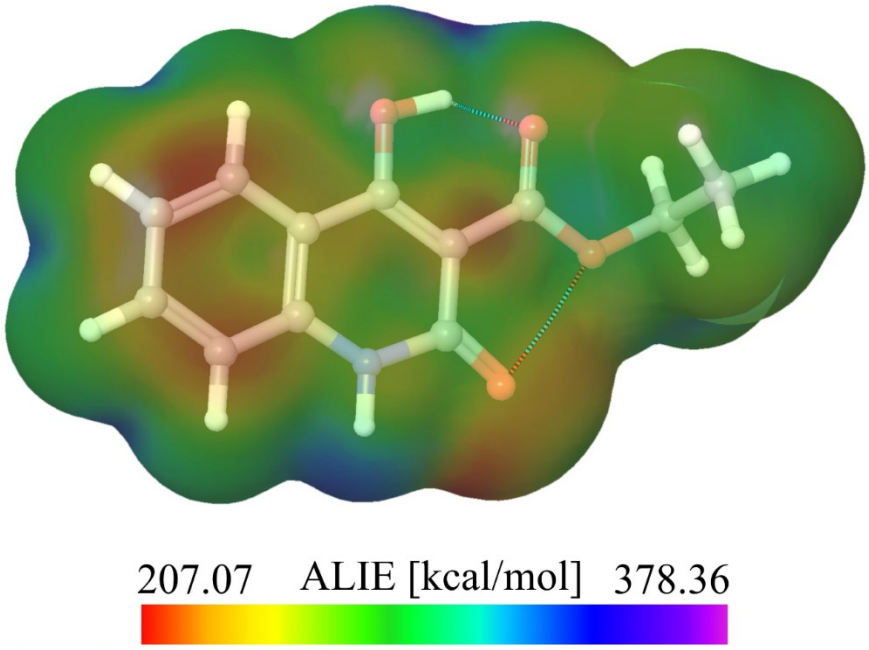

Fig. 6 ALIE surface of ethyl-4-hydroxy-2-oxo-1,2-dihydroquinoline-3-carboxylate molecule

Results presented in Fig.6 indicate that there are several molecule sites where ALIE has the lowest values. Namely, those molecule sites are benzene ring, oxygen atom O_{16} and carbon atom C_{15}, all characterized by ALIE values of ~207 kcal/mol. On the other side, near vicinity of hydrogen atoms H_{12} and H_{18} are characterized by the highest ALIE of ~378 kcal/mol. Fig.6 also contain information about the two formed intramolecular non-covalent interactions, between two oxygen atoms (O_{16} and O_{21}) and hydrogen atoms (H_{18} and O_{20}). The non-covalent interaction formed between hydrogen and oxygen atom is much stronger (corresponding strength is –0.062 electron/bohr^3) than the non-covalent interaction formed between two oxygen atoms (corresponding strength is -0.015 electron/bohr^3).

Fukui function is also a local descriptor, defined as the functional derivative of the chemical potential with respect to the external potential [74], while by using Maxwell relation it can be presented in the form of derivative of the electronic density with respect to the number of electrons [75, 76].This quantum molecular descriptor actually indicates the changes in electron density as a consequence of change in charge. Mapping of values of Fukui functions to the electron density surface provides a convenient way to determine molecule sites that could act as important reactive centers. In Jaguar program Fukui functions are calculated in finite difference approach according to the following equations:

$$f^{+} = \frac{\left(\rho^{N+\delta}(r) - \rho^{N}(r)\right)}{\delta}, \quad (2)$$

$$f^{-} = \frac{\left(\rho^{N-\delta}(r) - \rho^{N}(r)\right)}{\delta}. \quad (3)$$

where N stands for the number of electrons in reference state of the molecule, while δ stands for the fraction of electron which default value is set to be 0.01 [76]. Representative Fukui functions surfaces are presented in Fig.7. Color coding employed in Fig.7 is as following. Positive (purple) color in Fig.7a represent molecule sites where electron density has been increased as a consequence of addition of charge, while negative (red) color in Fig.7b represents molecule sites where electron density decreases with the removal of charge. According to the color coding it can be seen in Fig.7a that electron density increases, as a consequence of charge addition, in the near vicinity of carbon atoms C_6, C_{14} and C_{19}. On the other side electron density decreases, as a consequence of charge removal, in the near vicinity of oxygen atoms O_{20} and O_{21}.

Besides Fukui functions, Fukui indices are also widely used as local density functional descriptors to mock-up chemical reactivity and selectivity by designates the tendency of the electronic density to deform at a given position upon accepting or donating electrons [77-79]. Also, it is possible to define the corresponding condensed or atomic Fukui functions of the jth atom site as

$$f_j^{-} = q_j(N) - q_j(N-1) \quad (4)$$

$$f_j^{+} = q_j(N+1) - q_j(N) \quad (5)$$

$$f_j^{0} = [q_j(N+1) q - _j(N-1)] \quad (6)$$

In these equations, q_j is the atomic charge (evaluated from Mulliken population analysis, electrostatic derived charge etc. at the j^{th} atomic site is the neutral (N), anionic (N+1) or cationic (N-1) chemical species. Chattaraj et al. [80] have introduced the concept of generalized philicity. It contains almost all information about previously known different global and local reactivity and selectivity descriptor, in addition to the information regarding electrophilic/nucleophilic power of a given atomic site in a molecule. Morell et al. [81] have recently proposed a dual descriptor $\Delta f(r)$, which is defined as the difference between the nucleophilic and electrophilic Fukui function and is given by $\Delta f(r) > 0$, then the site is favoured for a nucleophilic attack, whereas if $\Delta f(r) < 0$, then the site may be favoured for an electrophilic attack. Under this situation, dual descriptors Δf (r) provide a clear difference between

nucleophilic and electrophilic attack at a particular site with their sign. That is they provide positive value for site prone for nucleophilic attack and a negative value prone for electrophilic attack. From the values reported in Table 3, according to the condition for dual descriptor, nucleophilic site for in our title compound is C_2, C_3,C_5, H_9, H_{10}, N_{11}, H_{12}, C_{13}, C_{14}, H_{18}, C_{19},O_{21}, H_{26}, H_{27} (positive value i.e. $\Delta f(r) > 0$. Similarly the electrophilic attack site is C_1, C_4, C_6, H_7, H_8, C_{15}, O_{17}, O_{20}, C_{22}, H_{23}, H_{24}, C_{25}, H_{28} (negative value i.e. $\Delta f(r) < 0$). The behaviour of molecules as electrophiles/nucleophiles during reaction depends on the local behaviour of molecules.

a) b)

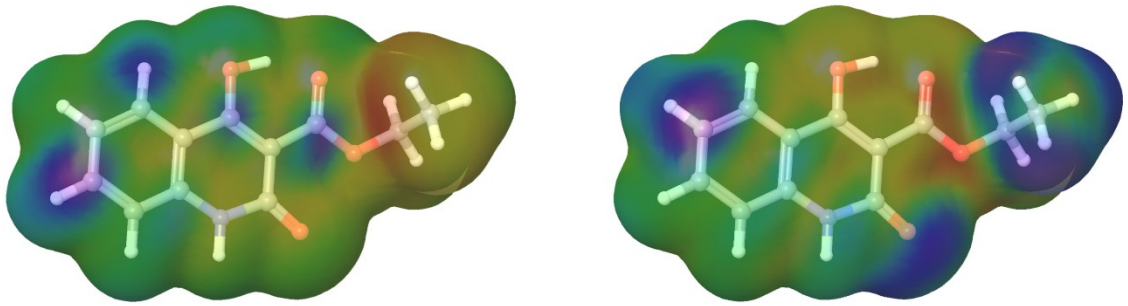

Fig. 7 Fukui functions a) f^+ and b) f^- of ethyl-4-hydroxy-2-oxo-1,2- dihydroquinoline-3-carboxylate molecule

2.4.6 NBO Analysis

The natural bond orbitals (NBO) calculations were performed using NBO 3.1 program [82] and the important interactions are presented in tables 4 and 5. The strong interactions are:C_{13}-O_{16} from N_{11} of $n_1(N_{11})\rightarrow\pi^*(C_{13}$-$O_{16})$, C_2-C_3 from N_{11} of $n_1(N_{11})\rightarrow\pi^*(C_2$-$C_3)$, N_{11}-C_{13} from O_{16} of $n_2(O_{16})\rightarrow\sigma^*(N_{11}$-$C_{13})$, C_{13}-C_{15} from O_{16} of $n_2(O_{16})\rightarrow\sigma^*(C_{13}$-$C_{15})$, C_{14}-C_{15} from O_{17} of $n_1(O_{17})\rightarrow\pi^*(C_{14}$-$C_{15})$, C_{19}-O_{21} from O_{20} of $n_2(O_{20})\rightarrow\sigma^*(C_{19}$-$O_{21})$. These interactions have high stabilization energies and electron densities, which are respectively, (0.00890, 0.45862, 0.08085, 0.06141, 0.35631, 0.07395e and 53.53, 45.39, 25.06, 18.29, 45.86, 23.37 kJ/mol. The natural orbitals with low and high occupation numbers are: $n_2(O_{16})$, $n_2(O_{17})$, $n_3(O_{20})$, $n_2(O_{21})$ and $n_1(O_{16})$, $n_1(O_{17})$, $n_1(O_{20})$, $n_1(O_{21})$. The orbital with low occupation numbers have higher energies, -0.23464, -0.31867, -0.27482, -0.31862a.u with considerable p-characters around 100.0% with low occupation numbers, 1.86676, 1.77071, 1.56926 and 1.75646. The orbital have high occupation numbers have low energies, -0.67847, -0.56174, -0.67554, -0.54974a.u with p-characters, 36.14, 59.46, 41.58, 59.44% and high occupation numbers, 1.97777, 1.97148, 1.95846, 1.96237.Thus a very close to pure p-type lone pair orbital participates in the electron donation to the σ* (C_{19}-O_{21}) orbital for $n_2(O_{20})\rightarrow\sigma^*(c_{19}$-

O_{21}), $\pi^*(C_{14}\text{-}C_{15})$ orbital for $n_2(O_{17})\rightarrow\pi^*(C_{14}\text{-}C_{15})$ and $\sigma^*(N_{11}\text{-}C_{13})$ orbital for $n_2(O_{16})\rightarrow\sigma^*(N_{11}\text{-}C_{13})$ interaction in the compound.

2.4.7 Nonlinear Optical Properties

The calculated first hyper polarizability of the title compound is 4.19×10^{-30} esu which is 32 times that of standard NLO material urea (0.13×10^{-30} esu) [83]. The reported value of first hyper polarizability of similar derivative is 2.24×10^{-30} esu [84]. The phenyl ring stretching vibrations at 1607, 1499 cm^{-1} in the IR spectrum have their counterparts in the Raman spectrum at 1603, 1503 cm^{-1} respectively with IR and Raman intensities are comparable. These types of organic molecules have conjugated π-electron system and large hyper polarizability which leads to nonlinear optical properties [85]. The C-N distances in the calculated molecular structure vary from 1.3743 to 1.4046 Å which are in between those of a C-N single and double bond and this suggest an extended π-electron delocalization over the molecular system which is also responsible for the nonlinearity of the molecule [86]. We conclude that the title compound is an attractive object for future studies of non-linear optical properties.

2.4.8 Reactive and Degradation Properties based on Autoxidation and Hydrolysis

Autoxidation and hydrolysis properties of molecules that are candidates for the practical applications can be predicted by calculations of BDE values and by calculations of RDF. It is very useful to predict to what extent drug candidate molecules are sensitive towards aforementioned mechanisms since it allows rationalization and optimization of experiments related to the forced degradation [87-90]. Drug molecules are sensitive towards autoxidation mechanism only at certain molecule sites, in which the BDE for hydrogen abstraction is in the range of 70 to 85 kcal/mol, according to the works of Wright et al. [91] and Gryn'ova et al. [92]. BDE values between 85 and 90 kcal/mol are questionable, but also possibly important. BDE values lower than 70 kcal/mol do not reflect sensitivity of drug molecules towards the autoxidation mechanism [91, 93, 94]. Results concerning BDE values for hydrogen abstraction and BDE for the rest of the single acyclic bonds in this work are provided in Fig.8. Results presented in Fig.8 concerning the BDE values for hydrogen abstraction indicate that investigated molecule has great stability towards autoxidation mechanism since all of the BDE values are much higher than 90 kcal/mol. Thanks to these results, it can be stated that EHODQC molecule is very stable in open air and in the presence of oxygen. On the other side the lowest BDE value for the rest of the single acyclic bonds has been calculated for the bond denoted with number 12 in Fig.8, indicating that degradation could start by detaching of the alkyl chain. Besides high

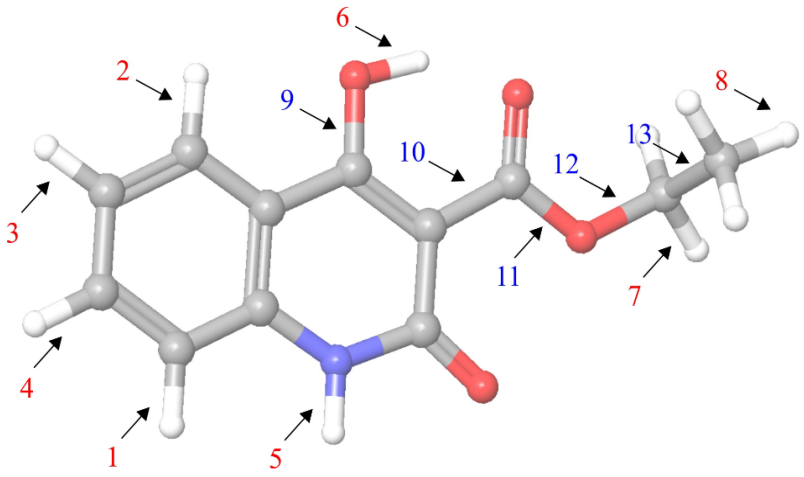

Bond	BDE [kcal/mol]
1	118.72
2	119.24
3	118.76
4	117.48
5	106.29
6	112.02
7	100.77
8	108.14
9	124.66
10	112.53
11	95.39
12	81.28
13	89.82

Fig. 8 BDEs of all single acyclic bonds of ethyl-4-hydroxy-2-oxo-1,2-dihydroquinoline-3-carboxylate molecule

stability towards autoxidation mechanism this study also indicates that EHODQC molecule is very stable in water, as indicated by RDFs. RDF, g(r), which determines the probability of finding a particle in the distance r from another particle [95], show that only five atoms of EHODQC molecule have relatively significant interactions with water molecules, Fig.9.Atoms that have relatively pronounced interactions with water molecules are carbon atoms C_1, C_{13} and C_{25}, hydrogen atom H_{12} and oxygen atom O_{16}. Carbon atoms have very similar g(r) profiles with similar peak distance located at around 3.5 Å, while there is significant difference in maximal g(r) values in favour of carbon atom C_{25}. Oxygen atom O_{16} is characterized with peak distance located under 3 Å. Of all atoms the most important, from the aspect of interactions with water molecules, is hydrogen atom H_{12}, with maximal g(r) value of almost 0.9 and with peak distance located at under 2 Å.

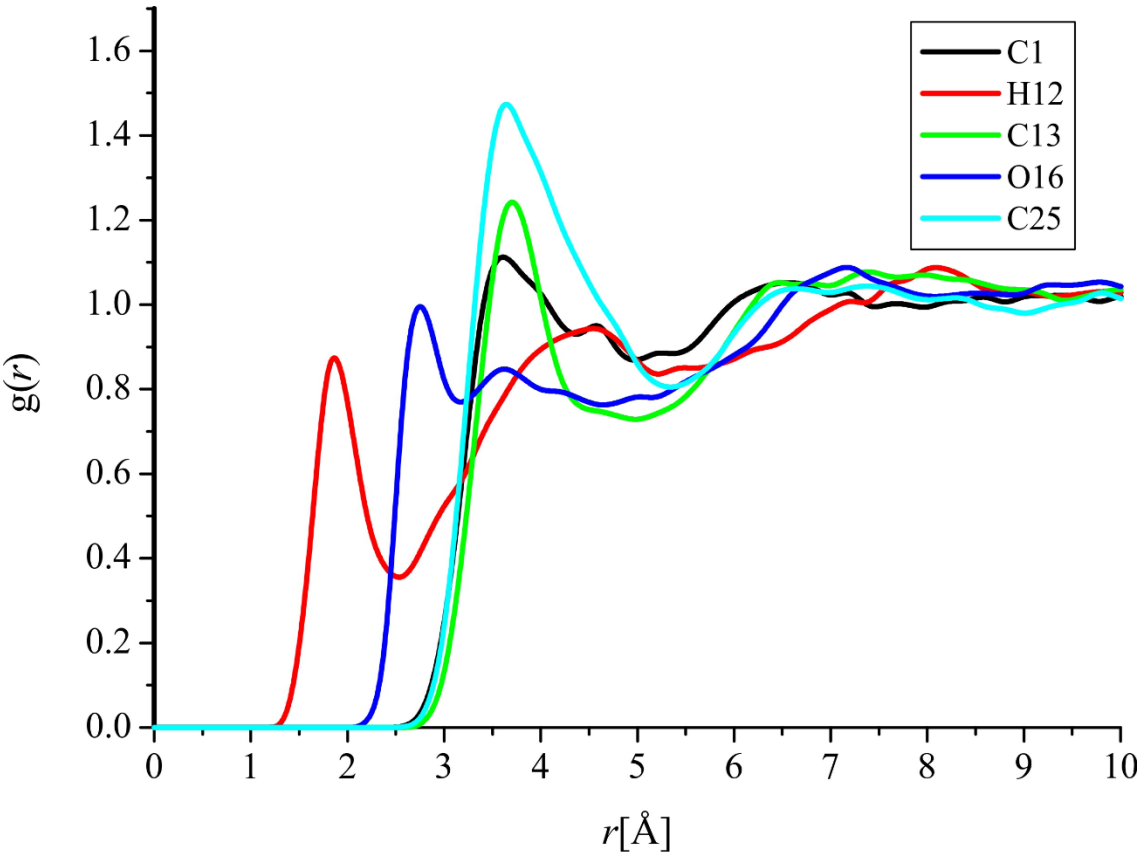

Fig. 9 RDFs of atoms of ethyl-4-hydroxy-2-oxo-1, 2-dihydroquinoline-3-carboxylate molecule with significant interactions with water molecules

2.4.9 Molecular Docking

It is evident from the literature that the pyridine derivatives show promising anti-tubercular activity [96]. Therefore we decided to evaluate in silico anti-tubercular potential of the title compound. Amongst the various targets for anti-TB drugs enoyl-acyl carrier protein (ACP) reductase being a well-established target [97, 98] was selected as the target macromolecule for docking simulations. ACP reductase is a key enzyme for the synthesis of the type II fatty acids. High resolution crystal structure of ACP reductase was downloaded from the RCSB PDB website (PDB ID: 1QG6) [99].All molecular docking calculations were performed on AutoDock-Vina software and as reported in literature [100, 101].Amongst the docked conformations, RMSD values below 2Å (Fig.10) binds well at the active site was analysed for detailed interactions in Discover Studio Visualizer 4. Docking study reveals that the synthesized molecules bind at the same site where the co-crystallized drug triclosan is attached (Fig 11). Lys163 and Ala189 form H-bonds with the title compound (Fig. 12). Formation of three hydrogen bonds predicts high affinity and specificity. The docked

compound form stable complex with ACP reductase as is evident from the interactions and the high binding affinity values (Table 6). These results suggest that the compound should

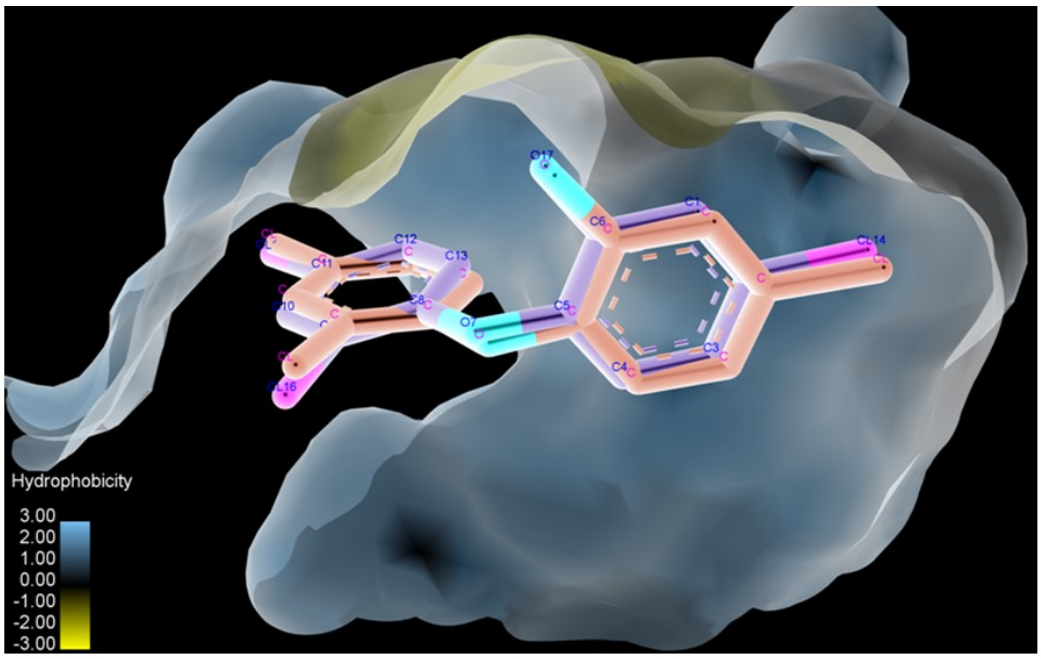

Fig. 10 Superimposition of docked conformation (purple) and the co-crystallized conformation (red) of triclosan shows RMSD value close to zero, confirming the reliability of docking protocol

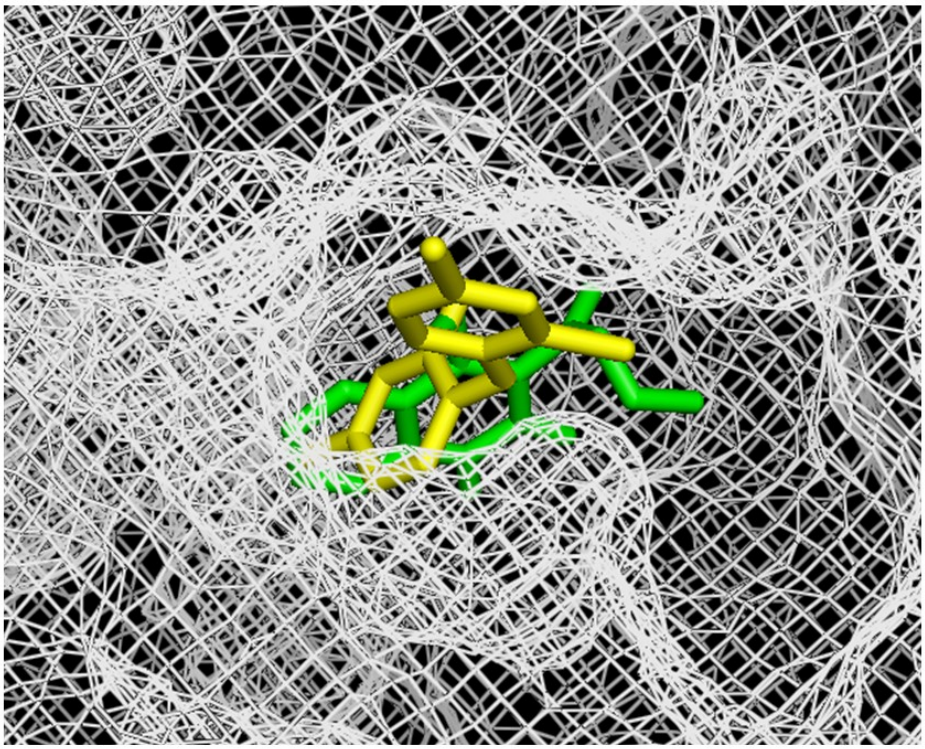

Fig. 11 Surface view of docked ligand at the active site of ACP reductase

exhibit inhibitory activity against ACP reductase and to be highly selective. Biological tests however need to be done to compliment the in silico predictions.

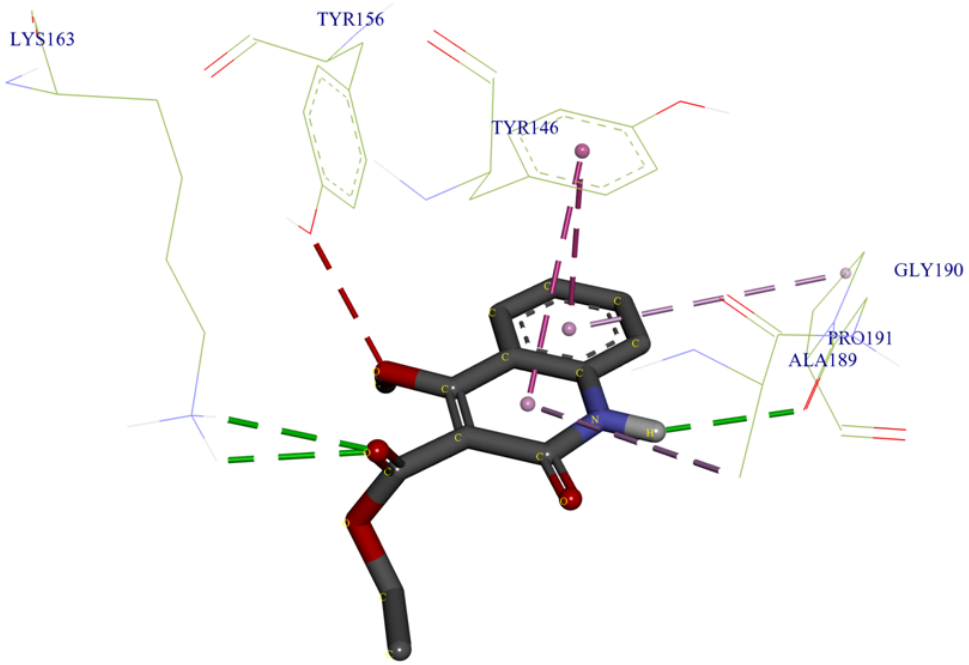

Fig. 12 Detailed interactions of the title compound with the inhibitor residues, dotted lines represent the interactions. H bonds, π-π T and alkyl-π interactions are represented by green, pink and violet dotted lines respectively.

2.5 Conclusion

The vibrational spectroscopic studies of ethyl-4-hydroxy-2-oxo-1,2-dihydroquinoline-3-carboxylate in the ground state were reported experimentally and theoretically. Potential energy distribution of normal modes of vibrations was done using GAR2PED program. The ring stretching modes in IR and Raman spectra are evidence for charge transfer interaction between the donor and the acceptor group through the π system. This along with the lowering of HOMO–LUMO band gap supports for the bioactivity of the molecule. NBO analysis predicts a strong inter molecular hyper conjugative interaction of (C_{19}-O_{21}) from O_{20} of $n_2(O_{20})$, (C_{14}-C_{15}) from $O_{17}$of $n_2(O_{17})$) and (N_{11}-C_{13}) from O_{16} of $n_2(O_{16})$. MEP predicts the most reactive part in the molecule. The calculated first hyper polarizability is comparable with the reported values of similar derivatives and is an attractive object for future studies in nonlinear optics. The minimum energy surfaces are obtained from the potential energy curve by PES scan studies. Thanks to DFT calculations of ALIE values in this work, beside benzene ring, we have determined oxygen atom O_{16} and carbon atom C_{15} as possibly prone to electrophile

attacks. Thanks to the mapping of the Fukui function values to the electron density surface we have also determined carbon atoms C_6, C_{14} and C_{19} and oxygen atoms O_{21} and O_{22} as possible important reactive centres. Calculations of BDE showed that title molecule is not sensitive towards autoxidation mechanism, which certainly hardens its degradation. This fact is also supported by the results of RDF after MD simulations which showed that only one atom, hydrogen atom H_{12}, have significantly pronounced interactions with water molecules.

Table 1. Optimized geometrical parameters of ethyl- 4- hydroxy-2- oxo-1, 2-dihydroquinoline- 3-carboxylate

Bond length (Å)		Bond angles(˚)		Dihedral angles(˚)	
C_1-C_2	1.4065	C_2-C_1-C_6	119.7	C_6-C_1-C_2-C_3	-0.0
C_1-C_6	1.3865	C_2-C_1-H_7	119.5	C_6-C_1-C_2-N_{11}	180.0
C_1-H_7	1.0868	C_6-C_1-H_7	120.8	H_7-C_1-C_2-C_3	180.0
C_2-C_3	1.4121	C_1-C_2-C_3	119.7	H_7-C_1-C_2-N_{11}	-0.0
C_2-N_{11}	1.3743	C_1-C_2-N_{11}	121.5	C_2-C_1-C_6-C_5	-0.0
C_3-C_4	1.4079	C_3-C_2-N_{11}	118.7	C_2-C_1-C_6-H_{10}	180.0
C_3-C_{14}	1.4473	C_2-C_3-C_4	119.5	H_7-C_1-C_6-C_5	180.0
C_4-C_5	1.3851	C_2-C_3-C_{14}	118.1	H_7-C_1-C_6-H_{10}	180.0
C_4-H_8	1.0842	C_4-C_3-C_{14}	122.3	C_1-C_2-C_3-C_4	0.0
C_5-C_6	1.4056	C_3-C_4-C_5	120.5	C_1-C_2-C_3-C_{14}	-180.0
C_5-H_9	1.0854	C_3-C_4-H_8	118.4	N_{11}-C_2-C_3-C_4	-180.0
C_6-H_{10}	1.0866	C_5-C_4-H_8	121.1	N_{11}-C_2-C_3-C_{14}	0.1
N_{11}-H_{12}	1.0133	C_4-C_5-C_6	119.6	C_1-C_2-N_{11}-H_{12}	-0.1
N_{11}-C_{13}	1.4046	C_4-C_5-H_9	120.3	C_1-C_2-N_{11}-C_{13}	180.0
C_{13}-C_{15}	1.4711	C_6-C_5-H_9	120.1	C_3-C_2-N_{11}-H_{12}	180.0
C_{13}-O_{16}	1.2232	C_1-C_6-C_5	121.0	C_3-C_2-N_{11}-C_{13}	-0.1
C_{14}-C_{15}	1.3992	C_1-C_6-H_{10}	119.2	C_2-C_3-C_4-C_5	-0.0
C_{14}-O_{17}	1.3262	C_5-C_6-H_{10}	119.8	C_2-C_3-C_4-H_8	-180.0
C_{15}-C_{19}	1.4686	C_2-N_{11}-H_{12}	119.8	C_{14}-C_3-C_4-C_5	180.0
O_{17}-H_{18}	1.0080	C_2-N_{11}-C_{13}	127.0	C_{14}-C_3-C_4-H_8	-0.1
H_{18}-O_{20}	1.5942	H_{12}-N_{11}-C_{13}	113.3	C_2-C_3-C_{14}-C_{15}	-0.0
C_{19}-O_{20}	1.2448	N_{11}-C_{13}-C_{15}	114.3	C_2-C_3-C_{14}-O_{17}	179.9
C_{19}-O_{21}	1.3288	N_{11}-C_{13}-O_{16}	118.4	C_4-C_3-C_{14}-C_{15}	-180.0
O_{21}-C_{22}	1.4500	C_{15}-C_{13}-O_{16}	127.3	C_4-C_3-C_{14}-O_{17}	-0.0
C_{22}-H_{23}	1.0921	C_3-C_{14}-C_{15}	121.6	C_3-C_4-C_5-C_6	-0.0
C_{22}-H_{24}	1.0923	C_3-C_{14}-O_{17}	115.5	C_3-C_4-C_5-H_9	-180.0
C_{22}-C_{25}	1.5209	C_{15}-C_{14}-O_{17}	123.0	H_8-C_4-C_5-C_6	180.0
C_{25}-H_{26}	1.0962	C_{13}-C_{15}-C_{14}	120.3	H_8-C_4-C_5-H_9	-0.0
C_{25}-H_{27}	1.0936	C_{13}-C_{15}-C_{19}	122.2	C_4-C_5-C_6-C_1	0.0
C_{25}-H_{28}	1.0946	C_{14}-C_{15}-C_{19}	117.5	C_4-C_5-C_6-H_{10}	-180.0
		C_{14}-O_{17}-H_{18}	108.2	H_9-C_5-C_6-C_1	-180.0
		C_{15}-C_{19}-O_{20}	122.3	H_9-C_5-C_6-H_{10}	-0.0
		C_{15}-C_{19}-O_{21}	116.0	C_2-N_{11}-C_{13}-C_{15}	-0.1
		O_{20}-C_{19}-O_{21}	121.8	C_2-N_{11}-C_{13}-O_{16}	179.9
		C_{19}-O_{21}-C_{22}	117.5	H_{12}-N_{11}-C_{13}-C_{15}	180.0

Bond length (Å)		Bond angles(˚)		Dihedral angles(˚)	
		O_{21}-C_{22}-H_{23}	103.5	H_{12}-N_{11}-C_{13}-O_{16}	-0.1
		O_{21}-C_{22}-H_{24}	109.1	N_{11}-C_{13}-C_{15}-C_{14}	0.2
		O_{21}-C_{22}-C_{25}	111.3	N_{11}-C_{13}-C_{15}-C_{19}	-179.8
		H_{23}-C_{22}-H_{24}	109.6	O_{16}-C_{13}-C_{15}-C_{14}	-179.9
		H_{22}-C_{23}-C_{25}	111.5	O_{16}-C_{13}-C_{15}-O_{19}	-179.8
		H_{24}-C_{22}-C_{25}	111.6	C_{3}-C_{14}-C_{15}-C_{13}	-0.2
		C_{22}-C_{25}-H_{26}	109.6	C_{3}-C_{14}-C_{15}-C_{19}	179.9
		C_{22}-C_{25}-H_{27}	110.8	O_{17}-C_{14}-C_{15}-C_{13}	180.0
		C_{22}-C_{25}-H_{28}	110.7	O_{17}-C_{14}-C_{15}-C_{19}	-0.0
		H_{26}-C_{25}-H_{27}	108.3	C_{3}-C_{14}-O_{17}-H_{18}	-179.8
		H_{26}-C_{25}-H_{28}	108.4	C_{15}-C_{14}-O_{17}-H_{18}	-0.0
		H_{27}-C_{25}-H_{28}	109.0	C_{13}-C_{15}-C_{19}-O_{20}	-179.8
				C_{13}-C_{15}-C_{19}-O_{21}	0.5
				C_{14}-C_{15}-C_{19}-O_{20}	0.1
				C_{14}-C_{15}-C_{19}-O_{21}	-178.6
				C_{15}-C_{19}-C_{21}-C_{22}	-179.8
				O_{20}-C_{19}-C_{21}-C_{22}	0.1
				C_{19}-C_{21}-C_{22}-H_{23}	-154.8
				C_{19}-C_{21}-C_{22}-H_{24}	-38.2
				C_{19}-C_{21}-C_{22}-C_{25}	85.3
				C_{21}-C_{22}-C_{25}-H_{26}	174.6
				C_{21}-C_{22}-C_{25}-H_{27}	-65.9
				C_{21}-C_{22}-C_{25}-H_{28}	55.2
				H_{23}-C_{22}-C_{25}-H_{26}	59.6
				H_{23}-C_{22}-C_{25}-H_{27}	179.1
				C_{23}-C_{22}-C_{25}-H_{28}	-59.9
				H_{24}-C_{22}-C_{25}-H_{26}	-63.2
				H_{24}-C_{22}-C_{25}-H_{27}	56.2
				H_{24}-C_{22}-C_{25}-H_{28}	177.3

Table 2. Calculated scaled wavenumbers, observed IR, Raman bands and vibrational assignments of the EHODQC compound.

B3LYP/6-311++G(d,p)			IR υ(cm^{-1})	Raman υ(cm^{-1})	Assignments
υ(cm^{-1})	IR_I	R_A			
3455	41.77	93.15	3458	-	υNH(100)
			3313	-	-
3111	5.33	113.33	3153	3141	υCH(98)
3090	16.16	237.70	3110	-	υCH(94)
3078	12.82	121.73	-	-	υCH(98)
3064	3.30	55.85	3060	3064	υCH(95)
3040	24.22	15.05	-	-	υCH_3(63), υCH_2(36)

B3LYP/6-311++G(d,p)			IR υ(cm^{-1})	Raman υ(cm^{-1})	Assignments
υ(cm^{-1})	IR_I	R_A			
3019	4.54	84.63	3033	-	$\upsilon CH_3(66)$, $\upsilon CH_2(34)$
3009	30.41	121.38	2990	-	$\upsilon CH_2(90)$
2980	22.91	104.21	-	2971	$\upsilon CH_2(99)$
2943	14.92	152.55	2940	2940	$\upsilon CH_3(100)$
2925	644.51	34.44	2930	2930	υOH(99)
1718	657.76	27.45	1752	1745	υC=O(68)
1632	157.87	131.63	1668	1669	$\upsilon C=O(56)$, $\upsilon C_{14}C_{15}(11)$
1618	258.72	108.04	1607	1603	$\upsilon Ph(41)$, $\upsilon C_{14}C_{15}(18)$
1586	98.00	35.45	-	-	$\upsilon Ph(53)$, $\upsilon C_{14}C_{15}(24)$
1557	197.35	58.52	1558	1556	$\upsilon C=C(45)$, υPh(20), δOH(15)
1484	44.68	35.14	1499	1503	υPh(39), δNH(33)
1478	8.34	6.13	1473	-	$\delta CH_3(82)$
1464	20.79	48.19	-	-	$\delta CH_2(40)$, υPh(43)
1459	4.98	10.49	-	-	$\delta CH_2(44)$, $\delta CH_3(22)$
1457	19.22	34.26	1447	1455	$\delta CH_3(62)$, $\delta CH_2(20)$
1408	223.12	60.84	-	-	$\upsilon C_{14}O_{17}(25)$, υPh(20),$\delta CH_2(11)$
1395	38.60	4.92	1392	-	δNH(39),δCH(21), υPh(25)
1386	15.27	5.06	-	-	$\delta CH_3(25)$, δNH(17),δCH(18)
1370	155.82	71.83	1370	-	$\delta CH_3(46)$,$\upsilon C_{15}C_{19}(11)$
1354	201.95	246.61	1348	1348	δOH(42), $\delta CH_3(20)$, $\upsilon C_{14}C_{15}(19)$
1336	135.32	41.89	-	-	υPh(74)
1293	135.42	13.15	1311	1305	$\delta CH_2(67)$, $\upsilon C_{19}O_{21}(12)$
1279	213.56	14.42	1273	-	υCOC(42), $\delta CH_2(13)$
1267	16.67	2.21	-	1271	δCH(55), υCN(43)
1229	77.81	11.83	1227	1230	δCH(55), υCO(44)
1226	47.35	71.46	-	1182	υCN(42), δCH(19)
1165	47.64	9.85	1167	1164	$\delta CH_2(19)$, $\delta CH_3(38)$
1155	6.42	8.81	-	-	δCH(52),$\delta CH_2(11)$
1143	25.99	14.55	-	-	δCH(50), υPh(19)
1096	21.07	6.22	1102	1107	δCH(69),υPh(12), υCO(11)

B3LYP/6-311++G(d,p)			IR υ(cm^{-1})	Raman υ(cm^{-1})	Assignments
υ(cm^{-1})	IR_I	R_A			
1085	62.74	5.34	-	1082	δCH_3(49),υCOC(38)
1067	89.67	5.91	-	-	υRing(52), δCH(20)
1023	7.96	21.72	1031	1033	υPh(59), δCH(22)
1001	32.07	8.56	997	1001	υCO(19), δCH(29), γCH(17)
950	0.02	0.03	941	944	γCH(88), δPh(10)
925	1.13	0.75	-	-	γCH(88)
897	3.17	2.89	907	-	δPh(40), δRing(21)
882	3.90	4.93	883	884	δPh(44),δCN(11)
876	98.09	0.72	864	866	γOH(97)
838	9.68	14.62	839	840	υCC(23),δCH_3(18)
834	0.47	3.83	-	-	γCH(79)
790	2.44	3.92	808	-	δCH_2(42), δCH_3(20)
757	0.24	0.53	757	757	γOH(19), γC=O(31), γRing(25)
748	9.24	5.70	-	-	δCH_2(42), δC=O(19), δCH_3(11)
745	71.92	3.50	-	-	γCH(62), γC=O(27)
730	8.47	1.49	-	-	γPh(56), γRing(21), γOH(11)
699	14.72	0.14	691	-	γC=O(47), τRing(36)
653	5.94	15.74	654	660	δPh(45), δRing(15)
648	0.08	1.69	-	-	γPh(44), γOH(39), γRing(12)
637	1.79	5.72	635	-	δC=O(28), δPh(20)
595	71.31	2.35	602	619	γNH(82)
589	22.18	1.31	-	-	δRing(28), δPh(17), δC=O(12)
527	2.41	12.38	532	540	δPh(52), δRing(18)
518	0.32	0.64	505	513	γPh(38), γRing(20)
458	24.22	2.01	-	-	δCO(34), δCH_3(11)
440	12.30	6.69	445	-	δC=C(28), δOH(14), δCH_2(13)
427	2.41	0.39	-	-	γPh(75)
409	5.90	1.18	410	409	δCO (31), δRing(10), δCO(10)
392	1.79	1.09	-	-	δCO(24), δCH2(19), δRing(12)
338	6.23	2.90	-	341	δCO(58), δC=O(25)

B3LYP/6-311++G(d,p)			IR υ(cm^{-1})	Raman υ(cm^{-1})	Assignments
υ(cm^{-1})	IR_I	R_A			
298	5.55	1.05	-	-	γCO(17), τCH_3(13)
276	1.36	1.24	-	-	τRing(25), γCO(17), τPh(17)
263	0.72	2.73	-	-	τRing(49),τPh(16)
247	0.52	1.70	-	-	τRing(45), γCO(35)
224	2.74	0.10	-	226	τCH_3(65), δCO(17)
166	0.04	1.98	-	-	τRing(49), γNH(14), τPh(12)
147	2.60	0.08	-	-	τCH_3(45), δCO(20)
104	0.43	0.82	-	104	τCO(34), τRing(24), τOH(17), γNH(10)
94	0.34	0.35	-	-	τRing(34), τC=O(25), τCH_3(23)
85	0.31	1.59	-	-	τRing(69), γNH(22)
52	0.53	1.34	-	-	τC=O41), τCH_2(18), τOH(12), δCH_2(10)
32	2.48	2.15	-	-	τRing(60), τC=O(52)

υ-stretching; δ-in-plane deformation; γ-out-of-plane deformation; τ-torsion

Ph-C_1-C_2-C_3-C_4-C_5-C_6; Ring-C_2-C_3-C_{14}-C_{15}-C_{13}-N_{11} .

Table 3 Values of Fukui functions considering Mulliken charges

Atom	q_j (N+1)	q_j(N-1)	q_j(N)	f_j^+	f_j^-	f_j^0	Δf(r)
C_1	-0.142293	-0.203788	-0.130935	-0.011358	0.072853	0.0307475	-0.084211
C_2	0.397044	0.337751	0.358690	0.038354	0.020939	0.0296465	0.017415
C_3	0.087898	0.073946	0.055177	0.032721	-0.018769	0.006976	0.05149
C_4	-0.157346	-0.225566	-0.140164	-0.017182	0.085402	0.03411	-0.102584
C_5	-0.089739	-0.136240	-0.132044	0.042305	0.004196	0.0232505	0.038109
C_6	-0.113064	-0.167402	-0.123269	0.010205	0.044133	0.027169	-0.033928

Atom	q_j (N+1)	q_j(N-1)	q_j(N)	f_j^+	f_j^-	f_j^0	Δf(r)
H_7	0.208702	0.070352	0.142708	0.065994	0.072356	0.069175	-0.006362
H_8	0.228807	0.097078	0.169244	0.059563	0.072166	0.0658645	-0.012603
H_9	0.226310	0.060882	0.131586	0.094724	0.070704	0.082714	0.02402
H_{10}	0.222168	0.059067	0.139777	0.082391	0.08071	0.0815505	0.001681
N_{11}	-0.733752	-0.777094	-0.808395	0.074643	-0.031301	0.021671	0.105944
H_{12}	0.389479	0.295208	0.333811	0.055668	0.038603	0.0471355	0.017065
C_{13}	0.620014	0.544074	0.465886	0.154128	-0.078188	0.03797	0.232316
C_{14}	0.352195	0.223663	0.203352	0.148843	-0.020311	0.064266	0.169154
C_{15}	-0.088565	-0.128033	0.030119	-0.118684	0.158152	0.019734	-0.276836
O_{16}	-0.364591	-0.561539	-0.400673	0.036082	0.160866	0.098474	-0.124784
O_{17}	-0.599466	-0.687947	-0.587260	-0.012206	0.100687	0.0442405	-0.112893
H_{18}	0.478373	0.427140	0.417089	0.061284	-0.010051	0.0256165	0.071335
C_{19}	0.684500	0.568837	0.492706	0.191794	-0.076131	0.0578315	0.267925
O_{20}	-0.543001	-0.647240	-0.517970	-0.025031	0.12927	0.0521195	-0.154301
O_{21}	-0.438560	-0.451449	-0.453291	0.014731	-0.001842	0.0064445	0.016573
C_{22}	-0.063963	-0.017939	-0.034400	-0.029563	-0.016461	-0.023012	-0.013102
H_{23}	0.186583	0.125269	0.168629	0.017954	0.04336	0.030657	-0.025406

Atom	q_j (N+1)	q_j(N-1)	q_j(N)	f_j^+	f_j^-	f_j^0	Δf(r)
H_{24}	0.190683	0.140152	0.166624	0.024059	0.026472	0.0252655	-0.002413
C_{25}	-0.471461	-0.45352	-0.421642	-0.049819	0.031878	0.0089705	-0.081697
H_{26}	0.178912	0.108153	0.141367	0.037545	0.033214	0.0353795	0.004331
H_{27}	0.178302	0.170806	0.165241	0.013061	-0.005565	0.003748	0.018626
H_{28}	0.175831	0.155378	0.168037	0.007794	0.012659	0.0102265	-0.004865

Table 4. NBO results showing the formation of Lewis and non-Lewis orbitals

Bond (A-B)	ED/Energy	EDA%	EDB%	NBO	S%	P%
$\sigma C_1–C_2$	1.97439	48.31	51.69	0.6950($SP^{1.96}$)C	33.77	66.23
-	-0.71723	-	-	+0.6122($SP^{1.72}$)C	36.76	63.24
σC_1-C_6	1.97929	50.48	49.52	0.7105($SP^{1.78}$)C	35.96	69.04
-	-0.71350	-	-	+0.7037($SP^{1.84}$)C	35.16	64.84
πC_1-C_6	1.70935	53.49	46.51	0.7314(SP^{1})C	0.00	100.0
-	-0.26927	-	-	+0.6820(SP^{1})C	0.00	100.0
σC_1-C_3	1.96604	49.94	50.06	0.7067($SP^{1.84}$)C	35.23	64.77
-	-0.71437	-	-	+0.7075($SP^{2.05}$)C	32.76	67.24
$\pi C_2–C_3$	1.59156	44.33	55.67	0.6658(SP^{1})C	0.00	100.0
-	-0.27151	-	-	+0.7461(SP^{1})C	0.00	100.0
σC_2-N_{11}	1.98678	39.25	60.75	0.6265($SP^{2.59}$)C	27.87	72.13
-	-0.83956	-	-	+0.7794($SP^{1.67}$)N	37.51	62.49
σC_3-C_4	1.97236	52.05	47.95	0.7215($SP^{1.83}$)C	35.31	64.69
-	-0.69983	-	-	+0.6924($SP^{1.98}$)C	33.53	66.47
σC_3-C_{14}	1.97295	50.58	49.42	0.7112($SP^{2.13}$)C	31.91	68.09
-	-0.70652	-	-	+0.7030($SP^{1.79}$)C	35.84	64.16
σC_4-C_5	1.98062	50.31	49.69	0.7093($SP^{1.79}$)C	35.79	64.21
-	-0.70799	-	-	+0.7049($SP^{1.84}$)C	35.18	64.82
πC_4-C_5	1.69226	47	53	0.6856(SP^{1})C	0.00	100.0
-	-0.26159	-	-	+0.7280(SP^{1})C	0.00	100.0
σC_5-C_6	1.98127	49.71	50.29	0.7050($SP^{1.92}$)C	34.20	65.80
-	-0.69646	-	-	+0.7092($SP^{1.86}$)C	34.94	65.06
σN_{11}-H_{12}	1.98561	72.84	27.16	0.8534($SP^{2.69}$)N	27.12	72.88
-	-0.67124	-	-	+0.5212(SP)H	100.0	0.00
σN_{11}-C_{13}	1.98905	63.27	36.73	0.7954($SP^{1.83}$)N	35.32	64.68
-	-0.80806	-	-	+0.6061($SP^{2.48}$)C	28.77	71.23
σC_{13}-C_{15}	1.97341	47.61	52.39	0.69($SP^{1.61}$)C	38.29	61.71
-	-0.69227	-	-	+0.7238($SP^{1.97}$)C	33.72	66.28
σC_{13}-O_{16}	1.99411	36.27	63.73	0.6023($SP^{2.07}$)C	32.62	67.38
-	-1.01611	-	-	+0.7983($SP^{1.77}$)O	36.11	63.89
πC_{13}-O_{16}	1.98363	31.62	68.38	0.5623(SP^{1})C	0.00	100.0
-	-0.34814	-	-	+0.8269(SP)O	0.00	100.0
σC_{14}-C_{15}	1.97636	49.54	50.46	0.7038($SP^{1.59}$)C	38.60	61.40
-	-0.74104	-	-	+0.7104($SP^{1.91}$)C	34.36	65.64
πC_{14}-C_{15}	1.70770	37.68	62.32	0.6138(SP^{1})C	0.00	100.0
-	-0.28315	-	-	+0.7894(SP^{1})c	0.00	100.0
σC_{14}-O_{17}	1.99376	34.22	65.78	0.5850($SP^{2.95}$)C	25.34	74.66

Bond (A-B)	ED/Energy	EDA%	EDB%	NBO	S%	P%
-	-0.93541	-	-	+0.8110($SP^{2.17}$)O	31.50	68.50
σC_{15}-C_{19}	1.97425	51.83	48.17	0.7199($SP^{2.13}$)C	31.91	68.09
-	-0.70917	-	-	+0.6941($SP^{1.46}$)C	40.68	59.32
σC_{19}-O_{20}	1.99633	34.79	65.21	0.5898($SP^{2.21}$)C	31.12	68.88
-	-1.01842	-	-	+0.8075($SP^{1.90}$)O	34.51	65.49
σC_{19}-O_{21}	1.99319	32.43	67.57	0.5695($SP^{2.56}$)C	28.12	71.88
-	-0.95104	-	-	+0.8220($SP^{2.06}$)O	32.69	67.31
σO_{21}-C_{22}	1.98739	69.97	30.03	0.8365($SP^{2.74}$)O	26.74	73.26
-	-0.77966	-	-	+0.5480($SP^{4.82}$)C	17.18	82.82
σC_{22}-C_{25}	1.99188	50.38	49.62	0.7098($SP^{2.35}$)C	29.83	70.17
-	-0.61798	-	-	+0.7044($SP^{2.73}$)C	26.80	73.20
n $_1N_{11}$	1.63732	-	-	SP^1	0.00	100.0
-	-0.27342	-	-	-	-	-
n_1O_{16}	1.97777	-	-	$SP^{0.57}$	63.86	36.14
-	-0.67847	-	-	-	-	-
n_2O_{16}	1.86676	-	-	$SP^{99.99}$	0.05	99.95
-	-0.23464	-	-	-	-	-
n_1O_{17}	1.97148	-	-	$SP^{1.47}$	40.54	59.46
-	-0.56174	-	-	-	-	-
n_2O_{17}	1.77071	-	-	SP^1	0.00	100.0
-	-0.31867	-	-	-	-	-
n_3O_{17}	1.61933	-	-	$SP^{2.58}$	27.96	72.04
-	-0.53432	-	-	-	-	-
n_1O_20	1.95846	-	-	$SP^{0.71}$	58.42	41.58
-	-0.67554	-	-	-	-	-
n_2O_{20}	1.83232	-	-	$SP^{13.11}$	7.09	92.91
-	-0.34222	-	-	-	-	-
n_3O_{20}	1.56926	-	-	$SP^{1.00}$	0.00	100.0
-	-0.27482	-	-	-	-	-
n_1O_{21}	1.96237	-	-	$SP^{1.47}$	40.56	59.44
-	-0.54974	-	-	-	-	-
n_2O_{21}	1.75646	-	-	$SP^{1.00}$	0.00	100.0
-	-0.31862	-	-	-	-	-

Table 5. Second-order perturbation theory analysis of Fock matrix in NBO basis corresponding to the intra molecular bonds of the title compound

Donor(i)	Type	ED/e	Acceptor(j)	Type	ED/e	E(2)[a]	E(j)-E(i)[b]	F(i,j)[c]
C_1-C_2	σ	1.97439	C_1-C_6	σ*	0.01336	2.46	1.27	0.050
	σ	-	C_2 -C_3	σ*	0.02906	4.30	1.24	0.065
	σ	-	C_2 -N_{11}	σ*	0.02831	1.72	1.14	0.039
	σ	-	C_3 -C_{14}	σ*	0.03163	2.58	1.20	0.050
	σ	-	N_{11}-C_{13}	σ*	0.08085	2.80	1.10	0.050
C_1-C_6	σ	1.97929	C_1-C_2	σ*	0.02047	2.84	1.24	0.053
	σ	-	C_2-N_{11}	σ*	0.02831	4.23	1.13	0.062
	σ	-	C_5-C_6	σ*	0.01589	2.33	1.24	0.048
C_1-C_6	π	1.70935	C_2-C_3	π*	0.45862	22.40	0.27	0.023
	π	-	C_4-C_5	π*	0.27624	15.19	0.29	0.059
C_2-C_3	σ	1.96604	C_1-C_2	σ*	0.02047	3.68	1.24	0.060
	σ	-	C_2-N_{11}	σ*	0.02831	1.42	1.13	0.036
	σ	-	C_3-C_4	σ*	0.02077	3.71	1.25	0.061
	σ	-	C_3-C_{14}	σ*	0.03163	2.64	1.19	0.050
	σ	-	C_{14}-O_{17}	σ*	0.01839	2.53	1.03	0.046

Donor(i)	Type	ED/e	Acceptor(j)	Type	ED/e	E(2)[a]	E(j)-E(i)[b]	F(i,j)[c]
C_2-C_3	π	1.59156	C_1-C_6	π*	0.30313	14.47	0.28	0.058
	π	-	C_2 -C_3	π*	0.45862	1.67	0.27	0.019
	π	-	C_4 -C_5	π*	0.27624	19.96	0.29	0.070
	π	-	C_{14}-C_{15}	π*	0.35631	24.02	0.26	0.070
C_2-N_{11}	σ	1.98678	C_1-C_2	σ*	0.02047	1.76	1.36	0.044
	σ	-	C_1-C_6	σ*	0.01336	1.07	1.39	0.034
	σ	-	C_2-C_3	σ*	0.02906	1.69	1.36	0.043
	σ	-	C $_3$-C_4	σ*	0.02077	1.80	1.37	0.044
	σ	-	N_{11}-C_{13}	σ*	0.08085	1.14	1.22	0.034
	σ	-	C_{13}-O_{16}	σ*	0.00890	1.62	1.35	0.042
C_3-C_4	σ	1.97236	C_2-C_3	σ*	0.02906	4.29	1.23	0.065
	σ	-	C $_2$-N_{11}	σ*	0.02831	3.13	1.12	0.053
	σ	-	C $_3$-C_{14}	σ*	0.03163	`3.35	1.18	0.056
	σ	-	C $_4$-C_5	σ*	0.01359	2.39	1.26	0.049
	σ	-	C_{14}-C_{15}	σ*	0.02917	1.91	1.23	0.043
C_3-C_{14}	σ	1.97295	C_1-C_2	σ*	0.02047	2.45	1.23	0.049
	σ	-	C $_2$-C_3	σ*	0.02906	2.64	1.23	0.051
	σ	-	C $_3$-C_4	σ*	0.02077	3.37	1.24	0.058
	σ	-	C $_4$-C_5	σ*	0.01359	1.43	1.27	0.038
	σ	-	C $_{14}$-C_{15}	σ*	0.02917	3.16	1.23	0.056
	σ	-	C $_{15}$-C_{19}	σ*	0.04477	2.66	1.15	0.050
C_4-C_5	σ	1.98062	C $_3$-C_4	σ*	0.02077	2.81	1.24	0.053
	σ	-	C $_3$-C_{14}	σ*	0.03163	3.43	1.19	0.057
	σ	-	C $_5$-C_6	σ*	0.01589	2.32	1.24	0.048
C_4-C_5	π	1.69226	C_1-C_6	π*	0.30313	22.66	0.27	0.070
	π	-	C $_2$-C_3	π*	0.45862	16.56	0.26	0.061
C_5-C_6	σ	1.98127	C_1-C_6	σ*	0.01336	2.41	1.25	0.049
	σ	-	C_4 -C_5	σ*	0.01359	2.38	1.26	0.049
N_{11}-C_{13}	σ	1.98905	C_1-C_2	σ*	0.02047	2.38	1.33	0.050
	σ	-	C_2-N_{11}	σ*	0.02831	1.78	1.23	0.042
	σ	-	C_{15}-C_{19}	σ*	0.04477	2.11	1.25	0.046
C_{13}-C_{15}	σ	-	C_{13}-O_{16}	σ*	0.00890	1.09	1.20	0.032
	σ	-	C_{14} -C_{15}	σ*	0.02917	3.37	1.22	0.057
	σ	-	C_{14}-O_{17}	σ*	0.01839	3.79	1.01	0.055
	σ	-	C_{15}-C_{19}	σ*	0.04477	1.75	1.13	0.040
	σ	-	C_{19}-O_{20}	σ*	0.02472	2.13	1.12	0.044
C_{13}-O_{16}	σ	1.99411	C_2-N_{11}	σ*	0.02831	1.83	1.43	0.046
	σ	-	C_{13}-C_{15}	σ*	0.06141	1.86	1.46	0.047
	σ	-	C_{14}-C_{15}	σ*	0.02917	1.08	1.54	0.037
	π	1.98363	C_{13}-C_{16}	π*	0.34926	1.62	0.34	0.023
	π	-	C_{14}-C_{15}	π*	0.35631	4.71	0.34	0.023
C_{14}-C_{15}	σ	1.97636	C $_3$-C_4	σ*	0.02077	2.35	1.27	0.049
	σ	-	C $_3$-C_{14}	σ*	0.03163	3.29	1.22	0.057
	σ	-	C_{13}-C_{15}	σ*	0.06141	2.35	1.18	0.048
	σ	-	C_{13}-O_{16}	σ*	0.00890	2.25	1.25	0.048
	σ	-	C_{15}-C_{19}	σ*	0.04477	2.50	1.18	0.049
	σ	-	C_{19}-O_{21}	σ*	0.07395	2.64	1.07	0.048
C_{14}-C_{15}	π	1.70770	C $_2$-C_3	π*	0.45862	9.28	0.28	0.048
	π	-	C_{13}-O_{16}	π*	0.34926	28.87	0.27	0.080
	π	-	C_{14}-C_{15}	π*	0.35631	6.31	0.27	0.037
C_{14}-O_{17}	σ	1.99376	C_2-C_3	σ*	0.02906	1.70	1.46	0.045
	σ	-	C_3-C_{14}	σ*	0.03163	0.76	1.41	0.029
	σ	-	C_{13}-C_{15}	σ*	0.06141	1.69	1.38	0.044
	σ	-	C_{14}-C_{15}	σ*	0.02917	1.02	1.46	0.035
C_{15}-C_{19}	σ	1.97425	C_3-C_{14}	σ*	0.03163	2.91	1.19	0.053
	σ	-	N_{11}-C_{13}	σ*	0.08085	1.64	1.09	0.038
	σ	-	C_{13}-C_{15}	σ*	0.06141	2.42	1.15	0.048

Donor(i)	Type	ED/e	Acceptor(j)	Type	ED/e	E(2)[a]	E(j)-E(i)[b]	F(i,j)[c]
	σ	-	C_{14}-C_{15}	σ*	0.02917	2.38	1.23	0.048
	σ	-	C_{19}-O_{20}	σ*	0.02472	0.54	1.14	0.022
	σ	-	C_{19}-O_{21}	σ*	0.07395	0.51	1.04	0.021
	σ	-	O_{21}-C_{22}	σ*	0.03753	3.39	0.90	0.049
C_{19}-O_{20}	σ	1.99633	C_{13}-C_{15}	σ*	0.06141	1.47	1.46	0.042
	σ	-	C_{15}-C_{19}	σ*	0.04477	1.24	1.46	0.038
C_{19}-O_{21}	σ	1.99319	C_{14}-C_{15}	σ*	0.02917	1.37	1.48	0.040
O_{21}-C_{22}	σ	1.98739	C_{15}-C_{19}	σ*	0.04477	3.22	1.22	0.056
	σ	-	C_{19}-O_{20}	σ*	0.02472	0.54	1.21	0.023
C_{22}-C_{25}	σ	1.99188	C_{19}-O_{21}	σ*	0.07395	0.56	0.95	0.021
LP N_{11}	σ	1.63732	C_2-C_3	π*	0.45862	45.39	0.27	0.102
	σ	-	C_{13}-O_{16}	π*	0.00890	53.53	0.26	0.106
LPO_{16}	σ	1.97777	N_{11}-C_{13}	σ*	0.08085	1.64	1.06	0.038
	σ	-	C_{13}-C_{15}	σ*	0.06141	2.72	1.12	0.050
	π	1.86676	C_2-N_{11}	σ*	0.02831	0.60	0.65.	0.180
	π	-	N_{11}-C_{13}	σ*	0.08085	25.06	0.61	0.112
	π	-	C_{13}-C_{15}	σ*	0.06141	18.29	0.68	0.101
LPO_{17}	σ	1.97148	C_3-C_{14}	σ*	0.03163	0.76	1.04	0.025
	σ	-	C_{14}-C_{15}	σ*	0.02910	7.34	1.09	0.080
LPO_{17}	π	1.77071	C_{14}-C_{15}	π*	0.35631	45.86	0.31	0.109
	n	1.61933	C_3-C_{14}	σ*	0.03163	5.05	1.01	0.070
	n	-	C_{14}-C_{15}	σ*	0.02910	0.77	1.06	0.028
LPO_{20}	σ	1.95846	C_{15}-C_{19}	σ*	0.04477	5.31	1.12	0.069
	σ	-	O_{21}-C_{22}	σ*	0.03753	0.58	0.86	0.020
	π	1.83232	C_{15}-C_{19}	σ*	0.04477	6.88	0.78	0.068
	π	-	C_{19}-O_{21}	σ*	0.07395	23.37	0.67	0.110
LPO_{21}	σ	1.96237	C_{15}-C_{19}	σ*	0.04477	0.63	0.99	0.022
	σ	-	C_{19}-O_{20}	σ*	0.02472	8.54	0.98	0.082
	π	1.75646	C_{22}-C_{25}	σ*	0.01138	4.41	0.68	0.052

Table 6. Binding affinity values for the nine poses predicted by AutoDock Vina

Mode	Affinity (kcal/mol)	Distance from best mode (Å)	
-	-	RMSD l.b.	RMSD u.b.
1	-7.1	0.000	0.000
2	-7.0	1.362	2.528
3	-6.7	2.849	3.370
4	-6.7	1.895	2.239
5	-6.7	1.833	2.067
6	-6.6	12.879	14.393
7	-6.6	2.474	3.478
8	-6.5	2.127	5.533
9	-6.5	2.211	5.710

2. 6 References

[1] M. Fujita, K. Chiba, Y. Tominaga, K. Hino, 7-(2-aminoethyl-1-azetidinyl)-4-oxoquinoline-3-carboxylic acids as potent antibacterial agents, design, synthesis and antibacterial activity, Chem. Pharm. Bull. 46 (1998) 787-796.

[2] M. Kidwai, K. R. Bhushan, P. Sapra, R. K. Saxena, R. Gupta, Alumina supported synthesis of antibacterial quinolines using microwaves, Bioorg. Med. Chem. 8 (2000) 69-72.

[3] R. Gupta, A. K. Gupta, S. Paul, P. L. Kachroo, Synthesis and biological activities of some 2-chloro-6/8-substituted-3-(3-alkyl/aryl-5,6-dihydro-s-triazolo[3,4-b][1,3,4]thiadiazol-6-yl)quinolines, Ind. J. Chem. 37B (1998) 1211-1213.

[4] R. Gupta, A. K. Gupta, S. Paul, Microwave assisted synthesis and biological activities of some 7/9-substituted-4-(3-alkyl/aryl-5,6-dihydro-s-triazolo[3,4-b][1,3,4]thiadiazol-6-yl)-tetrazolo[1,5-a]quinolines, Ind. J. Chem. 39B (2000) 847-852.

[5] J. Kos, I. Zadrazilova, E. Nevin, M. Soral, T. Gonec, P. Kollar, M. Oravec, A. Coffey, J. O'Mahony, T. Liptaj, K. Kralova, J. Jampilek, Ring-substituted 8-hydroxyquinoline-2-carboxanilides as potential anti-mycobacterial agents. Bioorg. Med. Chem. 23 (2015) 4188-4196.

[6] J. Zeigler, R. Linck, D. W. Wright, Heme aggregation inhibitors, anti-malarial drugs targeting an essential biomineralization process, Curr. Med. Chem. 8 (2001) 171-189.

[7] P. M. S. Chauhan, S. K. Srivastava, Present trends and future strategy in chemotherapy of malaria, Curr. Med. Chem. 8 (2001) 1535-1542.

[8] O. Famin, H. Krugliak, H. Ginsberg, Kinetics of inhibition of glutathione mediated degradation of ferriprotoporphyrin IX by anti-malarial drugs, Biochem. Pharmacol. 58 (1999) 59-68.

[9] F. M. D. Ismail, M. J. Dascombe, P. Carr, S. A. M. Meretter, P. Rouault, Novel aryl-bis-quinolines with anti-malarial activity in vivo, J. Pharm. Pharmacol. 50 (1998) 483-492.

[10] M. Go, T. Ngaam, A. L. Tan, K.Kuaha, P. Wilairat, Structure activity relationships of some indolo[3,2-c]quinolines with anti-malarial activity, Eur. J. Pharm. Sci. 6 (1998) 19-26.

[11] A. Dorn, S. R. Vippagunta, H. Mato;e. C. Jaquet, J. L. Vennerstrom, R. G. Ridley, An assessment of drug haematin binding as a mechanism for inhibition of haematin polymerisation by quinoline anti-malarials, Biochem. Pharmacol. 15 (1998) 727-736.

[12] S. Tiwari, P. M. S. Chauhan, A. P. Bhaduri, N. Fatima, R. K. Chatterjee, Syntheses and anti-filarial profile of 7-chloro-4-(substituted amino) quinolines, a new class of anti-filarial agents, Bioorg. Med. Chem. Lett. 10 (2000) 1409-1412.

[13] Y. Kuroda, M. Ogawa, H. Nasu, M. Terashima, M. Kasahara, Y. Kiyama, M. Wakita, Y. Fujiwara, N. Fujii, T. Nakagawa, Locations of local anestheticdibucaine in model membranes and the interaction beweendibucaine and a Na+ channel inactivation gate peptide as studied by 2H- and1H-NMR spectroscopies, Biophys. J. 71 (1996) 1191-1207

[14] J. Jampilek, M. Dolezal, V. Opletalova, J. Hartl, 5-Lipoxygenase, leukotrienes biosynthesis and potential antileukotrienic agents. Curr. Med. Chem. 13 (2006) 117-129.

[15] Z. F. Chen, P. Zhang, R. G.Xiong, D. J. Liu, X. Z. You, The first one dimensional metal organic coordination polymer with 4-quinoline carboxylate as building block [Cd(μ_2-H_2O)(4-quinolinecarboxylato-O,O)$_2$], Inorg. Chem. Commun. 5 (2002) 35-37.

[16] M. L. Martinez, W. C. Cooper, P. T. Chou, A novel excited state intramolecular proton transfer molecule, 10-hydroxybenzo[h]quinoline, Chem. Phys. Lett. 193 (1992) 151-154.

[17] E. L. Roberts, P. T. Chou, T. A. Alexander, R. A. Agbaria, I. M. Warner, Effects of organized media on the excited state intramolecular proton transfer in 10-hydroxybenzo[h]quinoline, J. Phys. Chem. 99 (1995) 5431-5437.

[18] K. Mekouar, J. -F.Mouscadet, D. Desmaële, F. Subra, H. Leh, D. Savoure, C. Auclair, J.d'Angelo, Styrylquinoline derivatives, a new class of potent HIV-1 integrase inhibitors that block HIV-1 replication in CEM cells, J. Med. Chem. 41 (1998) 2846-2857.

[19] R. Musiol, Quinoline-based HIV integrase inhibitors, Curr. Pharm. Des. 19 (2013) 1835-1849.

[20] J. F. Mouscadet, D. Desmaële, Chemistry and structure activity relationship of the styrylquinoline-type HIV integrase inhibitors, Molecules 15 (2010) 3048-3078.

[21] M. Serda, D. S. Kalinowski, A. Mrozek-Wilczkiewicz, R. Musiol, A. Szurko, A. Ratuszna, et al., Synthesis and Characterization of Quinoline-Based Thiosemicarbazones and Correlation of Cellular Iron-Binding Efficacy to Anti-Tumor Efficacy, Bioorg. Med. Chem. Lett. 22 (2012) 5527-5531.

[22] M. Serda, D. S. Kalinowski, N. Rasko, E. Potuckova, A. Mrozek-Wilczkiewicz, R. Musiol, et al., Exploring the anti-cancer Activity of Novel Thiosemicarbazones

Generated through the Combination of Retro-Fragments: Dissection of Critical Structure-Activity Relationships., PLoS One 9 (2014) e110291.

[23] A. Mrozek-Wilczkiewicz, D. S. Kalinowski, R. Musiol, J. Finster, A. Szurko, K. Serafin, et al., Investigating the anti-proliferative activity of styrylazanaphthalenes and azanaphthalenediones., Bioorg. Med. Chem. 18 (2010) 2664-71.

[24] J. Polanski, A. Kurczyk, A. Bak, R. Musiol, Privileged structures - dream or reality: preferential organization of azanaphthalenescaffold, Curr. Med. Chem. 19 (2012) 1921-45.

[25] R. Musiol, M. Serda, S. Hensel-Bielowka, J. Polanski, Quinoline-based antifungals, Curr. Med. Chem. 17 (2010) 1960-73.

[26] S. Armaković, S. J. Armaković, J. P. Šetrajčić, I. J. Šetrajčić, Active components of frequently used β-blockers from the aspect of computational study, J. Mol. Model.18 (2012) 4491-4501.

[27] S. J. Armaković, S. Armaković, N. L. Finčur, F. Šibul, D. Vione, J. P. Šetrajčić, B. Abramović, Influence of electron acceptors on the kinetics of metoprolol photocatalytic degradation in TiO 2 suspension, A combined experimental and theoretical study, RSC Advances, 5 (2015) 54589-54604.

[28] M. Blessy, R. D. Patel, P. N. Prajapati, Y. Agrawal, Development of forced degradation and stability indicating studies of drugs-A review, J. Pharm. Anal. 4 (2014) 159-165.

[29] B. Abramović, S. Kler, D. Šojić, M. Laušević, T. Radović, D. Vione, Photocatalytic degradation of metoprolol tartrate in suspensions of two TiO 2-based photocatalysts with different surface area.Identification of intermediates and proposal of degradation pathways, J. Hazard.Mater.198 (2011) 123-132.

[30] J. Molnar, J. Agbaba, B. Dalmacija, M. Klašnja, M. Watson, M. Kragulj, Effects of ozonation and catalytic ozonation on the removal of natural organic matter from groundwater, J. Environ. Engineering, 138 (2011) 804-808.

[31] J. J. Molnar, J. R. Agbaba, B. D. Dalmacija, M. T. Klašnja, M. B. Dalmacija, M. M. Kragulj, A comparative study of the effects of ozonation and TiO 2-catalyzed ozonation on the selected chlorine disinfection by-product precursor content and structure, Sci. Total Environ. 425 (2012) 169-175.

[32] D. V. Šojić, D. Z. Orčić, D. D. Četojević-Simin, N. D. Banić, B. F. Abramović, Efficient removal of sulcotrione and its formulated compound Tangenta® in aqueous TiO 2 suspension: Stability, photoproducts assessment and toxicity, Chemosphere, 138 (2015) 988-994.

[33] D. V. Šojić, D. Z. Orčić, D. D. Četojević-Simin, V. N. Despotović, B. F. Abramović, Kinetics and the mechanism of the photocatalytic degradation of mesotrione in aqueous suspension and toxicity of its degradation mixtures, J. Mol. Catalysis A: Chem. 392 (2014) 67-75.

[34] D. D. Četojević-Simin, S. J. Armaković, D. V. Šojić, B. F. Abramović, Toxicity assessment of metoprolol and its photodegradation mixtures obtained by using different type of TiO 2 catalysts in the mammalian cell lines, Sci. Total Environ. 463 (2013) 968-974.

[35] P. Lienard, J. Gavartin, G. Boccardi, M. Meunier, Predicting drug substancesautoxidation, Pharm. Res. 32 (2015) 300-310.

[36] G. L. de Souza, L. M. de Oliveira, R. G. Vicari, A. Brown, A DFT investigation on the structural and antioxidant properties of new isolated interglycosidic O-(1→ 3) linkage flavonols, J. Mol. Model. 22 (2016) 1-9.

[37] Z. Sroka, B. Żbikowska, J. Hładyszowski, The anti-radical activity of some selected flavones and flavonols, Experimental and quantum mechanical study, J. Mol. Model. 21 (2015) 1-11.

[38] H. Djeradi, A. Rahmouni, A. Cheriti, Anti-oxidant activity of flavonoids: a QSAR modeling using Fukui indices descriptors, J. Mol. Model. 20 (2014) 1-9.

[39] J. Jampilek, R. Musiol, M. Pesko, K. Kralova, M. Vejsova, J. Carroll, A. Coffey, J. Finster, D. Tabak, H. Niedbala, V. Kozik, J. Polanski, J. Csollei, J. Dohnal, Ring-substituted 4-hydroxy-1*H*-quinolin-2-ones: Preparation and biological activity, Molecules 14(3) (2009) 1145-1159.

[40] Gaussian 09, Revision B.01, M. J. Frisch, G. W. Trucks, H. B. Schlegel, G. E. Scuseria, M. A. Robb, J. R. Cheeseman, G. Scalmani, V. Barone, B. Mennucci, G. A. Petersson, H. Nakatsuji, M. Caricato, X. Li, H. P. Hratchian, A. F. Izmaylov, J. Bloino, G. Zheng, J. L. Sonnenberg, M. Hada, M. Ehara, K. Toyota, R. Fukuda, J. Hasegawa, M. Ishida, T. Nakajima, Y. Honda, O. Kitao, H. Nakai, T. Vreven, J. A. Montgomery, Jr., J. E. Peralta, F.Ogliaro, M. Bearpark, J. J. Heyd, E. Brothers, K. N. Kudin, V. N. Staroverov, T. Keith, R. Kobayashi, J. Normand, K. Raghavachari, A. Rendell, J. C. Burant, S. S. Iyengar, J. Tomasi, M. Cossi, N. Rega, J. M. Millam, M. Klene, J. E. Knox, J. B. Cross, V. Bakken, C. Adamo, J. Jaramillo, R. Gomperts, R.E. Stratmann, O. Yazyev, A. J. Austin, R. Cammi, C. Pomelli, J. W. Ochterski, R. L. Martin, K. Morokuma, V. G. Zakrzewski, G. A. Voth, P. Salvador, J. J. Dannenberg, S. Dapprich,

A. D. Daniels, O. Farkas, J. B. Foresman, J. V. Ortiz, J. Cioslowski, and D. J. Fox, Gaussian, Inc., Wallingford CT, 2010.

[41] J. B. Foresman, in: E. Frisch (Ed.), Exploring Chemistry with Electronic Structure Methods: A Guide to Using Gaussian, Gaussian Inc., Pittsburg, PA, 1996.

[42] Gauss View, Version 5, R. Dennington, T. Keith, J. Millam, SemichemInc.,Shawnee Mission, KS, 2009.

[43] J. M. L. Martin, C. Van Alsenoy, GAR2PED, A Program to Obtain a PotentialEnergy Distribution from a Gaussian Archive Record, University of Antwerp,Belgium, 2007.

[44] A. D. Bochevarov, E. Harder, T. F. Hughes, J. R. Greenwood, D. A. Braden, D. M. Philipp, D. Rinaldo, M. D. Halls, J. Zhang, R. A. Friesner, Jaguar: A high-performance quantum chemistry software program with strengths in life and materials sciences, Int. J. Quantum Chem. 113 (2013) 2110-2142.

[45] D. Shivakumar, J. Williams, Y. Wu, W. Damm, J. Shelley, W. Sherman, Prediction of absolute solvation free energies using molecular dynamics free energy perturbation and the OPLS force field, J. Chem. Theory and Comput. 6 (2010) 1509-1519.

[46] Z. Guo, U. Mohanty, J. Noehre, T. K. Sawyer, W. Sherman, G. Krilov, Probing the α-Helical Structural Stability of Stapled p53 Peptides: Molecular Dynamics Simulations and Analysis, Chem. Biol. Drug Design, 75 (2010) 348-359.

[47] K. J. Bowers, E. Chow, H. Xu, R. O. Dror, M. P. Eastwood, B. A. Gregersen, J. L. Klepeis, I. Kolossvary, M. A. Moraes, F. D. Sacerdoti, Scalable algorithms for molecular dynamics simulations on commodity clusters. in SC 2006 Conference, Proceedings of the ACM/IEEE. 2006. IEEE.

[48] I. Fabijanić, C. J. Brala, V. Pilepić, The DFT local reactivity descriptors of α-tocopherol, J. Mol. Model. 21 (2015) 1-7.

[49] A. D. Becke, Density-functional thermochemistry. III. The role of exact exchange, J. Chem. Phys. 98 (1993) 5648-5652.

[50] J. L. Banks, H. S. Beard, Y. Cao, A. E. Cho, W. Damm, R. Farid, A. K. Felts, T. A. Halgren, D. T. Mainz, J. R. Maple, Integrated modeling program, applied chemical theory (IMPACT), J. Comput. Chem. 26 (2005) 1752-1780.

[51] H. J. Berendsen, J. P. Postma, W. F. van Gunsteren, J. Hermans, Interaction models for water in relation to protein hydration, in Intermolecular forces, , Springer (1981) 331-342.

[52] A. Otero-de-la-Roza, E. R. Johnson, J. Contreras-García, Revealing non-covalent interactions in solids: NCI plots revisited, Phys. Chem. Chem. Phys. 14 (2012) 12165-12172.

[53] E. R. Johnson, E. R., S. Keinan, P. Mori-Sanchez, J. Contreras-Garcia, A.J. Cohen, W. Yang, Revealing noncovalent interactions, J. Am. Chem. Soc. 132 (2010) 6498-6506.

[54] Schrödinger Release 2015-4: Maestro, version 10.4, Schrödinger, LLC, New York, NY, 2015.

[55] J. Chowdhury, M. Ghosh, T. N. Misra, Surface enhanced Raman scattering of 2,2-biquinoline adsorbed on colloidal silver particles, Spectrochim. Acta 56 (2000) 2107-2115.

[56] G. Varsanyi, Assignments of Vibrational Spectra of Seven Hundred Benzene Derivatives, Wiley, New York 1974.

[57] N. P. G. Roeges, A Guide to the Complete Interpretation of the Infrared spectra of Organic Compounds, Wiley, New York 1994.

[58] R. T. Ulahannan, C. Y.Panicker, H. T. Varghese, C. VanAlsenoy, R. Musiol, J. Jampilek, P. L. Anto, Spectroscopic (FT-IR, FT-Raman) investigations and quantum chemical calculation sof 4-hydroxy-2-oxo-1,2-dihydroquinoline-7-carboxylic acid, Spectrochim. Acta 121 (2014) 404-414.

[59] N. B. Colthup, L. H. Daly, S. E. Wiberly, Introduction to IR and Raman Spectroscopy, Academic Press, New York,1990.

[60] R. M. Silverstein, F. X. Webster, Spectrometric Identification of Organic Compounds, ED. 6, John Wiley, Asia, 2003.

[61] C. Y. Panicker, H. T. Varghese, A. John, D. Philip, H. I. S. Nogueira, Vibrational spectra of melamine diborate, $C_3N_6H_62H_3BO_3$, Spectrochim. Acta 58 (2002) 1545-1551.

[62] Y. S. Mary, P. J. Jojo, C. Van Alsenoy, M. Kaur, M. S. Siddegowda, H. S. Yathirajan, H. I. S. Nogueira, S. M. A. Cruz, Vibrational spectroscopic studies (FT-IR, FT-Raman, SERS) and quantum chemical calculations on cyclobenzaprinium salicylate, Spectrochim. Acta 120 (2014) 340-350.

[63] L. J. Bellamy, The IR spectra of Complex Molecules,John Wiley and Sons, New York 1975.

[64] S. H. R. Sebastian, M. A. Al-Alshaikh, A. A. El-Emam, C. Y. Panicker, J. Zitko, M. Dolezal, C. Van Alsenoy, Spectroscopic quantum chemical studies, Fukui functions,

in vitro antiviral activity and molecular docking of 5-chloro-N-(3-nitrophenyl)pyrazine-2-carboxamide, J. Mol. Struct. 1119 (2016) 188-199.

[65] V. V. Menon, E. Foto, Y. S. Mary, E. Karatas, C. Y. Panicker, G. Yalcin, S. Armakovic, S. J. Armakovic, C. Van Alsenoy, I. Yildiz, Vibrational spectroscopic analysis, molecular dynamics simulations and molecular docking study of 5-nitro-2-phenoxymethyl benzimidazole, J. Mol. Struct. 1129 (2017) 86-97.

[66] G. Socrates, Infrared Characteristic Group Frequencies, John Wiley and Sons, NewYork,1981.

[67] C. Y. Panicker, K. R. Ambujakshan, H. T. Varghese, S. Mathew, S. Ganguli, A. K. Nanda, C. Van Alsenoy, FT-IR, FT-Raman and DFT calculations of 3-{[(4-fluorophenyl)methylene]amino}-2-phenylquinazolin-4(3H)-one, J. Raman. Spectrosc. 40 (2009) 527-536.

[68] F. J. Luque, J. M. Lopez, M. Orozco, Perspective on electrostatic interactions of a solute with a continuum, a direct utilization of ab initio molecular potentials for the prevision of solvent effects, Theor. Chem. Acc. 103 (2000) 343–345.

[69] P. Politzer, J. S. Murray, in: D. L. Beveridge, R. Lavery, (Eds.), Theoretical Biochemistry and Molecular Biophysics, Springer, Berlin, 1991.

[70] J. S. Murray, J. M. Seminario, P. Politzer, P. Sjoberg, Average local ionization energies computed on the surfaces of some strained molecules, Int. J. Quantum Chem. 38 (1990) 645-653.

[71] P. Politzer, F. Abu-Awwad, J. S. Murray, Comparison of density functional and Hartree–Fock average local ionization energies on molecular surfaces, Int. J. Quantum Chem. 69 (1998) 607-613.

[72] F. A. Bulat, A. Toro-Labbé, T. Brinck, J. S. Murray, P. Politzer, Quantitative analysis of molecular surfaces: areas, volumes, electrostatic potentials and average local ionization energies, J. Mol. Model. 16 (2010) 1679-1691.

[73] P. Politzer, J. S. Murray, F. A. Bulat, Average local ionization energy: a review, J. Mol. Model. 16 (2010) 1731-1742.

[74] A. Toro-Labbé, P. Jaque, J.S. Murray, P. Politzer, Connection between the average local ionization energy and the Fukui function, Chem. Phys. Lett. 407 (2005) 143-146.

[75] R. G. Parr, Density functional theory of atoms and molecules, in Horizons of Quantum Chemistry, 1980, Springer. p. 5-15.

[76] A. Michalak, F. De Proft, P. Geerlings, R. Nalewajski, Fukui functions from the relaxed Kohn-Sham orbitals, J. Phys. Chem. A103 (1999) 762-771.

[77] R. G. Parr, W.Yang, Functional Theory of Atoms and Molecules, OxfordUniversity Press, New York 1989.

[78] P. W. Ayers, R. G. Parr, Variational principles for describing chemical reactions, the Fukui function and chemical hardness revisited, J. Am. Chem. Soc. 122 (2000) 2010–2018.

[79] R. G. Parr, W. J. Yang, Density functional approach to the frontier electron theory of chemical reactivity, J. Am. Chem. Soc. 106 (1984) 4049-4050.

[80] P. K. Chattaraj, B. Maiti, U. Sarkar,Philicity: A unified treatment of chemical reactivity and selectivity, J. Phys. Chem. A 107 (2003) 4973-4965.

[81] C. Morell, A. Grand, A. Toro-Labbe, New dual descriptor for chemical reactivity, J. Phys. Chem. A 109 (2005) 205-212.

[82] NBO Version 3.1, E.D. Glendening, A.E. Reed, J.E. Carpenter, F. Weinhold.

[83] C. Adant, M. Dupuis, J. L. Bredas, Ab initio study of the nonlinear optical properties of urea, electron correlation and dispersion effects, Int. J. Quantum. Chem. 56 (1995) 497-507.

[84] G. Purohit, G. C. Joshi, Second order polarizabilities of some quinolines, Indian J. Pure Appl. Phys. 41 (2003) 922-927.

[85] Y. S. Mary, C. Y. Panicker, H. T. Varghese, K. Raju, T. E. Bolelli, I. Yildiz, C. M. Granadeiro, H. I. S. Nogueira, Vibrational spectroscopic studies and computational study of 4-fluoro-N-(2’-hydroxy-4’-nitrophenyl) phenylacetamide, J. Mol. Struct. 994 (2011) 223-231.

[86] S. R. Sheeja, N. A. Mangalam, M. R. P. Kurup, Y. S. Mary, K. Raju, H. T. Varghese, C. Y. Panicker, Vibrational spectroscopic studies and computational study of quinoline-2carbaldehyde benzyol hydrazone, J. Mol. Struct. 973 (2010) 36-46.

[87] Y. Xen, X. Sun, L. Fu, Z. Zhu, Z. Cui, DFT comparison of the OH-initiated degradation mechanisms for five chlorophenoxy herbicides, J. Mol. Model. 19 (2013) 2249-2263.

[88] L.-l. Ai, J.-y. Liu, Mechanism of OH-initiated atmospheric oxidation of E/Z-CF3CF=CFCF3: a quantum mechanical study, J. Mol. Model. 20 (2014) 1-10.

[89] W. Sang-aroon, V. Amornkitbamrung, V. Ruangpornvisuti, A density functional theory study on peptide bond cleavage at aspartic residues: direct vs cyclic intermediate hydrolysis, J. Mol. Model. 19 (2013) 5501-5513.

[90] J. Kieffer, É. Brémond, P. Lienard, G. Boccardi, In silico assessment of drug substances chemical stability, J. Mol. Struct. THEOCHEM, 954 (2010) 75-79.

[91] J. S. Wright, H. Shadnia, L. L. Chepelev, Stability of carbon-cantered radicals: Effect of functional groups on the energetics of addition of molecular oxygen, J. Comput. Chem. 30 (2009) 1016-1026.

[92] G. Gryn'ova, J. L. Hodgson, M. L. Coote, Revising the mechanism of polymer autoxidation, Org. Biomol. Chem. 9 (2011) 480-490.

[93] P. Lienard, J. Gavartin, G. Boccardi, M. Meunier, Predicting drug substances autoxidation, Pharm. Res. 32 (2015) 300-310.

[94] T. Andersson, A. Broo, E. Evertsson, Prediction of Drug Candidates' Sensitivity Toward Autoxidation: Computational Estimation of C-H Dissociation Energies of Carbon-Centered Radicals, J. Pharm. Sci. 103 (2014) 1949-1955.

[95] R. V. Vaz, J. R. Gomes, C. M. Silva, Molecular dynamics simulation of diffusion coefficients and structural properties of ketones in supercritical CO2 at infinite dilution, J. Supercritic. Fluids, 107 (2016) 630-638.

[96] G. C. Moraski, D. Lowell, A. P. Markley, A. Hipskind, H. Boshoff, S. Cho, S. G. Franzblau, M. J. Miller, Advent of imidazo [1, 2-a] pyridine-3-carboxamides with potent multi-and extended drug resistant anti-tuberculosis activity, ACS Med. Chem. Lett. 2(6) (2011) 466-470.

[97] R. J. Heath, Y. T. Yu, M. A. Shapiro, E. Olson, C.O. Rock, Broad spectrum antimicrobial biocides target the FabI component of fatty acid synthesis, J. Biol. Chem. 273 (1998) 30316-30320.

[98] J. C. Sacchettini, E. J. Rubin, J. S. Freundich, Drugs versus bugs: in pursuit of the persistent predator Mycobacterium tuberculosis, Nature Reviews Microbiology, 6 (2008) 41-52.

[99] W.H.J. Ward, G.A. Holdgate, S. Rowsell, E.G. McLean, R.A. Pauptit, E. Clayton, W.W. Nichols, J.G. Colls. C.A. Minshull, D.A. Jude, A. Mistry, D. Timms, R. Camble, N.J. Hales, C.J. Britton, W.F. Taylor, Kinetic and structural characteristics of the inhibition of enoyl (acyl carrier protein) reductase by triclosan, Biochemistry 38 (1999) 12514-12525.

[100] O. Trott, A.J. Olson, AutoDockVina: improving the speed and accuracy of docking with a new scoring function, efficient optimization, and multithreading, J. Comput. Chem. 31(2010) 455-461.

[101] J. A. War, K. Jalaja, Y. S. Mary, C. Y. Panicker, S. Armakovic, S. J. Armakovic, S. K. Srivastava, C. Van Alsenoy, Spectroscopic characterization of 1-[3-(1H-imidazol-1-yl)propyl]-3-phenylthiourea and assessment of reactive and optoelectronic properties employing DFT calculations and molecular dynamics simulations, J. Mol. Struct. 1129 (2017) 72-85.

CHAPTER III
FT-IR AND FT-RAMAN CHARACTERIZATION AND INVESTIGATION OF REACTIVE PROPERTIES OF N-(3-IODO-4-METHYLPHENYL) PYRAZINE-2-CARBOXAMIDE BY MOLECULAR DYNAMICS SIMULATIONS AND DFT CALCULATIONS

3.1. Introduction

Considerable attention has been devoted to pyrazine derivatives which have long been known for their diverse chemo-therapeutic properties. Pyrazinamide was early recognized as a first line drug for the treatment of tuberculosis [1, 2]. As a result of evolution of resistant strains of Mycobacterium tuberculosis [2], several pyrazine derivatives were prepared and proved to exhibit marked activity against multidrug resistant tuberculosis strains [3-8]. In addition, pyrazine nucleus was reported to constitute the essential pharmacophore in several pyrazine-based antiviral [9, 10], anticancer [11-13], anti-microbial [14], anti-malarial [15] trypanosomicidal [16] and insecticidal [17] agents. Moreover, pyrazine derivatives were reported as organic light-emitting diodes (OLEDs) [18, 19] and corrosion inhibitors [20, 22]. The title compound N-(3-iodo-4-methylphenyl)pyrazine-2-carboxamide (1) was found to be the most active anti-mycobacterial in vitro against M. tuberculosis H37Rv (minimum inhibitory concentration (MIC) < 2.0 mg/mL) [23]. The structure anti-mycobacterial activity relationship studies of N-phenylpyrazine-2-carboxam-ides showed the positive influence of halogen substitution in position 3 and methyl group in position 4 of the phenyl ring for the anti-mycobacterial activity [23-25]. Biologically active organic molecules are stable structures that are accumulating in the environment due to the frequent use an improper dumping. Their stability prevents degradation under natural conditions, while at the same time it was shown that they are toxic to aquatic organisms [26, 27]. Forced degradation via advanced oxidation processes is seen as substitute to conventional purification methods [26-32]. However, experiments and procedures based on forced degradation are complex and time consuming, so it is necessary to find ways how to perform their optimization and rationalization. This can be done by DFT calculations and MD simulations [33-36], since molecular modelling techniques can be used for prediction of reactive properties of investigated molecules. Results obtained by inexpensive computational experiments can further be used for understanding how forced degradation procedures can be improved. In the present work, the vibrational spectroscopic studies of N-(3-iodo-4-methylphenyl) pyrazine-2-carboxamide (NIMPC) are reported

experimentally and theoretically. The molecular docking studies are also reported due to the different potential biological activities of the title compound.

3.2. Experimental details

The title compound (Scheme 1) was prepared following the previously described procedure [23] via the reaction of pyrazine-2-carboxylic acid (A) (5 mmol) with thionyl chloride (7.5 mmol) in dry toluene to yield the corresponding acyl chloride (B), which was subsequently reacted with 3-iodo-4-methylaniline (5 mmol) in dry acetone with pyridine (5 mmol). The reaction was stirred at room temperature for1 hour, then poured into cold water. The crude product was collected, adsorbed on silica and purified by flash-chromatography (silica, gradient elution ethyl-acetate in hexane 0e30%). The yield of chromatographically pure product was 84% of theoretical yield related to acid (A). Elementary composition (CHON) of 1 was in the range of ± 0.4% of calculated values and the melting point was consistent with literature (141-142 ^{0}C) measured, 142-143 ^{0}C from literature [23]. The FT-IR spectrum (Fig. 1) was recorded using KBr pellets on a DR/JASCO FT-IR 6300 spectrometer. The FT-Raman spectrum (Fig. 2) was obtained on a Bruker RFS 100/s, Germany. For excitation of the spectrum, the emission of Nd:YAG laser was used with an excitation wavelength of 1064 nm, a maximal power 150 mW; measurement of solid sample.

Scheme 1. Synthesis of the title compound.

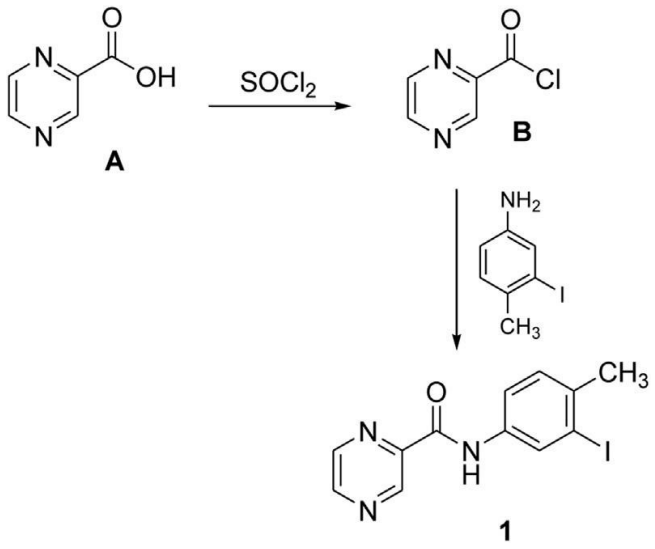

3.3. Computational details

Calculations of the title compound were carried with using the Gaussian09 program [37] using the B3LYP/ccpVDZ basis set to predict the molecular structure and wavenumbers in the gaseous phase and a scaling factor of 0.9613 had to be used for obtaining a considerably better agreement with the experimental data [38]. The structural parameters corresponding to the optimized geometry of the title compound (Fig. 3) are given in Table 1. The assignments of the calculated wavenumbers are done using GAR2PED [39] and Gauss view software [40]. In this work, the DFT calculations have also been performed by Jaguar 9.0 program [41], while the molecular modelling (MD) simulations have been performed by Desmond program [42-44]. Both of these programs have been used as implemented in Schrodinger Materials Science Suite 2015-4. DFT calculations with Jaguar program have been done with B3LYP exchange-correlation functional [45], with 6-311++G (d,p), 6-31 + G(d,p) and 6-311G(d,p) basis sets for the calculations of ALIE, Fukui functions and BDEs, respectively. In the case of MD simulations the OPLS 2005 force field [46] has been employed, with simulation time set to 10 ns within isothermal-isobaric (NPT) ensemble class. The MD simulations system was modelled by placing one NIMPC molecule into the cubic box with ~3000 water molecules. Other parameters include temperature of 300 K, pressure of 1.0325 bar and cut off radius of 12 Å. Simple point charge (SPC) model [47] was used for the description of solvent. Non-covalent interactions in Jaguar program have been investigated by the method developed by Johnson et al. [48, 49]. When Schrodinger€ Materials Science Suite 2015-4 was used, Maestro GUI [50] was used for the preparation of input files and analysis of results.

3.4. Results and discussion

In the following discussion, phenyl and pyrazine rings are designated as Ph and Pz respectively.

3.4.1. Geometrical parameters

The C-N and C-C bond lengths in the pyrazine ring of the title compound are 1.3366, 1.3392, 1.3424 and 1.3338 Å and 1.4013, 1.4037 Å, respectively, which are shorter than the normal C-N bond length (1.49 Å) and the C-C bond length (1.54 Å). The reported C-N and C-C bond lengths (B3LYP/SDD) of the pyrazine ring are 1.4104, 1.3577, 1.3577, 1.3608 Å and 1.4121, 1.3517 Å [51]. The bond lengths C_{10}-N_{12} and C_{13}-N_{12} (the carboxamide linker) are 1.3808 Å and 1.4111 Å which are also shorter than the normal C-N single bond and these bonds have some character of a double or conjugated bond [52]. The C-C bond lengths in the phenyl ring are in the range 1.3942-1.4071 Å. At N_{12} position, the angles C_{10}-N_{12}-H_{22} = 116.3^0, C_{10}-N_{12}-

C_{13} = 128.3^0 and C_{13}-N_{12}-H_{22} = 115.1^0, this asymmetry of angles is due to the weakening of the N-H bond. At C_{18} position, the angles C_{15}-C_{18}-I_{27}, C_{20}-C_{18}-I_{27}, C_{15}-C_{18}-C_{20} are 117.1, 120.9 and 122.0^0, respectively. This asymmetry is due to the iodine substitution in the phenyl ring. The bond angles C_4-C_5-N_6, C_4-C_5-C_{10}, C_{10}-C_5-N_6 are 121.3, 122.7 and 115.9^0, respectively. This asymmetry is attributed to the interaction of pyrazine ring and carboxamide group. The bond angles C_{18}-C_{20}-C_{23}, C_{16}-C_{20}-C_{23}, C_{18}-C_{20}-C_{16} at C_{20} are 123.6, 120.5, 116.0^0 and the asymmetry is due to the inter-action of the neighbouring groups.

3.4.2. IR and Raman spectra

The calculated scaled wavenumbers, observed IR, Raman bands and assignments are given in Table 2. According to literature, the N-H vibrations are expected in the regions, 3390 ± 60 cm^{-1} (stretching), 1500-1200 and 790 ± 70 cm^{-1} (bending modes) [53-56]. For the title compound, these modes were assigned at 3365 cm^{-1} (IR), 3370 cm^{-1} (Raman), 3464 (DFT) (stretching), 1486, 1225 602 cm^{-1} (IR), 600 cm^{-1} (Raman), 1485, 1223, 601 cm^{-1} (DFT)(bending). For the title compound, the N-H stretching mode has an IR intensity of 17.68 and Raman activity of 125.00 with a PED of 100%. The PED of N-H deformation modes of the title compound are in between 41 and 52%. For the deformation mode at 601 cm^{-1}, the IR intensity is low while the other two modes have high IR intensity for the title compound. In the present case, the N-H stretching mode is red shifted by 99 cm^{-1} in the IR spectrum from the computed value, which indicates the weakening of the N-H bond [57]. The C-N stretching modes are expected in the range 1275 ± 55 cm^{-1} [53] and the bands at 1211 cm^{-1} in the Raman spectrum and at 1214, 1105 cm^{-1} (DFT) with moderate IR intensities and PEDs around 40% are assigned as the C-N stretching modes of the title compound. The reported C-N stretching modes are at 1265, 1239 cm^{-1} in the IR spectrum and at 1261, 1248 cm^{-1} (DFT) [58]. For the title compound, the carbonyl stretching vibration is observed at 1695 cm^{-1} in the IR spectrum and at 1696 cm^{-1} in the Raman spectrum which is expected in the region 1715-1600 cm^{-1} [53] while the computed value is 1708 cm^{-1} with an IR intensity of 225.95 and Raman activity 176.10 and the PED is 64%. The CH_3 modes are expected in the regions, 3050-2900 cm^{-1} (stretching), 1485-1350, 1100-900 cm^{-1} (deformation modes) according to literature [53] and for the title compound, these modes are assigned at 2975, 2920 cm^{-1} (IR), 3005, 2970, 2918 cm^{-1} (Raman), 3001, 2973, 2915 cm^{-1} (DFT) (stretching), 1437, 1402, 1368, 1030 cm^{-1} (IR), 1403, 1370, 1028 cm^{-1} (Raman), 1436, 1404, 1364, 1032, 990 cm^{-1} (DFT) (bending). Analysis of vibrational spectra of substituted benzenes shows that the stretching vibrations of C-I corresponds to a band around

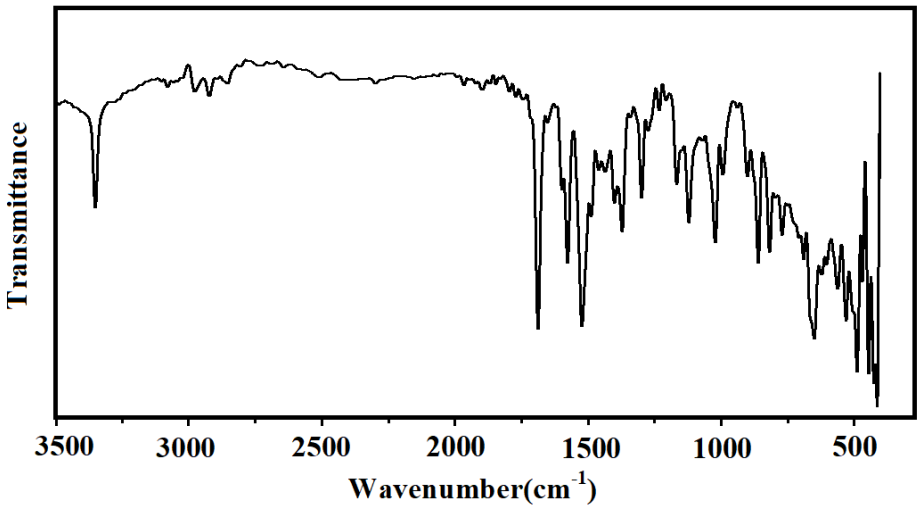

Fig. 1 FT-IR spectrum of N-(3-iodo-4-methyl phenyl) pyrazine-2- carboxamide

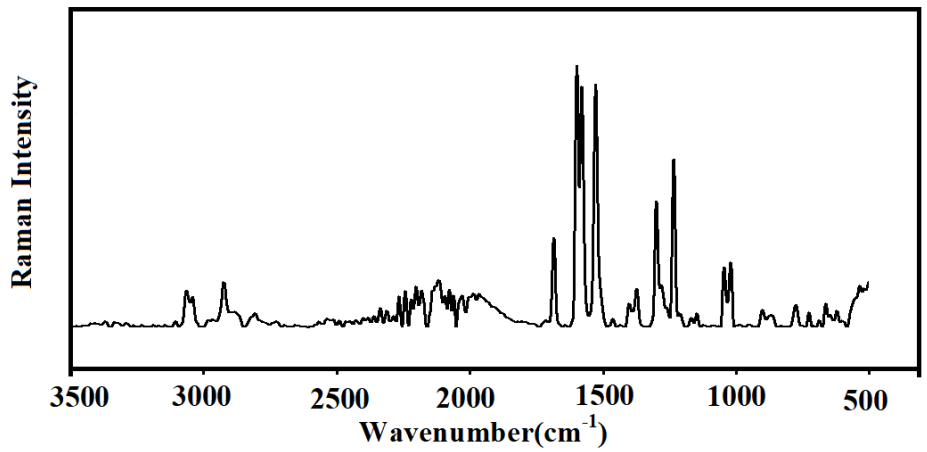

Fig. 2 FT-Raman spectrum of N-(3-iodo-4-methyl phenyl) pyrazine-2-carboxamide

340 cm^{-1} experimentally [59, 60]. The carbon-iodine stretching band of the title compound is assigned at 333 cm^{-1} theoretically. Zainuri et al. reported the CI stretching mode at 317 cm^{-1} [61]. For the title compound, the phenyl C-H stretching bands are observed at 3134, 3029 cm^{-1} in the IR spectrum and 3120, 3036 cm^{-1} in the Raman spectrum, while the computed values are in the range 3136-3032 cm-1 which are in agreement with the literature [53,62]. The phenyl ring stretching modes of the title compound are observed at 1590, 1458, 1342, 1290 cm^{-1} in the IR spectrum, at 1583, 1460, 1285 cm^{-1} in the Raman spectrum and at 1586, 1553, 1453, 1346 and 1287 cm^{-1} theoretically (DFT) [53]. The tri-substituted phenyl ring breathing mode of the title compound is assigned at 819 cm^{-1} (IR), 822 cm^{-1}(Raman) and 819 cm^{-1} (DFT)

with PED 58% which is in agreement with the literature [63]. The in-plane and out-of-plane C-H deformations of the phenyl ring are expected above and below 1000 cm^{-1} respectively [53] and these modes of the title compound were assigned at 1270, 1203, 1147 cm^{-1} (IR), 1263, 1149 cm^{-1} (Raman), 1265, 1201, 1149 cm 1 (DFT) (in-plane C-H bending modes) and 877 cm^{-1} (IR), 967, 878, 834 cm^{-1} (DFT) (out-of-plane bending modes). The IR bands in the region of 2676-1800 cm^{-1} and the large broadening seen in the IR spectrum support the intra-molecular hydrogen bonding [64]. The pyrazine C-H stretching modes of the title compound were observed 3070 cm^{-1} in IR spectrum and at 3064 cm^{-1} in Raman spectrum while the computed values are 3062, 3055, 3052 cm^{-1} theoretically which are expected in the range 3100-3000 cm^{-1} [65]. In the present case, the pyrazine ring stretching modes were observed at 1525,1120 cm^{-1} in the IR spectrum and at 1526,1175 cm^{-1} in the Raman spectrum while the PED analysis gives these modes at 1551, 1524, 1182, 1117, 1009 cm-^{1} which are in agreement with literature [66, 67]. In the present case, the pyrazine ring stretching modes have IR intensities in the range 2.82-38.52 and Raman activities 0.45 to 149.28 and the PEDs are around 60%. For the title compound, the ring breathing mode of the pyrazine ring was assigned at 954 cm^{-1} in the Raman spectrum and 952 cm^{-1} in (DFT) with low IR intensity and Raman activity, while the reported value is at 1015 cm^{-1} (DFT) [66]. For the title compound, the in-plane and out-of-plane CH bending modes of the pyrazine ring were assigned at1395, 1352, 1246 cm^{-1} and 959, 928, 855, 838 cm^{-1} theoretically. The experimentally observed values are 932, 860 cm^{-1} in the IR spectrum and 1240 cm^{-1} and 861 cm^{-1} in the Raman spectrum which are in agreement with the literature [66].

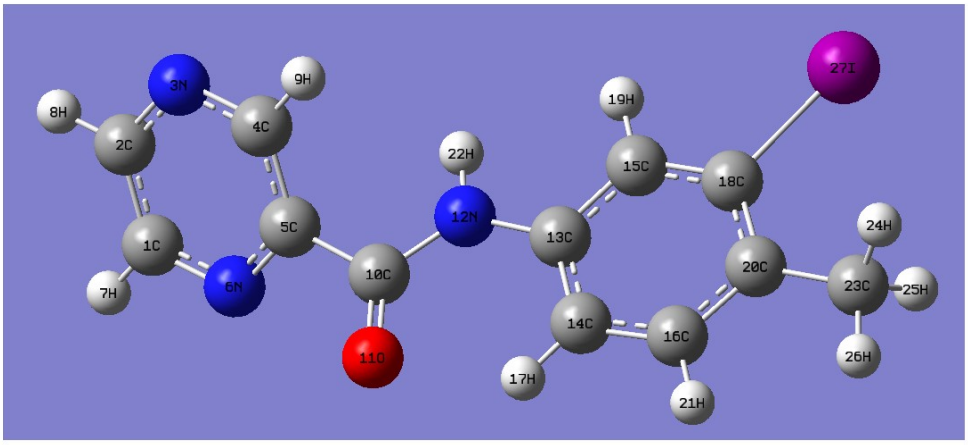

Fig. 3 Optimized geometry of N-(3-iodo-4-methyl phenyl) pyrazine-2-carboxamide

3.4.3. Natural bond orbital analysis

The natural bond orbitals (NBO) calculations were performed using the NBO 3.1 program [68] to find the various interactions in the molecular system and the important interactions are with stabilization energies, 10.82, 10.77, 22.62, 50.62 kJ/mol in $n_1(N_3) \rightarrow s^*(C_4\text{-}C_5)$, $n_1(N_6) \rightarrow s^*(C_4\text{-}C_5)$, $n_2(O_{11}) \rightarrow s^*(C_{10}\text{-}N_{12})$, $n_1(N_{12}) \rightarrow p^*(C_{10}\text{-}O_{11})$. The important hybrid orbital of the molecular system are: $n_2(O_{11})$ and $n_2(I_{27})$ with higher energies, 706.653, 712.219 kJ/mol and with low occupation numbers, 1.87640 and 1.97761 and the p-character is nearly 100%. The orbital $n_1(O_{11})$ and $n_1(I_{27})$ have lower energies, 1830.052 and 1617.151 kJ/mol with p-characters, 35.59 and 89.51% and high occupations numbers, 1.97534 and 1.99302.

3.4.4. Nonlinear optical properties

The calculated first hyperpolarizability of the title compound is 13×10^{-30} esu which is 100 times that of standard NLO material urea (0.13×10^{-30} esu) [69]. For a pyrazine derivative the first hyperpolarizability is reported at 9.77×10^{-30} esu [51]. We conclude that the title compound is an attractive object for future studies of nonlinear optical properties.

3.4.5. Frontier molecular orbitals

In order to understand global stability and reactive properties of the title compound we have investigated frontier molecular orbitals. Namely, the highest occupied molecular orbital (HOMO) and lowest unoccupied molecular orbital (LUMO) are the main molecular orbitals that take part in reactions with other molecular structures. Distribution of HOMO and LUMO provides important insight into the reactive properties of organic molecules, Fig. 4. Visualization presented in Fig. 4 indicates the importance of iodine atom, as HOMO is practically completely localized in the near vicinity of this atom. This result designates iodine atom to act as electron donor during the interactions with other molecules. On the other side LUMO orbital is mainly delocalized over the nitrogen containing six member ring, designating this part of the molecule to be electron acceptor during the interactions with other molecules. LUMO is also delocalized over the other six member ring, including nitrogen atom that connects two rings. Using information on the energies of HOMO and LUMO, useful and frequently used quantum-molecular descriptors such as the ionization energy and electron affinity can be calculated according to the following simple relations: $I = -E_{HOMO}$, $A = -E_{LUMO}$, $\eta = (-E_{HOMO} + E_{LUMO})/2$ and $\mu = (E_{HOMO} + E_{LUMO})/2$ [70]. Parr et al. [71] proposed the global electrophilicity power of a ligand as $\omega = \mu^2/2\eta$. For the title compound,

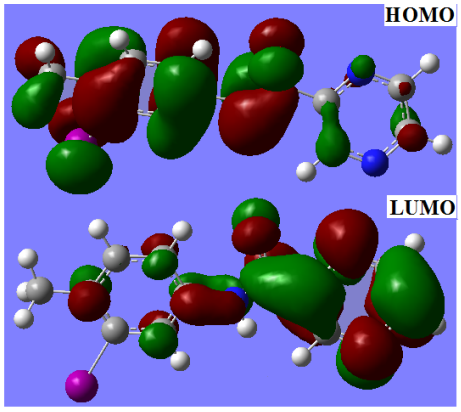

Fig. 4 HOMO-LUMO plot of N-(3-iodo-4-methyl phenyl) pyrazine-2- carboxamide

energy difference between HOMO and LUMO, HOMO-LUMO gap, is equal to 3.29 eV, which is relatively high value indicating significant stability of this potentially pharmaceutical molecule. Ionization potential, I, and electron affinity, A, are calculated to be 8.57 eV and 6.55 eV, respectively. The values of HOMO-LUMO gap and global hardness (η=1.64 eV) are almost the same as in the case of other pyrazine derivative that we have previously investigated [72]. Although the stability parameters of these derivatives are practically the same, there are significant differences in the values of chemical potential and global electrophilicity. Namely, the value of chemical potential of the presently investigated pyrazine derivative is 4.35 eV, which is higher than the value of 6.85 in the case of pyrazine derivative investigated in our previous paper [72]. Also, the calculated electrophilicity of the title molecule is 2.56 eV, which is significantly lower than the value of electrophilicity of derivative in the work of Joseph et al., 2013, with the value of 14.31 eV, meaning that the title molecule is much more stable.

3.4.6. Molecular electrostatic potential map

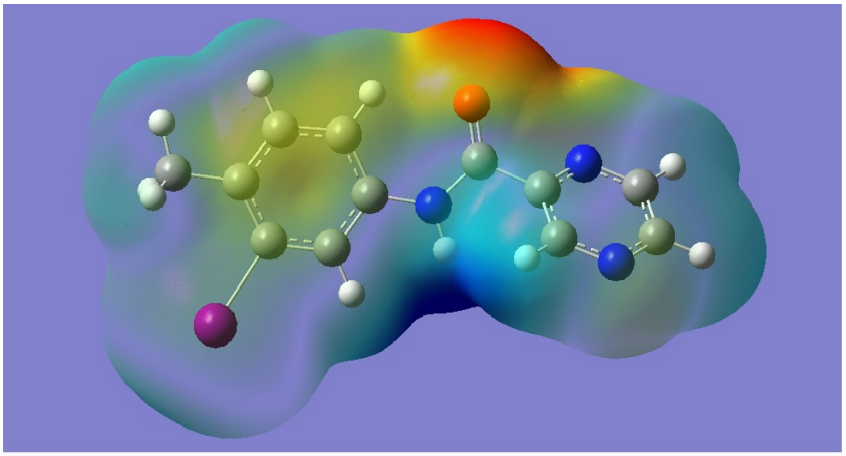

Fig. 5 MEP plot of N-(3-iodo-4-methyl phenyl) pyrazine-2- carboxamide

To predict the reactive sites of electrophilic and nucleophilic attacks for the investigated molecule, the molecular electrostatic potential (MEP) at the B3LYP/ccpVDZ optimized geometry was calculated [73-76]. The negative (red and yellow) regions of MEP were related to electrophilic reactivity and the positive (blue) regions to nucleophilic reactivity (Fig. 5). From the MEP, it is evident that the negative charge covers the carbonyl group and the positive region is over the N-H group. The high electronegativity of the carbonyl group makes it the most reactive part of the molecule.

3.4.7. ALIE surfaces, Fukui functions and non-covalent interactions

Local reactivity properties of organic molecules can be investigated by calculations of average local ionization energy (ALIE) values, as introduced by Sjoberg et al. [77, 78]. ALIE is defined as sum of orbital energies weighted by the orbital densities according to the following equation:

$$I(r) = \sum_i \frac{\rho_i(\vec{r})|\varepsilon_i|}{\rho(\vec{r})}. \quad (1)$$

where $\rho_i(\vec{r})$ denotes electronic density of the i-th molecular orbital at the point $\vec{r}$, ε_i denotes orbital energy, while $\rho(\vec{r})$ denotes total electronic density function. In case of this quantum-molecular descriptor important molecule sites from the aspect of electrophilic attacks can be visualized by mapping of its values to the electron density surface. In this way the areas with the lowest ALIE values indicate molecule sites where electrons are least tightly bound and therefore sites that are the most vulnerable to electrophilic attacks, Fig. 6. Analysis of the NIMPC's ALIE surface indicates three interesting molecule sites, possibly prone to electrophilic attacks. According to the Fig.6 these molecule sites are located in the near vicinity of iodine atom I_{27} and nitrogen atoms N_3 and N_6. These molecule sites are characterized by the lowest ALIE values of around 185 kcal/mol. On the other side molecule sites characterized by the highest ALIE values, where electrons are most tightly bonded, are near vicinities of hydrogen atoms H_7, H_8 and H_{22}, characterized by values of around 377 kcal/mol. According to the distribution of red colour in Fig. 6, iodine atom I_{27} is certainly the most vulnerable atom towards electrophilic attacks.

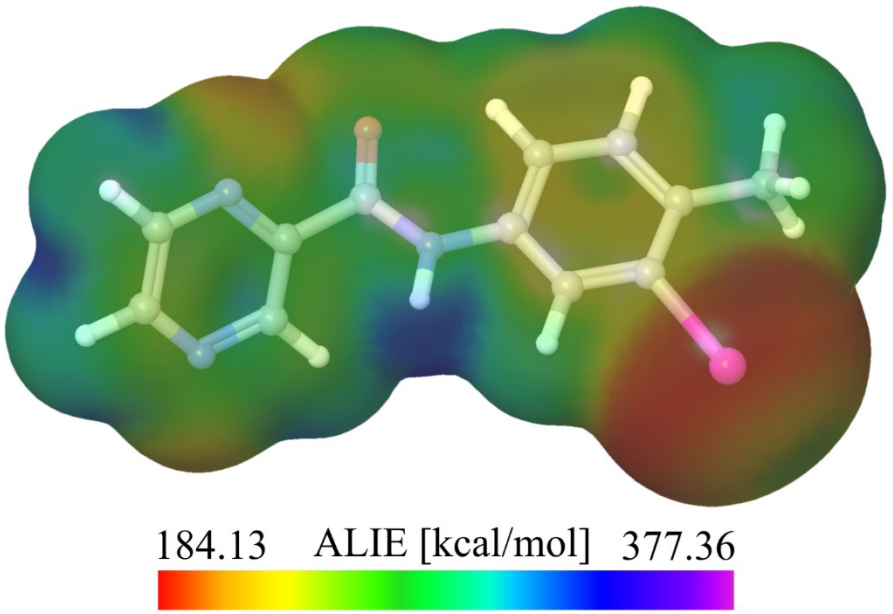

Fig. 6 ALIE surface of N-(3-iodo-4-methylphenyl) pyrazine-2-carboxamide molecule

Thanks to the analysis of electron density within NIMPC molecule intramolecular non-covalent interactions have been detected and visualized, Fig.7. In the case of NIMPC molecule there are two intramolecular non-covalent interactions formed between oxygen atom O_{11} and hydrogen atom H_{17} and between carbon atom C_{18} and iodine atom I_{27}. Non-covalent interaction between oxygen and hydrogen atom is much stronger than non-covalent interaction between carbon and iodine atom. Other interesting molecule sites from the aspect of local reactivity have been detected by calculations of Fukui functions, presented in Fig.8. This important quantum-molecular descriptor shows how electron density changes with the addition or removal of charge. These functions in Jaguar program are calculated with the help of finite difference approach, according to the following equations:

$$f^{+} = \frac{\left(\rho^{N+\delta}(r) - \rho^{N}(r)\right)}{\delta}, \tag{2}$$

$$f^{-} = \frac{\left(\rho^{N-\delta}(r) - \rho^{N}(r)\right)}{\delta}, \tag{3}$$

where N stands for the number of electrons in reference state of the molecule, while δ stands for the fraction of electron which default value is set to be 0.01 [79]. In this work Fukui functions have been visualized by mapping of their values to the electron density surface. Positive color in the case of Fukui f^{+}, Fig.8a, is purple color and shows molecule sites where the amount of electron density increased as charge has been added. On the other side, negative color in the case of Fukui f^{-} function, Fig.8b, is red color and shows molecule sites

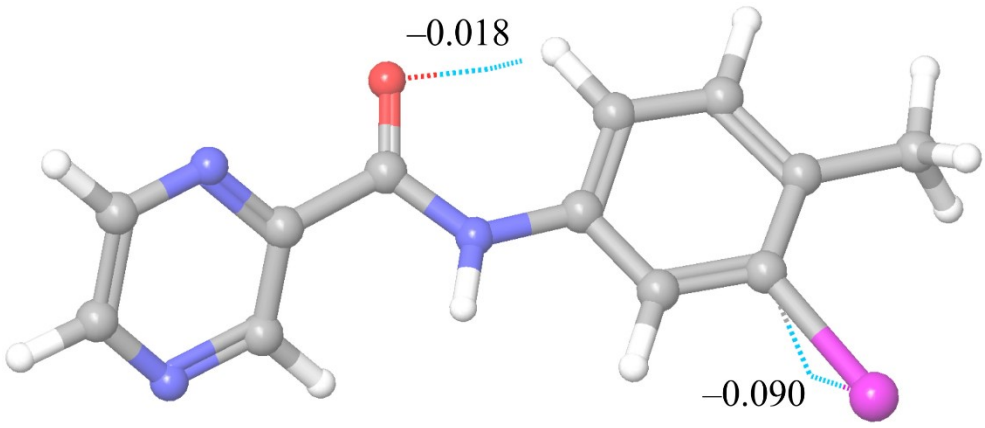

Fig. 7 Intramolecular non-covalent interactions and their strength

where the amount of electron density decreased as charge was removed. Results presented in Fig.8a indicate that carbon atom C_2 and nitrogen atom N_6 are molecule sites where electron density increases with the addition of charge, therefore designating these atoms as electrophilic. On the other side results presented in Fig.8b indicate that red color is localized also in the near vicinity of heterocyclic ring, this time in the near vicinity of carbon atoms C_4 and C_5, designating these parts of molecule as nucleophilic.

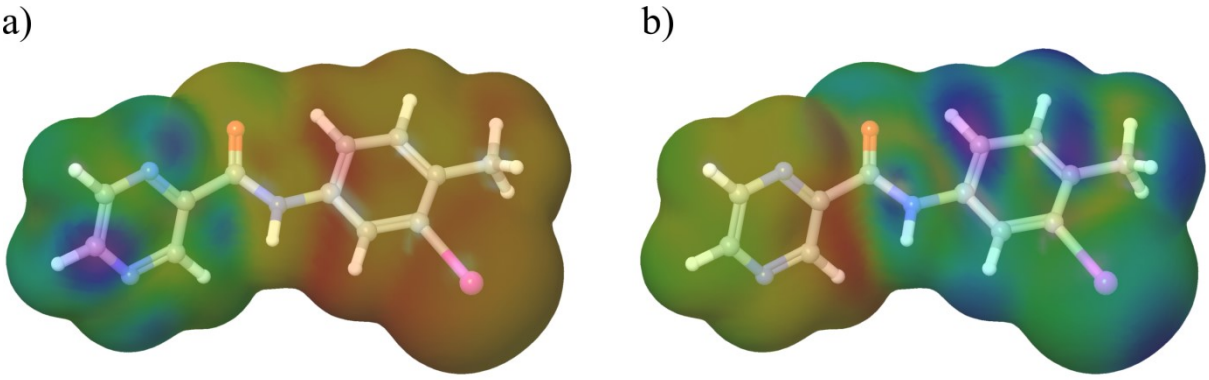

Fig. 8 Fukui functions a) f^+ and b) f^- of N-(3-iodo-4-methylphenyl) pyrazine-2-carboxamide molecule

3.4.8. Reactive and degradation properties based on autoxidation and hydrolysis

In order to predict the degradation properties based on autoxidation and hydrolysis mechanisms in this work, we have also calculated the bond dissociation energies (BDEs) and the radial distribution functions (RDFs). Calculations of BDE for hydrogen abstraction allow possibility to predict molecule sites where autoxidation process could start. These results also indicate to what extent the molecule is sensitive to open air and presence of oxygen, which is of particular

significance in pharmaceutical industry. In this regard, the BDE also contributes to the forced degradation studies, since they can be used for determination or confirmation of degradation path of a specific organic pharmaceutical molecule [80-83]. If the BDE for hydrogen abstraction ranges from 70 to 85 kcal/mol, then the molecule of interest is the most vulnerable to autoxidation mechanism, according to the study of Wright et al. [84]. Gryn'ova et al. [85] reported practically the same values, but also leaving "space" for the BDE values ranging between 85 and 90 kcal/mol, regarding to these values as possibly important for the autoxidation mechanism. BDE values for hydrogen abstraction lower than 70 kcal/mol, are not suitable for the autoxidation mechanism since the formed radicals are resistant to the O_2 insertion [84, 86, 87]. The BDE values of the title molecule are shown in Fig. 9. The red colored values correspond to the BDE values for hydrogen abstraction, while blue colored values correspond to the BDE values for the rest of the single acyclic bonds. High stability of the title molecule is confirmed by the results provided in Fig. 9. Since there are no BDE values for hydrogen abstraction lower than 90 kcal/mol, it can be stated that the title molecule is stable in open air and in the presence of oxygen. Concerning the BDE values for the rest of the single acyclic bonds, the lowest BDE value were calculated for the carbon-iodine bond between, indicating that degradation mechanism could start by detaching of the mentioned iodine atom.

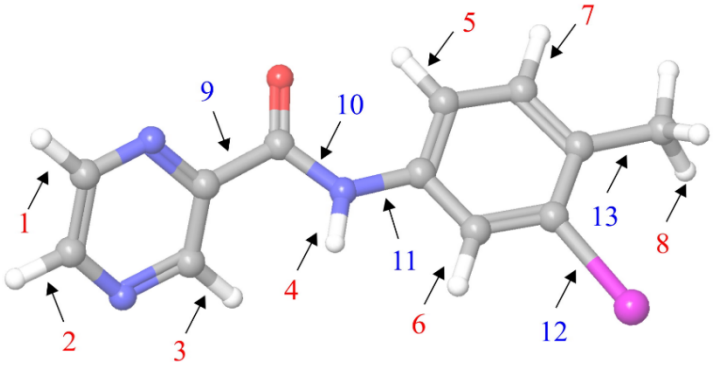

Bond	BDE [kcal/mol]
1	111.11
2	111.51
3	107.61
4	97.14
5	118.26
6	116.12
7	116.37
8	94.10
9	84.97
10	78.93
11	103.77
12	63.08
13	102.73

Fig. 9 BDEs of all single acyclic bonds

In order to determine to what extent hydrolysis mechanism could be important for the degradation of title molecule, we also calculated the RDF after MD simulations. In Fig. 10, the RDFs of atoms with the most pronounced interactions with water molecules have been presented. The RDF, g(r), indicated the probability of finding a particle in the distance r from another particle [88]. The results provided in Fig. 10 indicate that only four atoms of the title molecule have relatively significant interactions with water molecules. These atoms are carbon

atoms C_1, C_{10}, C_{23} and iodine atom I_{27}. All of these atoms have very similar g(r) profiles. The peak distance in all cases is located between 3.5 and 3.8 Å. According to the maximal g(r) values the most important RDF is certainly for iodine atom I_{27}. However, relatively high peak distances and absence of the hydrogen atoms with significant RDF profiles indicate that the title molecule is highly stable in water surrounding, which is significant from the pharmaceutical point of view.

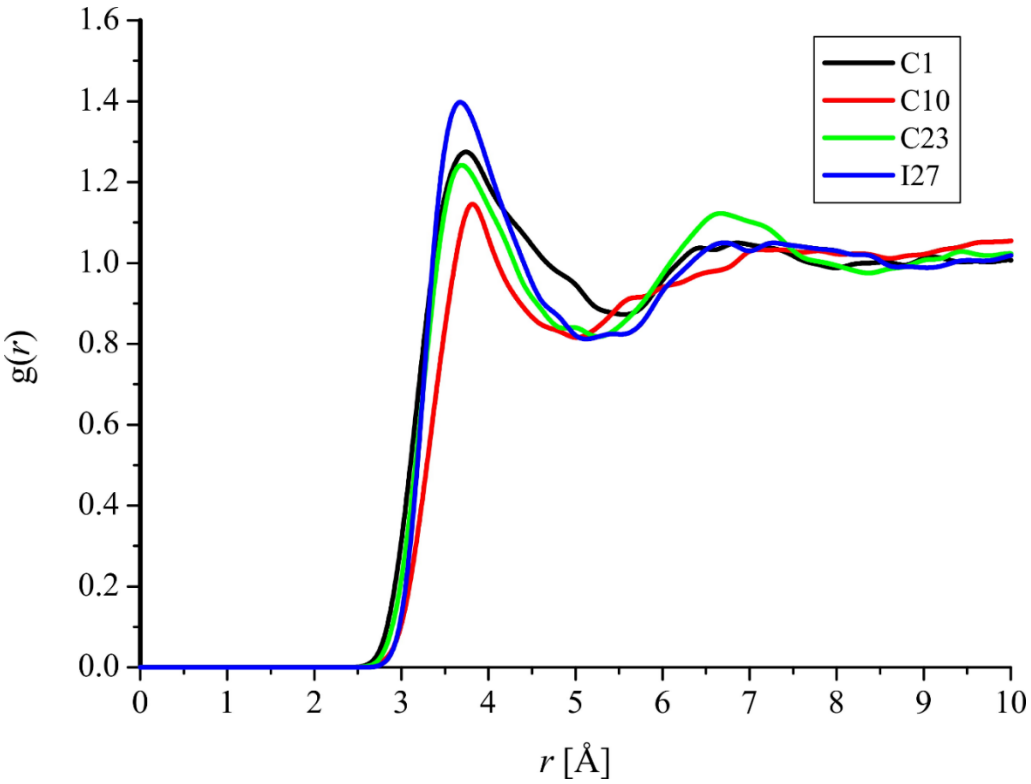

Fig. 10 RDFs of title compound with significant interaction with water molecule

3.4.9. Molecular docking

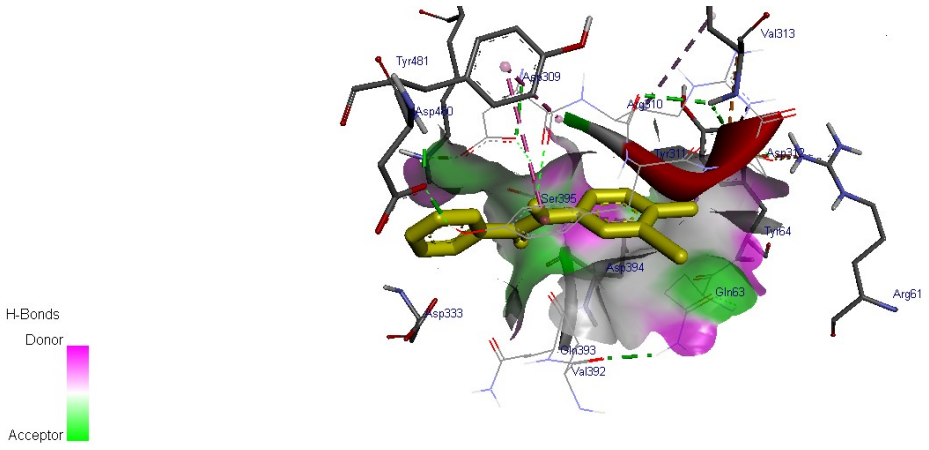

Fig. 11 the interaction of ligand with amino acids of mGluRs and H-bond surface

The metabotropic glutamate receptors (mGluRs) are family C G-protein-coupled receptors which participate in the modulation of synaptic transmission and neuronal excitability throughout the central nervous system. Large progress has been made in determining the mechanisms by which mGluRs are activated and the ligands that can modulate receptor activity. The widespread expression of mGluRs makes these receptors particularly attractive drug targets, and recent studies continue to validate the therapeutic utility of mGluR ligands in neurological and psychi-atric disorders such as Alzheimer's disease, Parkinson's disease, anxiety, depression, and schizophrenia [89]. The molecular docking simulations were performed on AutoDock Vina software [90] and the 3D crystal structure of metabotropic glutamate receptor 5 (mGluR5) was obtained from Protein Data Bank (PDB ID: 3LMK) [91]. The docking of the title compound with metabotropic glutamate receptor was done as previously reported [92]. The ligand (1) binds at the catalytic site of substrate by weak non-covalent interactions most prominent of which are H-bonding and alkyl-p interactions (Figs. 11 and 12). Backbone oxygen of Asp309 forms H-bond of 2.31 Å to ligand's carbox -amide hydrogen. Arg310, Tyr64, Val392 amino acids hold the benzene aromatic ring of 1 by alkyl-p interactions. The ligand (1) forms a stable complex with mGluR as is evident from the binding affinity (DG in kcal/mol) value 6.6 (Table 5). Shana et al. [92] reported that the ligand binds at the active sites of the protein by weak non-covalent interactions most prominent of which are H-bonding, alkyl-p and sigma-p interactions and predicted a binding free energy of -9.8 kcal/mol and the inhibitor forms a stable complex with FAK. These preliminary results suggest that the compound might exhibit inhibitory activity against mGluRs.

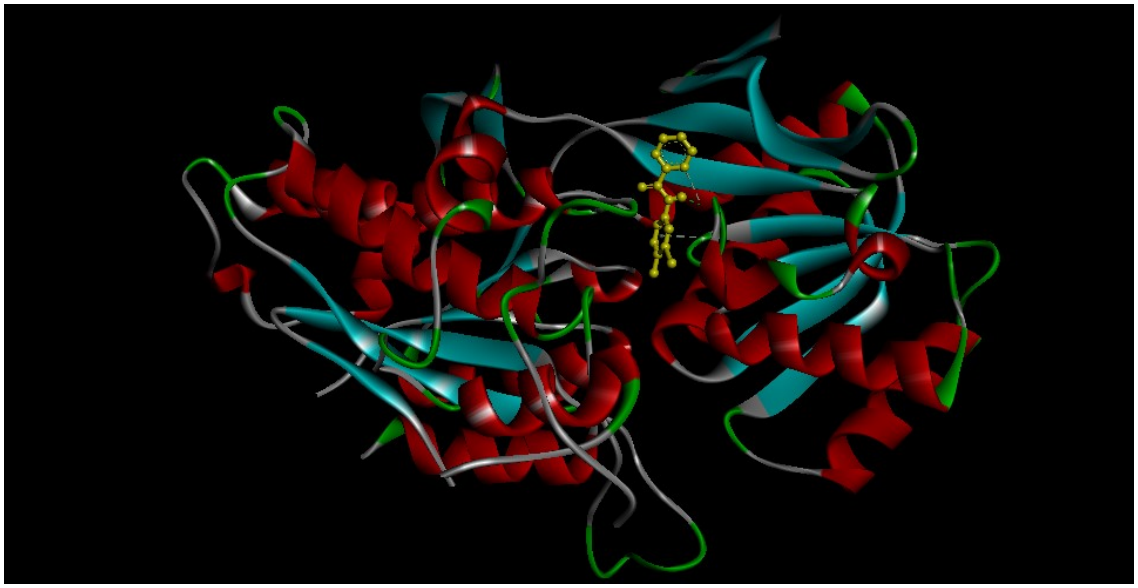

Fig. 12 The docked ligand embedded in the catalytic site of mGluRs

3.5. Conclusions

The experimental, structural and vibrational wavenumber assignments of the title compound were successfully analysed. The theoretically predicted geometrical parameters are in agreement with that of similar derivatives. The HOMO is delocalized over the iodine atom, methyl group and the phenyl ring while the LUMO is all over the molecule except iodine and methyl group. The MEP analysis showed that the negative charge covers the carbonyl group and the positive region is over the N-H group. Thanks to the DFT calculations of ALIE values, iodine atom I_{27} has been determined as the most important concerning the electrophilic attacks. The Fukui functions recognized heterocyclic ring as important reactive centre as well. The BDE values for hydrogen abstraction indicated that the title molecule is highly stable in open air and in the presence of oxygen. At the same time, the BDE for the rest of single acyclic bonds indicated that the degradation could start by detachment of iodine atom. High stability of the title molecule was also confirmed by RDFs, since there are only four atoms with significant interactions with water molecules and since there are not hydrogen atoms with significant profiles of RDFs. The title compound forms a stable complex with mGluR as is evident from the binding affinity value.

Table.1 Optimized Geometrical parameters of N-(3-iodo-4-methyl phenyl) pyrazine-2-carboxamide.

Bond Length(Å)		Bond Angle(^{0})		Dihedral Angle(^{0})	
C_1-C_2	1.4013	C_2-C_1-N_6	122.3	N_6-C_1-C_2-C_3	-0.5
C_2-N_3	1.3366	C_1-C_2-N_3	122.0	C_2-N_3-C_4-C_5	-0.1
C_4-C_5	1.4037	C_2-N_3-C_4	115.7	C_4-C_5-N_6-C_1	1.4
C_5-C_{10}	1.5170	C_5-C_4-H_9	121.2	N_6-C_5-C_{10}-O_{11}	-35.8
N_{12}-C_{13}	1.4111	N_6-C_5-C_{10}	115.9	O_{11}-C_{10}-N_{12}-C_{13}	-1.1
C_{13}-C_{15}	1.4048	C_5-C_{10}-N_{12}	113.6	N_{12}-C_{13}-C_{14}-C_{16}	-179.6
C_{15}-C_{18}	1.3949	C_{10}-N_{12}-H_{22}	116.3	C_{14}-C_{13}-C_{15}-C_{28}	0.0
C_{16}-H_{21}	1.0929	N_{12}-C_{13}-C_{15}	117.2	C_{13}-C_{15}-C_{18}-I_{27}	-180.0
C_{20}-C_{23}	1.5065	C_{13}-C_{14}-H_{17}	119.7	C_{15}-C_{18}-C_{20}-C_{16}	0.0
C_{23}-H_{26}	1.0994	C_{13}-C_{15}-H_{19}	119.8	I_{27}-C_{18}-C_{20}-C_{23}	-0.1
C_1-N_6	1.3338	C_{14}-C_{16}-H_{21}	118.3	C_2-C_1-C_6-C_5	-0.6
C_2-H_8	1.0947	C_{15}-C_{18}-I_{27}	117.1	N_3-C_4-C_5-N_6	-1.1
C_4-H_9	1.0951	C_{16}-C_{20}-C_{23}	120.5	C_4-C_5-C_{10}-O_{11}	140.8
C_{10}-O_{11}	1.2181	C_{20}-C_{23}-H_{25}	111.6	N_6-C_5-C_{10}-N_{12}	145.0
N_{12}-H_{22}	1.0133	H_{24}-C_{23}-H_{26}	108.1	C_{10}-N_{12}-C_13-C_{14}	-2.2
C_{14}-C_{16}	1.3942	C_2-C_1-H_7	120.8	C_{15}-C_{13}-C_{14}-C_{16}	0.0
C_{15}-H_{19}	1.0918	C_1-C_2-H_8	120.9	C_{13}-C_{14}-C_{16}-C_{20}	-0.1
C_{18}-C_{20}	1.4071	N_3-C_4-C_5	122.5	C_{14}-C_{16}-C_{20}-C_{18}	0.0

Bond Length(Å)		Bond Angle(^{0})		Dihedral Angle(^{0})	
C23-H_{24}	1.1025	C_4-C_5-N_6	121.3	C_{15}-C_{18}-C_{20}-C_{23}	-180.0
C1-H_7	1.0948	C_1-N_6-C_5	116.2	C_1-C_2-N_3-C_4	0.8
N3-C_4	1.3392	O_{11}-C_{10}-N_{12}	124.9	N_3-C_4-C_5-C_{10}	-177.5
C5-N_6	1.3424	C_{13}-N_{12}-H_{22}	115.1	C_4-C_5-C_{19}-N_{12}	-38.4
C10-N_{12}	1.3808	C_{14}-C_{13}-C_{15}	119.1	C_5-C_{10}-N_{12}-C_{13}	178.0
C13-C_{14}	1.4033	C_{16}-C_{14}-H_{17}	121.2	C_{10}-N_{12}-C_{13}-C_{15}	178.2
C14-H_{17}	1.0863	C_{18}-C_{15}-H_{19}	119.9	N_{12}-C_{13}-C_{15}-C_{18}	179.7
C16-C_{20}	1.4048	C_{20}-C_{16}-H_{21}	118.2	C_{13}-C_{15}-C_{18}-C_{20}	-0.1
C18-I_{27}	2.1208	C_{20}-C_{18}-I_{27}	120.9	C_{14}-C_{16}-C_{20}-C_{23}	-180.0
C23-H_{25}	1.1024	C_{18}-C_{20}-C_{23}	123.6	I_{27}-C_{18}-C_{20}-C_{16}	179.9
		C_{20}-C_{23}-H_{26}	110.6		
		H_{25}-C_{23}-H_{26}	108.1		
		N6-C_1-H_7	116.9		
		N3-C_2-H_8	117.1		
		N_3-C_4-H_9	116.3		
		C_4-C_5-C_{10}	122.7		
		C_5-C_{10}-O_{11}	121.5		
		C_{10}-N_{12}-C_{13}	128.3		
		N_{12}-C_{13}-C_{14}	123.7		
		C_{13}-C_{14}-C_{16}	119.0		
		C_{13}-C_{15}-C_{18}	120.4		
		C_{14}-C_{16}-C_{20}	123.5		
		C_{15}-C_{18}-C_{20}	122.0		
		C_{16}-C_{20}-C_{18}	116.0		
		C_{20}-C_{23}-H_{24}	111.5		
		H_{24}-C_{23}-H_{25}	106.8		

Table 2 Calculated scaled wavenumbers, observed IR, Raman bands and vibrational assignments of the title compound

B3LYP/cc-pVDZ			IR	Raman	Assignments
$\upsilon(cm^{-1})$	IR_I	R_A	$\upsilon(cm^{-1})$	$\upsilon(cm^{-1})$	
3464	17.68	125.00	3365	3370	υNH(100)
3136	8.83	58.93	3134	3120	υCHPh(98)
3062	4.80	59.39	3070	3064	υCHPz(98)
3055	15.61	128.58	-	-	υCHPz(96)
3052	33.75	381.75	-	-	υCHPz(95)
3034	2.60	113.83	-	3036	υCHPh(98)
3032	24.59	52.78	3029	-	υCHPh(98)
3001	15.52	77.74	-	3005	υCH_3(99)
2973	8.91	89.13	2975	2970	υCH_3(100)
2915	20.99	266.62	2920	2918	υCH_3(100)
1708	225.95	176.10	1695	1696	υC=O(64), δNH(19)
1586	92.44	516.36	1590	1583	υPh(65),δCHPh(23)
1553	58.25	17.16	-	-	υPh(52),δNH(21)
1551	38.52	84.50	-	-	υPz(60),δCHPz(13)

B3LYP/cc-pVDZ			IR	Raman	Assignments
$\upsilon(cm^{-1})$	IR_I	R_A	$\upsilon(cm^{-1})$	$\upsilon(cm^{-1})$	
1524	2.82	149.28	1525	1526	υPz(67),δCHPz(22)
1485	520.52	422.51	1486		δNH(47), υPh(10), δCHPh(10)
1453	24.20	3.28	1458	1460	υPh(48), δCH_3(17), δCHPh(27)
1436	13.88	13.46	1437		δCH_3(97)
1404	30.31	8.59	1402	1403	δCH_3(51), δCHPh(10), υPh(17)
1395	8.06	14.86	-	-	δCHPz(57), υPz(20)
1364	19.05	5.39	1368	1370	δCH_3(91)
1352	82.00	97.49	-	-	δCHPz(62), υPz(17)
1346	4.94	12.93	1342	-	υPh(49), δCHPh(22)
1287	100.73	167.38	1290	1285	υPh(60), υCN(14)
1265	1.14	4.25	1270	1263	δCHPh(53), υPh(13)
1246	17.51	38.60	-	1240	δCHPz(41), υPz(23)
1223	25.81	96.34	1225	-	δNH(41), υCC(22), υPh(12)
1214	20.37	230.08	-	1211	υCN(38), υPh(19), δCHPh(11)
1201	18.97	4.33	1203	-	δCHPh(43), υCC(12), υPh(13)
1182	10.47	18.15	-	1175	υPz(90)
1149	7.36	26.47	1147	1149	δCHPh(58), υPh(15)
1117	2.98	14.03	1120	-	υPz(59), δCHPz(23)
1105	109.96	1.45	-	-	υCN(41), υPz(22)
1032	5.83	26.22	1030	1028	δCH_3(64), δCHPh(20)
1009	2.98	0.45	-	-	υPz(60)
998	37.61	19.09	997		δPh(49), υPh(26)
990	26.25	38.60	-	-	δCH_3(46), γCHPh(18), υPh(11)
967	28.10	1.77	-	-	γCHPh(67), δCH_3(21)
959	0.16	0.69	-	-	γCHPz(89)
952	1.72	0.61	-	954	υPz(63), δPz(18)
928	1.40	2.13	932	-	γCHPz(81)
878	18.56	6.25	877	-	γCHPh(64),τPh(25)
855	24.08	20.71	860	861	γCHPz(58), τPz(11)
838	8.26	4.12	-	-	γCHPz(29), δC=O(14), τPz(18)
834	16.45	1.55	-	-	γCHPh(85)
819	7.14	2.73	819	822	υPh(58), δPh(13), γCHPz(12)
761	5.75	7.02	766	766	τPz(55), γCHPz(28)
754	4.25	22.15	752	-	δPz(27), υCC(16), δPh(26)
714	2.77	6.95	712	720	γC=O(33), δPz(27)
702	7.69	0.83	698	705	δPz(32), τPh(16), γC=O(17)
683	3.28	1.09	-	685	τPh(60), γCC(25)
646	14.58	4.44	648	647	δPh(71), υCI(10)
601	0.52	4.21	602	600	γNH(52), τC=O(21)
560	1.13	1.52	562	558	δPz(76)
543	17.33	21.90	-	540	γCN(28), τPh(28), γCC(14)
529	47.48	2.10	530	525	δPh(16), δC=O(21), γCC(11),
476	6.80	2.78	475	-	δPh(39), τPz(31)
429	1.15	0.28	428	-	τPh(63), γCI(23)
422	10.66	1.50	419	420	τPz(36), δCC(19), δCN(18)
399	10.45	0.57	398	-	τPz(53), δCC(18)

B3LYP/cc-pVDZ			IR	Raman	Assignments
$\upsilon(cm^{-1})$	IR_I	R_A	$\upsilon(cm^{-1})$	$\upsilon(cm^{-1})$	
365	3.32	0.77	-	-	γCC(25), τPz(16), τPh(26)
336	3.90	2.80	-	340	τPh(29), γCC(25), δC=O(11)
333	0.31	1.60	-	-	δCN(19), υCI(16), δCC(15)
272	2.06	2.80	-	-	δCC(30), δPh(28), τCH3(25)
209	0.94	5.61	-	215	τPz(35), τPh(32)
199	0.57	2.26	-	197	υCI(38), δCI(23), δPh(20)
176	4.07	3.43	-	177	τNH(26), δCI(19), τCH3(28)
153	1.70	1.74	-	155	τCC(48), γCI(12)
148	0.76	0.66	-	-	τCC(50), γCI(13), τPh(14)
130	0.55	1.84	-	-	δCI(27), τPh(11), τPz(14)
118	0.91	3.56	-	-	τPh(37), τPz(27), τCH3(39)
64	2.85	4.07	-	62	τCC(45), τNH(31)
50	0.54	3.99	-	-	δC=O(30), γCC(14), δNH(12),
34	0.79	1.05	-	-	τC=O(46), τCC(11), τPh(15)
23	0.57	4.44	-	-	τNH(47), τCC(39)

Pz=Pyrazine; Ph-Phhenyl;

Table 3. Second-order perturbation theory analysis Of Fock matrix in NBO basis corresponding to the intramolecular bonds of the title compound

Donor(2i)	type	ED/e	Acceptor(j)	Type	ED/e	E(2)[a]	E(j)-E(i)[b]	F(I,j)[c]
C_1-C_2	σ	1.99242	C_5-C_{10}	σ*	0.07333	0.57	1.1	0.023
C_1-N_6	σ	1.9831	C_5-C_{10}	σ*	0.07333	3.96	1.21	0.063
-	π	1.69267	C_2-N_3	π*	0.34631	20.88	0.29	0.07
-	π	-	C_4-C_5	π*	0.30781	23.83	0.31	0.077
C_2-N_3	π	1.69618	C_1-N_6	π*	0.33281	20	0.3	0.069
-	π	-	C_4-C_5	π*	0.30781	23.4	0.31	0.077
N_3-C_4	σ	1.98525	C_4-C_5	σ*	0.04499	0.84	1.32	0.034
-	σ	-	C_5-C_{10}	σ*	0.07333	3.17	1.21	0.056
C_4-C_5	σ	1.98613	C_5-N_6	σ*	0.02556	0.68	1.18	0.025
-	σ	-	C_5-C_{10}	σ*	0.07333	1.16	1.11	0.033
-	σ	-	C_{10}-O_{11}	σ*	0.02668	1.8	1.21	0.042
-	π	1.6049	C_1-N_6	π*	0.01502	19.24	0.27	0.065
-	π	-	C_2-N_3	π*	0.01734	19.21	0.26	0.064
-	π	-	C_{10}-O_{11}	σ*	0.02668	1.2	0.76	0.03
-	π	-	C_{10}-O_{11}	π*	0.28383	11.03	0.3	0.053
-	π	-	C_{10}-N_{12}	σ*	0.07419	1.81	0.68	0.034
C_5-N_6	σ	1.98208	C_4-C_5	σ*	0.04499	1.07	1.33	0.034
-	σ	-	C_5-C_{10}	σ*	0.07333	0.79	1.21	0.028
-	σ	-	C_{10}-O_{11}	π*	0.28383	0.62	0.86	0.022
-	σ	-	C_{10}-N_{12}	σ*	0.07419	1.23	1.24	0.035
C_5-C_{10}	σ	1.96658	C_1-N_6	σ*	0.01502	4.73	1.12	0.065

Donor(2i)	type	ED/e	Acceptor(j)	Type	ED/e	E(2)[a]	E(j)-E(i)[b]	F(I,j)[c]
-	σ	-	N_3-C_4	σ*	0.01746	3.32	1.11	0.054
-	σ	-	C_4-C_5	σ*	0.04499	0.98	1.15	0.03
-	σ	-	C_5-N_6	σ*	0.02556	0.81	1.11	0.027
-	σ	-	N_{12}-C_{13}	σ*	0.0341	6.05	1.04	0.071
C_{10}-O_{11}	σ	1.98963	C_4-C_5	σ*	0.04499	1.81	1.46	0.046
-	σ	-	C_5-C_{10}	σ*	0.07333	1.11	1.35	0.035
-	π	1.97719	C_4-C_5	π*	0.30781	2.93	0.39	0.033
-	π	-	C_5-N_6	σ*	0.02556	1.15	0.84	0.028
-	π	-	C_{10}-O_{11}	π*	0.28383	0.76	0.41	0.017
C_{10}-N_{12}	σ	1.98625	C_5-N_6	σ*	0.02556	1.34	1.27	0.037
-	σ	-	N_{12}-C_{13}	σ*	0.0341	1.46	1.2	0.037
-	σ	-	C_{13}-C_{15}	σ*	0.02554	2.01	1.35	0.047
N_{12}-C_{13}	σ	1.98296	C_5-C_{10}	σ*	0.07333	2.13	1.16	0.045
-	σ	-	C_{10}-N_{12}	σ*	0.07419	1.14	1.19	0.033
-	σ	-	C_{13}-C_{14}	σ*	0.02367	0.97	1.32	0.032
-	σ	-	C_{13}-C_{15}	σ*	0.02554	0.81	1.13	0.029
-	σ	-	C_{14}-C_{16}	σ*	0.01386	2.02	1.35	0.047
-	σ	-	C_{15}-C_{18}	σ*	0.02139	2.65	1.33	0.053
N_{12}-H_{22}	σ	1.98277	C_{10}-O_{11}	σ*	0.02668	4.09	1.14	0.061
-	σ	-	C_{13}-C_{14}	σ*	0.02367	4.2	1.2	0.063
C_{13}-C_{14}	σ	1.97161	N_{12}-C_{13}	σ*	0.0341	0.89	1.06	0.027
-	σ	-	C_{13}-C_{15}	σ*	0.02554	3.08	1.21	0.054
-	σ	-	C_{14}-C_{16}	σ*	0.01386	1.61	1.25	0.04
C_{13}-C_{15}	σ	1.96286	C_{10}-N_{12}	σ*	0.07419	4.71	1.09	0.064
-	σ	-	N_{12}-C_{13}	σ*	0.0341	0.54	1.06	0.021
-	σ	-	C_{13}-C_{14}	σ*	0.02367	2.66	1.22	0.051
-	σ	-	C_{15}-C_{18}	σ*	0.02139	2.77	1.23	0.052
-	σ	-	C_{18}-I_{27}	σ*	0.04424	3.95	0.74	0.048
C_{14}-C_{16}	σ	1.9755	N_{12}-C_{13}	σ*	0.0341	5.61	1.05	0.069
-	σ	-	C_{13}-C_{14}	σ*	0.02367	1.86	1.21	0.042
-	σ	-	C_{16}-C_{20}	σ*	0.02776	2.15	1.23	0.046
-	σ	-	C_{18}-I_{27}	σ*	0.04424	0.54	0.72	0.018
-	σ	-	C_{20}-C_{23}	σ*	0.01683	4.11	1.07	0.059
C_{15}-C_{18}	σ	1.97713	N_{12}-C_{13}	σ*	0.0341	4.19	1.09	0.06
-	σ	-	C_{13}-C_{15}	σ*	0.02554	2.02	1.24	0.045
-	σ	-	C_{18}-C_{20}	σ*	0.03805	2.62	1.25	0.051
-	σ	-	C_{20}-C_{23}	σ*	0.01683	4.58	1.11	0.064
C_{16}-C_{20}	σ	1.9615	C_{14}-C_{16}	σ*	0.01386	1.74	1.24	0.042
-	σ	-	C_{18}-C_{20}	σ*	0.03805	3.19	1.2	0.055
-	σ	-	C_{18}-I_{27}	σ*	0.04424	5.37	0.72	0.056
-	σ	-	C_{20}-C_{23}	σ*	0.01683	1.15	1.07	0.031
C_{18}-C_{20}	σ	1.97707	C_{15}-C_{18}	σ*	0.02139	2.41	1.24	0.049

Donor(2i)	type	ED/e	Acceptor(j)	Type	ED/e	E(2)[a]	E(j)-E(i)[b]	F(I,j)[c]
-	σ	-	C_{16}-C_{20}	σ*	0.02776	2.01	1.26	0.045
-	σ	-	C_{20}-C_{23}	σ*	0.01683	2.02	1.1	0.042
C_{18}-I_{27}	σ	1.97181	C_{13}-C_{15}	σ*	0.02554	6.14	1	0.07
-	σ	-	C_{16}-C_{20}	σ*	0.02776	6.13	1.03	0.071
C_{20}-C_{23}	σ	1.97834	C_{14}-C_{16}	σ*	0.01386	3.52	1.17	0.057
-	σ	-	C_{15}-C_{18}	σ*	0.02139	4.1	1.15	0.061
-	σ	-	C_{16}-C_{20}	σ*	0.02776	1.28	1.16	0.034
-	σ	-	C_{18}-C_{20}	σ*	0.03805	1.92	1.14	0.042
LPN_3	σ	1.9297	C_1-C_2	σ*	0.03712	9.97	0.84	0.083
-	σ	-	C_4-C_5	σ*	0.04499	10.82	0.84	0.085
LPN_6	σ	1.92814	C_1-C_2	σ*	0.03712	10.13	0.84	0.083
-	σ	-	C_4-C_5	σ*	0.04499	10.77	0.83	0.085
-	σ	-	C_5-C_{10}	σ*	0.07333	2.05	0.72	0.034
LPO_{11}	σ	1.97534	C_5-C_{10}	σ*	0.07333	2.63	1.05	0.048
-	σ	-	C_{10}-N_{12}	σ*	0.07419	2.63	1.07	0.048
-	π	1.8764	C_5-C_{10}	σ*	0.07333	18.42	0.62	0.097
-	π	-	C_{10}-N_{12}	σ*	0.07419	22.62	0.65	0.109
LPN_{12}	σ	1.66033	C_{10}-O_{11}	σ*	0.02668	1.58	0.74	0.033
-	σ	-	C_{10}-O_{11}	π*	0.28383	50.62	0.29	0.109
LPI_{27}	σ	1.99302	C_{15}-C_{18}	σ*	0.02139	1.14	1.13	0.032
-	σ	-	C_{18}-C_{20}	σ*	0.03805	1.2	1.13	0.033
-	π	-	C_{15}-C_{18}	σ*	0.02139	2.01	0.79	0.036

Table 4. NBO results showing the formation of Lewis and non-Lewis orbitals

Bond(A-B)	ED/e[a]	EDA%	EDB%	NBO	s%	p%
σC_1-C_2	1.99242	49.98	50.02	$0.7070(sp^{1.70})C$	37.01	62.99
-	-0.74671	-	-	$+0.7072(sp^{1.70})C$	37.05	62.95
σC_1-N_6	1.98310	39.60	60.40	$0.6293(sp^{2.22})C$	31.10	68.90
-	-0.85493	-	-	$+0.7772(sp^{1.93})N$	34.17	65.83
πC_1-N_6	1.69267	43.75	56.25	$0.6614(sp^{1.00})C$	0.00	100.0
-	-0.33281	-	-	$+0.7500(sp^{1.00})N$	0.00	100.0
σC_2-N_3	1.98707	39.78	60.22	$0.6307(sp^{2.23})C$	30.94	69.06
-	-0.85730	-	-	$+0.7760(sp^{1.90})N$	34.44	65.56
πC_2-N_3	1.69618	43.01	56.99	$0.6558(sp^{1.00})C$	0.00	100.0
-	-0.33504	-	-	$+0.7549(sp^{1.00})N$	0.00	100.0
σN_3-C_4	1.98525	59.85	40.15	$0.7736(sp^{1.91})N$	34.39	65.61
-	-0.85637	-	-	$+0.6337(sp^{2.22})C$	31.03	68.97
σC_4-C_5	1.98613	49.38	50.62	$0.7027(sp^{1.68})C$	37.28	62.72
-	-0.75470	-	-	$+0.7115(sp^{1.71})C$	36.93	63.07
πC_4-C_5	1.60490	48.60	51.40	$0.6972(sp^{1.00})C$	0.01	99.99
-	-0.30576	-	-	$+0.7169(sp^{99.99})C$	0.01	99.99
σC_5-N_6	1.98208	40.50	59.50	$0.6364(sp^{2.24})C$	30.89	69.11
-	-0.85925	-	-	$+0.7713(sp^{1.86})N$	34.93	65.07
σC_5-C_{10}	1.96658	51.75	48.25	$0.7194(sp^{2.11})C$	32.15	67.85
-	-0.67998	-	-	$+0.6946(sp^{1.88})C$	34.72	65.28
σC_{10}-O_{11}	1.98963	34.54	65.46	$0.5877(sp^{2.14})C$	31.89	68.11
-	-0.99557	-	-	$+0.8091(sp^{1.95})O$	33.87	66.13
πC_{10}-O_{11}	1.97719	32.01	67.99	$0.5658(sp^{58.79})C$	1.67	98.33
-	-0.41169	-	-	$+0.8245(sp^{57.54})O$	1.71	98.29
σC_{10}-N_{12}	1.98625	36.25	63.75	$0.6021(sp^{2.15})C$	31.78	68.22
-	-0.84359	-	-	$+0.7984(sp^{1.78})N$	35.95	64.05

σN_{12}-C_{13}	1.98296	62.91	37.09	0.7932($sp^{1.69}$)N	37.17	62.83
-	-0.80884	-	-	+0.6090($sp^{2.67}$)C	27.27	72.73
σN_{12}-H_{22}	1.98277	71.44	28.56	0.8452($sp^{2.73}$)N	26.83	73.17
-	-0.69032	-	-	+0.5345(sp)H	100.0	0.00
σC_{13}-C_{14}	1.97161	51.27	48.73	0.7160($sp^{1.68}$)C	37.29	62.71
-	-0.70384	-	-	+0.6981($sp^{1.96}$)C	33.79	66.21
σC_{13}-C_{15}	1.96286	50.26	49.74	0.7089($sp^{1.83}$)C	35.35	64.65
-	-0.70799	-	-	+0.7053($sp^{1.83}$)C	35.37	64.63
σC_{14}-C_{16}	1.97550	50.03	49.97	0.7073($sp^{1.80}$)C	35.72	64.28
-	-0.69533	-	-	+0.7069($sp^{1.80}$)C	35.70	64.30
πC_{14}-C_{16}	1.66454	50.27	49.73	0.7090($sp^{1.00}$)C	0.00	100.0
-	-0.25694	-	-	+0.7052($sp^{1.00}$)C	0.00	100.0
σC_{15}-C_{18}	1.97713	49.99	50.01	0.7070($sp^{1.75}$)C	36.43	63.57
-	-0.73198	-	-	+0.7072($sp^{1.53}$)C	39.50	60.50
πC_{15}-C_{18}	1.72137	48.10	51.90	0.6935($sp^{1.00}$)C	0.00	100.0
-	-0.28163	-	-	+0.7204($sp^{1.00}$)C	0.00	100.0
σC_{16}-C_{20}	1.96150	49.30	50.70	0.7022($sp^{1.77}$)C	36.11	63.89
-	-0.69114	-	-	+0.7120($sp^{1.93}$)C	34.08	65.92
σC_{18}-C_{20}	1.97707	50.40	49.60	0.7100($sp^{1.43}$)C	41.14	58.86
-	-0.72486	-	-	+0.7042($sp^{1.94}$)C	34.02	65.98
σC_{18}-I_{27}	1.97181	53.64	46.36	0.7324($sp^{4.08}$)C	19.69	80.31
-	-0.49613	-	-	+0.6809($sp^{8.62}$)I	10.40	89.60
σC_{20}-C_{23}	1.97834	50.91	49.09	0.7135($sp^{2.14}$)C	31.88	68.12
-	-0.62828	-	-	+0.7006($sp^{2.35}$)C	29.86	70.14
n_1 N_3	1.92970	-	-	$sp^{2.20}$	31.22	68.78
-	-0.36938	-	-	-	-	-
n_1 N_6	1.92814	-	-	$sp^{2.23}$	30.94	69.06
-	-0.36351	-	-	-	-	-
n_1 O_{11}	1.97534	-	-	$sp^{0.55}$	64.41	35.59
-	-0.69703	-	-	-	-	-

$n_2 O_{11}$	1.87640	-	-	$sp^{99.99}$	0.05	99.95
-	-0.26915	-	-	-	-	-
$n_1 N_{12}$	1.66033	-	-	$sp^{99.99}$	0.06	99.94
-	-0.29132	-	-	-	-	-
$n_1 C_{13}$	1.02319	-	-	$sp^{1.00}$	0.00	100.0
-	-0.13407	-	-	-	-	-
$n_1 I_{27}$	1.99302	-	-	$sp^{0.12}$	10.49	89.51
-	-0.61594	-	-	-	-	-
$n_2 I_{27}$	1.97761	-	-	$sp^{99.99}$	0.13	99.87
-	-0.27127	-	-	-	-	-
$n_3 I_{27}$	1.95133	-	-	$sp^{1.00}$	0.00	100.0
-	-0.26950	-	-	-	-	-

Table 5 The binding affinity values of different poses of the title compound predicted by AutoDock Vina

Mode	Affinity(Kcal/mole)	Distance from best mode(Å)	
-	-	RMSD l.b	RMSD u.b
1	-6.6	0.000	0.000
2	-6.2	21.414	24.151
3	-6.2	1.487	2.080
4	-6.0	21.754	24.426
5	-5.6	18.358	20.149
6	-5.5	26.367	27.361
7	-5.4	21.945	24.695
8	-5.4	22.683	25.091
9	-5.4	3.071	6.994

3.6 References

[1] H. I. Boshoff, V. Mizrahi, C. E. Barry III, Effects of pyrazinamide on fatty acid synthesis by whole mycobacterial cells and purified fatty acid synthase I, J. Bacteriol. 184 (2002) 2167-2172.

[2] M. Njire, Y. Tan, J. Mugweru, C. Wang, J. Guo, W. W. Yew, S. Tan, T. Zhang, Pyrazinamide resistance in Mycobacterium tuberculosis: review and update, Adv. Med. Sci. 61 (2016) 63-71.

[3] A. N. Unissa, L. E. Hanna, S. Swaminathan, A note on derivatives of Isoniazid, Rifampicin, and Pyrazinamide showing activity against resistant Mycobacte-rium tuberculosis, Chem. Biol. Drug. Des. 87 (2016) 537-550.

[4] J. Zitko, P. Paterova, V. Kubícek, J. Mandíkova, F. Trejtnar, J. Kunes, M. Dolezal, Synthesis and antimycobacterial evaluation of pyrazinamide derivatives with benzylamino substitution, Bioorg. Med. Chem. Lett. 23 (2013) 476-479.

[5] T. S. Chitre, K. D. Asgaonkar, P. B. Miniyar, A. B. Dharme, M. A. Arkile, A. Yeware, D. Sarkar, V. M. Khedkar, P. C. Jha, Synthesis and docking studies of pyrazine-thiazolidinone hybrid scaffold targeting dormant tuberculosis, Bioorg. Med. Chem. Lett. 26 (2016) 2224-2228.

[6] D. Sriram, P. Yogeeswari, S. P. Reddy, Synthesis of pyrazinamide Mannich bases and its antitubercular properties, Bioorg. Med. Chem. Lett. 16 (2006) 2113-2116.

[7] M. Abdel-Aziz, H. M. Abdel-Rahman, Synthesis and anti-mycobacterial evaluation of some pyrazine-2-carboxylic acid hydrazide derivatives, Eur. J. Med. Chem. 45 (2010) 3384-3388.

[8] M. Dolezal, P. Cmedlova, L. Palek, J. Vinsova, J. Kunes, V. Buchta, J. Jampilek, K.Kralova, Synthesis and anti-mycobacterial evaluation of substituted pyrazinecarboxamides, Eur. J. Med. Chem. 43 (2008) 1105-1113.

[9] M. Saudi, J. Zmurko, S. Kaptein, J. Rozenski, J. Neyts, A. V. Aerschot, Synthesis and evaluation of imidazole-4,5- and pyrazine-2,3-dicarboxamides targeting dengue and yellow fever virus, Eur. J. Med. Chem. 87 (2014) 529-539.

[10] S. Velazquez, S. De Castro, J. Balzarini, M.J. Camarasa, From b-amino-g-sultone to new bicyclic pyridine and pyrazine heterocyclic systems: discovery of a novel class of HIV-1 non-nucleoside inhibitors, Anti-vir. Res. 82 (2009) A26-A27.

[11] H. Zhang, Y. Wang, P. Zhu, J. Liu, S. Xu, H. Yao, J. Jiang, W. Ye, X. Wu, J. Xu, Design, synthesis and antitumor activity of triterpenoid pyrazine derivatives from 23-hydroxybetulinic acid, Eur. J. Med. Chem. 97 (2015) 235-244.

[12] L. Racane, S. K. Pavelic, I. Ratkaj, V. Stepanic, K. Pavelic, V. Tralic-Kulenovic, G. Karminski-Zamola, Synthesis and antiproliferative evaluation of some new amidino-substituted bis-benzothiazolyl-pyridines and pyrazine, Eur. J. Med. Chem. 55 (2012) 108-116.

[13] Y. B. Zhang, X. L. Wang, W. Liu, Y. S. Yang, J. F. Tang, H. L. Zhu, Design, synthesis and biological evaluation of heterocyclic azoles derivatives containing pyrazine moiety as potential telomerase inhibitors, Bioorg. Med. Chem. 20 (2012) 6356-6365.

[14] C. G. Bonde, N. J. Gaikwad, Synthesis and preliminary evaluation of some pyr-azine containing thiazolines and thiazolidinones as antimicrobial agents, Bioorg. Med. Chem. 12 (2004) 2151-2161.

[15] Y. K. Zhang, J. J. Plattner, E. E. Easom, R. T. Jacobs, D. Guo, V. Sanders, Y. R. Freund, B. Campo, P. J. Rosenthal, W. Bu, F. J. Gamo, L. M. Sanz, M. Ge, L. Li, J. Ding, Y. Yang, Benzoxaborole anti-malarial agents. Part 4. Discovery of potent 6-(2-(alkoxycarbonyl)pyrazinyl-5-oxy)-1,3-dihydro-1-hydroxy-2,1-benzoxaboroles, J. Med. Chem. 58 (2015) 5344-5354.

[16] R. Rahmani, K. Ban, A. J. Jones, L. Ferrins, D. Ganame, M. L. Sykes, V. M. Avery, K. L. White, E. Ryan, M. Kaiser, S. A. Charman, J. B. Baell, 6-Arylpyrazine-2-carboxamides: a new core for trypanosoma brucei inhibitors, J. Med. Chem. 58 (2015) 6753-6765.

[17] M. Tomizawa, S. Kagabu, I. Ohno, K. A. Durkin, J. E. Casida, Potency and selectivity of trifluoro acetylimino and pyrazinoylimino nicotinic insecticides and their fit at a unique binding site Niche, J. Med. Chem. 51 (2008) 4213-4218.

[18] B. Gao, Q. Zhou, Y. Geng, Y. Cheng, D. Ma, Z. Xie, L. Wang, F. Wang, New fluorescent dipolar pyrazine derivatives for non-doped red organic light-emitting diodes, Mater. Chem. Phys. 99 (2006) 247-252.

[19] G. Ge, J. He, H. Guo, F. Wang, D. Zou, Highly efficient phosphorescent iridium (III) diazine complexes for OLEDs: different photophysical property between iridium III) pyrazine complex and iridium (III) pyrimidine complex, J. Organomet. Chem. 694 (2009) 3050-3057.

[20] M. Abdallah, M. Sobhi, H.M. Al-Tass, Corrosion inhibition of aluminum in hydrochloric acid by pyrazinamide derivatives, J. Mol. Liq. 223 (2016) 1143-1150.

[21] M. Kissi, M. Bouklah, B. Hammouti, M. Benkaddour, Establishment of equiv-alent circuits from electrochemical impedance spectroscopy study of corrosion inhibition of steel by pyrazine in sulphuric acidic solution, App. Surf. Sci. 252 (2006) 4190-4197.

[22] X. Li, S. Deng, H. Fu, Three pyrazine derivatives as corrosion inhibitors for steel in 1.0 M H2SO4 solution, Corros. Sci. 53 (2011) 3241-3247.

[23] M. Dolezal, J. Zitko, D. Kesetovicova, J. Kunes, M. Svobodova, Substituted N-phenylpyrazine-2-carboxamides: synthesis and antimycobacterial evaluation, Molecules 14 (2009) 4180-4189.

[24] J. Zitko, B. Servusova, P. Paterova, J. Mandikova, V. Kubicek, R. Kucera, V.Hrabcova, J. Kunes, O. Soukup, M. Dolezal, Synthesis, antimycobacterial activity and in vitro cytotoxicity of 5-Chloro-N-phenylpyrazine-2-carboxamides, Molecules 18 (2013) 14807-14825.

[25] B. Servusova, J. Vobickova, P. Paterova, V. Kubicek, J. Kunes, M. Dolezal, J. Zitko, Synthesis and antimycobacterial evaluation of N-substituted-5-chloropyrazine-2-carboxamide, Bioorg. Med. Chem. Lett. 23 (2013) 3589-3591.

[26] B. Abramovic, S. Kler, D. Sojic, M. Lausevic, T. Radovic, D. Vione, Photocatalytic degradation of metoprolol tartrate in suspensions of two TiO2-based photo-catalysts with different surface area. Identification of intermediates and proposal of degradation pathways, J. Hazard. Mater 198 (2011) 123-132.

[27] S. J. Armakovic, S. Armakovic, N. L. Fincur, F. Sibul, D. Vione, J. P. Setrajcic, B. Abramovic, Influence of electron acceptors on the kinetics of metoprolol photocatalytic degradation in TiO2 suspension. A combined experimental and theoretical study, RSC Adv. 5 (2015) 54589-54604.

[28] J. Molnar, J. Agbaba, B. Dalmacija, M. Klasnja, M. Watson, M. Kragulj, Effects of ozonation and catalytic ozonation on the removal of natural organic matter from groundwater, J. Environ. Eng. 138 (2012) 804-808.

[29] J. J. Molnar, J. R. Agbaba, B. D. Dalmacija, M. T. Klasnja, M. B. Dalmacija, M. M. Kragulj, A comparative study of the effects of ozonation and TiO2-catalyzed ozonation on the selected chlorine disinfection by-product precursor content and structure, Sci. Total Environ. 425 (2012) 169-175.

[30] D. V. Sojic,D. Z. Orcic, D. D. Cetojevic-Simin, N. D. Banic, B. F. Abramovic, Efficiremoval of sulcotrione and its formulated compound Tangenta in aqueous TiO_2

suspension: stability, photoproducts assessment and toxicity, Chemosphere 138 (2015) 988-994.

[31] D. V. Sojic, D. Z. Orcic, D. D. Cetojevic-Simin, V. N. Despotovic, B. F. Abramovic, Kinetics and the mechanism of the photocatalytic degradation of mesotrio in aqueous suspension and toxicity of its degradation mixtures, J. Mol. Catal. A Chem. 392 (2014) 67-75.

[32] D. D. Cetojevic-Simin, S. J. Armakovic, D. V. Sojic, B. F. Abramovic, Toxicity assessment of metoprolol and its photo degradation mixtures obtained by using different type of TiO_2 catalysts in the mammalian cell lines, Sci. Total Environ. 463 (2013) 968-974.

[33] P. Lienard, J. Gavartin, G. Boccardi, M. Meunier, Predicting drug autoxidation, Pharm. Res. 32 (2015) 300-310.

[34] G. L. C. de Souza, L. M. F. de Oliveira, R. G. Vicari, A. Brown, A DFT investigation on the structural and antioxidant properties of new isolated interglycosidic O-(1/3) linkage flavonols, J. Mol. Model 22 (2016) 1-9.

[35] Z. Sroka, B. Zbikowska, J. Hładyszowski, The anti-radical activity of some selected flavones and flavonols. Experimental and quantum mechanical study. J. Mol. Model 21 (2015) 1-11.

[36] H. Djeradi, A. Rahmouni, A. Cheriti, Antioxidant activity of flavonoids: a modeling using Fukui indices descriptors, J. Mol. Model 20 (2014) 1-9.

[37] M. J. Frisch, G. W. Trucks, H. B. Schlegel, G. E. Scuseria, M. A. Robb, J. R. Cheeseman, G. Scalmani, V. Barone, B. Mennucci, G. A. Petersson H. Nakatsuji, M. Caricato, X. Li, H. P. Hratchian, A. F. Izmaylov, J. Bloino, G. Zheng, J. L. Sonneberg, M. Hada, M. Ehara, K. Toyota, R. Fukuda, J. Hasegawa,M. Ishida, T. Nakajima, Y. Honda, O.Kitao, H. Nakai, T. Vreven,J.A. Montgomery, J.E. Peralta, F. Ogliaro, M. Bearpark, J. J. Heyd, E. Brothers, K. N. Kudin, V. N. Staroverov, T. Keith, R. Kobayashi, J. Normand, K. Raghavachari, A. Rendell, J. C. Knox, J. B. Cross,V. Bakken, C. Adamo, J. Jaramillo, R. Gomperts, R. E. Stratmann, O. Yazyev, A. J. Austin, R. Cammi, C. Pomelli, J. W. Ochterski, R. L. Martin, K. Morokuma, V. G. Zakrzewski, G. A. Voth, P. Salvador, J. J. Dannenberg, S. Dapprich, A. D. Daniels, O. Farkas, J. B. Foresman, J. V. Ortiz, J. Cioslowski, D. J. Fox, Gaussian 09, Revision B.01, Gaussian Inc., Wallingford CT, 2010.

[38] J. B. Foresman, in: E. Frisch (Ed.), Exploring Chemistry with Electronic Struc-ture Methods, A Guide to Using Gaussian, Pittsburg, PA, 1996.

[39] J. M. L. Martin, C. Van Alsenoy, GAR2PED, a Program to Obtain a Potential En-ergy Distribution from a Gaussian Archive Record, University of Antwerp, Belgium, 2007.

[40] R. Dennington, T. Keith, J. Millam, Gaussview, Version 5, Semichem Inc., Shawnee Missions KS, 2009.

[41] A. D. Bochevarov, E. Harder, T. F. Hughes, J. R. Greenwood, D.A. Braden, D. M. Philipp, D. Rinaldo, M. D. Halls, J. Zhang, R. A. Friesner, Jaguar: a high-performance quantum chemistry software program with strengths in life and materials sciences, Int. J. Quantum Chem. 113 (18) (2013) 2110-2142.

[42] D. Shivakumar, J. Williams, Y. Wu, W. Damm, J. Shelley, W. Sherman, Pre-diction of absolute solvation free energies using molecular dynamics free energy perturbation and the OPLS force field, J. Chem. Theory Comput. 6 (2010) 1509-1519.

[43] Z. Guo, U. Mohanty, J. Noehre, T. K. Sawyer, W. Sherman, G. Krilov, Probing the a-helical structural stability of stapled p53 peptides: molecular dynamics simulations and analysis, Chem. Biol. Drug. Des. 75 (2010) 348-359.

[44] I. Fabijanic, C. J. Brala, V. Pilepic, The DFT local reactivity descriptors of a-tocopherol, J. Mol. Model 21 (2015) 1-7.

[45] A. D. Becke, Density-functional thermochemistry. III. The role of exact ex-change, J. Chem. Phys. 98 (1993) 5648-5652.

[46] J. L. Banks, H. S. Beard, Y. Cao, A. E. Cho, W. Damm, R. Farid, A. K. Felts, T. A. Halgren, D. T. Mainz, J. R. Maple, R. Murphy, D. M. Philippe, M. P. Repasky, L. Y. Zhang, B. J. Berine, R. A. Friesnery, E. Gallicchio, R. M. Levy, Integrated modeling program, applied chemical theory (IMPACT), J. Comput. Chem. 26 (2005) 1752-1780.

[47] H. J. C. Berendsen, J. P. M. Postma, W. F. van Gunsteren, J. Hermans, Interaction Models for Water in Relation to Protein Hydration, in Intermolecular Forces, Springer, 1981, 331-342.

[48] A. Otero-de-la-Roza, E. R. Johnson, J. Contreras-García, Revealing non-covalent interactions in solids: NCI plots revisited, Phys. Chem. Chem. Phys. 14 (2012) 12165-12172.

[49] E. R. Johnson, S. Keinan, P. Mori-Sanchez, J. Contreras-Garcia, A. J. Cohen, W. Yang, Revealing non-covalent interactions, J. Am. Chem. Soc. 132 (2010) 6498-6506.

[50] Schrodinger€ Release 2015-4: Maestro, Version 10.4, Schrodinger, LLC, New York, NY, 2015.

[51] T. Joseph, H. T. Varghese, C. Y. Panicker, K. Viswanathan, M. Dolezal, C. Van Alsenoy, Spectroscopic (FT-IR, FT-Raman), first order hyperpolarizability, NBO

analysis, HOMO and LUMO analysis of N-[(4-(trifluoromethyl)phenyl] doi.org/10.1016/j.arabjc.2013.08.004.

[52] W. He, G. Zhou, J. Li, A. Tian, Molecular design of analogues of 2,6-diamino-3,5-dinitropyrazine-1-oxide, J. Mol. Struct. THEOCHEM 668 (2004) 201-208.

[53] N. P. G. Roeges, A Guide to the Complete Interpretation of Infrared Spectra of Organic Structures, Wiley, New York, 1994.

[54] N. B. Colthup, L. H. Daly, S. E. Wiberly, Introduction to Infrared and Raman Spectroscopy, 2, Academic Press, New York, 1975.

[55] G. Varsanyi, Assignments of Vibrational Spectra of Seven Hundred Benzene Derivatives, Wiley, New York, 1974.

[56] Y. S. Mary, C. Y. Panicker, H. T. Varghese, K. Raju, T. E. Bolelli, I. Yildiz, C. M. Granadeiro, H. I. S. Nogueiro, Vibrational spectroscopic studies and computational study of 4-fluoro-N-(2'-hydroxy-4'-nitrophenyl)phenyl-acetamide, J. Mol. Struct. 994 (2011) 223-231.

[57] M. Barthes, G. De Nunzio, M. Ribet, Polarons or proton transfer in chains of peptide groups ? Synth. Met. 76 (1996) 337-340.

[58] J. Lukose, C. Y. Panicker, P. S. Nayak, B. Narayana, B. K. Sarojini, C. Van Alsenoy, A. A. Al-Saadi, Synthesis, structural and vibrational investigation on 2-phenyl-N-(pyrazine-2-yl)acetamide combining XRD diffraction, FT-IR and NMR spectroscopies with DFT calculations, Spectrochim. Acta A 135 (2015) 608-616.

[59] E. Loh, Raman spectra of iodine derivatives of tyrosine and thyronine, J. Raman Spectrosc. 3 (1975) 327-333.

[60] R. A. Yadav, J. S. Singh, O. Sala, The Raman and infrared spectra and normal coordinate analysis for 1,2-diiodotetraflurobenzene, J. Raman Spectrosc. 14 (1983) 353-357.

[61] D. A. Zainuri, S. Arshad, N. C. Khalib, I. A. Razak, R. R. Pillai, S. F. Sulaiman, N. S. Hashim, K. L. Ooi, S. Armakovic, S. J. Armakovic, C. Y. Panicker, synthesis, XRD crystal structure, spectroscopic characterization (FT-IR, 1H and 13C NMR), DFT studies, chemical reactivity and bond dissociation energy studies using molecular dynamics simulations and evaluation of antimicrobial and antioxidant activities of a novel chalcone derivative, (E)-1-(4-bromophenyl)-3-(4-iodophenyl)prop-2-en-1-one, J. Mol. Struct. 1128 (2017) 520-533.

[62] J. Coats, R. A. Meyers (Eds.), Encyclopedia of Analytical Chemistry, Interpre-tation of Infrared Spectra, a Practical Approach, John Wiley and Sons, Chi-chester, 2000.

[63] R. I. Al-Wabli, K. S. Resmi, Y. S. Mary, C. Y. Panicker, M. I. Attia, A. A. El-Emam, C. Van Alsenoy, Vibrational spectroscopic studies, Fukui functions, HOMO-LUMO, NLO, NBO analysis and molecular docking study of (E)-1-(1,3-benzodioxol-5-yl)-4,4-dimethylpent-1-en-3-one, a potential precursor to bioactive agents, J. Mol. Struct. 1123 (2016) 375-383.

[64] D. Philip, A. John, C.Y. Panicker, H.T. Varghese, FT-Raman, FT-IR and surface enhanced Raman scattering spectra of sodium salicylate, Spectrochim. Acta A 57 (2001) 1561-1566.

[65] J. F. Arenas, J. T. I. Navarrete, J. C. Ottero, J. I. Marcos, A. Cardenete, Vibrational spectra of [1H4]pyrazine and [2H4] pyrazine, J. Chem. Soc. Faraday Trans. 2 (81) (1985) 405-415.

[66] H. Endredi, F. Billes, F. S. Holly, Vibrational spectroscopical and quantum chemical study of the chlorine substitution of pyrazine, J. Mol. Struct. THEO-CHEM 633 (2003) 73-82.

[67] J. Lukose, C. Y. Panicker, P. S. Nayak, B. Narayana, B. K. Sarojini, C. Van Alsenoy, A. A. Al-Saadi, Synthesis, structural and vibrational investigation on 2-phenyl-N-(pyrazine-2-yl)acetamide combining XRD diffraction, FT-IR and NMR spectroscopies with DFT calculations, Spectrochim. Acta A 135 (2015) 608-616.

[68] E. D. Glendening, A. E. Reed, J. E. Carpenter, F. Weinhold, NBO Version 3.1, TCI, University of Wisconsin, Madison, 1998.

[69] M. Adant, M. Dupuis, J. L. Bredas, Ab initio study of the nonlinear optical properties of urea: electron correlation and dispersion effects, Int. J. Quantum. Chem. 56 (1995) 497-507.

[70] K. Fukui, Role of frontier orbitals in chemical reactions, Science 218 (1982) 747-754.

[71] R. G. Parr, R. G. Pearson, Absolute hardness: companion parameter to absolute electronegativity, J. Am. Chem. Soc. 105 (1983) 7512-7516.

[72] T. Joseph, H. T. Varghese, C. Y. Panicker, K. Viswanathan, M. Dolezal, T. K. Manojkumar, C. Van Alsenoy, Vibrational spectroscopic investigations and computational study of 5-tert-Butyl-N-(-trifluoromethylphenyl)pyrazine-2-carboxamide, Spectrochim. Acta 113 (2013) 203-214.

[73] E. Scrocco, J. Tomasi, Electronic molecular structure, reactivity and intermo-lecular forces: aneuristic Interpretation by means of electrostatic Molecular Potentials, Adv. Quantum. Chem. 103 (1978) 115-193.

[74] F. J. Luque, J. M. Lopez, M. Orozco, Perspective on electrostatic interactions of a solute with a continuum a direct utilization of ab initio molecular potentials for the prevision of solvent effect, Theor. Chem. Acc. 103 (2001) 343-345.

[75] P. Politzer, J. S. Murray, A comprehensive survey, protein, in: D.L. Beveridge, R.Lavery (Eds.), Chap. 13 Theoretical Biochemistry and Molecular Biophysics, vol. 2, Adenine Press, Schenectady, NY, 1991.

[76] E. Scrocco, J. Tomasi, The electrostatic molecular potential as a tool for the interpretation of molecular properties, Top. Curr. Chem. 42 (1973) 95-170.

[77] J. S. Murray, J. M. Seminario, P. Politzer, P. Sjoberg, Average local ionization energies computed on the surfaces of some strained molecules, Int. J. Quan-tum Chem. 38 (1990) 645-653.

[78] P. Politzer, F. Abu-Awwad, J. S. Murray, Comparison of density functional and Hartree-Fock average local ionization energies on molecular surfaces, Int. J. Quantum Chem. 69 (1998) 607-613.

[79] A. Michalak, F. De Proft, P. Geerlings, R. Nalewajski, Fukui functions from the relaxed Kohn-Sham orbitals, J. Phys. Chem. A 103 (1999) 762-771.

[80] X. Ren, Y. Sun, X. Fu, L. Zhu, Z. Cui, DFT comparison of the OH-initiated degradation mechanisms for five chlorophenoxy herbicides, J. Mol. Model 19 (2013) 2249-2263.

[81] L.-l. Ai, J.-y. Liu, Mechanism of OH-initiated atmospheric oxidation of E/Z-CF3CF¼ CFCF3: a quantum mechanical study, J. Mol. Model 20 (2014) 2179.

[82] W. Sang-aroon, V. Amornkitbamrung, V. Ruangpornvisuti, A density functional theory study on peptide bond cleavage at aspartic residues: direct vs cyclic intermediate hydrolysis, J. Mol. Model 19 (2013) 5501-5513.

[83] J. Kieffer, E. Bremond, P. Lienard, G. Boccardi, In silico assessment of drug substances chemical stability, J. Mol. Struct. THEOCHEM 954 (2010) 75-79.

[84] J. S. Wright, H. Shadnia, L. L. Chepelev, Stability of carbon-centered radicals: effect of functional groups on the energetics of addition of molecular oxygen, J. Comput. Chem. 30 (2009) 1016-1026.

[85] G. Gryn'ova, J. L. Hodgson, M. L. Coote, Revising the mechanism of polymer autoxidation, Org. Biomol. Chem. 9 (2011) 480-490.

[86] P. Lienard, J. Gavartin, G. Boccardi, M. Meunier, Predicting drug substances autoxidation, Pharm. Res. 32 (2015) 300-310.

[87] T. Andersson, A. Broo, E. Evertsson, Prediction of drug candidates' sensitivity toward autoxidation: computational estimation of C H dissociation energies of carbon-centered radicals, J. Pharm. Sci. 103 (2014) 1949-1955.

[88] R. V. Vaz, J. R. B. Gomes, C. M. Silva, Molecular dynamics simulation of diffusion coefficients and structural properties of ketones in supercritical CO2 at infinite dilution, J. Supercritic. Fluids 107 (2016) 630-638.

[89] C. M. Niswender, P. J. Conn, Metabotropic glutamate receptors: physiology, pharmacology and disease, Ann. Rev. Pharmacol. Toxicol. 50 (2010) 295-322.

[90] O. Trott, A. J. Olson, AutoDock Vina: improving the speed and accuracy of docking with a new scoring function, efficient optimization and multi-threading, J. Comput. Chem. 31 (2010) 455-461.

[91] A. Wehenkel, P. Fernandez, M. Bellinzoni, V. Catherinot, N. Barilone, G.Labesse, M. Jackson, P.M. Alzari, The structure of PknB in complex with mitoxantrone, an ATP-competitive inhibitor, suggests a mode of protein ki-nase regulation in mycobacteria, FEBS Lett. 580 (2006) 3018-3022.

[92] P. S. Shana, M. A. Al-Alshaikh, C. Y. Panicker, A. A. El-Emam, M. Arisoy, O. Temiz-Arpaci, C. Van Alsenoy, Synthesis, vibrational spectroscopic investigations, molecular docking, anti-bacterial and anti-microbial studies of 5-ethyl-sulphonyl-2-(p-aminophenyl) benzoxazole, J. Mol. Struct. 1115 (2016) 94-104.

CHAPTER IV
SPECTROSCOPIC INVESTIGATIONS (IR, RAMAN), DFT CALCULATIONS, WITH NBO, MEP, HOMO-LUMO, NLO AND MOLECULAR DOCKING STUDIES OF3-[(4-CARBOXYPHENYL)CARBAMOYL]-4-HYDROXY-2-OXO-1,2-DIHYDROXY QUINOLINE-6-CARBOXYLIC ACID.

4.1 Introduction

Quinoline derivatives possess number of medicinal properties like anti-bacterial [1] anti-filarial [2] anti-malerial [3] anti-fungal [4] cardiovascular [5] anti-tuberculosis [6]. 8-hydroxy quinolone derivative can be used as an active compound of pharmaceutical product [7] nuclear medicine [8] treating cancer [9] and neurodegeneration disorder [10]. Recent years DFT, molecular docking and vibrational studies of quinolone derivatives are reported [11, 12]. Some quinolone derivatives are used as lifesaving drugs and have many applications like optical switches sensors in electro chemistry and in the area of inorganic chemistry [13, 14]. Amino quinoline derivatives are a good candidate for the inhibition of human immuno virus (HIV) [15]. In order to analyse the effect of halogen substitution, in the parent molecule the hydrogen atoms 7H, 8H and 9H are replaced by chlorine, fluorine and bromine atoms which are designated as 7Cl, 8Cl, 9Cl for chlorine, 7F, 8F, 9F for fluorine and 7Br, 8Br, 9Br for bromine, respectively.

4.2 Experimental Details

3-[(4-Carboxyphenyl) carbamoyl]-4-hydroxy-2-oxo-1,2-dihydroquinoline-6-carboxylic acid was prepared by a microwave-assisted reaction of 4-aminobenzoic acid with triethyl methanetricarboxylate [16] (Scheme 1). All reagents were purchased from Aldrich. Kieselgel 60, 0.040-0.063 mm (Merck, Darmstadt, Germany) was used for column chromatography. TLC experiments were performed on alumina-backed silica gel 40 F254 plates (Merck). The plates were illuminated under UV (254 nm) and evaluated in iodine vapour. The melting points were determined on Boetius PHMK 05 (VEB Kombinat Nagema, Radebeul, Germany) and are uncorrected. Elemental analyses were carried out on an automatic Perkin-Elmer 240 microanalyser (Boston, USA). The purity of the final compounds was checked by the HPLC separation module Waters Alliance 2695 XE (Waters Corp., Milford, MA, USA). The detection wavelength 210 nm was chosen. The peaks in the chromatogram of the solvent (blank) were deducted from the peaks in the chromatogram of the sample solution. The purity of individual compounds was determined from the area peaks in the chromatogram of the sample solution. UV spectra (λ, nm) were determined on a Waters Photodiode Array Detector 2996 (Waters

Corp.) in ca 6×10^{-4} mol methanolic solution and log ε (the logarithm of molar absorption coefficient ε) was calculated for the absolute maximum λ_{max} of individual target compounds. All ^{1}H NMR spectra were recorded on a Bruker AM-500 (499.95 MHz for ^{1}H), Bruker Bio Spin Corp., Germany. Chemicals shifts are reported in ppm (δ) to internal $Si(CH_3)_4$, when diffused easily exchangeable signals are omitted.

3-[(4-Carboxyphenyl) carbamoyl]-4-hydroxy-2-oxo-1,2-dihydroquinoline-6-carboxylic acid

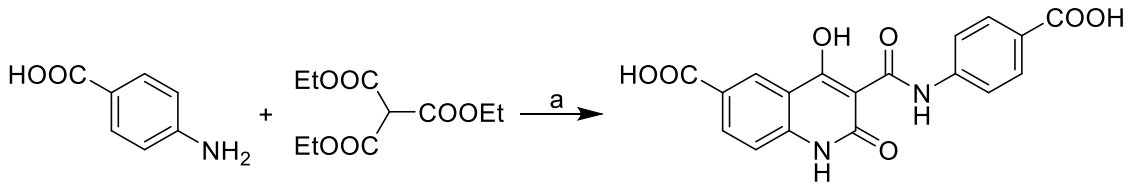

Scheme 1. Preparation of the target compound: (a) microwave irradiation

4-Aminobenzoic acid (0.7 g, 0.005 mol) was mixed with triethyl methanetricarboxylate (2.12 mL, 0.01 mol) and heated in microwave reactor at 50% of power during 15 min and 3 min at 90%. The temperature reached 231 °C during heating. Et_2O was added to the cooled mixture and the precipitate was washed with hot (55 °C) MeOH to obtain the pure product as a yellow crystalline compound. Yield 62%. Mp 340-350 °C. Anal. Calc. for $C_{18}H_{12}N_2O_7$ (368.29): C 58.70%, H 3.28%; found: C 58.09%, H 3.54%. HPLC purity 97.52%. UV (nm), λ_{max}/log ε: 251.3/3.53. IR (cm^{-1}): 3621, 1180 (OH), 3034 (CH_{arom}), 2970, 1689 (acid), 1680 (lactam), 1642 (C=O), 1635 ($C=C_{cycle}$), 1630 (amide), 1599 (Ph), 1520 (NH). ^{1}H NMR (DMSO-*d*$_6$, 500 MHz) δ: 7.41 (d, *J*=8.5 Hz, 1H), 7.70 (d, *J*=9.1 Hz, 2H), 7.90 (d, *J*=9.1 Hz, 2H), 8.15 (d, *J*=8.5 Hz, 1H), 8.50 (s, 1H), 12.40 (s, 1H), 12.95 (s, 1H), 16 (s, 1H).

The FT-IR spectrum (Fig.1) was recorded using KBr pellets on a DR/Jasco FT-IR 6300 spectrometer. The FT-Raman spectrum (Fig. 2) was obtained on a Bruker RFS 100/s, Germany. For excitation of the spectrum the emission of Nd:YAG laser was used, excitation wavelength 1064 nm, maximal power 150mW, measurement on solid sample.

4.3 Computational Details

Calculations of the wavenumbers, molecular geometry, polarizability values, frontier molecular orbital analysis were carried out with Gaussian 09 program [17] using the B3LYP/6-311++G(d,p) quantum chemical calculation method. A scaling factor of 0.9613 is used to scale the theoretically obtained wavenumbers [18] and the assignments of the vibrational wavenumbers are done by using GaussView [19] and GAR2PED software [20]. Parameters corresponding to optimized geometry of the title compound (Fig. 3) are given in Table 1.

4.4 Results and Discussions

4.4.1 Optimized Geometrical Parameters

For the title compound the bond lengths of C_2-C_3 = 1.4084 Å, C_3-C_4 = 1.4130 Å and C_4-C_5 = 1.4045 Å and these values are greater than that of C_1-C_2 (1.3824 Å) and C_5-C_6 (1.3916 Å) due to adjacent quinoline ring and the reported values are C_2-C_3 = 1.4020 Å, C_3-C_4 = 1.4171 Å, C_5-C_4 = 1.4043 Å [21]. The values of bond lengths C_{12}-C_{14} (1.4579 Å) and C_{14}-C_{18} (1.4854 Å) are high which is due to the adjacent C=O and carboxylic groups. The bond angle C_3-C_4-C_5 (119.5°) is lesser than 120° because of the presence of quinoline ring. The angles C_4-C_{13}-C_{14} and C_3-N_{10}-C_{12} are 121.2° and 126.0° respectively, which can be assumed as due to the presence of OH group which is electropositive. According to literature the corresponding reported bond angles are C_1-C_2-C_3 (119.6°), C_2-C_3-C_4 (119.4°), C_2-N_{14}-C_{20} (125.8°), C_3-C_{15}-C_{18} (121.3°) and N_{14}-C_{20}-C_{18} (114.2°) respectively [22]. The presence of higher electro negative group C=O would be the reason for the greater bond angle of N_{10}-C_{12}-C_{14} (116.0°).

4.4.2 IR and Raman Spectra

The observed IR and Raman bands and calculated (scaled) wavenumbers and assignments are given in Table 2. The C_{12}=O_{16} and C_{13}=C_{14} stretching vibrations are assigned at 1678 cm^{-1} (DFT), 1670 cm^{-1} (IR) and at 1562 cm^{-1} (DFT), 1551 cm^{-1} (IR), 1548 cm^{-1} (Raman) respectively. The C=O stretching mode has high IR intensity and PED of 37%. The C=O stretching vibration in the spectra of carboxylic acid give rise to strong bands in the region 1600-1700 cm^{-1} [23]. The bands observed at 1746, 1741 cm^{-1}theoretically with IR intensities 362.66, 401.22, Raman activities 269.81, 1619.61 and with PEDs of 73, 72% are assigned as C_{35}=O_{36}, C_{31}=C_{32} stretching modes of the title compound. The stretching band of C_{13}-O_{15} is expected in the region 1220 ± 40 cm^{-1} [24-26] and the band at 1292 cm^{-1} (DFT) is assigned as C-O stretching vibration with IR intensity of 165.45 of the title compound while the reported value is 1206 cm^{-1}(DFT) [27]. The O-H stretching vibration gives rise to a band at 3050 ± 150 cm^{-1} [23]. The band observed at 2666 cm^{-1} experimentally and 2793 cm^{-1} in DFT calculation is assigned as the O-H stretching vibration. The downshift of the O-H stretching mode is due to the strong hydrogen bonded system present in the title compound as reported in literature [28, 29]. The O-H in-plane and out-of-plane deformation modes are expected at 1395 ± 55 cm^{-1} and at 905 ± 70 cm^{-1} respectively [23]. For the title compound the band at 1352 cm^{-1} (DFT) is assigned as the in-plane O-H deformation band. Similarly the band at 922 cm^{-1} (DFT) is assigned as the O-H out-of-plane deformation band of the title compound. The in-plane O-H bending mode has a IR intensity and high Raman activity of 68.14

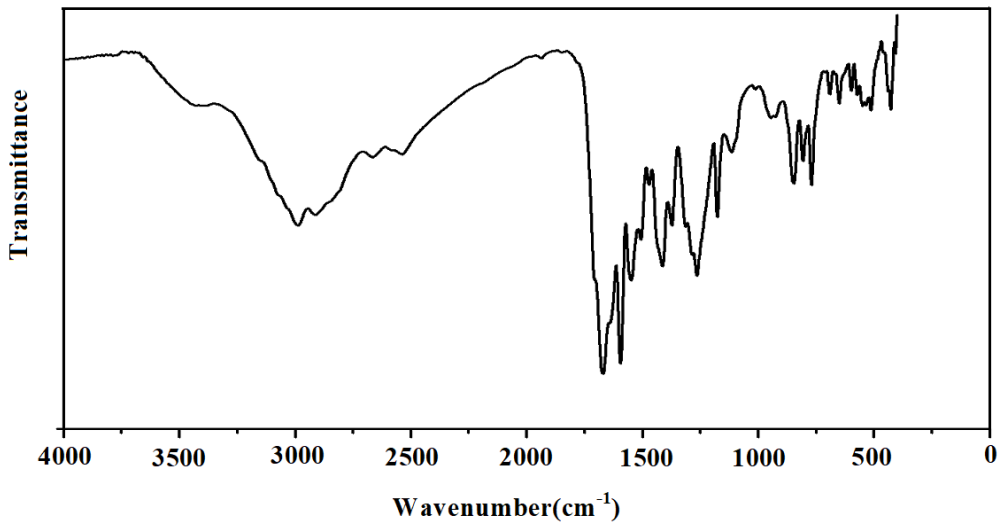

Fig 1. FT-IR spectrum of 3-[(4- carboxyphenyl) carbamoyl] -4-hydroxy-2-oxo-1, 2-dihydroquinoline-6-carboxylic acid

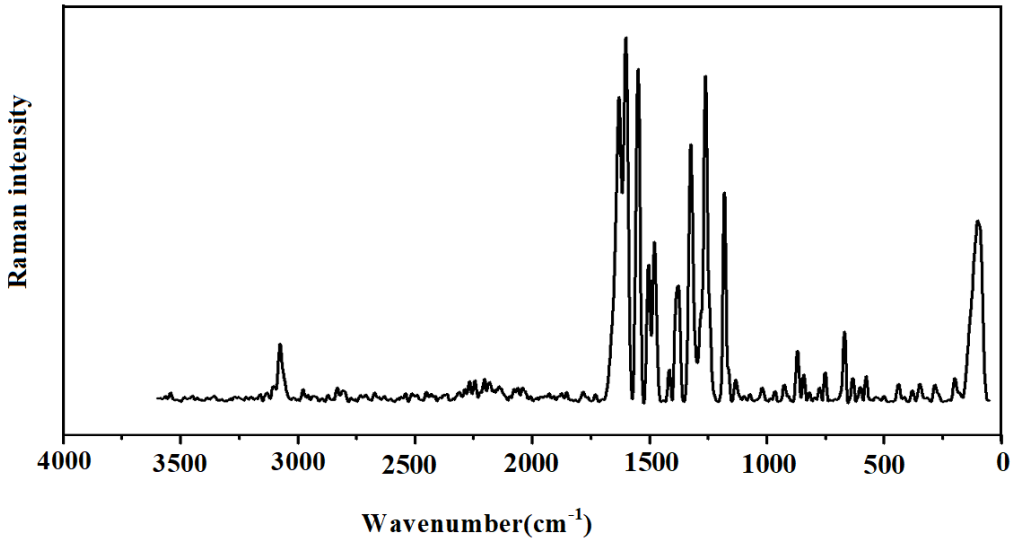

Fig 2. FT-Raman spectrum of 3-[(4-carboxyphenyl) carbamoyl] -4-hydroxy-2-oxo-1, 2-dihydroquinoline-6-carboxylic acid

and 955.36. Rajeev et al. [27] reported a band at 1412 cm^{-1} as the in-plane O-H deformation. The N-H stretching vibrations are expected [30] in the range 3500-3300 cm^{-1}. In the present study the bands observed at 3440, 3392 cm^{-1} in the IR spectrum and 3454 cm^{-1} theoretically are assigned as N-H stretching vibrational mode which has a PED of 100%, IR intensity 50.89 and Raman activity 108.89. In the present case the N-H stretching mode splits into a doublet and downshifted from the computed value which indicates the weakening of the N-H bond [31, 32]. N-H group shows bands at 1510-1500, 1350-1250 and 740-730 cm^{-1} [33]. According to literature if N-H is a part of a closed ring [33] the N-H deformation band is absent in the region 1510-1500 cm^{-1}. In the present case the N-H in-plane deformation band is observed at

1439 cm^{-1} theoretically and this mode has IR intensity 35.79, Raman activity 131.12 with a PED 22%. The out-of-plane deformation bands of N-H are expected in the range 650 ± 50 cm^{-1} and the bands observed at 612 cm^{-1} (DFT) assigned as γNH mode of the title compound. This mode has 73% PED with 60.95 as IR intensity and a low Raman activity less than 10.00. In the present case, the quinoline C-C stretching ring modes are observed at 1413 cm^{-1} in the IR spectrum, 1414 cm^{-1} in the Raman spectrum, 1413 cm^{-1} theoretically with high IR intensity and the C-N stretching modes are at 1114 cm^{-1} in the IR spectrum, 1233, 1082 cm^{-1} theoretically. Both the modes possess moderate IR intensities. Rajeev et al. reported the quinoline stretching modes at 1610, 1445, 1020 cm^{-1} (C-C), 1262 cm^{-1} (C-N) in the IR spectrum, 1609, 1051, 1022 cm^{-1} (C-C), 1202 cm^{-1} (C-N) in the Raman spectrum, 1607, 1433, 1045, 1035 cm^{-1} (C-C), 1270, 1230 cm^{-1} (C-N) theoretically [27]. The DFT calculations give the C-H stretching modes of the phenyl ring I and phenyl ring II of the title compound at 3128, 3101, 3067 cm^{-1} and 3151, 3099, 3098, 3061 cm^{-1}. Similarly the bands observed at 3132, 3103, 3078 cm^{-1} (Raman) and 3157, 2990 cm^{-1} (IR) are assigned as C-HI and C-HII stretching modes of the phenyl rings of parent molecule [23]. The bands observed at 1470, 1372 and 1593, 1505, 1314 cm^{-1}in IR spectrum, 1477 and 1602, 1503, 1382, 1323 cm^{-1} in Raman spectrum and at 1618, 1580, 1485, 1369, 1342 and 1609, 1591,1538, 1496,1403,1321 cm^{-1} theoretically are assigned as phenyl rings stretching modes of the title compound which are expected in the region 1620-1250 cm^{-1} [23]. In asymmetric tri-substituted benzene, when all the three substituents are heavy, the ring breathing mode appears above 1100 cm^{-1} [34]. For the tri-substituted phenyl ring PhI, the ring breathing mode is assigned at1066 cm^{-1} theoretically with moderate IR intensity and PED 18%. Madhavan et al. [35] reported the ring breathing mode for a compound having two tri-substituted benzene rings at 1110 and 1083 cm^{-1} respectively. In the present case, the band observed at 1070 cm^{-1} in Raman spectrum and 1072 cm^{-1} theoretically with a PED contribution of 16% and high IR intensity is assigned as the ring breathing mode of the phenyl ring II which is expected in region 1020-1070 cm^{-1} [24]. Panicker et al. [36] reported the ring breathing mode of di-substituted benzene at 1018 cm^{-1} (IR), 1034 cm^{-1} (Raman) and 1019 cm^{-1} (DFT). For the title compound, the bands observed at 1284, 1114 cm^{-1} (IR), 1134, 1099, cm^{-1} (Raman) and 1288, 1245, 1152, 1137, 1106, 1104 cm^{-1} (DFT) are assigned as the C-H in-plane bending modes of the phenyl rings. The C-H out-of-plane deformations are expected below 1000 cm^{-1} [23] and for the title compound the theoretical calculations give bands at 951, 949, 938, 925, 842, 828, 815,794 cm^{-1} as γCH modes of the phenyl rings. Experimentally these bands are observed at 970, 926, 841, 818, 799 cm^{-1} in the Raman spectrum.

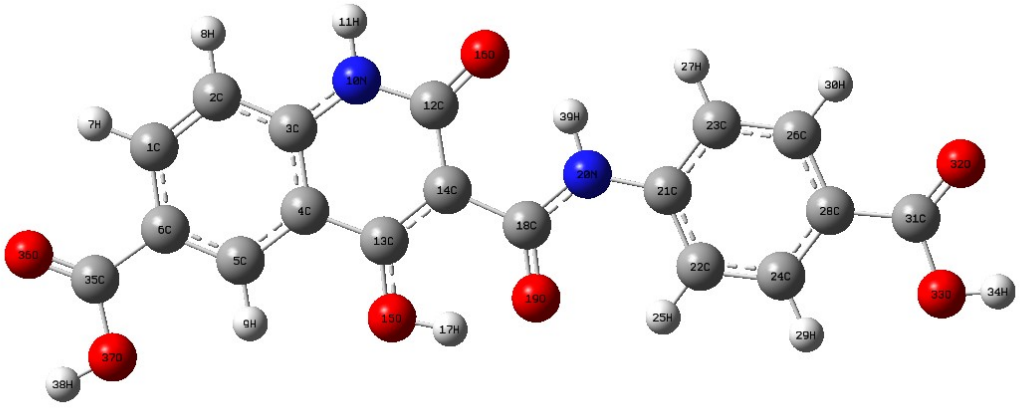

Fig. 3 Optimized geometry of 3-[(4-carboxyphenyl) carbamoyl]-4-hydroxy-2-oxo-1,2-dihydroxyquinoline-6-carboxylic acid.

4.4.3 Frontier Molecular Orbitals

Frontier molecular orbital study is used to explain the chemical behaviour and stability of the molecular system. The atomic orbital components of the frontier molecular orbitals are shown in Fig. 4. The delocalization of HOMO and LUMO over the molecular system shows the charge transfer within the molecular system. The HOMO-LUMO gap is found to be 3.157 eV. The chemical descriptors can be evaluated by using HOMO and LUMO orbital energies, E_{HOMO}, and E_{LUMO} as: ionization energy I= -E_{HOMO}, electron affinity A= -E_{LUMO}, hardness η = (I-A)/2, chemical potential μ = -(I+A)/2 and electrophilicity index ($\omega = \mu^2/2\eta$ [37]. For the title compound CHODQC I = 8.482, A = 5.325, η = 1.579, μ = -6.904 and ω = 15.093 eV (Table 3). For the title molecule, HOMO is delocalized over the phenyl group (PhII), amide group and partially over the quinoline ring while the LUMO is delocalized strongly over the entire molecule except carboxyl group of quinoline ring.

For 7Cl, HOMO is delocalized strongly over the quinoline ring and substituted chlorine atom while LUMO is delocalized strongly over the entire molecule except N-H groups. For 8Cl and 9Cl HOMO is over the phenyl ring PhI and partially over the pyridine ring and LUMO is over the entire molecule except carboxyl group of PhI and carbonyl group of pyridine ring. For 7Br HOMO is over the entire molecule except carboxyl group of PhI and LUMO is over the entire molecule. For 8Br and 9Br HOMO is over the entire molecule except carboxyl group of PhI and carbonyl group of pyridine ring and LUMO is over the entire molecule except carboxyl group of PhI and N-H group of pyridine ring. For 7F, HOMO is over the entire molecule except arboxyl group of PhI

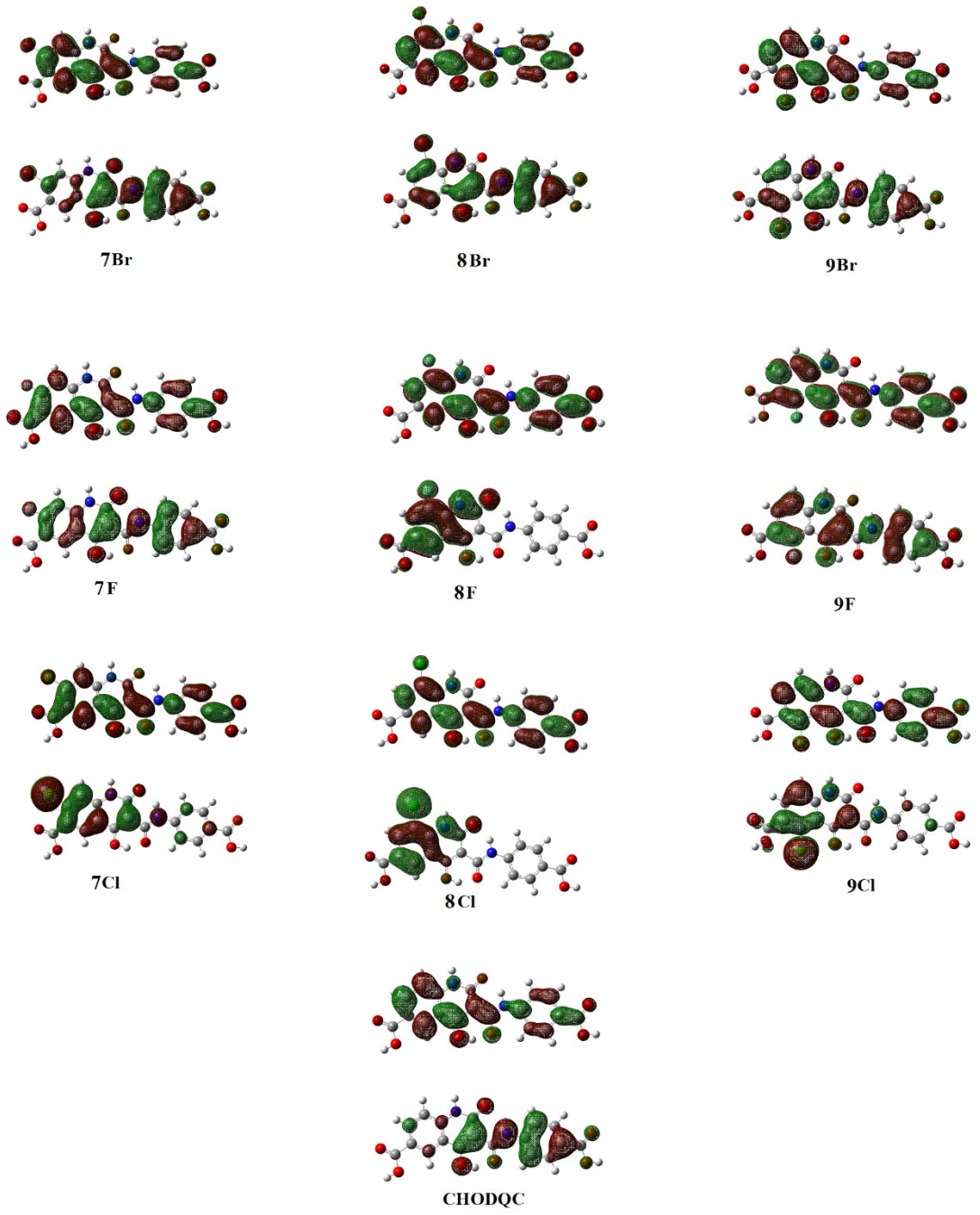

Fig.4 HOMO–LUMO plots of 3-[(4-carboxyphenyl) carbamoyl]-4-hydroxy-2-oxo-1,2-dihydroxyquinoline-6-carboxylic acid with halogen substitution

and N-H of pyridine while LUMO is over the entire molecule except N-H group of amide group. For 8F, HOMO is over the entire quinoline ring while for 9F, HOMO is over the entire molecule. LUMO is delocalized over the entire molecule except carboxyl group of PhI,

carbonyl group of pyridine and NH group of amide for 8F and 9F. The chemical potential decreases for the halogen substitution in the order 7Cl, 8Cl, 9Cl less than 7F, 8F, 9F less than 7Br, 8Br, 9Br less than parent. Chemical potential value of 8Cl is deviated maximum from the parent molecule while all other halogen substitution shows minimum deviation. Halogen substitution results in reduction in the μ value in comparison with the parent molecule and for 8Cl it is minimum. Halogen substitution also results a decrease in electrophilicity index and is minimum for 8Cl. Global hardness is higher for 8Cl because of its large HOMO-LUMO gap which results a decrease in polarizability.

4.4.4 Molecular Electrostatic Potential

Molecular electrostatic potential and electron density are related to each other to find the reactive sites for electrophilic and nucleophilic sites [38, 39]. The negative (red and yellow) regions of MEP map (Fig.5) were related to electrophilic reactivity while the positive (blue) regions to nucleophilic reactivity. For the parent molecule, most electrophilic (red and Yellow) regions are C=O group of both carboxyl group, slightly over PhII and the nucleophilic regions (blue) are deeply over the NH bond of quinoline ring, slightly over the hydrogen atom of the OH groups. For 7Cl, 8Cl and 9Cl, electrophilic regions are strongly over the carbonyl group of both carboxyl group and slightly over the phenyl ring while the nucleophilic regions are over the N-H group of quinoline ring and slightly over the hydrogen atoms of the O-H groups and more intense in the case of 8Cl. For fluorine substitution the electrophilic regions are similar to that of chlorine substitution while the nucleophilic regions are same that of chlorine substitution but blue region of N-H bond of quinoline in 8F is more pronounced. For bromine substitution also the electrophilic and nucleophilic behaviour is identical to that of chlorine and fluorine substitution while blue region around bromine is higher than that in fluorine substitution. The nucleophilic region of fluorine substitution is less than that in chlorine and bromine substitution.

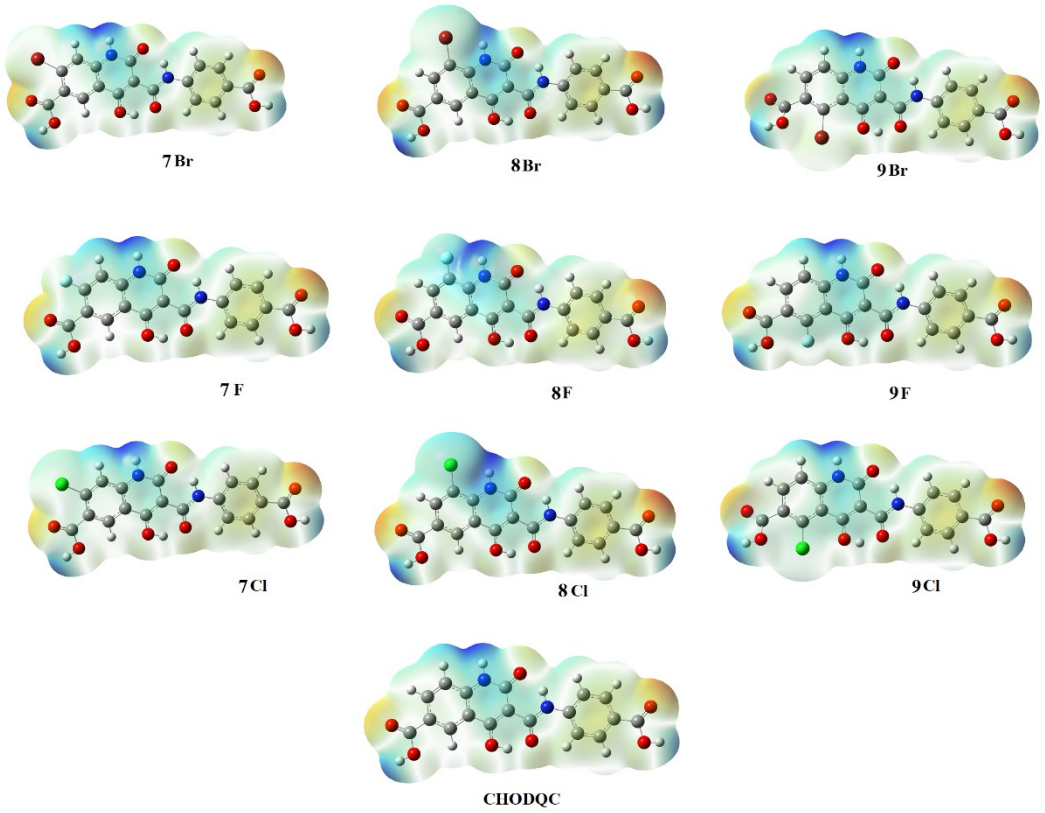

Fig.5 MEP map of 3-[(4-carboxyphenyl) carbamoyl]-4-hydroxy-2-oxo-1,2-dihydroxyquinoline-6-carboxylic acid with halogen substitution.

4.4.5 NBO Analysis

The natural bond orbitals (NBO) calculations were performed using NBO 3.1 program [40]. The strong interactions are: $LPO_{37} \rightarrow C_{35}\text{-}O_{36}$, $LPO_{36} \rightarrow C_{35}\text{-}O_3$ $LPO_{33} \rightarrow C_{31}\text{-}O_{32}$, $LPO_{32} \rightarrow C_{31}\text{-}O_{33}$, $LPN_{20} \rightarrow C_{18}\text{-}O_{19}$, $LPO_{15} \rightarrow C_{13}\text{-}C_{14}$, $LPN_{10} \rightarrow C_{12}\text{-}O_{16}$, $LPC_4 \rightarrow C_{13}\text{-}C_{14}$ and $LPC_4 \rightarrow C_5\text{-}C_6$ with energies, 21.44, 16.30,, 21.43, 16, 26, 28.99, 22.49, 27.67, 37.81 and 35.32 kcal/mol. 100% p-character is found in lone pairs of O37,O36, O33, O32, O16,O15 and N10 atoms. The important results are tabulated in Tables 4 and 5.

4.4.6 Nonlinear Optical Properties

The calculated first hyper polarizability of the title compound is 15.827×10^{-30} esu which is 121.75 times that of standard NLO material urea (0.13×10^{-30} esu) (table 6) [41]. The reported value of first hyper polarizability of similar derivative is 2.24×10^{-30} esu [42]. The phenyl ring stretching vibrations at 1607, 1499 cm^{-1} in the IR spectrum have their counterparts in the Raman spectrum at 1603, 1503 cm^{-1} respectively with IR and Raman intensities are comparable. These types of organic molecules have conjugated π-electron system and large hyper polarizability which leads to nonlinear optical properties [43]. The C-N distances in the

calculated molecular structure vary from 1.3743 to 1.4046 Å which are in between those of a C-N single and double bond and this suggest an extended π-electron delocalization over the molecular system which is also responsible for the nonlinearity of the molecule [44]. We conclude that the title compound is an attractive object for future studies of non-linear optical properties.

4.4.7 Molecular Docking

Antimalarial drugs constitute a major part of antiprotozoal drugs. Malaria remains a major health problem, mainly in sub-Saharan Africa and parts of Asia and South America [45] with over 200 million clinical infections and nearly half a million deaths annually. Malaria is caused by protozoan parasites belonging to the genus Plasmodium and is transmitted via the bite of a female Anopheles mosquito. There are four major species of the parasite that cause malaria in humans, namely, Plasmodium falciparum, P. vivax, P. ovale, and P. malaria, while a fifth parasite, P. knowlesi, is now recognized [46]. Historically, a range of drugs has been used to treat or prevent malaria , including several derived from the quinoline ring system such as quinine, chloroquine (CQ), amodiaquine, piperaquine, mefloquine, and primaquine [47]. Quinoline and its related derivative comprise a class of heterocycles, which has been exploited immensely than any other nucleus for the development of potent antimalarial agents. Various chemical modifications of quinoline have been attempted to achieve analogs with potent antimalarial properties against sensitive as well as resistant strains of Plasmodium sp., together with minimal potential undesirable side effects [48]. From PASS (Prediction of Activity Spectra) [49] analysis we have to choose the favorable target for docking study and different types of activities predicted as in Table 7. We choose the activity ubiquinol-cytochrome-c reductase inhibitor with Pa value 0.858 and high resolution crystal structure of corresponding receptor atovaquone-inhibited cytochrome BC1 complex with PDBID: 4PD4 was downloaded from the RCSB protein data bank website.

Atovaquone is a drug that inhibits the respiratory chain of Plasmodium falciparum, but with serious limitations like known resistance, low bioavailability and high plasma protein binding [50]. cyt bc1 inhibitors are generally classified as slow-onset anti-malarials, we found that a single dose of endochin-like quinolone-400 (ELQ-400) rapidly induced stasis in blood-stage parasites, which was associated with a rapid reduction in parasitemia in vivo. ELQ-400 also exhibited a low propensity for drug resistance and was active against atovaquone- resistant

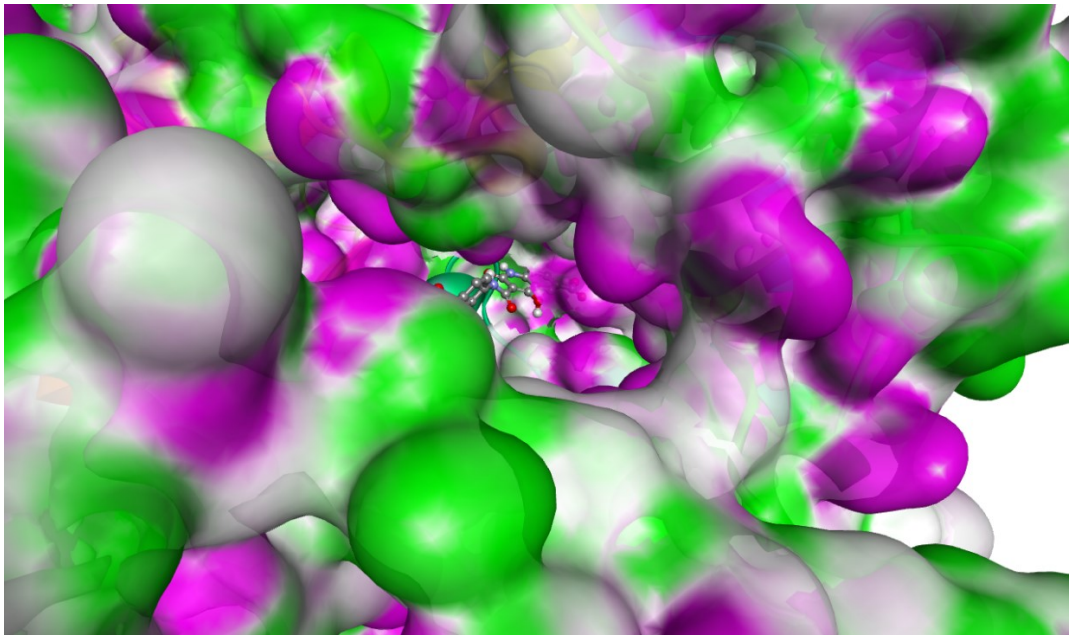

Fig.6 The docked ligand of 3-[(4-carboxyphenyl) carbamoyl]-4-hydroxy-2-oxo-1,2-dihydroxyquinoline-6-carboxylic acid in the active site of receptor

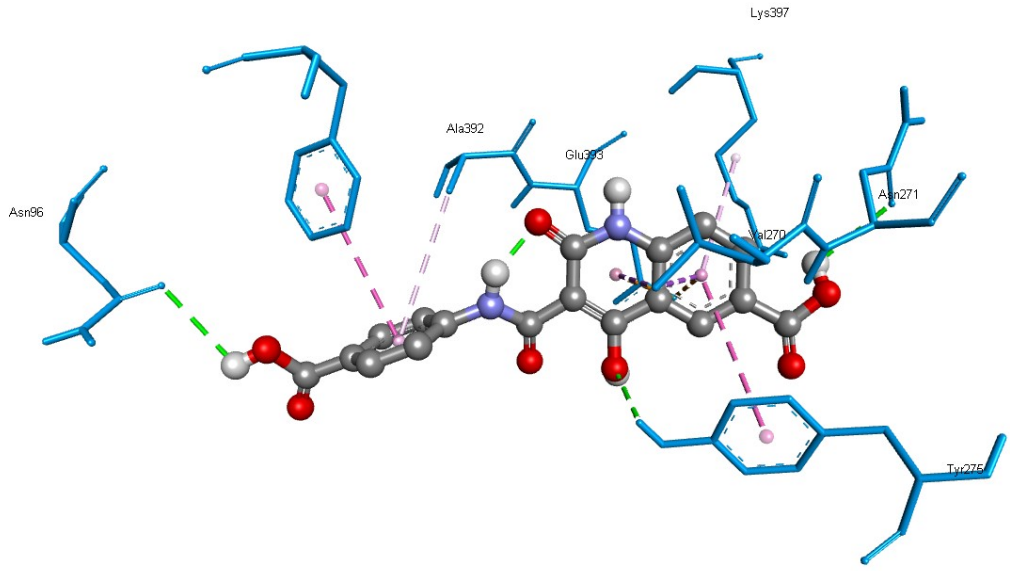

Fig.7 Ligand interactions of 3-[(4-carboxyphenyl) carbamoyl]-4-hydroxy-2-oxo-1,2-dihydroxyquinoline-6-carboxylic acid with amino acids.

P. falciparum strains with point mutations in cyt bc1. ELQ-400 shows that cyt bc1 inhibitors can function as single-dose, blood-stage anti-malarials and is the first compound to provide combined treatment, prophylaxis, and transmission blocking activity for malaria after a single oral administration [51]. This remarkable efficacy suggests that metabolic therapies, including

cyt bc_1 inhibitors, may be valuable additions to the collection of single-dose anti-malarials in current development.

All docking calculations were performed on AutoDock4.2 [52], Auto Dock-Vina software [53] and as in literature [54]. The amino acids of the receptor Tyr275, Asn96, Asn271 forms H-bond with OH group and other electrostatic interactions are detailed in Fig.6. The docked ligand forms a stable complex with the receptors atovaquone-inhibited cytochrome BC1 complex as depicted in Fig.7 and the binding free energy value is -9.1 kcal/mol (Table 8). These preliminary results suggest that the compound having inhibitory activity against the antimalarial receptor atovaquone-inhibited cytochrome BC1 complex. Thus the title compound can be developed as drug used for the treatment of malaria.

4.5 Conclusions

The vibrational spectroscopic studies of 3-[(4-carboxyphenyl) carbamoyl]-4-hydroxy-2-oxo-1, 2-dihydroquinoline-6-carboxylic acid in the ground state were reported theoretically and experimentally. Potential energy distribution of normal mode vibration was done using GAR2PED programme.The vibrational wave number of the title compound successfully analyzed. For the title compound HOMO is delocalized over the phenyl group, amide group and LUMO is over the entire molecule except carboxyl group of quinoline ring. In addition to that the halogen substituted HOMO-LUMO calculation showed a decrease in the electrophilicity index and is minimum for substituted chlorine at the eight position of the compound. The molecular electrostatic potential analysis results that the negative charge covers part of the oxygen atom in carboxylic acid and positive charge over the nitrogen atom in the quinoline ring. The title compound form a stable complex with ubiquinol-cytochrome c re ductase inhibitor as is evident from the binding affinity values.

Table 1. Optimized geometrical Parameters of 3-[(4-carboxyphenyl) carbamoyl]-4-hydroxy-2-oxo-1, 2-dihydroquinoline-6-carboxylic acid

Bond length(º)		Bond angle(º)		Dihedral angle(º)	
C_1-C_2	1.3824	C_2-C_1-C_6	120.9	C_6-C_1-C_2-C_3	-0.0
C_1-C_6	1.4113	C_2-C_1-H_7	120.8	C_2-C_1-C_6-C_5	-0.0
C_1-H_7	1.0863	C_1-C_2-C_3	119.6	C_2-C_1-C_6-C_{35}	180.0
C_2-C_3	1.4084	C_1-C_2-H_8	120.7	C_1-C_2-C_3-C_4	0.0
C_2-H_8	1.0880	C_6-C_1-H_7	118.3	C_1-C_2-C_3-N_{10}	180.0
C_3-C_4	1.4130	C_1-C_6-C_5	119.6	C_2-C_3-C_4-C_5	0.0
C_3-N_{10}	1.3745	C_1-C_6-C_{35}	117.8	C_2-C_3-C_4-C_{13}	-180.0
C_4-C_5	1.4045	C_3-C_2-H_8	119.7	N_{10}-C_3-C_4-C_5	-180.0
C_4-C_{13}	1.4498	C_2-C_3-C_4	120.1	N_{10}-C_3-C_4-C_{13}	0.0
C_5-C_6	1.3916	C_2-C_3-N_{10}	121.3	C_2-C_3-N_{10}-C_{12}	-180.0
C_5-H_9	1.0841	C_4-C_3-N_{10}	118.6	C_4-C_3-N_{10}-C_{12}	0.0

Bond length(º)		Bond angle(º)		Dihedral angle(º)	
C_6-C_{35}	1.4849	C_3-C_4-C_5	119.5	C_3-C_4-C_5-C_6	-0.0
N_{10}-H_{11}	1.0127	C_3-C_4-C_{13}	118.4	C_{13}-C_4-C_5-C_6	180.0
N_{10}-C_{12}	1.3914	C_3-N_{10}-H_{11}	119.9	C_3-C_4-C_{13}-C_{14}	-0.0
C_{12}-C_{14}	1.4579	C_3-N_{10}-C_{12}	126.0	C_3-C_4-C_{13}-O_{15}	-180.0
C_{12}-O_{16}	1.2374	C_5-C_4-C_{13}	122.1	C_5-C_4-C_{13}-C_{14}	180.0
C_{13}-C_{14}	1.3989	C_4-C_5-C_6	120.3	C_5-C_4-C_{13}-O_{15}	-0.0
C_{13}-O_{15}	1.3198	C_4-C_5-H_9	119.0	C_4-C_5-C_6-C_1	0.0
C_{14}-C_{18}	1.4854	C_4-C_{13}-C_{14}	121.2	C_4-C_5-C_6-C_{35}	-180.0
O_{15}-H_{17}	1.0122	C_4-C_{13}-O_{15}	115.9	C_1-C_6-C_{35}-O_{36}	0.0
O_{16}-H_{39}	1.7992	C_6-C_5-H_9	120.7	C_1-C_6-C_{35}-O_{37}	180.0
H_{17}-O_{19}	1.5785	C_5-C_6-C_{35}	122.5	C_5-C_6-C_{35}-O_{36}	-190.0
C_{18}-O_{19}	1.2507	C_6-C_{35}-O_{36}	124.7	C_5-C_6-C_{35}-O_{37}	-0.0
C_{18}-N_{20}	1.3596	C_6-C_{35}-O_{37}	113.0	C_3-N_{10}-C_{12}-C_{14}	-0.0
N_{20}-C_{21}	1.4047	H_{11}-N_{10}-C_{12}	114.0	C_3-N_{10}-C_{12}-O_{16}	180.0
N_{20}-H_{39}	1.0244	N_{10}-C_{12}-C_{14}	116.0	N_{10}-C_{12}-C_{14}-C_{13}	0.0
C_{21}-C_{22}	1.4068	N_{10}-C_{12}-O_{16}	118.0	N_{10}-C_{12}-C_{14}-C_{18}	180.0
C_{21}-C_{23}	1.4092	C_{14}-C_{12}-O_{16}	126.0	O_{16}-C_{12}-C_{14}-C_{13}	-180.0
C_{22}-C_{24}	1.3924	C_{12}-C_{14}-C_{13}	119.8	O_{16}-C_{12}-C_{14}-C_{18}	0.0
C_{22}-H_{25}	1.0814	C_{12}-C_{14}-C_{18}	122.1	C_4-C_{13}-C_{14}-C_{12}	-0.0
C_{23}-C_{26}	1.3864	C_{12}-C_{16}-H_{39}	99.6	C_4-C_{13}-C_{14}-C_{18}	-180.0
C_{23}-H_{27}	1.0896	C_{14}-C_{13}-O_{15}	123.0	O_{15}-C_{13}-C_{14}-C_{12}	180.0
C_{24}-C_{28}	1.4017	C_{13}-C_{14}-C_{18}	118.1	O_{15}-C_{13}-C_{14}-C_{18}	0.0
C_{24}-H_{29}	1.0859	C_{13}-O_{15}-H_{17}	106.1	C_{12}-C_{14}-C_{18}-O_{19}	180.0
C_{26}-C_{28}	1.4030	C_{14}-C_{18}-O_{19}	120.2	C_{12}-C_{14}-C_{18}-N_{20}	0.0
C_{26}-H_{30}	1.0863	C_{14}-C_{18}-N_{20}	116.8	C_{13}-C_{14}-C_{18}-O_{19}	0.0
C_{28}-C_{31}	1.4815	O_{15}-H_{17}-O_{19}	149.6	C_{13}-C_{14}-C_{18}-N_{20}	180.0
C_{31}-O_{32}	1.2132	O_{19}-C_{18}-N_{20}	123.0	C_{14}-C_{18}-N_{20}-C_{21}	-180.0
C_{31}-O_{33}	1.3596	C_{18}-O_{19}-H_{17}	103.1	O_{19}-C_{18}-N_{20}-C_{21}	0.0
O_{33}-H_{34}	0.9720	C_{18}-N_{20}-C_{21}	129.2	C_{18}-N_{20}-C_{21}-C_{22}	-0.0
C_{35}-O_{36}	1.2120	C_{18}-N_{20}-H_{39}	113.5	C_{18}-N_{20}-C_{21}-C_{23}	180.0
C_{35}-O_{37}	1.3554	C_{21}-N_{20}-H_{39}	117.3	N_{20}-C_{21}-C_{22}-C_{24}	-180.0
O_{37}-H_{38}	0.9722	N_{20}-C_{21}-C_{22}	124.3	C_{23}-C_{21}-C_{22}-C_{24}	0.0
		N_{20}-C_{21}-C_{23}	116.3	N_{20}-C_{21}-C_{23}-C_{26}	180.0
		N_{20}-H_{39}-O_{16}	141.9	C_{22}-C_{21}-C_{23}-C_{26}	-0.0
		C_{22}-C_{21}-C_{23}	119.4	C_{21}-C_{22}-C_{24}-C_{28}	0.0
		C_{21}-C_{22}-C_{24}	119.5	C_{21}-C_{23}-C_{26}-C_{28}	0.0
		C_{21}-C_{22}-H_{25}	119.7	C_{22}-C_{24}-C_{28}-C_{26}	-0.0
		C_{21}-C_{23}-C_{26}	120.5	C_{22}-C_{24}-C_{28}-C_{31}	180.0
		C_{21}-C_{23}-H_{27}	119.5	C_{23}-C_{26}-C_{28}-C_{24}	0.0
		C_{24}-C_{22}-H_{25}	120.8	C_{23}-C_{26}-C_{28}-C_{31}	-180.0
		C_{22}-C_{24}-C_{28}	121.2	C_{24}-C_{28}-C_{31}-O_{32}	180.0
		C_{22}-C_{24}-H_{29}	119.4	C_{24}-C_{28}-C_{31}-O_{33}	-0.0
		C_{26}-C_{23}-H_{27}	120.0	C_{26}-C_{28}-C_{31}-O_{32}	0.0
		C_{23}-C_{26}-C_{28}	120.4	C_{26}-C_{28}-C_{31}-O_{33}	180.0
		C_{23}-C_{26}-H_{30}	120.8		
		C_{28}-C_{24}-H_{29}	119.5		
		C_{24}-C_{28}-C_{26}	119.1		

Bond length(º)		Bond angle(º)		Dihedral angle(º)	
		C_{24}-C_{28}-C_{31}	122.8		
		C_{28}-C_{26}-H_{30}	118.8		
		C_{26}-C_{28}-C_{31}	118.2		
		C_{28}-C_{31}-O_{32}	125.2		
		C_{28}-C_{31}-O_{33}	113.1		
		O_{32}-C_{31}-O_{33}	121.7		
		C_{31}-O_{33}-H_{34}	105.8		
		O_{36}-C_{35}-O_{37}	122.3		
		C_{35}-O_{37}-H_{38}	106.2		

Table 2. IR, Raman bands and calculated (scaled) wavenumbers of CHODQC and assignments

No	B3LYP/6-311++G(d, p)			IR ν(cm^{-1})	Raman ν (cm^{-1})	Assignments
	ν(cm^{-1})	IR_I	R_A			
111	3545	64.41	295.68	-	3542	$\nu O_{33}H_{34}$(99)
110	3545	85.56	236.91	-	-	$\nu O_{37}H_{38}$(99)
109	3454	50.89	108.89	3440 3392	-	$\nu N_{10}H_{11}$(100)
108	3231	398.20	431.45	-	-	$\nu N_{20}H_{39}$(99)
107	3151	2.95	39.19	3157	-	νCHII(98)
106	3128	2.89	37.14	-	3132	νCHI(99)
105	3101	1.58	143.23	-	3103	νCHI(95)
104	3099	1.69	95.44	-	-	νCHII(95)
103	3098	2.12	95.49	-	-	νCHII(93)
102	3067	6.25	85.67	-	3078	νCHI(95)
101	3061	7.07	48.71	2990	-	νCHII(95)
100	2793	903.66	56.85	2666	-	$\nu O_{15}H_{17}$(99)
99	1746	362.66	269.81	-	-	$\nu C_{35}O_{36}$(73)
98	1741	401.29	169.61	-	-	$\nu C_{31}O_{32}$(72)
97	1678	512.03	10.06	1670	-	$\nu C_{12}O_{16}$(37)
96	1625	138.36	620.76	-	1630	$\nu C_{18}O_{19}$(26)
95	1618	74.61	349.28	-	-	νPhI(23)
94	1609	170.19	11.78	-	1602	νPhII(47)
93	1591	978.08	1638.12	1593	-	νPhII(44)
92	1580	208.84	1.94	-	-	νPhI(49)
91	1562	41.76	118.04	1551	1548	$\nu C_{13}C_{14}$(32), νPh1(15), $\delta O_{15}H_{17}$(10)

No	B3LYP/6-311++G(d, p)			IR ν(cm^{-1})	Raman ν (cm^{-1})	Assignments
	ν(cm^{-1})	IR_I	R_A			
90	1538	986.10	1388.60	-	-	νPhII(27), $\delta C_{18}O_{19}$(13)
89	1496	26.65	130.96	1505	1503	νPhII(38), δCHII(45)
88	1485	165.35	350.03	1470	1477	νPhI(24), δCHI(20), νC_3N_{10}(11)
87	1439	35.79	131.12	-	-	$\delta N_{10}H_{11}$(22), νPhI(13)
86	1413	213.93	438.67	1413	1414	νC_4C_{13}(40), $\nu C_{13}O_{15}$(28)
85	1403	14.30	86.10	-	1382	νPhII(42), δCHII(27)
84	1369	5.58	23.41	1372	-	νPhI(51), δCHI(12), $\delta N_{10}H_{11}$(12)
83	1352	68.74	955.36	-	-	$\delta O_{15}H_{17}$(17), $\nu C_{13}C_{14}$(17), $\upsilon C_{18}O_{19}$(10)
82	1342	111.52	191.03	-	-	νPhI(26), $\delta C_{18}O_{19}$(15)
81	1338	67.92	1.95	-	-	$\delta O_{37}H_{38}$(10), $\nu C_{35}O_{37}$(12)
80	1336	473.63	189.54	-	-	$\delta O_{33}H_{34}$(13), $\nu C_{31}O_{33}$(12)
79	1321	60.41	257.62	1314	1323	νPhII(73)
78	1292	165.43	5.51	-	-	$\nu C_{13}O_{15}$(28) , $\nu C_{12}C_{14}$(24), $\nu N_{10}C_{12}$(16)
77	1288	13.42	128.21	1284		δCHII(62)
76	1251	103.81	403.81	1261	1260	$\delta C_{18}O_{19}$ (19), $\nu C_{18}N_{20}$(10)
75	1245	27.98	711.98	-	-	δCHI(23), νPhII(10), $\nu C_{21}N_{20}$(16)
74	1233	20.23	111.26	-	-	νC_3N_{10}(27), $\delta N_{10}H_{11}$(14), $\delta C_{18}O_{19}$ (19)
73	1210	29.32	0.61	-	-	$\delta C_{18}O_{19}$ (36)
72	1184	195.44	11.90	-	1183	$\delta O_{33}H_{34}$(31), δCHII(20), $\delta C_{28}C_{31}$(13)
71	1173	207.87	95.65	1173	-	$\delta O_{37}H_{38}$(31), C_6C_{35}(13)
70	1152	305.17	415.54	-	-	δCHII(48), $\delta O_{33}H_{34}$(14)
69	1137	10.52	14.28	-	1134	δCHI(42)
68	1106	75.21	24.52	1114	-	δCHII(12)
67	1104	98.68	4.34	-	1099	δCHII(36)
66	1082	59.18	15.91	-	-	$\nu C_{12}N_{10}$(15), $\nu C_{31}O_{33}$(15)
65	1072	204.93	7.50	-	1070	νPhII(16), $\nu C_{31}O_{33}$(33)
64	1066	39.09	0.59	-	-	νPhI(18), δCHII(12), $\nu C_{35}O_{37}$(31)
63	994	6.99	18.05	1014	1020	δPhII(53), νPhII(32)
62	951	0.97	3.82	-	970	γCHII(79), γPhII(17)

No	B3LYP/6-311++G(d, p)			IR ν(cm^{-1})	Raman ν (cm^{-1})	Assignments
	ν(cm^{-1})	IR_I	R_A			
61	949	0.16	0.50	-	-	γCHI(86)
60	948	7.70	4.16	946	-	δPhI(13), $\delta C_{18}O_{19}$(22)
59	938	0.47	0.41	-	-	γCHII(90)
58	925	8.72	1.32	-	926	γCHII(78)
57	922	118.10	0.48	-	-	$\gamma O_{15}H_{17}$(96)
56	896	7.84	16.48	-	870	δPhI(17), $\delta C_{18}O_{19}$(26)
55	846	3.44	26.96	846	-	$\delta C_{18}O_{19}$(29), $\delta N_{20}H_{39}$ (18), νPhII(11)
54	842	28.35	0.08	-	841	γCHII(63)
53	828	36.23	2.99	-	-	γCHII(67), $\gamma N_{20}H_{39}$(17)
52	815	9.54	3.18		818	γCHI(70)
51	812	9.74	30.00	807	-	$\delta C_{18}O_{19}$(41), δring(11)
50	794	38.68	1.37	-	799	γCHII(50), $\gamma N_{20}H_{39}$(20), $\gamma N_{20}C_{18}$(15)
49	762	49.05	4.20	768	776	$\gamma C_{31}O_{32}$(22), γPhII(25), $\gamma C_{21}N_{20}$(10)
48	759	2.41	2.35	-	-	$\delta C_{13}O_{15}$(23), γring(32), $\gamma C_{14}C_{18}$(10)
47	754	62.10	0.65	-	754	$\gamma C_{35}O_{36}$(41), γPhI(15), γCHI(11)
46	744	45.76	5.18	-	-	$\nu C_{28}C_{31}$(10)
45	736	36.51	2.95	-	-	$\gamma C_{12}O_{16}$ (29), $\gamma C_{18}O_{19}$(15), γPhI(14)
44	709	18.04	22.94	-	-	δPhI(10)
43	701	12.14	1.59	-	-	$\gamma N_{10}H_{11}$ (13), $\gamma C_{18}O_{19}$ (29), γring (17)
42	694	37.34	2.03	688	-	γPhII(56), $\gamma C_{21}N_{20}$(11), $\gamma C_{28}C_{31}$(31)
41	659	9.95	2.43	-	668	γPhI(21), γring(10), $\delta C_{13}O_{15}$(10)
40	650	11.28	21.35	648	-	δPhI(34), δring(11)
39	637	37.11	1.29	-	636	δC_6C_{35}(29), $\delta C_{12}O_{16}$(12), δPhI(15)
38	625	18.22	5.69	-	-	δPhII(44)
37	614	39.63	5.78	-	-	δPhII(35), $\delta C_{31}O_{32}$(14), $\delta C_{12}O_{16}$(10)
36	612	60.95	2.41	-	-	$\gamma N_{10}H_{11}$(73)

No	B3LYP/6-311++G(d, p)			IR ν(cm^{-1})	Raman ν (cm^{-1})	Assignments
	ν(cm^{-1})	IR_I	R_A			
35	601	96.01	6.18	-	600	γring(10), $\gamma O_{37}H_{38}$ (10)
34	597	34.60	9.87	596	-	$\gamma C_{28}C_{31}$(61)
33	578	6.03	5.27	572	578	$\delta C_{18}O_{19}$(41), $\delta C_{31}O_{32}$(18)
32	549	27.23	18.37	547	-	δring(16), δPhI(17), δC_6C_{35}(15)
31	516	18.76	0.89	535	-	δring(46), $\delta C_{35}O_{36}$(13)
30	511	25.17	2.65	511	-	γring(22), γC_6C_{35}(13), γPhI(37)
29	498	13.14	5.76	-	500	$\gamma C_{21}N_{20}$(29), γPhII(39), $\gamma C_{28}C_{31}$ (13)
28	489	7.07	1.35	-	-	δPhII(25), $\delta C_{28}C_{31}$(45)
27	471	47.81	1.55	459	-	$\delta C_{35}O_{36}$(39)
26	438	28.55	1.58	438	437	$\delta C_{13}O_{15}$(16), $\delta N_{20}H_{39}$(13), $\delta C_{12}O_{16}$(11)
25	433	4.83	0.13	426	-	γPhI(54)
24	415	13.12	5.03	-	-	$\delta C_{18}O_{19}$(41), $\delta C_{13}O_{15}$(10)
23	405	0.21	0.06	406	-	γPhII(80)
22	394	22.32	2.29	-	379	$\delta C_{21}N_{20}$ (13), $\delta C_{12}O_{16}$ (17), $\delta C_{18}C_{14}$(23)
21	368	8.65	4.57	-	347	$\delta C_{31}O_{32}$(17), δring (28), δPhII(12)
20	317	0.36	0.74	-	-	$\gamma C_{14}C_{18}$ (13), γPhI (13), γring(13)
19	308	1.65	0.04	-	-	γring(21), $\gamma C_{28}C_{31}$(11), γC_6C_{35}(10)
18	307	13.3	0.88	-	-	$\delta C_{18}O_{19}$(18), $\delta C_{21}N_{20}$(21)
17	297	0.74	6.20	-	286	$\delta C_{35}C_6$ (17), δC_6O_{35}(14), δPhI(18)
16	253	0.37	1.19	-	-	$\gamma C_{14}C_{18}$ (49), δPhII(25)
15	247	0.86	0.78	-	-	$\gamma C_{18}C_{14}$ (19), δPhI(12)
14	181	0.43	0.85	-	196	δPhII(24), δC_6C_{35} (10)
13	176	0.10	2.02	-	-	τring(41), $\gamma O_{15}H_{17}$(15)
12	158	1.90	0.19	-	-	τring(24), $\gamma N_{10}H_{11}$(21)
11	150	5.09	0.13	-	-	$\delta C_{28}C_{31}$(14), $\delta C_{18}O_{19}$ (13)
10	142	0.29	0.34	-	-	τring(20), $\tau C_{14}C_{18}$(20)
9	116	3.03	0.67	-	-	δC_6C_{35}(35)
8	104	0.13	1.20	-	101	$\tau C_{14}C_{18}$(36), $\gamma O_{15}H_{17}$(21), τring(18)
7	78	2.32	1.57	-	-	τPhI(10), τring(11), $\tau C_{18}N_{20}$(15)

No	B3LYP/6-311++G(d, p)			IR ν(cm^{-1})	Raman ν (cm^{-1})	Assignments
	ν(cm^{-1})	IR_I	R_A			
6	75	0.00	0.49	-	-	$\tau C_{28}C_{31}$(60)
5	57	1.71	1.37	-	-	τring (15), τPhI(14), τC_6C_{35}(57)
4	49	0.00	0.75	-	-	τring(33), τPhII(8)
3	47	0.03	0.80	-	-	$\delta N_{20}H_{39}$ (34), $\delta C_{21}N_{20}$ (11)
2	27	0.69	1.35	-	-	$\tau N_{20}C_{21}$(57)
1	16	0.00	0.84	-	-	τring(12), $\tau C_{18}N_{20}$(29), $\tau C_{14}C_{18}$(21)

Table 3. Energetic parameters of the CHODQC and halogen substitutions

	HOMO	LUMO	I = - E_{HOMO}	A = - E_{LUMO}	ΔE	η = (I-A)/2	μ = -(I+A)/2	ω = $\mu^2/2\eta$
CHODQC	-8.482	-5.325	8.482	5.325	3.157	1.579	-6.904	15.093
7chlroirne	-8.105	-5.176	8.105	5.176	2.929	1.465	-6.641	15.052
8chlroine	-7.885	-4.622	7.885	4.622	3.263	1.632	-6.254	11.983
9chlroine	-8.039	-5.140	8.039	5.140	2.899	1.450	-6.590	14.975
7fluorine	-8.423	-5.172	8.423	5.172	3.251	1.626	-6.798	14.211
8fluorine	-8.276	-5.182	8.276	5.182	3.094	1.547	-6.729	14.635
9fluorine	-8.404	-5.151	8.404	5.151	3.253	1.627	-6.778	14.118
7bromine	-8.461	-5.288	8.461	5.288	3.173	1.587	-6.875	14.892
8bromine	-8.484	-5.298	8.484	5.298	3.186	1.593	-6.891	14.905
9bromine	-8.427	-5.283	8.427	5.283	3.144	1.572	-6.855	14.946

Table 4. NBO result showing the formation of Lewis and non-Lewis orbitals

Bond (A-B)	ED/Energy	EDA%	EDB%	NBO	S%	P%
σC_1-C_2 -	0.98856 -0.73127	49.65 -	50.35 -	$0.7046(sp^{1.79})C$ $+0.7096(sp^{1.75})C$	35.80 36.32	64.20 63.68
πC_1-C_2 -	0.84908 -0.28780	45.37 -	54.63 -	$0.6736(sp^{1.00})C$ $+0.7391(sp^{1.00})C$	0.00 0.00	100.0 100.0
σC_1-C_6 -	0.98652 -0.71144	49.22 -	50.78 -	$0.7016(sp^{1.88})C$ $+0.7126(sp^{1.93})C$	34.78 34.11	65.22 65.89
σC_2-C_3 -	0.98554 -0.73032	48.51 -	51.49 -	$0.6965(sp^{1.90})C$ $+0.7176(sp^{1.77})C$	34.43 36.06	65.57 63.94
σC_3-C_4 -	0.98180 -0.72658	49.95 -	50.05 -	$0.7068(sp^{1.81})C$ $+0.7074(sp^{2.04})C$	35.65 32.91	64.35 67.09

Bond (A-B)	ED/Energy	EDA%	EDB%	NBO	S%	P%
σC_3-N_{10}	0.99237	38.03	61.97	0.6167($sp^{2.55}$)C	28.14	71.86
-	-0.85958	-	-	+0.7872($sp^{1.62}$)N	38.17	61.83
σC_4-C_5	0.98465	51.42	48.58	0.7171($sp^{1.84}$)C	35.15	64.85
-	-0.71830	-	-	+0.6970($sp^{1.88}$)C	34.72	65.28
σC_4-C_{13}	0.98382	50.54	49.46	0.7109($sp^{2.13}$)C	31.90	68.10
-	-0.71446	-	-	+0.7033($sp^{1.82}$)C	35.45	64.55
σC_5-C_6	0.98730	49.44	50.56	0.7031($sp^{1.82}$)C	35.41	64.59
-	-0.72601	-	-	+0.7110($sp^{1.79}$)C	35.88	64.12
πC_5-C_6	0.82480	42.74	57.26	0.6538($sp^{1.00}$)C	0.00	100.0
-	-0.28108	-	-	+0.7567($sp^{1.00}$)C	0.00	100.0
σC_6-C_{35}	0.98528	51.82	48.18	0.7199($sp^{2.34}$)C	29.96	70.04
-	-0.70075	-	-	+0.6941($sp^{1.49}$)C	40.15	59.85
σN_{10}-C_{12}	0.99174	63.95	36.05	0.7997($sp^{1.85}$)N	35.15	64.85
-	-0.82886	-	-	+ 0.6004($sp^{2.44}$)C	29.03	70.97
σC_{12}-C_{14}	0.98436	48.15	51.85	0.6939($sp^{1.62}$)C	38.21	61.79
-	-0.70828	-	-	+0.7201($sp^{2.03}$)C	33.05	66.95
σC_{12}-O_{16}	0.99437	35.12	64.88	0.5926($sp^{2.05}$)C	32.83	67.17
-	-1.01364	-	-	+0.8055($sp^{1.87}$)O	34.90	65.10
πC_{12}-O_{16}	0.98730	30.20	69.80	0.5495($sp^{99.99}$)C	0.00	100.0
-	-0.37506	-	-	+0.8355($sp^{1.00}$)O	0.01	99.99
σC_{13}-C_{14}	0.98751	49.53	50.47	0.7038($sp^{1.63}$)C	38.09	61.95
-	-0.75255	-	-	+0.7104($sp^{1.87}$)C	34.88	65.12
πC_{13}-C_{14}	0.84461	38.75	61.25	0.6225($sp^{1.00}$)C	0.00	100.0
-	-0.29939	-	-	+0.7826($sp^{1.00}$)C	0.00	100.0
σC_{13}-O_{15}	0.99445	33.10	66.90	0.5753($sp^{2.78}$)C	26.48	73.52
-	-0.93982	-	-	+0.8179($sp^{2.30}$)O	30.31	69.69
σC_{14}-C_{18}	0.98111	51.18	48.82	0.7154($sp^{2.12}$)C	32.04	67.96
-	-0.70381	-	-	+0.6987($sp^{1.66}$)C	37.58	62.42
σC_{18}-O_{19}	0.99269	32.35	67.65	0.5688($sp^{2.33}$)C	30.05	69.95
-	-0.82174	-	-	+0.8225($sp^{2.08}$)O	32.43	67.57
πC_{18}-O_{19}	0.97381	31.11	68.89	0.5577($sp^{99.99}$)C	0.42	99.58
-	-0.53501	-	-	+0.8300($sp^{99.99}$)O	0.79	99.21
σC_{18}-N_{20}	0.99039	40.13	59.87	0.6335($sp^{2.12}$)C	32.03	67.97
-	-0.83505	-	-	+0.7737($sp^{1.95}$)N	33.85	66.15
σN_{20}-C_{21}	0.98948	59.54	40.46	0.7716($sp^{1.61}$)N	38.38	61.26
-	-0.85498	-	-	+0.6361($sp^{2.36}$)C	29.73	70.27
σC_{21}-C_{22}	0.98732	51.04	48.96	0.7144($sp^{1.81}$)C	35.65	64.35
-	-0.70552	-	-	+0.6997($sp^{1.96}$)C	33.78	66.22
σC_{21}-C_{23}	0.98568	51.52	48.48	0.7177($sp^{1.90}$)C	34.54	65.46
-	-0.69940	-	-	+0.6963($sp^{1.94}$)C	34.03	65.97
σC_{22}-C_{24}	0.98909	49.60	50.40	0.7042($sp^{1.74}$)C	36.46	63.54
-	-0.72682	-	-	+0.7100($sp^{1.79}$)C	35.81	64.19
πC_{22}-C_{24}	0.82033	40.71	59.29	0.6380($sp^{1.00}$)C	0.00	0.00
-	-0.27619	-	-	+0.7700($sp^{1.00}$)C	100.0	100.0
σC_{23}-C_{26}	0.98969	49.40	50.60	0.7029($sp^{1.76}$)C	36.19	63.81
-	-0.72456	-	-	+0.7113($sp^{1.80}$)C	35.75	64.25
πC_{23}-C_{26}	0.80982	39.89	60.11	0.6316($sp^{1.00}$)C	0.00	0.00

Bond (A-B)	ED/Energy	EDA%	EDB%	NBO	S%	P%
-	-0.27298	-	-	+0.7753($sp^{1.00}$)C	100.0	100.0
σC_{24}-C_{28}	0.98827	49.44	50.56	0.7031($sp^{1.91}$)C	34.37	65.63
-	-0.71450	-	-	+0.7110($sp^{1.82}$)C	35.50	64.50
σC_{26}-C_{28}	0.98708	49.41	50.59	0.7029($sp^{1.91}$)C	34.36	65.64
-	-0.71181	-	-	+0.7112($sp^{1.88}$)C	34.75	65.25
σC_{28}-C_{31}	0.98597	51.28	48.72	0.7161($sp^{2.37}$)C	29.71	70.29
-	-0.70258	-	-	+0.6980($sp^{1.50}$)C	39.97	60.03
σC_{31}-O_{32}	0.99631	34.18	65.82	0.5373($sp^{1.98}$)C	0.00	100.0
-	-1.05946	-	-	+0.8434($sp^{1.80}$)O	0.00	100.0
πC_{31}-O_{32}	0.98183	33.53	66.74	0.5847($sp^{1.00}$)C	0.00	100.0
-	-0.39740	-	-	+0.8113($sp^{1.00}$)O	0.00	100.0
σC_{31}-O_{33}	0.99564	30.75	69.25	0.5547($sp^{2.78}$)C	26.48	73.52
-	-0.92044	-	-	+0.8321($sp^{2.17}$)O	31.57	68.43
σC_{35}-O_{36}	0.99620	34.08	65.92	0.5838($sp^{1.98}$)C	33.57	66.43
-	-1.05599	-	-	+0.8119($sp^{1.80}$)O	35.70	64.30
πC_{35}-O_{36}	0.98967	30.73	69.27	0.5543($sp^{1.00}$)C	0.00	100.0
-	-0.39675	-	-	+0.8323($sp^{1.00}$)O	0.00	100.0
σC_{35}-O_{37}	0.99554	30.77	69.23	0.5547($sp^{2.79}$)C	26.41	73.59
-	-0.91820	-	-	+0.8321($sp^{2.16}$)O	31.66	68.34
n_1N_{10}	0.81511	-	-	$sp^{99.99}$	0.03	99.97
-	-0.29998	-	-	-	-	-
n_1O_{15}	0.98581	-	-	$sp^{1.44}$	41.23	58.77
-	-0.57445	-	-	-	-	-
n_2O_{15}	0.88442	-	-	$sp^{99.99}$	0.01	99.99
-	-0.33551	-	-	-	-	-
n_3O_{15}	0.80785	-	-	$sp^{2.49}$	28.33	71.67
-	-0.54637	-	-	-	-	-
n_1O_{16}	0.98710	-	-	$sp^{0.54}$	64.66	35.34
-	-0.69479	-	-	-	-	-
n_2O_{16}	0.91141	-	-	$sp^{99.99}$	0.42	99.58
-	-0.26540	-	-	-	-	-
n_1O_{19}	0.98252	-	-	$sp^{0.82}$	55.06	44.94
-	-0.64215	-	-	-	-	-
n_2O_{19}	0.91962	-	-	$sp^{6.35}$	13.60	86.40
-	-0.39219	-	-	-	-	-
n_1N_{20}	0.86698	-	-	$sp^{2.76}$	26.62	73.38
-	-0.33229	-	-	-	-	-
n_1O_{32}	0.98829	-	-	$sp^{0.55}$	64.35	35.65
-	-0.71587	-	-	-	-	-
n_2O_{32}	0.93126	-	-	$sp^{1.00}$	0.01	99.99
-	-0.29119	-	-	-	-	-
n_1O_{33}	0.98979	-	-	$sp^{1.15}$	46.43	53.57
-	-0.61362	-	-	-	-	-
n_2O_{33}	0.91343	-	-	$sp^{1.00}$	0.00	100.0
-	-0.35262	-	-	-	-	-
n_1O_{36}	0.98819	-	-	$sp^{0.55}$	64.33	35.67
-	-0.71428	-	-	-	-	-

Bond (A-B)	ED/Energy	EDA%	EDB%	NBO	S%	P%
n_2O_{36} -	0.93154 -0.28884	- -	- -	$sp^{1.00}$ -	0.01 -	99.99 -
n_1O_{37} -	0.98969 -0.60952	- -	- -	$sp^{1.16}$ -	46.37 -	53.63 -
n_2O_{37} -	0.91664 -0.34980	- -	- -	$sp^{1.00}$ -	0.00 -	100.0 -

Table 5. Second-order perturbation theory analysis of Fock matrix in NBO basis corresponding to the intra molecular bonds of the CHODQC

Donor(i)	type	ED/e	Acceptor(j)	Type	ED/e	E(2)[a]	E(j)-E(i)[b]	F(ij)[c]
C_5-C_6	σ	0.98733	C_{35}-O_{36}	σ *	0.13399	1.25	1.20	0.049
-	π	0.82446	C_{35}-O_{36}	π*	0.13399	14.41	0.24	0.076
-	π	-	C_1-C_2	π*	0.12995	11.73	0.28	0.074
C_{13}-C_{14}	σ	0.98754	C_4-C_5	σ*	0.01001	1.84	1.26	0.061
-	σ	-	C_{18}-N_{20}	σ*	0.02628	1.55	1.16	0.054
-	π	0.84525	C_{12}-O_{16}	π*	0.00515	16.45	0.26	0.084
-	π	-	C_{18}-O_{19}	π*	0.13952	16.22	0.25	0.082
LPC_4	σ	0.54382	C_5-C_6	π*	0.15882	35.28	0.15	0.111
-	σ	-	C_{13}-C_{14}	π*	0.17309	37.81	0.13	0.106
LPN_{10}	σ	0.81494	C_{12}-O_{16}	π*	0.18382	27.67	0.26	0.108
LPO_{15}	σ	0.98597	C_{13}-C_{14}	σ*	0.01569	4.22	1.06	0.085
-	π	0.88385	C_{13}-C_{14}	π*	0.17309	22.49	0.32	0.110
LPO_{16}	σ	0.98828	N_{10}-C_{12}	σ*	0.03861	0.94	1.04	0.040
-	π	-	N_{10}-C_{12}	σ*	0.03861	11.50	0.62	0.107
-	π	-	C_{12}-C_{14}	σ*	0.02821	8.07	0.69	0.095
LPO_{19}	π	0.92775	C_{18}-N_{20}	σ*	0.02662	8.34	0.79	0.105
LPN_{20}	π	-	C_{18}-O_{19}	π*	0.98887	28.99	0.23	0.104
LPO_{32}	π	0.93175	C_{28}-C_{31}	σ*	0.98606	7.71	0.67	0.093
LPO_{32}	π	-	C_{31}-O_{33}	σ*	0.99564	16.26	0.54	0.119
LPO_{33}	σ	-	C_{31}-O_{32}	π*	0.99259	21.43	0.30	0.106
LPO_{36}	π	0.98819	C_{35}-O_{37}	σ*	0.99554	16.30	0.54	0.119
LPO_{37}	π	0.91664	C_{35}-O_{36}	π*	0.13399	21.44	0.31	0.105

Table 6 Polarizability values of CHODQC and halogen substitutions

	μ debye	α x10^{-23}esu	β x 10^{-30}esu	γ x 10^{-37}esu	MR=1.333παN,
CHODQC	3.7723	3.835	15.827	-37.219	MR = 25.210 x alpha
7Cl	2.2885	4.090	14.706	-43.982	96.684
8Cl	3.3286	4.014	19.209	-41.111	103.113
9Cl	4.2570	4.019	16.340	-40.007	101.323
7F	2.4881	3.852	14.266	-40.117	97.113
8F	3.3922	3.835	18.475	-38.524	96.684
9F	4.0094	3.844	15.433	-38.203	96.911
7Br	2.6165	4.200	14.325	-46.681	105.886
8Br	3.4016	4.103	18.702	-42.842	103.441
9Br	4.3456	4.097	14.845	-41.671	103.289

Table 7. PASS prediction for the activity spectrum of raj compound. Pa represents probability to be active and Pi represents probability to be inactive.

Pa	Pi	Activity
0.858	0.015	Ubiquinol-cytochrome-c reductase inhibitor
0.855	0.012	Methylenetetrahydrofolate reductase (NADPH) inhibitor
0.823	0.020	Testosterone 17beta-dehydrogenase (NADP+) inhibitor
0.777	0.017	Taurine dehydrogenase inhibitor
0.731	0.004	5 Hydroxytryptamine release inhibitor
0.732	0.014	Glutathione thiolesterase inhibitor
0.709	0.016	NADPH-cytochrome-c2 reductase inhibitor
0.705	0.015	2-Dehydropantoate 2-reductase inhibitor
0.700	0.012	Pterin deaminase inhibitor
0.690	0.005	N-methylhydantoinase (ATP-hydrolysing) inhibitor
0.711	0.026	Glutamate-5-semialdehyde dehydrogenase inhibitor
0.688	0.007	Aminobutyraldehyde dehydrogenase inhibitor
0.687	0.012	Kidney function stimulant
0.668	0.016	Fatty-acyl-CoA synthase inhibitor
0.673	0.029	Fusarinine-C ornithinesterase inhibitor

0.656	0.015	L-glutamate oxidase inhibitor
0.656	0.023	UDP-N-acetylglucosamine 4-epimerase inhibitor
0.641	0.008	Erythropoiesis stimulant
0.653	0.021	2-Hydroxyquinoline 8-monooxygenase inhibitor
0.639	0.007	Histamine release inhibitor
0.659	0.028	Ribulose-phosphate 3-epimerase inhibitor
0.646	0.017	Insulysin inhibitor
0.653	0.029	Dehydro-L-gulonate decarboxylase inhibitor

Table 8 The binding affinity values of different poses of the compound predicted by AutoDock Vina

Mode	Affinity (kcal/mol)	Distance from best mode (Å)	
-	-	RMSD l.b.	RMSD u.b.
1	-9.1	0.000	0.000
2	-8.7	23.021	25.648
3	-8.6	21.625	24.204
4	-8.5	4.709	6.627
5	-8.5	22.282	24.626
6	-8.2	15.464	16.890
7	-8.0	17.626	19.186
8	-8.0	2.659	10.111
9	-7.8	22.017	24.050

4.6 References

[1] M. Kidway, K. R. Bhushan, P. Sapra, R. K. Saxena, R. Guptha, Alumina-supported of antibacterial qunolines used microwaves, Bioorg. Med. chem. 8 (2000) 69-72.

[2] S. Tewari, P. M. S. Chauhan, A. P. Bhaduri, M. Fatima, R. K. Chatterji, Synthesis and anti-filarial agents Bioorg. Med. Chem. Lett. 10 (2000) 1409-1412.

[3] T. Narendar, S. K. Tanvir, M. S. Rao, K. Srivastava, S. K. Puri Prenylated chalcones isolated from Ctotalaria genus inhibits invitro growth of human malaria parasite plasmodium falciparum Bioorg. Med. Chem. lett. 15 (2005) 2453-2455.

[4] R. F Hector An overview of anti-fungal drugs and their use for treatments of deep and superficial mycoses in animals, Clin. Tech. Small Anim. Pract. 20 (2005) 240-249.

[5] K. M. Khan, Z. S. Saify, Z. A. Khan, M. Ahmed, M. Saeed, M. Schick, H. J. Kohlbau, W. Voelter, Antibiotics, Antiviral drugs, chemotherapeutics. cytostatics-syntheses and cytotoxic antimicrobial, antifungal and cardiovascular activity of new quinoline derivatives, Arzheim. Forsch-Drug Res. 50 (2000) 915-924.

[6] A. Nayyar, A. Malde, E. Coutinho, R. Jain, Synthesis, anti-tuberculosis activity and 3D-QSAR study of ring-substituted-2/4-quinoline carbaldehyde derivatives, Bioorg. Med. Chem. 14 (2006) 7302-7310.

[7] B. Sureshkumar, Y. Sheena Mary, C. Yohannan Panicker, K. S. Resmi, S. Suma, Stevan Armaković, Sanja J. Armaković, C. Van Alsenoy. Spectroscopic analysis of 8-hydroxyquinoline-5-sulphonic acid and investigation of its reactive properties by DFT and molecular dynamics simulations. J. Mol. Struct. 1150 (2017) 540-552.

[8] G. Bandoli, A. Dolmella, F. Tisato, M. Porchia, F. Refosco Mononuclear six coordinated Ga (III) complexes, a comprehensive survey, Coord. Chem. Rev. 253 (2009) 56-77.

[9] L. E. Scott, C. Orvig, Medicinal inorganic chemistry approaches to passivation and removal of aberrant metal ions in disease Chem. Rev. 109 (2009) 4885-4910.

[10] M. J. Hannon, Metal based anticancer drugs, from a past anchored in platinum chemistry to a post genomic future of diverse chemistry and biology Pure Appl. Chem. 79 (2007) 2243-2261.

[11] R. T. Ulahannan, C. Y. Panicker, H. T. Varghese, R. Musiol, J. Jampilek, C. Van Alsenoy, J. A. War, S. K. Srivastava, Molecular structure, FT-IR, FT-Raman, NBO, HOMO and LUMO, MEP, NLO and molecular docking study of 2-[(E)-2-(2-bromophenyl)-ethenyl quinoline-6-carboxylic acid Spectrochim. Acta. 151 (2015) 184-197.

[12] E. Fazal, C. Y. Panicker, H. T. Varghese, S. Nagarajan, B. S. Sudha, J. A. War, S. K. Srivastava, S. B. Harikumar, P. L. Anto, Vibrational spectroscopic and molecular docking study of 4-methylphenylquinoline-2-carboxylate Spectrochim. Acta 143 (2015) 213-222.

[13] S. A. Khan, A. M. Asiri, S. H. Al-Thaqafy, H. M. F. Aidallah, S. A. El-Daly, Synthesis, characterization and spectroscopic behavior of novel 2-oxo-1,4-disubstituted-1,2,5,6-tetrahydrobenzo[h]quinoline-3-carbonitrildyes, Spectrochim. Acta 133 (2014) 141-148.

[14] C. B. Sangani, J. A. Makawana, X. Zhang, S. C. Teraiya, I. Lin, H. L. Zhu, Design, synthesis and molecular modeling of pyrazole-quinoline-pyridine hybrids as a new class of antimicrobial and anticancer agents, Eur. J. Med. Chem.76 (2014) 549-557.

[15] L. Strekowski, J. L. Mokrosz, A. H. Vidya, A. Czarny, M. T. Cegla, R. L. Wydra, S. E. Patterson, R. S. Schinazi, Synthesis and quantitative structure- Activity relationship analysis of 2-(aryl or heteroaryl) qunoline-4-amines a new class of anti-HIV-1agents, J. med. Chem. 34 (1991) 1739-1746.

[16] J. Jampilek, R. Musiol, M. Pesko, K. Kralova, M. Vejsova, J. Carroll, A. Coffey, J. Finster, D. Tabak, H. Niedbala, V. Kozik, J. Polanski, J. Dohnal, Ring-substituted 4-hydroxy-1H-quinolin-2-ones: Preparation and biological activity. Molecules, 14 (2009) 1145-1159.

[17] Gaussian 09, Revision B.01, M. J. Frisch, G. W. Trucks, H. B. Schlegel, G. E. Scuseria, M.A. Robb, J. R. Cheeseman, G. Scalmani, V. Barone, B. Mennucci, G. A. Petersson, H. Nakatsuji, M. Caricato, X. Li, H. P. Hratchian, A. F. Izmaylov, J. Bloino, G. Zheng, J. L. Sonnenberg, M. Hada, M. Ehara, K. Toyota, R. Fukuda, J. Hasegawa, M. Ishida, T. Nakajima, Y. Honda, O. Kitao, H. Nakai, T. Vreven, J. A. Montgomery, Jr., J. E. Peralta, F.Ogliaro, M. Bearpark, J. J. Heyd, E. Brothers, K. N. Kudin, V. N. Staroverov, T. Keith, R. Kobayashi, J. Normand, K. Raghavachari, A. Rendell, J. C. Burant, S. S. Iyengar, J. Tomasi, M. Cossi, N. Rega, J. M. Millam, M. Klene, J. E. Knox, J. B. Cross, V. Bakken, C. Adamo, J. Jaramillo, R. Gomperts, R.E. Stratmann, O. Yazyev, A. J. Austin, R. Cammi, C. Pomelli, J. W. Ochterski, R. L. Martin, K. Morokuma, V. G. Zakrzewski, G. A. Voth, P. Salvador, J. J. Dannenberg, S. Dapprich, A. D. Daniels, O. Farkas, J. B. Foresman, J. V. Ortiz, J. Cioslowski, and D. J. Fox, Gaussian, Inc., Wallingford CT, 2010.

[18] J. B. Foresman, in: E. Frisch (Ed.), Exploring Chemistry with Electronic Structure Methods: A Guide to Using Gaussian, Gaussian Inc., Pittsburg, PA, 1996.

[19] Gauss View, Version 5, R. Dennington, T. Keith, J. Millam, SemichemInc., Shawnee Mission, KS, 2009.

[20] J. M. L. Martin, C. Van Alsenoy, GAR2PED, A Program to Obtain a Potential Energy Distribution from a Gaussian Archive Record, University of Antwerp, Belgium, 2007.

[21] J. Chowdhury, M.Ghosh, T.N. Misra, Surface enhanced Raman scattering of 2,2-biquinoline adsorbed on colloidal silver particles, Spectrochim. Acta 56 (2000) 2107-2115.

[22] R. T. Ulahannan, C. Y. Panicker, H. T. Varghese, C. Van Alsenoy, R. Musiol, J. Jampilek, P. L. Anto Spectroscopic (FT-IR, FT-Raman) investigations and quantum chemical calculations of 4-hydroxy-2-oxo-1,2-dihydroquinoline-7-carboxylic acid Spectrochim. Acta 121 (2014) 404-414.

[23] N. P. G. Roeges, A Guide to the Complete Interpretation of the Infrared spectra of Organic Compounds, Wiley, New York 1994.

[24] G. Varsanyi, Assignments of Vibrational Spectra of Seven Hundred Benzene Derivatives, Wiley, New York 1974.

[25] N. B. Colthup, L. H. Daly, S. E. Wiberly, Introduction to IR and Raman Spectroscopy, Academic Press, New York, 1990.

[26] R. M. Silverstein, F. X. Webster, Spectrometric Identification of Organic Compounds, ED. 6, John Wiley, Asia, 2003.

[27] R. T. Ulahannan, C. Y. Panicker, H. T. Varghese, C. Van Alsenoy, R. Musiol, J. Jampilek, P. L. Anto, Spectroscopic (FT-IR, FT-Raman) investigations and quantum chemical calculation sof 4-hydroxy-2-oxo-1,2-dihydroquinoline-7-carboxylic acid, Spectrochim. Acta 121 (2014) 404-414.

[28] C. Y. Panicker, H. T. Varghese, A. John, D. Philip, H. I. S. Nogueira, Vibrational spectra of melamine diborate, $C_3N_6H_62H_3BO_3$, Spectrochim. Acta 58 (2002) 1545-1551.

[29] Y. S. Mary, P. J. Jojo, C. Van Alsenoy, M. Kaur, M. S. Siddegowda, H. S. Yathirajan, H. I. S. Nogueira, S. M. A. Cruz, Vibrational spectroscopic studies (FT-IR, FT-Raman, SERS) and quantum chemical calculations on cyclobenzaprinium salicylate, Spectrochim. Acta 120 (2014) 340-350.

[30] L. J. Bellamy, The IR spectra of Complex Molecules, John Wiley and Sons, New York 1975.

[31] S. H. R. Sebastian, M. A. Al-Alshaikh, A. A. El-Emam, C. Y. Panicker, J. Zitko, M. Dolezal, C. Van Alsenoy, Spectroscopic quantum chemical studies, Fukui functions,

in vitro antiviral activity and molecular docking of 5-chloro-N-(3-nitrophenyl) pyrazine-2-carboxamide, J. Mol. Struct. 1119 (2016) 188-199.

[32] V. V. Menon, E. Foto, Y. S. Mary, E. Karatas, C. Y. Panicker, G. Yalcin, S. Armakovic, S. J. Armakovic, C. Van Alsenoy, I. Yildiz, Vibrational spectroscopic analysis, molecular dynamics simulations and molecular docking study of 5-nitro-2-phenoxymethyl benzimidazole, J. Mol. Struct. 1129 (2017) 86-97.

[33] G. Socrates, Infrared Characteristic Group Frequencies, John Wiley and Sons, New York, 1981.

[34] G. Varsanyi, Assignments of Vibrational Spectra of Seven Hundred Benzene derivatives,Wiley, New York, 1974.

[35] V. S. Madhvan, H. T. Varghese, S. Mathew, J. Vinsova, C. Y. Panicker, FT-IR, FT-Raman and DFT calculations of 4-Chloro-2-(3,4-dichlorophenyl carbamoyl) phenyl acetate, Spectrochim. Acta 72 (2009) 547-553.

[36] C. Y. Panicker, K. R. Ambujakshan, H. T. Varghese, S. Mathew, S. Ganguli, A. K. Nanda, C. Van Alsenoy, FT-IR, FT-Raman and DFT calculations of 3-{[(4-fluorophenyl)methylene]amino}-2-phenylquinazolin-4(3H)-one, J. Raman. Spectrosc. 40 (2009) 527-536.

[37] A. S. El-Azab, Y. S. Mary, C. Y. Panicker, A. A.-M A-Aziz, A. Magda, El-Sherbeny, C. V. Alsenoy, DFT and experimental (FT-IR and FT-Raman) investigation of vibrational spectroscopy and molecular docking studies of 2-(4-oxo-3-phenyl-3,4-dihydroquinazolin-2-ylthio)-N-(3,4,5 trimethoxy phenyl) acetamide, J. Mol Struct. 1113 (2016) 133-145.

[38] F. J. Luque, J. M. Lopez, M. Orozco, Perspective on electrostatic interactions of a solute with a continuum, a direct utilization of ab initio molecular potentials for the prevision of solvent effects, Theor. Chem. Acc. 103 (2000) 343–345.

[39] P. Politzer, J. S. Murray, in: D. L. Beveridge, R. Lavery, (Eds.), Theoretical Biochemistry and Molecular Biophysics, Springer, Berlin, 1991.

[40] E. D. Glendening, A. E. Reed, J. E. Carpenter, F. Weinhold, NBO Version 3.1.

[41] C. Adant, M. Dupuis, J. L. Bredas, Ab initio study of the nonlinear optical properties of urea, electron correlation and dispersion effects, Int. J. Quantum. Chem. 56 (1995) 497-507.

[42] G. Purohit, G. C. Joshi, Second order polarizabilities of some quinolines, Indian J. Pure Appl. Phys. 41 (2003) 922-927.

[43] Y. S. Mary, C. Y. Panicker, H. T. Varghese, K. Raju, T. E. Bolelli, I. Yildiz, C. M. Granadeiro, H. I. S. Nogueira, Vibrational spectroscopic studies and computational study of 4-fluoro-N-(2'-hydroxy-4'-nitrophenyl) phenylacetamide, J. Mol. Struct. 994 (2011) 223-231.

[44] S. R. Sheeja, N. A. Mangalam, M. R. P. Kurup, Y. S. Mary, K. Raju, H. T. Varghese, C. Y. Panicker, Vibrational spectroscopic studies and computational study of quinoline-2carbaldehyde benzyol hydrazone, J. Mol. Struct. 973 (2010) 36-46.

[45] M. Cunha-Rodrigues, M. Prudencio, M. M. Mota, W. Haas, Antimalarial drugs-host targets (re) visited, Biotechnol. J. 1 (2006) 321-332.

[46] C. Daneshvar, T. M. Davis, J. Cox-Singh, M. Z. Rafa'ee, S. K. Zakaria, P. C. Divis, B. Singh, Clinical and laboratory features of human Plasmodium knowlesi infection, Clin. Infect. Dis. 49 (2009) 852-860.

[47] B. Gunsaru, S. J. Burgess, W. Morrill, J. X. Kelly, S. Shomloo, M. J. Smilkstein, K. Liebman, D. H. Peyton, Simplified reversed chloroquines to overcome malaria resistance to quinoline-based drugs, Antimicrob. Agents Chemother. 61 (2017) 1913-1916.

[48] B. Sandhya, S. Kumar, S. Drabu, R. Kumar, Structural modifications of quinoline-based antimalarial agents: Recent developments, J. Pharm. Bioallied. Sci. 2 (2010) 64-71.

[49] A. Lagunin, A. Stepanchikova, D. Filimonov, V. Poroikov, PASS: prediction of activity spectra for biologically active substances, Bioinformatics 16 (2000) 747-748.

[50] A. C. R. Sodero, B. Abrahim-Vieira, P. H. M. Torres, P. G. Pascutti, C. R. S. Garcia, V. F. Ferreira, D. R. da Rocha, S. B. Ferreira, F. P. Silva, Atovaquone is a drug that inhibits the respiratory chain of Plasmodium falciparum, but with serious limitations like known resistance, low bioavailability and high plasma protein binding, Mem. Inst. Oswaldo. Cruz, 112 (2017) 299-308.

[51] A. M. Stickles, L. M. Ting, J. M. Morrisey, Y. Li, M. W. Mather, E. Meermeier, A. M. Pershing, I. P. Forquer, G. P. Miley, S. Pou, R. W. Winter, D. J. Hinrichs, J. X. Kelly, K. Kim, A. B. Vaidya, M. K. Riscoe, A. Nilsen, Inhibition of Cytochrome bc1 as a Strategy for Single-Dose, Multi-Stage Antimalarial Therapy, Am. J. Trop. Med. Hyg. 92 (2015) 1195-1201.

[52] G. M. Morris, R. Huey, W. Lindstrom, M. F. Sanner, R. K. Belew, D. S. Goodsell, A. J. Olson, Autodock4 and AutoDockTools4: automated docking with selective receptor flexibility, J. Comput. Chem. 16 (2009) 2785-2791.

[53] O. Trott, A. J. Olson, AutoDock Vina: Improving the speed and accuracy of docking with a new scoring function, efficient optimization and multithreading, J. Comput. Chem. 31 (2010) 455-461.

[54] J. A. War, K. Jalaja, Y. S. Mary, C. Y. Panicker, S. Armakovic, S. J. Armakovic, S. K. Srivastava, C. Van Alsenoy, Spectroscopic characterization of 1-[3-(1H-imidazol-1-yl)propyl]-3-phenylthiourea and assessment of reactive and optoelectronic properties employing DFT calculations and molecular dynamics simulations, J. Mol. Struct. 1129 (2017) 72-85.

CHAPTER V
SPECTROSCOPIC CHARACTERIZATION, DOCKING STUDIES OF 6-CHLORO-*N*-(3-IODO-4-METHYLPHENYL)-PYRAZINE-2-CARBOXAMIDE AND INVESTIGATION OF ITS REACTIVE PROPERTIES BY DFT CALCULATIONS.

5.1 Introduction

Pyrazine products are used as inhibitors of protein kinases, as representatives with antifungal, antibacterial, anticancer and antiviral activities [1]. Pyrazine moieties are found as medical and agricultural drug intermediates, in a variety of vegetables, bell pepper, beets, asparagus and peanuts, in beef, blackberry, corn, grape fruit juice, and breakfast cereal and is mainly used to confect the essence of cocoa, coffee, meat or potato flavor [2]. Pyrazinamide is a member of the pyrazine family and it is known as a very effective antimycobacterial agent, with a well-established role in tuberculosis treatment [3]. Pyrazine carboxamide is among the first line drugs for the treatment of tuberculosis and it kills or stops the growth of certain bacteria that cause tuberculosis [4]. Pyrazinoic acid disrupts membrane energetics and inhibits membrane transport function in mycobacterium tuberculosis [5]. Silymarin, an active polyphenolic fraction of Silybum marianum, is an ancient herbal remedy used to treat a range of liver disorders, including hepatitis, cirrhosis, and as a hepatoprotective nutritional supplement against poisoning from alcohol, chemical, wild mushroom, and environmental toxins. Silymarin consists of a group of flavonolignans, namely silydianin, silychristin, silybin, and isosilybin [6]. Its antioxidant activity is due to its free radical scavenging property, an increase in superoxide dismutase activity, peroxide formation and the inhibition of lipid [7-8]. The pyrazine ring is a part of many polycyclic compounds of biological and/or industrial significance. The widespread occurrence of pyrazines in nature, especially in the flavours of many food systems, their effectiveness at very low concentrations is responsible for the high interest in these compounds. Some substituted pyrazine carboxamides, tested in vitro, showed not only antimycobacterial and antifungal activities [9-10] but also may play role as herbicidal chemical agents due to their inhibition properties in photosynthetic electron transport in photosystem 2. [11]. Many pyrazinamide derivatives inhibited photosynthetic electron transport (PET) in plant chloroplasts [12-15] and they were found to act as photosystem (PS) 2 inhibitors. In order to analyze the effect of halogen substitution, in the parent molecule, the position of iodine atom is replaced by bromine, chlorine and fluorine atoms respectively and which are designated as 10Br, 10Cl, 10F. Similarly the positions of hydrogen atom in the parent molecule CIMPC, 16H, 18H and 20H are replaced by iodine, bromine, chlorine and fluorine

atoms respectively which are designated as 16I, 16Br, 16Cl, 16F, 18I, 18Br, 18Cl, 18F and 20I, 20Br, 20Cl, 20F.

5.2 Experimental Details

The condensation of 6-chloropyrazine-2-carboxylic acid chloride with 3-iodo-4-methylaniline yielded 6-chloro-*N*-(3-iodo-4-methylphenyl)-pyrazine-2-carboxamide [16]. A mixture of 6-chloropyrazine-2-carboxylic acid (50.0 mmol) and thionyl chloride (5.5 mL, 75.0 mmol) in dry toluene (20 mL) was refluxed for about 1 h. Excess of thionyl chloride was removed by repeated evaporation with dry toluene *in vacuo*. The crude acyl chloride dissolved in dry acetone (50 mL) was added dropwise to a stirred solution of the 3-iodo-4-methylaniline (50.0 mmol) in 50 mL of dry pyridine at room temperature. After the addition was complete, stirring continued for another 30 min. The reaction mixture was then poured into 100 mL of cold water and the crude amide was collected and recrystallized from aqueous ethanol (scheme 1).6-Chloro-*N*-(3-iodo-4-methylphenyl)-pyrazine-2-carboxamide (CAS Registry Number: 1072927-31-1). Yield 83%; Anal. Calcd. For $C_{12}H_9ClIN_3O$ (373.6): 38.58% C, 2.43% H, 11.25% N; Found: 38.80% C, 2.62% H, 11.37% N. Mp 173.4-174.5 °C; Log *P*: 3.33; Clog *P*: 3.54369; TLC: *R*F = 0.81; 1H-NMR δ: 9.38 (1H, s, H3), 9.32 (1H, bs, NH), 8.81 (1H, s, H5), 8.21 (1H, d, *J*=2.2 Hz, H2′), 7.68 (1H, dd, *J*=8.2 Hz, *J*=2.2 Hz, H6′), and 7.24 (1H, d, *J*=8.2 Hz, H5′), 2.42 (3H, s, CH3); 13C-NMR δ: 159.2, 147.6, 147.4, 143.7, 142.2, 138.3, 135.3, 129.9, 129.7, 119.8, 100.8, and 27.5.

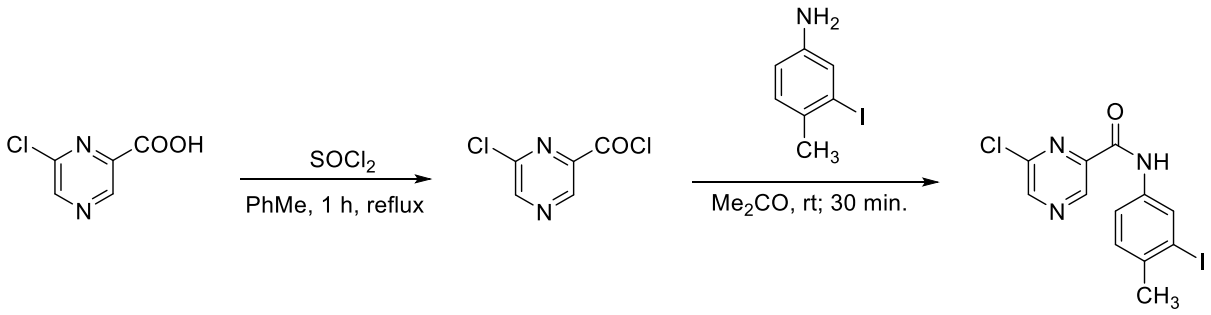

Scheme 1:

Pyrazine derivatives have been synthesized and successfully evaluated as agents with diverse pharmacological effects, including but not limited to anti-proliferative, anti-infective, and effects on cardiovascular or nervous system, and some of them have become clinically used

drugs worldwide [17]. Pyrazinamide (PZA), a first-line anti-TB drug, was discovered through an effort to find anti-tubercular nicotinamide derivatives. Our research is focused on PZA analogues with a -CONH- bridge connecting the pyrazine and benzene rings. This moiety can form centrosymmetric dimer pairs with the peptidic carboxamido group of some peptides, needed for binding to the receptor site, possibly by formation of hydrogen bonds. 6-Chloro-*N*-(3-iodo-4-methylphenyl)-pyrazine-2-carboxamide had minimal antimycobacterial activity (MIC = 8 mg/L) against M. tuberculosis comparable with the standard PZA (MIC = 8 mg/L) [18]. The photosynthesis inhibition, antialgal activity and the effect of a series of pyrazine derivatives as abiotic elicitors on the accumulation of flavonoids in a callus culture of Ononis arvensis (L.) were investigated and the most active inhibitor of the oxygen evolution rate in spinach chloroplasts was 6-Chloro-*N*-(3-iodo-4-methylphenyl)-pyrazine-2-carboxamide (IC_{50} = 51.0 μmol/L). The maximal flavonoid production (about 900%) was reached after a twelve-hour elicitation process with 6-Chloro-*N*-(3-iodo-4-methylphenyl)-pyrazine-2-carboxamide [19].

The FT-IR spectrum (Fig. 1) was recorded using KBr pellets on a DR/JASCO FT-IR 6300 spectrometer. The FT-Raman spectrum (Fig. 2) was obtained on a Bruker RFS 100/s, Germany. For excitation of the spectrum, the emission of Nd:YAG laser was used with an excitation wavelength of 1064 nm, a maximal power 150 mW; measurement of solid sample.

5.3 Computational Details

Calculations of the title compound were carried with using the Gaussian09 program [20] using the B3LYP/ccpVDZ basis set to predict the molecular structure and wavenumbers in the gaseous phase and a scaling factor of 0.9613 had to be used for obtaining a considerably better agreement with the experimental data [21]. The structural parameters corresponding to the optimized geometry of the title compound (Fig. 3) are given in Table 1. The assignments of the calculated wavenumbers are done using GAR2PED [22] and Gauss view software [23].

5.4 Results and Discussion

In the following discussion, phenyl and pyrazine rings are designated as Ph and Pz respectively.

5.4.1 Geometrical Parameters

The C-N and C-C bond lengths in the pyrazine ring of the title compound are 1.3318, 1.3394, 1.3440, 1.3185 Å and 1.3971, 1.4038 Å, respectively, which are shorter than the normal

C-N bond length (1.49 Å) and the C-C bond length (1.54 Å). The reported C-N and C-C bond lengths of the pyrazine ring are 1.4104, 1.3577, 1.3577, 1.3608 Å and 1.4121, 1.3517 Å [24]. The bond lengths C_9-N_{11} and C_{12}-N_{11} (the carboxamide linker) are 1.3657 Å and 1.4074 Å which are also shorter than the normal C-N single bond and these bonds have some character of a double or conjugated bond [25]. The C-C bond lengths in the phenyl ring are in the range 1.3890-1.4043Å. At N_{11} position, the angles C_9-N_{11}-H_{21} = 114.3°, C_9-N_{11}-C_{12} = 128.8° and C_{12}-N_{11}-H_{21} = 116.9°, this asymmetry of angles is due to the weakening of the N-H bond. At C_{17} position, the angles C_{14}-C_{17}-I_{26}, C_{19}-C_{17}-I_{26}, C_{14}-C_{17}-C_{19} are 116.4, 120.2 and 123.4° respectively. This asymmetry is due to the iodine substitution in the phenyl ring. The bond angles C_4-C_5-N_6, C_4-C_5-C_9, C_9-C_5-N_6 are 121.2, 120.0 and 118.8°, respectively. This asymmetry is attributed to the interaction of pyrazine ring and carboxamide group. The bond angles C_{17}-C_{19}-C_{22}, C_{15}-C_{19}-C_{22}, C_{17}-C_{19}-C_{15} at C_{19} are 123.9, 120.2, 115.9° and the asymmetry is due to the interaction of the neighboring groups.

5.4.2 IR and Raman Spectra

The calculated scaled wavenumbers, observed IR, Raman bands and assignments are given in Table 2. According to literature, the N-H vibrations are expected in the regions, 3390 ± 60 cm^{-1} (stretching), 1500-1200 and 790 ± 70 cm^{-1} (bending modes) [26-29]. For the title compound, these modes were assigned at 3330 cm^{-1} (IR), 3494 cm^{-1} (Raman), 3418 (DFT) (stretching), 1509(DFT)(in-plane bending), 674 cm^{-1} (IR), 668 cm^{-1} (Raman), 667 cm^{-1} (DFT)(out-of-plane bending). For the title compound, the N-H stretching mode has an IR intensity of 76.90 and Raman activity of 247.15 with a PED of 91%. The PED of N-H deformation modes of the title compound are in between 14 and 44%. For the deformation mode at 667 cm^{-1}, the IR intensity is low while the other mode have high IR intensity for the title compound. In the present case, the N-H stretching mode is red shifted by 88 cm^{-1} in the IR spectrum from the computed value, which indicates the weakening of the N-H bond [30]. The C-N stretching modes are expected in the range 1275 ± 55 cm^{-1} [26] and the bands at 1232 cm^{-1} (DFT) with low IR intensities and PED around 28%, at 1230(IR) spectrum and 1237 cm^{-1}(Raman) spectrum are assigned as the C-N stretching modes of the title compound. The reported C-N stretching modes are at 1265, 1239 cm^{-1} in the IR spectrum and at 1261, 1248 cm^{-1} (DFT) [31]. For the title compound, the carbonyl stretching vibration is observed at 1670 cm^{-1} in the IR spectrum and at 1667 cm^{-1} in the Raman spectrum which is expected in the region 1715-1600 cm^{-1} [26] while the computed value is 1706 cm^{-1} with an IR intensity of 198.96 and Raman activity 153.36 and the PED is 66%. According to literature [26], the CH_3

modes are expected in the regions, 3050-2900 cm^{-1} (stretching), 1485-1350, 1100-900 cm^{-1} (deformation modes) and for the title compound, these modes are assigned at 3024, 2982, 2925 cm^{-1} (IR), 2957, 2924 cm^{-1} (Raman), 3010, 2987, 2934 cm^{-1} (DFT) (stretching), 1433, 1031 cm^{-1} (IR), 1035 cm^{-1} (Raman), in between 1462-989 cm^{-1} (DFT) (bending). Analysis of vibrational spectra of substituted benzenes shows that the stretching vibrations of C-I corresponds to a band around 340 cm^{-1} experimentally [32, 33]. The carbon-iodine stretching band of the title compound is assigned at 311 cm^{-1} theoretically, 271cm^{-1} experimentally. Zainuri et al. reported the CI stretching mode at 317 cm^{-1} [34]. For the title compound, the phenyl CH stretching bands are observed at 3062 cm^{-1} in the IR spectrum and 3063 cm^{-1} in the Raman spectrum, while the computed values are in the range 3159-3059 cm^{-1} which are in agreement with the literature [26, 35]. The phenyl ring stretching modes of the title compound are observed at 1580, 1485, 1298 cm^{-1} in the IR spectrum, at 1598, 1561, 1302 cm^{-1} in the Raman spectrum and at 1596, 1571,1476, 1373, 1291 cm^{-1} theoretically (DFT) [26]. The tri-substituted phenyl ring breathing mode of the title compound is assigned at 862(IR), 866(Raman) and 858 cm^{-1} (DFT) with PED 21% which is in agreement with the literature [36]. The in-plane and out-of-plane C-H deformations of the phenyl ring are expected above and below 1000 cm^{-1} respectively [26] and these modes of the title compound were assigned at 1269, 1248, 1193 cm^{-1} (DFT) (in-plane CH bending modes) and 926 (IR), 908, 890, 794 cm^{-1} (DFT) (out-of-plane bending modes). The IR bands in the region of 2676-1800 cm^{-1} and the large broadening seen in the IR spectrum support the intra-molecular hydrogen bonding [37].

The pyrazine C-H stretching modes of the title compound were observed at 3116, 3093 cm^{-1} theoretically which are expected in the range 3100-3000 cm^{-1} [38]. In the present case, the pyrazine ring stretching modes were observed at 1520, 1121 cm^{-1} in the IR spectrum and at 1525, 1395 cm^{-1} in the Raman spectrum while the PED analysis gives these modes in a range 1548-1140 cm^{-1} which are in agreement with literature [39,40]. In the present case, the pyrazine ring stretching modes have IR intensities in the range 2.18 to 59.64 and Raman activities 6.05 to 477.37 and the PEDs are around 50%. For the title compound,

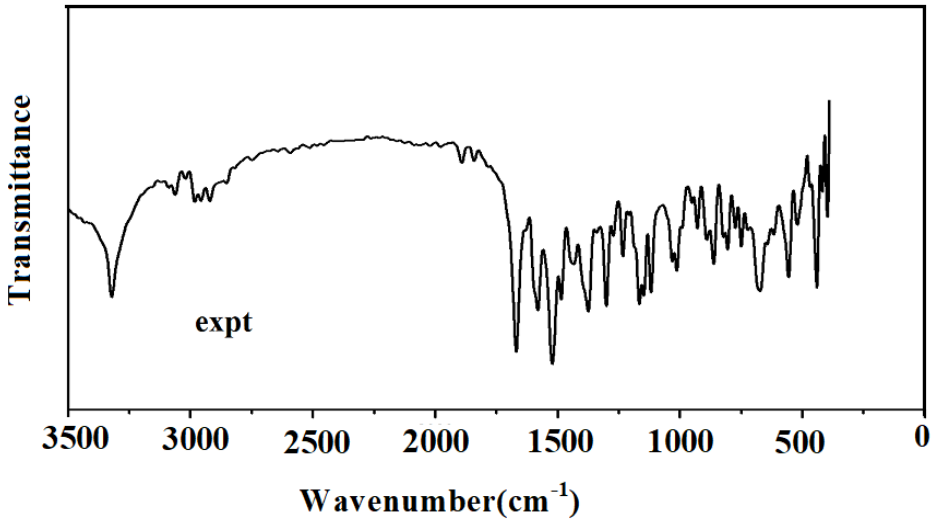

Fig. 1 FT-IR spectrum of 6-Chloro-N-(3-iodo-4- methylphenyl)-pyrazine-2-carboxamide

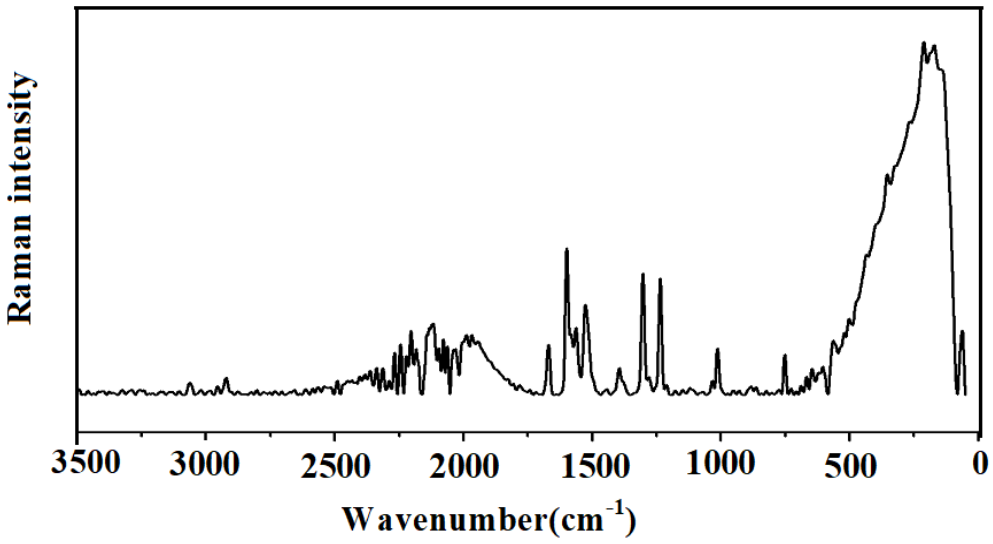

Fig. 2 FT-IR spectrum of 6-Chloro-N-(3-iodo-4- methylphenyl)-pyrazine-2-carboxamide

the ring breathing mode of the pyrazine ring was assigned at 991 cm^{-1} in the DFT with low IR intensity and Raman activity, while the reported value is at 1015 cm^{-1} (DFT) [39]. For the title compound, the in-plane and out-of-plane CH bending modes of the pyrazine ring were assigned at1384, 1158, 943, and 884 cm^{-1} theoretically. The experimentally observed values are 1377, 1166, 1179,958 cm^{-1} which are in agreement with the literature [39].

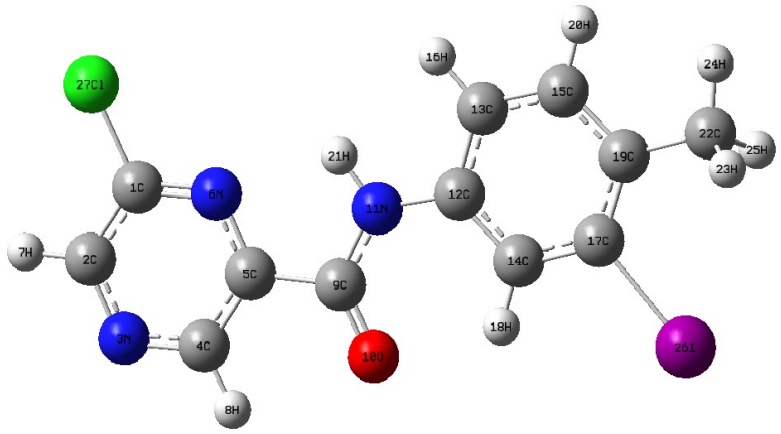

Fig. 3 Optimized geometry of 6-Chloro-*N*-(3-iodo-4-methylphenyl)-pyrazine-2-carboxamide

5.4.3 Natural Bond Orbital Analysis

The NBO (Natural Bond Orbital) calculations were performed using NBO 3.1 program [41] and the important interactions are presented in the table 3 and 4. The important interactions are: $LPCl_{27} \rightarrow C_1\text{-}N_6$, $LPN_{11} \rightarrow C_{12}\text{-}C_{13}$, $LPN_{11} \rightarrow C_9\text{-}O_{10}$, $LPO_{10} \rightarrow C_9\text{-}N_{11}$, $LPO_{10} \rightarrow C_5\text{-}C_9$, $C_{15}\text{-}C_{19} \rightarrow C_{14}\text{-}C_{17}$ and $C_{15}\text{-}C_{19} \rightarrow C_{12}\text{-}C_{13}$ with energies, 14.26, 31.00, 50.74, 22.46, 18.84, 23.23 and 22.77 kcal/mol. 100% p-character is found in Cl_{27}, I_{26}, N_{11} and O_{10}.

5.4.4 Nonlinear optical properties

The calculated first hyper polarizability of the title compound is 24.973×10^{-30} esu which is 192.1 times that of standard NLO material urea (0.13×10^{-30} esu) [42]. For a pyrazine derivative the first hyper polarizability is reported at 9.77×10^{-30} esu [24]. We conclude that the title compound is an attractive object for future studies of nonlinear optical properties. In CIMPC substitution increases the dipole moment in the order 26>18>16>20. Highest dipole moment value is noticed for 26C and lowest value for 20I. Highest polarizability value is noticed for 20I and lowest value for 18I. For first order hyper polarizability, β value decreased to a large extent for 18^{th} position for F, Cl and I except Br. Highest β value is noticed for 20I and lowest value for 18Cl.(Table 5)

5.4.5 Frontier Molecular Orbitals

In order to understand global stability and reactive properties of the title compound we have investigated frontier molecular orbitals. Namely, the highest occupied molecular orbital (HOMO) and lowest unoccupied molecular orbital (LUMO) are the main molecular orbitals

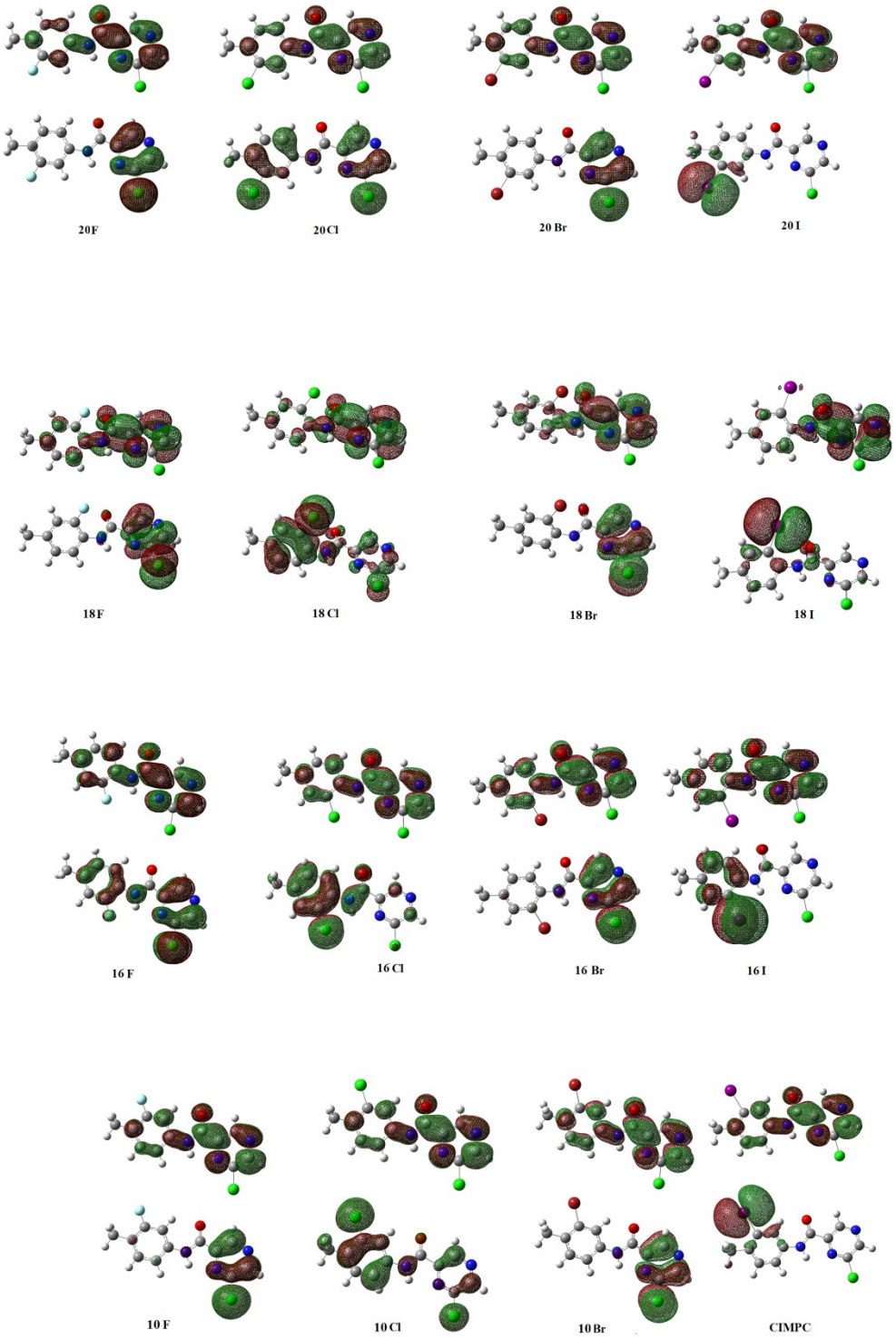

Fig. 4 HOMO-LUMO plots of 6-Chloro-*N*-(3-iodo-4-methylphenyl)-pyrazine-2-carboxamide

that take part in reactions with other molecular structures. Distribution of HOMO and LUMO provides important insight into the reactive properties of organic molecules, Figure 4. Frontier molecular orbital study is used to explain the chemical behaviour and stability of the molecular system. The atomic orbital components of the frontier molecular orbitals are shown in Fig. 4. The delocalization of HOMO and LUMO over the molecular system shows the charge transfer within the molecular system. The HOMO–LUMO gap is found to be 0.834 eV. The chemical descriptors can be evaluated by using HOMO and LUMO orbital energies, E_{HOMO} and E_{LUMO} as: ionization energy $I = -E_{HOMO}$, electron affinity $A = -E_{LUMO}$, hardness $\eta = (I-A)/2$, chemical potential $\mu = -(I+A)/2$ and electrophilicity index $\omega = \mu 2/2\eta$. For the title compound, I = 5.934, A = 5.100, η = 0.417, μ = -5.517 and ω = 36.496 eV.

For the title compound the HOMO is delocalized over the entire iodine atom and slightly over the phenyl ring and CH_3 group while the LUMO is delocalized over the entire molecule except iodine, chlorine atom and CH_3 group. For halogen substitution 10Br, HOMO is delocalized only over the pyrazine ring. For 10Cl substitution HOMO is delocalized over the entire molecule except the C=O group and the nitrogen atom (position 3) of pyrazine ring. For 10F HOMO is over entire pyrazine ring except nitrogen (position 3). While for 10Br, 10Cl and 10F the LUMO delocalization is same over the entire molecule except the CH_3 group, chlorine atom and corresponding halogen atoms.

For halogen substitution 16I HOMO is delocalized the entire phenyl ring and iodine atom. For 16Br the HOMO is over entire pyrazine ring except nitrogen atom (position 3). For 16Cl HOMO is delocalized entire phenyl ring, C=O group and slightly over the pyrazine ring. For 16F the HOMO is delocalized over entire pyrazine ring except nitrogen atom (positon 3) and slightly over the phenyl ring and nitrogen atom of carboxamide group. For halogen substitution 16I, 16Br, 16Cl and 16F the LUMO delocalization is the same over the entire molecule except the CH_3 group, chlorine atom and the corresponding halogen atoms and this is also as in the previous halogen substitutions.

For halogen substitutions 18I the HOMO is strongly delocalized over the iodine atom. For halogen substitution 18Br the HOMO is over entire pyrazine ring except nitrogen atom (Position 3). For 18Cl substitution the HOMO is delocalized strongly over the entire phenyl ring and slightly over the pyrazine ring and carboxamide group. For halogen substitution 18F the HOMO is delocalized over entire pyrazine ring. For halogen substitutions 18I and 18F the LUMO is localized same over entire pyrazine ring and carboxamide group. Similarly for halogen substitutions 18Br and 18Cl the LUMO delocalization is strong over entire pyrazine ring except chlorine atoms.

For halogen substitution 20I the HOMO is delocalized strongly around the iodine atom. For the halogen substitutions 20Br and 20F the HOMO is delocalized strongly over the entire pyrazine ring except the nitrogen atom (Position 3). For halogen substitution 20Cl the HOMO is strongly delocalized over entire pyrazine ring except nitrogen atom (position 3) and also substituted chlorine atom and partially over phenyl ring. For 20I and 20Cl the LUMO is delocalized strongly over the pyrazine ring except chlorine atom and slightly over carboxamide and phenyl group. For halogen substitution 20Br the LUMO is over entire molecule except CH_3 group, bromine and chlorine atoms. For halogen substitution 20F LUMO is delocalized over the entire pyrazine ring except chlorine atom, slightly over carboxamide group and phenyl ring.

The average value of chemical potential decreases for the halogen substitution in the order 10I, 16I, 18I, 20I less than 10Cl, 16Cl, 18Cl, 20Cl less than 10F, 16F, 18F, 20F less than 10Br, 16Br, 18Br, 20Br. Chemical potential value of 16Br is deviated maximum from the parent molecule while all other halogen substitution shows considerable deviation. Halogen substitution results in increase in the μ value in comparison with the parent molecule, which is a minimum. Halogen substitution also results a decrease in electrophilicity index and is minimum for 18Br. Global hardness is higher for 18Br because of its large HOMO-LUMO gap which results a decrease in polarizability (Table 6).

5.4.6 Molecular Electrostatic Potential Map

Molecular electrostatic potential and electron density are related to each other to find the reactive sites for electrophilic and nucleophilic sites [43, 44]. The negative (red and yellow) regions of MEP map (Fig. 5) were related to electrophilic reactivity while the positive (blue) regions to nucleophilic reactivity. For the parent molecule, most electrophilic (red and yellow) regions are around C=O of carboxamide group, deeply over entire phenyl ring, and slightly near nitrogen atom (position 3) and the nucleophilic regions (blue) are deeply over iodine atom and slightly over the pyrazine ring. For halogen substitutions 10Br, 10Cl, 10F, the electrophilic regions are strongly over the C=O group of carboxamide, slightly over the phenyl ring and nitrogen atom (position 3) while the nucleophilic regions are over the N-H of carboxamide group and the pyrazine ring but the blue region deeply over pyrazine ring in 10Br is more pronounced. For iodine substitution in 16I the electrophilic regions are around C=O of carboxamide group, deeply over phenyl ring and slightly near N-H bond and the blue region is deeply over iodine atom and pyrazine ring. For halogen substitution 16Br, the electrophilic regions are at C=O region, slightly over phenyl ring and deeply over N-H bond. For chlorine and fluorine substitution 16Cl, 16F the electrophilic regions are similar to that of bromine

substitution while the nucleophilic regions are similar to that of bromine substitution but blue region of chlorine atom in 16Cl is more pronounced. For halogen substitutions 18Br, 18Cl, 18F the electrophilic behavior is around C=O and slightly over phenyl ring is identical to that of 18I where red region is slightly over nitrogen atom (position 3) while the nucleophilic region is identical to that of 18I. For the halogen substitutions 20Br, 20Cl and 20F the red region is over C=O, slightly over phenyl ring and near nitrogen atom (position 3) while the blue region is near N-H bond and over pyrazine ring. For halogen substitution 20I the electrophilic region is deeply over C=O, entire phenyl ring and near nitrogen atom (position 3) while the nucleophilic region is deeply over iodine atom and around pyrazine ring.

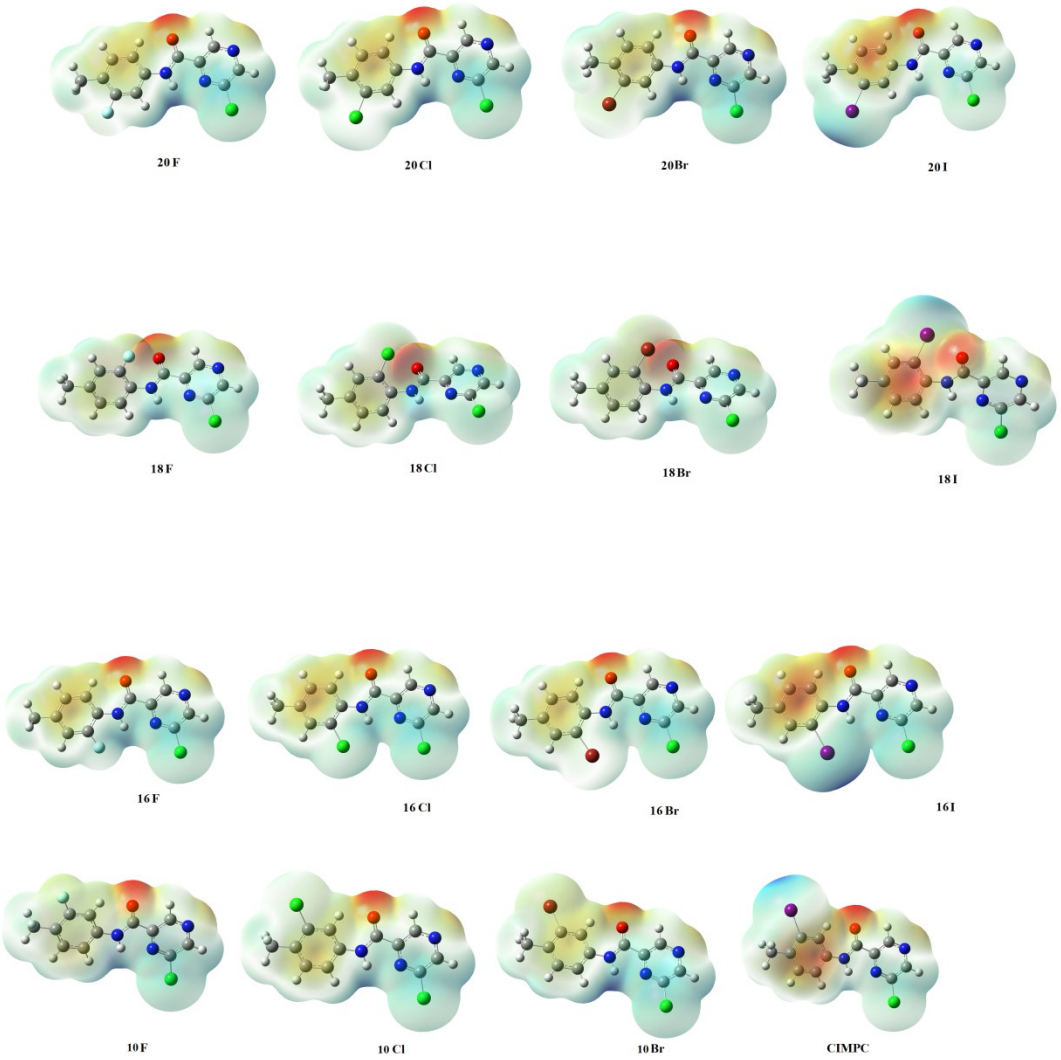

Fig.5 MEP plot of 6-Chloro-*N*-(3-iodo-4-methylphenyl)-pyrazine-2-carboxamide

5.4.7 Molecular docking

Molecular docking was employed to recognize the active site of the receptor, and acquire the best geometry of ligand-receptor complex. Based on the structure of a compound, PASS (Prediction of Activity Spectra) [45] is an online tool which predicts different types of activities and given in the Table 7. We choose the activity Vanilloid 1 agonist with Pa value 0.708 and high resolution crystal structure of corresponding protein transient receptor potential cation channel (PDB ID: 4DX1) was downloaded from the RCSB protein data bank website. Transient receptor potential vanilloid 1 (TRPV1), a non-selective cation channel. TRPV1 is thought to be a central transducer of hyperalgesia and a prime target for controlling pain pharmacologically because it is a point where many proalgesic pathways converge and it is upregulated and sensitized by inflammation and injury [46].A novel transient receptor potential vanilloid 1 (TRPV1) agonist, inhibits TNF-alpha production through the activation of capsaicin-sensitive afferent neurons and treatment of chronic inflammation [47]. Pharmacologically active agents, pyrazine as novel anti-inflammatory drug. pyrazine N-

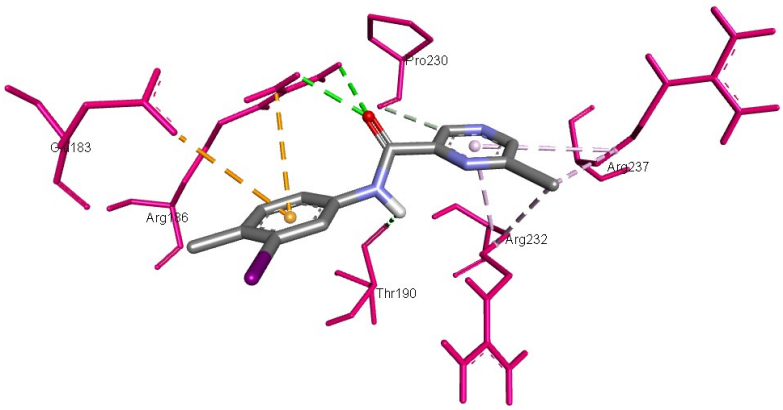

Fig.6 Interactive plots of amino acids of the receptor with the ligand

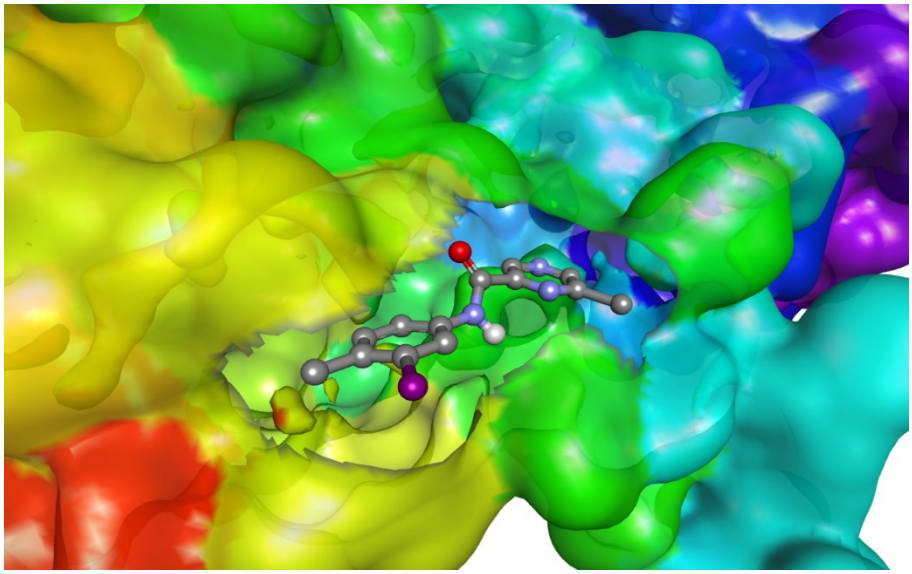

Fig.7. The docked ligand of 6-Chloro-N-(3-iodo-4-methylphenyl)-pyrazine-2-carboxamide at the active site of the receptor

acylhydrazone (NAH) derivatives evaluated in several animal models of pain and inflammation [48]. Thus we choose title compound as ligand and transient receptor potential cation channel as target for docking study.

All molecular docking calculations were performed on AutoDock4.2 [49] and Auto Dock Vina software [50]. The original ligand as well as water molecules were removed from the crystal structure, and polar hydrogens and united atom Kollman charges were assigned for the receptor using the graphical user interface Auto Dock Tools (ADT). The Lammarckian Genetic Algorithm (LGA) [51] was employed to calculate the energy between ligand and receptor. The compound docked the active site of receptors with the grid centre dimension 40×40×40. The conformations with the lowest binding energy is extracted and analysed for detailed interactions in Discovery Studio Visualizer 4.0 software. The ligand binds at the active site of the substrates by weak non-covalent interactions. The amino acids Arg186 forms two H-bond with carbonyl group while Thr190 has a H-bond with N-H group. Pro230 having an H-bond with pyrazine rind and electrostatic interactions are detailed in Fig.6. The docked ligand forms a stable complex with transient receptor potential cation channel as depicted in Fig.7 and the binding free energy value is -5.9 kcal/mol, tabulated in Table 8. These preliminary results suggest that the compound having inhibitory activity against the anti-inflammatory receptor transient receptor potential cation channel. Thus the title compound can be developed as drug used for the treatment of pain and inflammation.

5.5 Conclusion

FT-IR and FT Raman spectra of 6-chloro-N-(3-iodo-4 methyl phenyl) pyrazine-2-carboxamide were recorded and analyzed. The vibrational wavenumbers were computed at B3LYP/6 31Gen theory. The data obtained from theoretical calculation are used to assign vibrational band obtained experimentally. The geometrical parameters of the title compound are in agreement with similar derivatives. For the title compound the HOMO is delocalized over the entire iodine atom and LUMO is delocalized over the entire except iodine atom also halogen substituted HOMO-LUMO calculations are conducted the lowering of HOMO-LUMO band gap support the bioactive property of the molecule. The molecular electrostatic potential study showed that for the parent molecule most electrophilic regions are around C=O of carboxamide group and the nucleophilic region deeply over iodine atom. The NBO analysis performed in this study enabled us to know about the conjugate interactions taking place within the molecular spices.

Tables

Table1. Optimized geometrical parameters of 6-chloro-N-(3-iodo-4 methyl phenyl)

pyrazine 2 carboxamide

Bond length (Å)		Bond angles(˚)		Dihedral angles(˚)	
C_1-C_2	1.4038	C_2-C_1-N_6	122.4	N_6-C_1-C_2-C_3	0.0
C_1-N_6	1.3185	C_2-C_1-Cl_{27}	119.6	N_6-C_1-C_2-C_7	-180.0
C_1-Cl_{27}	1.7509	C_1-C_2-C_3	120.8	Cl_{27}-C_1-C_2-C_3	-180.0
C_2-N_3	1.3318	C_1-C_2-H_7	121.0	C_2-C_1-N_6-C_5	-0.0
C_2 H_7	1.0864	N_6 C_1 Cl_{27}	118.0	Cl_{27} C_1 N_6 C_5	180.0
N_3-C_4	1.3394	C_1-N_6-C_5	116.8	$C1_{27}$-C_2-C_3-C_4	-0.0
C_4-C_5	1.3971	C_3-C_2-H_7	118.2	C_2-C_3-C_4-C_5	-0.0
C_4-H_8	1.0848	C_2-C_3-C_4	117.3	C_3-C_4-C_5-N_6	0.0
C_5-N_6	1.3440	C_3-C_4-C_5	121.5	C_3-C_4-C_5-C_9	-180.0
C_5-C_9	1.5094	C_3-C_4-H_8	118.2	C_4-C_5-N_6-$C1_{27}$	-0.0
C_9-O_{10}	1.2267	C_5-C_4-H_8	120.3	C_9-C_5-N_6-C_1	180.0
C_9-N_{11}	1.3657	C_4-C_5-N_6	121.2	C_4-C_5-C_9-O_{10}	0.0
N_{11}-C_{12}	1.4074	C_4-C_5-C_9	120.0	C_4-C_5-C_9-N_{11}	-180.0

Bond length (Å)		Bond angles(˚)		Dihedral angles(˚)	
N_{11}-H_{21}	1.0152	N_6-C_5-C_9	118.8	N_6-C_5-C_9-O_{10}	-180.0
C_{12}-C_{13}	1.4014	C_5-C_9-O_{10}	120.5	N_6-C5-C_9-N_{11}	0.0
C_{12}-C_{14}	1.4030	C_5-C_9-N_{11}	113.2	C_5-C9-N_{11}-C_{12}	-180.0
C_{13}-C_{15}	1.3890	C_{10}-C_9-N_{11}	126.4	O_{10}-C_9-N_{11}-C_{12}	0.0
C_{13}-H_{16}	1.0875	C_9-N_{11}-C_{12}	128.8	C_9-N_{11}-C_{12}-C_{13}	180.0
C_{14}-C_{17}	1.3927	C_9-N_{11}-H_{21}	114.3	C_9-N_{11}-C_{12}-C_{14}	-0.0
C_{14}-H_{18}	1.0875	C_{12}-N_{11}-H_{21}	116.9	N_{11}-C_{12}-C13-C_{15}	-180.0
C_{15}-C_{19}	1.4043	C_{11}-C_{12}-C_{13}	117.8	C_{14}-C_{12}-C_{13}-C_{15}	0.0
C_{15}-H_{20}	1.0869	C_{11}-C_{12}-C_{14}	122.9	N_{11}-C_{12}-C_{14}-C_{17}	180.0
C_{17}-C_{19}	1.4018	C_{13}-C_{12}-C_{14}	119.3	C_{13}-C_{12}-C_{14}-C_{17}	-0.0
C_{17}-I_{26}	2.1547	C_{12}-C_{13}-C_{15}	120.1	C_{12}-C_{13}-C_{15}-C_{19}	-0.0
C_{19}-C_{22}	1.5075	C_{12}-C_{13}-H_{16}	120.0	C_{12}-C_{14}-C1$_7$-C_{19}	-0.0
C_{22}-H_{23}	1.0964	C_{12}-C_{14}-C_{17}	119.0	C_{12}-C_{14}-C_{17}-I_{26}	-180.0
C_{22}-H_{24}	1.0942	C_{12}-C_{14}-H_{18}	119.5	C_{13}-C_{15}-C_{19}-C_{17}	-0.0
C_{22}-H_{25}	1.0964	C_{15}-C_{13}-C_{16}	119.9	C_{13}-C_{15}-C_{19}-C_{22}	180.0
		C_{13}-C_{15}-C_{19}	122.4	C_{14}-C_{17}-C_{19}-C_{15}	0.0
		C_{13}-C_{15}-H_{20}	119.0	C_{14}-C_{17}-C_{19}-C_{22}	180.0
		C_{17}-C_{14}-H_{18}	121.6	I_{26}-C_{17}-C_{19}-C_{15}	180.0
		C_{14}-C_{17}-C_{19}	123.4	I_{26}-C_{17}-C_{19}-C_{22}	
		C_{14}-C_{17}-I_{26}	116.4		
		C_{19}-C_{15}-H_{20}	118.6		
		C_{15}-C_{19}-C_{17}	115.9		
		C_{15}-C_{19}-C_{22}	120.2		
		C_{19}-C_{17}-I_{26}	120.2		
		C_{17}-C_{19}-C_{22}	123.9		
		C_{19}-C_{22}-H_{23}	111.5		
		C_{19}-C_{22}-H_{24}	110.6		
		C_{19}-C_{22}-H_{25}	111.5		
		H_{23}-C_{22}-H_{24}	108.1		
		H_{23}-C_{22}-H_{25}	106.8		
		H_{24}-C_{22}-H_{25}	108.1		

Table 2. Calculated scaled wavenumbers, observed IR, Raman bands and vibrational assignments of the 6-chloro-N-(3-iodo-4 methyl phenyl) pyrazine-2-carboxamide

B3LYP/6-31G*			IR(υcm^{-1})	Raman(υcm^{-1})	Assignments
$\nu(cm^{-1})$	IR_I	R_A			
3418	76.90	247.15	3330	3494	νNH(91)
3159	10.23	29.34	-	-	νCHPh(99)
3116	0.48	70.55	-	-	νCHPz(99)
3093	4.95	146.37	-	-	νCHPz(99)
3077	17.56	159.69	-	-	νCHPh(99)
3059	11.72	51.55	3062	3063	νCHPh(99)
3010	16.98	72.38	3024	-	νCH_3(79)
2987	12.08	99.59	2982	2957	νCH_3(78)
2934	24.50	261.06	2925	2924	νCH_3(93)
1706	198.96	153.36	1670	1667	νC=O(66)
1596	29.42	617.65	1580	1598	νPh(54), δCHPh(14)
1571	239.88	635.27	-	1561	νPh(42), δNH(15)
1548	11.57	477.37	-	-	νPz(69), δCHPz(19)
1523	38.45	203.67	1520	1525	νPz(75)
1509	391.56	550.79	-	-	δNH(34), υPh(27)
1476	95.98	74.90	1485	-	υPh(51), υCHPh(39)
1462	64.19	173.43	-	-	δCH_3(75)
1453	6.12	19.35	1433	-	δCH_3(95)
1406	2.18	17.01	-	1395	νPz(41), δCHPz(28)
1392	1.03	33.04	-	-	δCH_3(62), $\upsilon C_{19}C_{22}$(19)
1384	70.36	153.67	1377	-	δCHPz(43), νPh(10), δCHPh(12), υPz(14)
1373	83.38	1.72	-	-	νPh(26), δCHPz(22), υCHPh(16)
1291	51.05	422.73	1298	1302	νPh(69)
1269	3.80	100.71	-	-	δCHPh(39)
1248	17.99	199.57	-	-	δCHPh(15), νC_5C_9(17), υPz(13)
1232	9.95	458.13	1230	1237	νCN(28), νPh(31), δCN(14)
1212	4.22	46.39	-	-	υPz(81)

B3LYP/6-31G*			IR(υcm^{-1})	Raman(υcm^{-1})	Assignments
ν(cm^{-1})	IR_I	R_A			
1193	2.75	26.02	-	-	δCHPh(29), υPh(13), δPh(11), $\upsilon C_{19}C_{22}$(27)
1158	139.97	3.37	1166	1179	δCHPz(26), νPh(11), νPz(34), δPz(13)
1145	29.06	6.05	1147	-	νPz(27), δCHPh(22)
1140	59.64	19.73	1121	1118	νPz(42), δCHPh(24), δCHPz(17)
1103	42.21	9.99	-	-	νPz(42), νCN(26)
1033	4.17	0.19	1031	1035	δCH_3(89)
1007	35.55	23.23	1009	1015	νPh(27), δPh(43)
991	42.31	70.72	-	-	υPz(56), δPz(25)
989	3.85	9.31	-	-	δCH_3(70)
943	0.89	1.42	-	958	γCHPz(88)
908	0.75	2.02	926	-	γCHPh(91)
902	21.17	16.0	889	886	δCN(21), υC_9C_5(16), υCCl(11), δPz(13)
890	14.86	1.18	-	-	γCHPh(79)
884	8.28	0.06	-	-	γCHPz(73)
858	62.66	32.03	862	866	υPh(21), δPh(15)
794	29.54	3.18	-	-	γCHPh(79)
785	27.42	2.56	776	-	νCCl(10), δCO(20), δPz(20)
753	4.92	5.54	749	749	δPz(39), γC_5C_9(27), γCO(27)
732	13.78	16.72	723		δPh(23), δPz(10), $\nu C_{19}C_{22}$(23)
707	0.44	0.20	-	-	δCO(17), γPz(56)
685	8.56	1.35	-	691	γPh(74)
667	63.76	1.63	674	668	γNH(44), γCO(29)
650	25.67	14.45	644	648	δPh(70)
629	1.18	6.23	614	603	δPz(66)
562	0.03	2.34	550	566	$\gamma C_{19}C_{22}$(12), γPh(30)
535	20.34	14.29	516	504	γCO(28), δPh(22)
498	1.25	0.95	-	-	γPz(24), γCCl(35), γCO(10)

B3LYP/6-31G*			IR(υcm^{-1})	Raman(υcm^{-1})	Assignments
ν(cm^{-1})	IR$_I$	R$_A$			
485	9.43	2.57	-	-	δPh(27), δPz(26), υC$_9$C$_5$(12)
449	20.88	0.24	441	435	γPz(63), γC$_5$C$_9$(15)
430	4.740	0.67	-	-	γPh(62)
423	0.74	1.92	396	-	δC$_{19}$C$_{22}$(35), δCN(16)
383	7.11	8.94	366	-	υCCl(39), δPz(18)
337	0.49	2.24	357	354	γPh(25), γC$_{19}$C$_{22}$(35)
330	9.25	1.33	-	-	γCO(36), δCN(23)
311	6.34	7.57	-	271	υCI(40), δCCl(36)
244	0.89	6.23	-	-	δPh(18), υC$_5$C$_9$(11)
221	5.28	1.22	-	211	υCI(33), δCCl(23)
199	0.55	1.20	-	-	γCI(16), γC N(14), τPh(13), τCO(12)
196	0.49	1.98	-	-	δCI(41), δC19C22(15)
172	0.04	1.88	-	168	τPz(69), γCCl(16)
157	0.03	0.00	-	-	τCH$_3$(86)
142	1.83	3.94	-	-	γCI(24), τPh(13), γC$_5$C$_9$(19)
127	1.47	1.80	-	-	τPh(48), τCN(14)
87	1.39	3.03	-	-	δC$_5$C$_9$(28), τCI(27), τCN(14)
72	2.89	1.76	-	-	τC$_5$C$_9$(50), τCN(27), τPh(11)
49	0.15	0.03	-	-	τCO(40), τC$_5$C$_9$(15), τC$_{I9}$C$_{22}$, τCN(14)
35	0.64	0.01	-	-	τCO(37), τCN(27)
18	0.00	0.11	-	-	τCN(63), τCO(16)

Pz=Pyrazine; Ph-Phenyl

Table 3. Second-order perturbation theory analysis of Fock matrix in NBO basis corresponding to the intra molecular bonds of CIMPC

Donor(i)	type	ED/e	Acceptor(j)	Type	ED/e	E(2)[a]	E(j)-E(i)[b]	F(ij)[c]
C_1-N_6	σ	1.98582	C_1-C_2	σ*	0.05017	0.89	1.36	0.031
-	π	1.73005)	C_2-N_3	π*	0.32058	18.49	0.31	0.069
-	π	-	C_4-C_5	π*	0.04365	20.70	0.33	0.075
C_2-N_3	π	1.70809	C_1-N_6	π*	0.38561	20.02	0.29	0.069
-	π	-	C_4-C_5	π*	0.29757	22.45	0.32	0.075
C_4-C_5	σ	1.98640	C_1-N_6	σ*	0.03033	0.61	1.21	0.024
-	π	1.62140	C_1-N_6	π*	0.38561	20.47	0.26	0.065
-	π	-	C_2-N_3	π*	0.32058	19.14	0.27	0.065
-	π	-	C_9-O_{10}	π*	0.28710	10.70	0.31	0.053
C_{12}-C_{13}	σ	1.97164	N_{11}-C_{12}	σ*	0.03414	0.87	1.06	0.027
-	π	1.63542	C_{14}-C_{17}	π*	0.39086	22.68	0.27	0.070
-	π	-	C_{15}-C_{19}	π*	0.34201	20.85	0.29	0.070
C_{14}-C_{17}	σ	1.97706	N_{11}-C_{12}	σ*	0.03414	4.21	1.08	0.060
	π	1.72017	C_{12}-C_{13}	π*	0.38599	18.51	0.30	0.068
	π	-	C_{15}-C_{19}	π*	0.34201	19.17	0.31	0.070
C_{15}-C_{19}	π	1.63333	C_{12}-C_{13}	π*	0.38599	22.77	0.27	0.070
-	π	-	C_{14}-C_{17}	π*	0.39086	23.23	0.26	0.070
LPN_3	σ	1.92158	C_1-C_2	σ*	0.05017	11.01	0.82	0.085
LPN_3	σ	-	C_4-C_5	σ*	0.04365	10.63	0.84	0.085
LPN_6	σ	1.89228	C_1-C_2	σ*	0.05017	11.12	0.81	0.086
LPN_6	σ	-	C_4-C_5	σ*	0.04365	10.21	0.83	0.084
LPO_{10}	π	-	C_5-C_9	σ*	0.07420	18.84	0.62	0.098
LPO_{10}	π	-	C_9-N_{11}	σ*	0.07354	22.46	0.65	0.109
LPN_{11}	σ	-	C_9-O_{10}	π*	0.28710	50.74	0.29	0.109
LPN_{11}	σ	-	C_{12}-C_{13}	π*	0.38599	31.00	0.31	0.088
$LPCl_{27}$	n	1.91841	C_1-N_6	π*	0.38561	14.26	0.27	0.060

Table 4. NBO results showing the formation of Lewis and non-Lewis orbitals of CIMPC

Bond(A-B)	ED/ea	EDA%	EDB%	NBO	s%	p%
σC_1-C_2	1.99140	50.76	49.24	0.7125($sp^{1.40}$)C	41.67	58.33
-	-0.78221	-	-	+0.7017($sp^{1.77}$)C	36.14	63.86
σC_1-N_6	1.98582	39.57	60.43	0.6290($sp^{1.87}$)C	34.86	65.14
-	-0.98582	-	-	+0.7774($sp^{1.75}$)N	36.41	63.59
πC_1-N_6	1.73005	45.46	54.54	0.6742($sp^{1.00}$)C	0.00	100.00
-	-0.36803	-	-	+0.7385($sp^{1.00}$)N	0.00	100.00
σC_1-Cl_{27}	1.98115	43.96	56.04	0.6630($sp^{3.28}$)C	23.38	76.62
-	-0.70944	-	-	+0.7486($sp^{5.94}$)C	14.42	85.58
σC_2-N_3	1.98229	40.06	59.94	0.6329($sp^{2.18}$)C	31.47	68.53
-	--0.34997		-	+0.7742($sp^{1.90}$)N	34.49	65.51
πC_2-N_3	1.70809	42.91	57.09	0.6551($sp^{1.00}$)C	0.00	100.00
-	-0.87490	-	-	+0.7556($sp^{1.00}$)N	0.00	100.00
σN_3-C_4	1.98489	59.97	40.03	0.7744($sp^{1.90}$)N	34.45	65.55
-	-0.86687	-	-	+0.6327(sp2.24)C	30.82	69.18
σC_4-C_5	1.98640	49.27	50.73	0.7019($sp^{1.69}$)C	37.19	62.81
-	-0.76925	-	-	+0.7122($sp^{1.70}$)C	37.09	62.91
πC_4-C_5	1.62140	49.06	50.94	0.7004($sp^{1.00}$)C	0.01	99.99
-	-0.31939	-	-	+0.7137($sp^{99.99}$)C	0.01	99.99
σC_5-N_6	1.97150	39.88	60.12	0.6315($sp^{2.28}$)C	30.46	69.54
-	-0.87076	-	-	+0.7754($sp^{1.86}$)N	34.96	65.04
σC_5-C_9	1.96638	52.10	47.90	0.7218($sp^{2.08}$)C	32.43	67.57
-	-0.69127	-	-	+0.6921($sp^{1.91}$)C	34.35	65.65
σC_9-O_{10}	1.98952	34.60	65.40	0.5883($sp^{2.13}$)C	31.90	68.10
-	-1.00167	-	-	+0.8087($sp^{1.97}$)O	33.67	66.33
πC_9-O_{10}	1.97656	32.17	67.83	0.5672($sp^{55.54}$)C	1.77	98.23
-	-0.42140	-	-	+0.8236($sp^{54.69}$)O	1.80	98.20
σC_9-N_{11}	1.98598	36.36	63.64	0.6030($sp^{2.12}$)C	32.03	67.97
-	-0.85300	-	-	+0.7978($sp^{1.78}$)N	35.92	64.08
σN_{11}-C_{12}	1.98280	63.01	36.99	0.7938($sp^{1.69}$)N	37.19	62.81
-	-0.81409	-	-	+0.6082($sp^{2.68}$)C	27.16	72.84

Bond(A-B)	ED/ea	EDA%	EDB%	NBO	s%	p%
σC_{12}-C_{13}	1.97164	51.28	48.72	0.7161(sp1.68)C	37.34	62.66
-	-0.70877	-	-	+0.6980($sp^{1.96}$)C	33.79	66.21
πC_{12}-C_{13}	1.63542	51.24	48.76	0.758($sp^{1.00}$)C	0.00	100.00
-	-0.26987	-	-	+0.6983($sp^{1.00}$)C	0.00	100.00
σC_{12}-C_{14}	1.96297	50.28	49.72	0.7091($sp^{1.82}$)C	35.41	64.59
-	-0.71281	-	-	+0.7051($sp^{1.83}$)C	35.35	64.65
σC_{13}-C_{15}	1.97541	50.06	49.94	0.7075($sp^{1.80}$)C	35.73	64.27
-	-0.69942	-	-	+0.7067($sp^{1.80}$)C	35.67	64.33
σC_{14}-C_{17}	1.97706	50.02	49.98	0.7072($sp^{1.74}$)C	36.45	63.55
-	-0.73587	-	-	+0.7070($sp^{1.53}$)C	39.45	60.55
πC_{14}-C_{17}	1.72017	48.11	51.89	0.6936($sp^{1.00}$)C	0.00	100.00
	-0.28552	-	-	+0.7203($sp^{1.00}$)C	0.00	100.00
σC_{15}-C_{19}	1.96170	49.31	50.69	0.7022($sp^{1.77}$)C	36.11	63.89
-	-0.69504	-	-	+0.7120($sp^{1.93}$)C	34.07	65.93
πC_{15}-C_{19}	1.63333	49.99	50.01	0.7070($sp^{1.00}$)C	0.00	100.00
-	-0.25852	-	-	+0.7072($sp^{1.00}$)C	0.00	100.00
σC_{17}-C_{19}	1.97709	50.40	49.60	0.7100($sp^{1.43}$)C	41.11	58.89
-	-0.72842	-	-	+0.7042($sp^{1.94}$)C	34.01	65.99
σC_{17}-I_{26}	1.97175	53.77	46.23	0.7333($sp^{4.06}$)C	19.78	80.22
-	-0.49972	-	-	+0.6799($sp^{8.65}$)C	10.37	89.63
σC_{19}-C_{22}	1.97831	50.95	49.09	0.7138($sp^{2.14}$)C	31.89	68.11
-	-0.63165	-	-	+0.7004($sp^{2.35}$)C	29.84	70.16
$n1N_3$	1.92158	-	-	Sp2.21	31.11	68.89
-	-0.38057			-	-	-
$n1N_6$	1.89228	-	-	Sp2.49	28.68	71.32
-	-0.37174			-	-	-
$n1O_{10}$	1.97545	-	-	Sp0.55	64.52	35.48
-	-0.70487			-	-	-
$n2O_{10}$	1.87439	-	-	Sp99.99	0.06	99.94
-	-0.27662			-	-	-
$n1N_{11}$	1.65763	-	-	Sp99.99	0.07	99.93
-	-0.29824			-	-	-

Bond(A-B)	ED/ea	EDA%	EDB%	NBO	s%	p%
n1I_{26} -	1.99300 -0.61887	-	-	Sp0.12 -	89.54 -	10.46 -
n2I_{26} -	1.97743 -0.27418	-	-	Sp99.99 -	0.14 -	99.86 -
n3I_{26} -	1.95066 -0.27235	-	-	Sp0.17 -	0.00 -	100.00 -
n1Cl_{27} -	1.99197 -0.94724	-	-	Sp0.17 -	85.15 -	14.85 -
n2Cl_{27} -	1.97091 -0.33659	-	-	Sp99.99 -	0.44 -	99.56 -
n3Cl_{27} -	1.91841 -0.33348		-	Sp1.00 -	0.00 -	100.00 -

Table 5. Polarizability values of CIMPC and halogen substitutions

	μ debye	α x 10^{-23}esu	β x 10^{-30} esu	γ x10^{-37} esu
CIMPC	3.5147	2.782	24.973	-21.240
10Br	3.3623	2.756	25.460	-19.876
10Cl	3,5352	2.671	24.853	-18.287
10F	3.0499	2.500	26.287	-15.968
16Br	1.1896	2.727	21.866	-16.345
16Cl	1.1041	2.650	21.835	-15.686
16F	1.3843	2.503	24.355	-14.868
16I	1.6246	2.790	32.504	-17.348
18Br	2.9675	2.605	36.782	-16.441
18Cl	3.1251	2.527	3.269	-15.783
18F	2.8580	2.409	8.735	-14.933
18I	1.7722	1.795	5.402	-17.668
20Br	0.8064	2.756	26.477	-19.683
20Cl	0.7935	2.671	25.702	-18.086
20F	0.9418	2.500	26.808	-15.878
20I	0.7531	2.845	38.874	-21.595

Table 6. Chemical descriptors of CIMPC and halogen substitutions

	HOMO	LUMO	$I = -E_{HOMO}$	$A = -E_{LUMO}$	ΔE	$\eta = (I-A)/2$	$\mu = -(I+A)/2$	$\omega = \mu^2/2\eta$
CIMPC	-0.21808	-0.18744	5.934	5.100	0.834	0.417	-5.517	36.496
10Br	-0.29757	-0.18747	8.097	5.101	2.996	1.498	-6.599	14.535
10Cl	-0.29652	-0.18722	8.069	5.094	2.975	1.488	-6.582	14.557
10F	-0.29755	-0.18727	8.097	5.096	3.001	1.501	-6.597	14.497
16Br	-0.29750	-0.18761	8.095	5.105	2.990	1.495	-6.600	14.569
16Cl	-0.28821	-0.18699	7.842	5.088	2.754	1.377	-6.465	15.177
16F	-0.29707	-0.18725	8.084	5.095	2.989	1.495	-6.590	14.524
16I	-0.22020	-0.18879	5.992	5.137	0.885	0.428	-5.565	36.179
18Br	-0.29766	-0.18473	8.100	5.027	3.073	1.537	-6.564	14.016
18Cl	-0.29480	-0.18431	8.021	5.015	3.006	1.503	-6.518	14.133
18F	-0.29757	-0.18523	8.097	5.040	3.057	1.529	-6.569	14.111
18I	-0.21454	-0.18622	5.838	5.067	0.771	0.386	-5.453	38.517
20Br	-0.29756	-0.18742	8.097	5.100	2.997	1.499	-6.599	14.525
20Cl	-0.29713	-0.18705	8.085	5.090	2.995	1.498	-6.588	14.487
20F	-0.29754	-0.18709	8.096	5.091	3.005	1.503	-6.594	14.465
20I	-0.21820	-0.18876	5.937	5.136	0.801	0.401	-5.537	38.227

Table 7. PASS prediction for the activity spectrum of CIMPC compound. Pa represents probability to be active and Pi represents probability to be inactive.

Pa	Pi	Activity
0.708	0.003	Vanilloid 1 agonist
0.675	0.078	Ubiquinol-cytochrome-c reductase inhibitor
0.477	0.003	Vanilloid agonist
0.431	0.056	Platelet derived growth factor receptor kinase inhibitor
0.370	0.007	Lymphocytopoiesis inhibitor
0.408	0.083	Erythropoiesis stimulant
0.466	0.142	Nicotinic alpha6beta3beta4alpha5 receptor antagonist
0.350	0.027	Imidazoline I1 receptor agonist
0.363	0.050	CF transmembrane conductance regulator agonist
0.335	0.038	Antineoplastic (pancreatic cancer)
0.324	0.030	Thyroxine 5-deiodinase inhibitor
0.374	0.085	Peptide agonist
0.364	0.076	Centromere associated protein inhibitor
0.316	0.037	Thiamine pyridinylase inhibitor
0.352	0.074	Autoimmune disorders treatment
0.362	0.093	5 Hydroxytryptamine release inhibitor
0.302	0.037	Antihelmintic
0.284	0.022	Pancreatic disorders treatment
0.352	0.095	RNA-directed RNA polymerase inhibitor
0.317	0.062	Antituberculosic
0.276	0.023	Blasticidin-S deaminase inhibitor
0.285	0.038	Sodium channel blocker
0.296	0.057	Antiparasitic
0.235	0.003	Sodiumhydrogen exchanger 5 inhibitor
0.362	0.143	Nicotinic alpha2beta2 receptor antagonist
0.236	0.023	Aurora-C kinase inhibitor
0.231	0.018	Complement inhibitor

Table 8. The binding affinity values of different poses of the compound CIMPC predicted by Autodock Vina.

Mode	Affinity (kcal/mol)	Distance from best mode (Å)	
-	-	RMSD l.b.	RMSD u.b.
1	-5.9	0.000	0.000
2	-5.7	1.649	2.135
3	-5.6	18.110	20.686
4	-5.4	3.679	6.984
5	-5.4	17.560	19.338
6	-5.3	17.033	18.815
7	-5.3	17.397	19.392
8	-5.3	12.883	15.474
9	-5.3	3.992	7.341

5.6 References

[1] D. R. Boubee, C. V. Leeuwen, D. Dubourdieu, Organoleptic impact of 2-methoxy-3-isobutylpyrazine on red brodeaux and loire wines, effect of environmental conditions on concentrations in grapes during ripening, J. Agric. Food Chem. 48 (2000) 4830-4834.

[2] H. Endredi, F. Billes, S. Holly, Vibrational spectroscopic and quantum chemical study of chlorine substitution of pyrazine, J. Mol. Struct. Theochem. 633 (2003) 73-82.

[3] A. Somoskovi, M. M. Wade, Z. Sun, Y. Zhang, Iron enhances the antituberculous activity of pyrazinamide, J. Antimicrob. Chemother. 53 (2004) 192-196.

[4] V. Opletalova, Jırı. Hartl, A. Patel, K. Palat Jr., V. Buchta, Ring substituted 3-phenyl-1-(2-pyrazinyl)-2-propen-1-ones as potential photosynthesis-inhibiting, anti-fungal and anti-mycobacterial agents, Il. Farmaco 57 (2002) 135-144.

[5] Y. Zhang, M. M. Wade, A. Scorpio, H. Zhang Z. Sun, Mode of action of pyrazinamide: disruption of Mycobacterium tuberculosis membrane transport and energetics by pyrazinoic acid, J. of Antimicrob. Chemother. 52 (2003) 790–795.

[6] V. Křen, D. Walterova, Silybin and silymarin–New effects and applications, Biomed. Pap. 149 (2005) 29-41.

[7] S. S. Raza, M. M. Khan, M. Ashafaq, A. Ahmad, G. Khuwaja, A. Khan, Silymarin protects neurons from oxidative stress associated damages in focal cerebral ischemia: A behavioral, biochemical and immune histological study in Wistar rats, J. Neurol. Sci. 309 (2011) 45-54.

[8]. N. K. Singhal, G. Srivastava, D. K. Patel, S. K. Jain, M. P. Singh, Melatonin or silymarin reduces maneb- and paraquat-induced Parkinson's disease phenotype in the mouse, J. Pineal Res. 50 (2011) 97-109.

[9] W. J. Chung, A. Kornilov, B. H Brodsky, M. Higgins, T. Sanchez, L. B. Heifets,. M. H. Cynamon, J. Welch, Inhibition of M. tuberculosis in vitro in monocytes and in mice by aminomethylene pyrazinamide analogs, Tuberculosis 88 (2008) 410-419.

[10] B. Servusová, D. Eibinová, M. Doležal, V. Kubícek, P. Paterová, M. Peško, Substituted N-benzylpyrazine-2-carboxamides: Synthesis and biological evaluation, Molecules 17 (2012) 13183-98.

[11] D. M. Kráľová, K. Herbicides, Theory and Applications: Synthesis and Evaluation of Pyrazine Derivatives with Herbicidal Activity. In Tech; 2011.

[12] M. Doležal, K. Kráľová, Synthesis and Evaluation of Pyrazine Derivatives with Herbicidal Activity. In Herbicides, Theory and Applications; S Soloneski, M.L. Larramendy, Eds.; In Tech: Vienna, Austria, (2011) 581-610.

[13] M. Dolezal, J. Zitko, Z. Osicka, J. Kunes, M. Vejsova, V. Buchta, J. Dohnal, J. Jampilek, K. Kralova, Synthesis, antimycobacterial, antifungal and photosynthesis-inhibiting activity of chlorinated N-phenylpyrazine-2-carboxamides. Molecules 15 (2010) 8567-8581.

[14] M. Dolezal, P. Cmedlova, L. Palek, J. Vinsova, J. Kunes, V. Buchta, J. Jampilek, K Kralova, Synthesis and antimycobacterial evaluation of substituted pyrazine carboxamides. Eur. J. Med. Chem. 43 (2008) 1105–-1113.

[15] M. Doležal, L. Tumová, D. Kešetovičová, J. Tuma, K. Kráľová, Substituted N-phenylpyrazine-2-carboxamides, their synthesis and evaluation as herbicides and abiotic elicitors. Molecules 12 (2007) 2589-2598

[16] M. Dolezal, L. Tumova, D. Kesetovicova, J. Tuma, K. Kralova, Substituted *N*-Phenylpyrazine-2-carboxamides, Their Synthesis and Evaluation as Herbicides and Abiotic Elicitors, Molecules 12 (2007) 2589-2598.

[17] M. Dolezal, J. Zitko, Pyrazines Derivatives: a patent review (June 2012-present). Exp. Opin. Ther. Pat. 25 (2015) 33-47.

[18] M. Dolezal, J. Zitko, D. Kesetovicova, J. Kunes, M. Svobodova, Substituted *N*-Phenylpyrazine-2-carboxamides: Synthesis and Antimycobacterial Evaluation. *Molecules* 14 (2009) 4180-4189.

[19] M. Dolezal, L. Tumova, D. Kesetovicova, J. Tuma, K. Kralova, Substituted *N*-Phenylpyrazine-2-carboxamides, Their Synthesis and Evaluation as Herbicides and Abiotic Elicitors. Molecules 12 (2007) 2589-2598.

[20] Gaussian 09, Revision B.01, M. J. Frisch, G. W. Trucks, H. B. Schlegel, G. E. Scuseria, M. A. Robb, J. R. Cheeseman, G. Scalmani, V. Barone, B. Mennucci, G. A. Petersson, H. Nakatsuji, M. Caricato, X. Li, H. P. Hratchian, A. F. Izmaylov, J. Bloino, G. Zheng, J. L. Sonneberg, M. Hada, M. Ehara, K. Toyota, R. Fukuda, J. Hasegawa, M. Ishida, T. Nakajima, Y. Honda, O. Kitao, H. Nakai, T. Vreven, J. A. Montgomery, J. E. Peralta, F. Ogliaro, M. Bearpark, J. J. Heyd, E. Brothers, K. N. Kudin, V. N. Staroverov, T. Keith, R. Kobayashi, J. Normand, K. Raghavachari, A. Rendell, J. C. Knox, J. B. Cross, V. Bakken, C. Adamo, J. Jaramillo, R. Gomperts, R. E. Stratmann, O. Yazyev, A. J. Austin, R. Cammi, C. Pomelli, J. W. Ochterski, R. L. Martin, K. Morokuma, V. G. Zakrzewski, G. A. Voth, P. Salvador, J. J. Dannenberg, S. Dapprich, A. D. Daniels, O. Farkas, J. B. Foresman, J. V. Ortiz, J. Cioslowski, D. J. Fox, Gaussian Inc., Wallingford CT, 2010.

[21] J. B. Foresman, A Guide to Using Gaussian, Pittsburg, PA, in E: Frisch (Ed.), Exploring Chemistry with Electronic Structure Methods, 1996.

[22] J. M. L. Martin, C. Van Alsenoy, GAR2PED, A Program to obtain a potential energy distribution from a Gaussian archive record, University of Antwerp, Belgium, 2007.

[23] R. Dennington, T. Keith, J. Millam, Gaussview, Version 5, Semichem Inc., Shawnee Missions KS, 2009.

[24] T. Joseph, H. T. Varghese, C. Y. Panicker, K. Viswanathan, M. Dolezal, C. Van Alsenoy, Spectroscopic (FT-IR, FT-Raman), first order hyperpolarizability, NBO analysis, HOMO and LUMO analysis of *N*-[(4-(trifluoromethyl)phenyl]pyrazine-2-carboxamide by density functional methods, Arabian J. Chem. "In Press" doi.org/ 10.1016/ j.arabjc.2013.08.004.

[25] W. He, G. Zhou, J. Li, A. Tian, Molecular design of analogues of 2,6-diamino-3,5-dinitropyrazine-1-oxide, J. Mol. Struct. THEOCHEM 668 (2004) 201-208.

[26] N. P. G. Roeges, A Guide to the Complete Interpretation of Infrared Spectra of Organic Structures, Wiley, New York, 1994.

[27] N. B. Colthup, L. H. Daly, S. E. Wiberly, Introduction to infrared and Raman spectroscopy, Ed. 2, Academic Press, New York, 1975.

[28] G. Varsanyi, Assignments of Vibrational Spectra of Seven Hundred Benzene Derivatives, Wiley, New York 1974.

[29] Y. S. Mary, C. Y. Panicker, H. T. Varghese, K. Raju, T. E. Bolelli, I. Yildiz, C. M. Granadeiro, H. I. S. Nogueiro, Vibrational spectroscopic studies and computational study of 4-fluoro-*N*-(2'-hydroxy-4'-nitrophenyl)phenylacetamide, J. Mol. Struct. 994 (2011) 223-231.

[30] M. Barthes, G. De Nunzio, M. Ribet, Polarons or proton transfer in chains of peptide groups, Synth. Met. 76 (1996) 337-340.

[31] J. Lukose, C. Y. Panicker, P. S. Nayak, B. Narayana, B. K. Sarojini, C. Van Alsenoy, A. A. Al-Saadi, Synthesis, structural and vibrational investigation on 2-phenyl-*N*-(pyrazine-2-yl)acetamide combining XRD diffraction, FT-IR and NMR spectroscopies with DFT calculations, Spectrochim. Acta A 135 (2015) 608-616.

[32] E. Loh, Raman spectra of iodine derivatives of tyrosine and thyronine, J. Raman Spectrosc. 3 (1975) 327-333.

[33] R. A. Yadav, J. S. singh, O. Sala, The Raman and infrared spectra and normal coordinate analysis for 1,2-diiodotetraflurobenzene, J. Raman Spectrosc. 14 (1983) 353-357.

[34] D. A. Zainuri, S. Arshad, N. C. Khalib, I. A. Razak, R. R. Pillai, S. F. Sulaiman, N. S. Hashim, K. L. Ooi, S. Armaković, S. J. Armaković, C. Y. Panicker, synthesis, XRD

crystal structure, spectroscopic characterization (FT-IR, 1H and 13C NMR), DFT studies, chemical reactivity and bond dissociation energy studies using molecular dynamics simulations and evaluation of antimicrobial and antioxidant activities of a novel chalcone derivative, (*E*)-1-(4-bromophenyl)-3-(4-iodophenyl)prop-2-en-1-one, J. Mol. Struct. 1128 (2017) 520-533.

[35] J. Coats, R. A. Meyers (Ed.), Encyclopedia of analytical chemistry, interpretation of Infrared spectra, a practical approach, in: John Wiley and Sons, Chichester, 2000.

[36] R. I. Al-Wabli, K. S. Resmi, Y. S. Mary, C. Y. Panicker, M. I. Attia, A. A. El-Emam, C. Van Alsenoy, Vibrational spectroscopic studies, Fukui functions, HOMO-LUMO, NLO, NBO analysis and molecular docking study of (*E*)-1-(1,3-benzodioxol-5-yl)-4,4-dimethylpent-1-en-3-one, a potential precursor to bioactive agents, J. Mol. Struct. 1123 (2016) 375-383.

[37] D. Philip, A. John, C.Y. Panicker, H.T. Varghese, FT-Raman, FT-IR and surface enhanced Raman scattering spectra of sodium salicylate, Spectrochim. Acta A 57 (2001) 1561-1566.

[38] J. F. Arenas, J. T. I. Navarrete, J. C. Ottero, J. I. Marcos, A. Cardenete, Vibrational spectra of [$^{1}H_4$]pyrazine and [$^{2}H_4$]pyrazine, J. Chem. Soc. Faraday Trans. 2 (81) (1985) 405-415.

[39] H. Endredi, F. Billes, F. S. Holly, Vibrational spectroscopical and quantum chemical study of the chlorine substitution of pyrazine, J. Mol. Struct. THEOCHEM. 633 (2003) 73-82.

[40] J. Lukose, C. Y. Panicker, P. S. Nayak, B. Narayana, B. K. Sarojini, C. Van Alsenoy, A. A. Al-Saadi, Synthesis, structural and vibrational investigation on 2-phenyl-*N*-(pyrazine-2-yl) acetamide combining XRD diffraction, FT-IR and NMR spectroscopies with DFT calculations, Spectrochim. Acta A 135 (2015) 608-616.

[41] E. D. Glendening, A. E. Reed, J. E. Carpenter, F. Weinhold. NBO Version 3.1, Gaussian Inc., Pittsburgh.

[42] M. Adant, M. Dupuis, J. L. Bredas, *Ab initio* study of the nonlinear optical properties of urea: Electron correlation and dispersion effects, Int. J. Quantum. Chem. 56 (1995) 497-507.

[43] F. J. Luque, J. M. Lopez, M. Orozco, Perspective on electrostatic interactions of a solute with a continuum, a direct utilization of ab initio molecular potentials for the prevision of solvent effects, Theor. Chem. Acc. 103 (2000) 343-345.

[44] P. Politzer, J. S. Murray, in: D. L. Beveridge, R. Lavery, (Eds.), Theoretical Biochemistry and Molecular Biophysics, Springer, Berlin, 1991.

[45] A. Lagunin, A. Stepanchikova, D. Filimonov, V. Poroikov, PASS: prediction of activity spectra for biologically active substances, Bioinformatics 16 (2000) 747-748.

[46] F. Tsuji, H. Aono, Role of Transient Receptor Potential Vanilloid 1 in Inflammation and Autoimmune Diseases, Pharmaceuticals 5 (2012) 837-852.

[47] F. Tsuji, M. Murai, K. Oki, Seki I, K. Ueda, H. Inoue, L. Nagelkerken, M. Sasano, H . Aono, Transient receptor potential vanilloid 1 agonists as candidates for anti-inflammatory and immunomodulatory agents, Eur. J. Pharmacol. 627 (2010) 332-339.

[48] Y. K. C. D. Silva, C. V. Augusto, M. L. D. C. Barbosa, G. M. D. A. Melo, A. C. D. Queiroz, T. D. L. M. F. Dias, W. B. Júnior, E. J. Barreiro, L. M. Lima, M. S. A. Moreira, Synthesis and pharmacological evaluation of pyrazine N-acylhydrazone derivatives designed as novel analgesic and anti-inflammatory drug candidates, Bioor. Med. Chem. 18 (2010) 5007-5015.

[49] G. M. Morris, R. Huey, W. Lindstrom, M. F. Sanner, R. K. Belew, D. S. Goodsell, A. J. Olson, AutoDock4 and AutoDockTools4: Automated docking with selective receptor flexibility, J. Comput. Chem. 16 (2009) 2785-91.

[50] O. Trott, A. J. Olson, AutoDock Vina: improving the speed and accuracy of docking with a new scoring function, efficient optimization and multi-threading, J. Comput. Chem. 31 (2010) 455-461.

[51] G. M. Morris, D. S. Goodsell, R. S. Halliday, R. Huey, W. E. Hart, R. Belew, A. J. Olson, Automated docking using a Lamarckian genetic algorithm and an empirical binding free energy function, J. Comput. Chem. 19 (1998) 1639-1662.

CHAPTER VI

A THEORETICAL STUDY ON MOLECULAR STRUCTURE, CHEMICAL REACTIVITY AND MOLECULAR DOCKING STUDIES ON 1,7,8,9-TETRA CHLORO-10,10-DIMETHOXY-4-[3-(4-BENZYLPIPERAZIN-1-YL)PROPYL]-4-AZATRICYCLO[5.2.1.$0^{2,6}$] DEC-8-ENE-3, 5-DIONE.

6.1 Introduction

The Piperazines or cyclizines is a cyclic-organic compound that consists of a six membered ring containing two opposing nitrogen atoms. Piperazine exists as a small alkaline deliquescent crystals and was introduced as a solvent for uric acid. Inside the body the drug is partly oxidized and partly eliminated unchanged. Outside the body, piperazine has an ability to dissolve uric acid and producing a soluble urate [1, 2]. Piperazine derivatives used as nucleoside reverse transcriptase inhibitors for the treatment of HIV Virus [3]. Aryl piperazine derivatives exhibit a wide class of biological activities such as: anti-arrythmic [4, 5], anti-cancer [6, 7], anti-viral [8, 9], anti-oxidative [10], and anti-bacterial [11].Compounds of this type show high affinity for dopaminergic [12], α1-adrenergic [13], and serotoninergic receptors [14, 15]. A large class of aryl piperazine derivatives of 1,7,8,9-Tetrachloro-10,10-dimethoxy-4-azatricyclo[5.2.1.$0^{2,6}$] dec-8-ene-3,5-dione were evaluated in vitro against agents of different virus classes, such as the single-stranded RNA+ viruses, Yellow fever virus and Bovine viral diarrhea virus, both belonging to the Flaviridae, a HIV-1 (Retrovirus), and HBV (Hepadnavirus) [16]. Complexes of diarylpiperidin-4-one were found as the new variety of anti-microbial agents with activity against pathogenic bacterial species and fungal strains [17]. In order to analyse the effect of halogen substitution, in the parent molecule, the position of four chlorine atoms are replaced by bromine, and fluorine atoms respectively and which are designated as TDBPA, TDBPA Br, TDBPA F,

6.2 Experimental Details

1,7,8,9-Tetrachloro-10,10-dimethoxy-4-azatricyclo[5.2.1.$0^{2,6}$]dec-8-ene-3,5-dione (1) was synthesized (scheme 1) as previously described [18]. 1,7,8,9-Tetrachloro-4-(3-chloropropyl)-10,10-dimethoxy-4-azatricyclo[5.2.1.$0^{2,6}$]dec-8-ene-3,5-dione (2) was prepared as follows: A mixture of imide 1 (0.5 g, 0.00138 mol), 1-bromo-3-chloropropane (0.6 g, 0.00415 mol) and anhydrous K_2CO_3 (0.5 g,0.0036 mol) in acetonitrile (50 mL) was refluxed for 8 h. The inorganic precipitate was filtered off, the solvent was evaporated [19].The title compound, 1,7,8,9-tetrachloro-10,10-dimethoxy-4-[3-(4-benzylpiperazin-1-yl)propyl]-4-azatricyclo[5.2.1.$0^{2,6}$] dec-8-ene-3, 5-dione (3) was prepared as follows: A mixture of compound 2(0.3 g, 0.0007 mol), 1-benzylpiperazine 0.21 g (0.0013 mol),anhydrous K_2CO_3

(0.3 g, 0.0022 mol) and KI (0.2 g, 0.0012 mol) was dissolved in acetonitrile (50 mL) and refluxed for 30 h. The solvent was evaporated, then the residue was purified by column chromatography (eluent: $CH_2Cl_2ACH_3OH$, 95:5) [31]. Yield 75%,m.p. 245.5–2460C. Anal. Calculated: 48.06% C, 4.71% H, 7.01% Found: 48.03% C, 4.59% H, 6.80% N The FT-IR spectrum (Fig.1) was recorded using KBr pellets on a DR/Jasco FT-IR 6300 spectrometer. The FT-Raman spectrum (Fig. 2) was obtained on a Bruker RFS 100/s, Germany. For excitation of the spectrum the emission of Nd:YAG laser was used, excitation wavelength 1064 nm, maximal power 150 mW, measurement on solid sample.

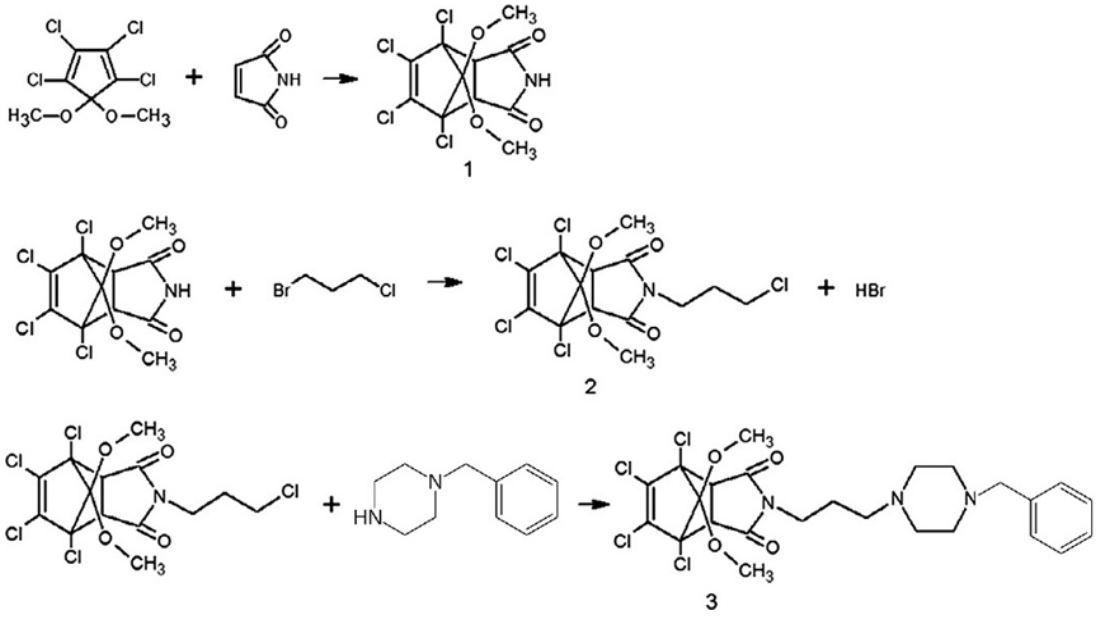

Scheme 1: Pathway of compound synthesis

6.3 Computational Details

Calculations of the title compound were carried with using the Gaussian09 program [20] using the B3LYP/6-311++G(d,p) basis set to predict the molecular structure and wavenumbers in the gaseous phase and a scaling factor of 0.9613 had to be used for obtaining a considerably better agreement with the experimental data [21]. The structural parameters corresponding to the optimized geometry of the title compound (Fig. 3) are given in Table 1. The assignments of the calculated wavenumbers are done using GAR2PED [22] and Gauss view software [23]

6.4 Result and Discussion

6.4.1 Geometrical Parameters

No data is available regarding the X-ray crystallography of the molecule, to the best our knowledge .Moreover, the reported structural parameters of the parental molecule significantly correlates with our theoretical predictions attesting the authenticity of our results.

The bond angles of imido fragment of title compound give theoretically as C_{16}-N_{15}-C_{13} = 114.0, O_{18}-C_{13}-N_{15} = 124.6,O_{18}-C_{13}-C_4 = 127.4, N_{15}-C_{13}-C_4 = 107.9, C_{13}-C_4-C_5 = 105.0, C_{13}-C_4-H_{10} = 107.3, C_5-C_4-H_{10} = 114.2, C_{16}-C_5-H_{12} = 107.6, C_4-C_5-H_{12} = 114.1, O_{17}-C_{16}-N_{15} = 124.7, O_{17}-C_{16}-C_5 = 127.3, N_{15}-C_{16}-C_5 = 107.9° respectively, where as the reported values of similar derivatives are 114.7, 124.0, 128.5, 107.4,105.8, 112.3 , 113.8 , 113.3, 113.1, 126.3, 129.2, 106.5◦ and 111.0, 126.1, 128.4, 105.5,109.9, 115.0, 136.0, 118.0, 118.0, 123.7, 131.4, 104.9° [24]. Conley et al. [24] reported the dihedral angles, C_{16}-N_{15}-C_{13}-O_{18} = 179.5, C_{16}-N_{15}-C_{13}-C_4 = 4.0, O_{18}-C_{13}-C_4-C_5 = 177.5, N_{15}-C_{13}-C_4-C_5 = 0.5, C_{13}-C_4-C_5-C_{16} = 1.7, C_{13}-N_{15}-C_{16}-C_5 = 5.1, C_4-C_5-C_{16}-O_{17} = 176.7, C_4-C_5-C_{16}-N_{15} = 4.0° whereas for the title compound the corresponding values are 177.3, 6.7, 177.6, 1.7, 3.1, 8.8, 176.5 and 7.0° respectively. Pinho e Melo et al. [25] reported the bond lengths N_{15}-C_{16} = 1.3654, N_{15}-C_{13} = 1.4484 Å, bond angles C_{16}-N_{15}-C_{13} = 116.8, C_{16}-N_{15}-C_{19} = 121.6, C_{13}-N_{15}-C_{19} = 121.6, C_5-C_{16}-N_{15} = 121.9, N_{15}-C_{13}-C_4 = 107° and dihedral angles C_{13}-N_{15}-C_{16}-C_5 = 177.2, C_{16}-N_{15}-C_{13}-C_4 = 169.9° which are in agreement with our calculated values. Lee and Swager [26] reported the bond lengths O_{17}-C_{16} = 1.1954, O_{18}-C_{13} = 1.2054, N_{15}-C_{16} = 1.3776, N_{15}-C_{13} = 1.3765 Å and the bond angles C_5-C_{16}-N_{15} = 106.3, C_4-C_{13}-N_{15} = 106.5°. The B3LYP calculations give the bond lengths within the imido fragment as C_{16}-O_{17} = 1.2095, N_{15}-C_{16} = 1.3917, C_{13}-O_{18} = 1.2077, C_{13}-N_{15} = 1.3933, C_{13}-C_4 = 1.5337, C_{16}-C_5 = 1.5373, C_5-C_4 = 1.5534 Å. Conley et al. [24] reported the corresponding values as 1.2025, 1.3985, 1.2104, 1.4054, 1.4865, 1.5155, 1.555 Å and 1.1974, 1.3995, 1.2004, 1.3824, 1.4866, 1.4826, 1.3436 Å for different similar derivatives. The N_{15}-C_{19} bond length (1.4617 Å) is longer than N_{15}-C_{13} (1.3933 Å) and N_{15}-C_{16} (1.3917 Å) bond lengths. This indicates, as expected, a delocalized p-electron system along the imide part of the molecule (O_{18}-C_{13}-N_{15}-C_9-O_{17}) as reported by Bartkowska et al. [27]. Bartkowska et al. [27] reported the bond lengths, C13-O18 = 1.2032, N_{15}-C_{13} = 1.3913, C_{13}-C_4 = 1.5193, C_4-C_5 = 1.5453, C_{16}-O_{17} = 1.2073, N_{15}-C_{16} = 1.3880 Å and the bond angles, N_{15}-C_{19}-C_{28} = 111.3 O_{18}-C_{13}-N_{15} = 124.3, O_{18}-C_{13}-C_4 = 127.8, N_{15}-C13-C4 = 107.8, O_{17}-C_{16}-N_{15} = 127.2, N_{15}-C_{16}-C_5 = 107.0, C_{16}-N_{15}-C_{13} = 114.2,C_{16}-N_{15}-C_{19} = 123.8 and C_{13}-N_{15}-C_{19} = 121.7° whereas the corresponding values in the present case are 1.2077, 1.3933, 1.5337,1.5534, 1.2095, 1.3917 Å and 113.0, 124.6, 127.4,

107.9,124.7,107.9, 114.0, 123.3,122.4°. For the title compound the C_4-H_{10}, C_5-H_{12}, bond lengths are 1.0945, 1.0948 Å whereas reported values are 0.96, 0.9601 Å [24]. The cyclohexene ring fragment is a sterically strained system. Presumably, this is the reason for elongation of skeletal C-C bonds, C_1-C_2, C_2-C_3, C_3-C_4, C_5-C_6, and C_6-C_1. The C-C bond lengths in the five member ring (C_5-C_{16}, C_4-C_{13}) are elongated to a lesser extent. These may be explained by change of the substitution pattern in the nitrogen containing five member ring as reported by Tarabara et al. [28]. The methoxy groups, O_{14}-C_{11}-H_{23}, $_{24}$, $_{27}$ and O_9-C_8-H_{20}, $_{21}$, $_{22}$ inclined almost equally with respect to the other parts of the six member ring. The bond angles C_1-C_6-C_7, C_5-C_6-C_7, C_2-C_3-C_7, C_4-C_3-C_7, C_6-C_1-C_2 and C_4-C_3-C_2 are respectively 99.5, 102.3, 99.6, 102.8, 107.9 and 104.7°. In addition the declination of the five member ring from the cyclohexene ring are given by the angles C_6-C_5-C_{16} and C_3-C_4-C_{13} by 118.7 and 119.2° which are almost equal as reported in the literature [28]. The conjugation in the imido group is essentially disturbed; the torsion angles C_{13}-N_{15}-C_{16}-C_5, C_{16}-N_{15}-C_{13}-C_4 are 8.8, -6.7° and the C_{13}-$N_{15}$and C_{16}-N_{15} bond lengths are elongated to 1.4037, 1.4021 Å relative to the average value 1.371 Å [29]. For the cyclohexene ring, Manohar et al. [30] reported the bond lengths C_1-C_2 = 1.3194, C_1-C_6 = 1.5174, C_6-C_5 = 1.5523, C_6-C_7 = 1.5484, C_5-C_4 = 1.5353, C_4-C_3 = 1.5543, C_3-C_7 = 1.5473, C_3-C_2 = 1.5144 Å and the corresponding bond lengths of the title compound are 1.3472, 1.5334, 1.5705, 1.5870, 1.5693, 1.5750, 1.5903, 1.5311 Å. The bond angles reported by Manohar et al. [30] are C_3-C_4-C_5 = 102.9, C_3-C_2-C_1 = 107.5, C_3-C_7-C_6 = 92.4, C_2-C_3-C_4 = 107.2, C_6-C_5-C_4 = 103.1, C_6-C_1-C_2 = 107.7, C_5-C_6-C_1 = 106.8, C_2-C_3-C_7 = 99.52, C_4-C_3-C_7 = 101.12, C_5-C_6-C_7 = 101.1, C_1-C_6-C_7 = 99.4Å where as the corresponding calculated(DFT) values of the title compound are 103.1, 107.3 91. 4,104.7, 103.1, 107.9, 105.7, 99.6, 102.8, 102.3, 99.5°. In the present case, the oxygen atoms O_{17} and O_{18} are equally inclined from the N_{15} atom given by the angles O_{17}-C_{16}-N_{15}, O_{18}-C_{13}-N_{15} (124.6°) and from C_4 and C_5 atoms given by the angles O_{17}-C_{16}-C_5, O_{18}-C_{13}-C_4 (127.3°) as reported in the literature [31]. There are four types of CC bonds involved in the title compound, strained CC bonds of R1, RII, RIII, RIV, propyl group and of the carbon–carbon bridge. The CC bond lengths are in the range 1.5265-1.5638, 1.5337-1.5534, 1.5340-1.5342 Å, in R1, RII, propyl group, 1.5854, 1.5100 Å in the carbon–carbon bridge and 1.5255 in benzyl fragment respectively. The CH bond lengths are C_4-H_{10} = 1.0945 and C_5-H_{12} = 1.0948 Å. The CH bond lengths are in the range 1.0950-1.1126 Å for the bridging CH_2 groups, and for the CH_3 groups, CH bond lengths are in the range of 1.0931-1.0957 Å. The optimized carbon-carbon bridge angles C_3-C_7-C_6 = 91.3 is similar to the structures reported by Manohar et al. [30]. The propyl group is tilted from the RII, as is evident from torsion angles, C_5-C_{16}-N_{15}-C_{19} (177.1°), C_{16}-N_{15}-C_{19}-C_{28} (92.2°), C_4-C_{13}-

N_{15}-C_{19} (179.2°) and C_{13}-N_{15}-C_{19}-C_{28} (81.5°). The double bonds C_{16}-O_{17} and C_{13}-O_{18} are conjugated with the p-system of the RII, with the torsion angles O_{17}-C_{16}-N_{15}-C_{13}, C_{16}-N_{15}-C_{13}-C_4 being 174.6, 6.7 and O_{18}-C_{13}-N_{15}-C_{16}, C_{13}-N_{15}-C_{16}-C_5 being 177.3, 8.8 respectively as reported by Kasyan et al. [32]. At N_{15} position, the bond angles C_{16}-N_{15}-C_{19} = 123.3, C_{13}-N_{15}-C_{19} = 122.4 and C_{16}-N_{15}-C_{13} = 114.0° and this asymmetry of angles reveal the steric repulsion of the atoms H_{26}, H_{25} and O_{17}, O_{18} [32]. For the piperazine ring, El-Emam et al. [33] reported the bond lengths N_{38}-C_{40} = 1.4650, N_{38}-C_{39} = 1.4630, C_{39}-C_{46} = 1.5140, N_{47}-C_{45} = 1.4580, N_{47}-C_{46} = 1.4710, C_{40}-C_{45} = 1.5110 and the corresponding bond lengths of the title compound are 1.4714, 1.4574, 1.5400, 1.4540, 1.4646, 1.5438 Å respectively. The DFT calculations give the bond angles within the piperazine ring N_{38}-C_{39}-C_{46} = 110.2, N_{38}-C_{40}-C_{45} = 111.6, N_{47}-C_{45}-C_{40} = 109.5, N_{47}-C_{46}-C_{39} = 110.8, C_{45}-N_{47}-C_{46} = 112.3°. El-Emam et al. [33] reported the corresponding values as 110.0, 109.7, 109.7, 110.0 and 110.0 for different similar derivatives. Karczmarzyk et al. [34] reported the dihedral angles C_{40}-N_{38}-C_{39}-C_{46} = 61.1, C_{45}-N_{47}-C_{46}-C_{39} = 60.1, N_{38}-C_{39}-C_{46}-N_{47} = 61.5, C_{46}-N_{47}-C_{45}-C_{40} = 58.2, C_{39}-N_{38}-C_{40}-C_{45} = 58.9, N_{47}-C_{45}-C_{40}-N_{38} = 57.5° which are in agreement with our calculated values.

6.4.2 IR and Raman Spectra

In the following discussion, the cyclohexene ring is designated as RI, the imido fragment ring is designated as RII, piperazine ring is designated as RIII, Phenyl ring is designated as RIV and the calculated (scaled) wavenumbers, observed IR and Raman bands and assignments are given in Table 2. The assignments of the benzene ring vibrations are made by referring [35] the case of benzene derivatives with mono substitution as summarized by Roeges. According to Roeges, the CH stretching modes for mono substituted benzene are found in the region 3105-3000 cm^{-1} [35]. For the title compound, the bands observed at 3069 cm^{-1} in the IR spectrum and 3068, 3053 cm^{-1} in the Raman spectrum are assigned as CH stretching mode of the phenyl ring. The calculated (DFT) values are at 3078, 3066, 3058, 3046 and 3044 cm^{-1} [35]. The bands observed at 1621, 1477, 1438 and 1307 cm^{-1} in the IR spectrum and at 1610 and 1573 cm^{-1} in the Raman spectrum are assigned as υIV ring-stretching modes. Theoretically these modes are assigned at 1598, 1579, 1479, 1437 and 1309 cm^{-1}. These vibrations are expected in the region 1620-1300 cm^{-1} [35]. For the title compound, the ring breathing mode of phenyl ring is found at 979 cm^{-1} theoretically [35].The bands observed at 1140,1065 cm^{-1} in the IR spectrum and 1161,1014 cm^{-1} in the Raman spectrum are assigned as the in-plane bending vibrations of CH modes. DFT calculations give these modes at 1164,1161,1140,1068 and 1016 cm^{-1}. For the title compound, the bands at 921, 891, 828 cm^{-1}

in the IR spectrum and 930, 893, 824,735 cm^{-1} in the Raman spectrum are assigned as the out-of-plane CH deformations of the phenyl ring. The γCH bands are found theoretically at 950, 924, 893, 828 and 731 cm^{-1}. In aromatic methoxy compounds, $\upsilon_{as}CH_3$ bands are expected in the region [35] 2985 ± 20 and 2955 ± 20 cm^{-1} and the symmetrical stretching mode $\upsilon_{s}CH_3$ is expected in the range 2845 ± 45 cm^{-1} in which all the

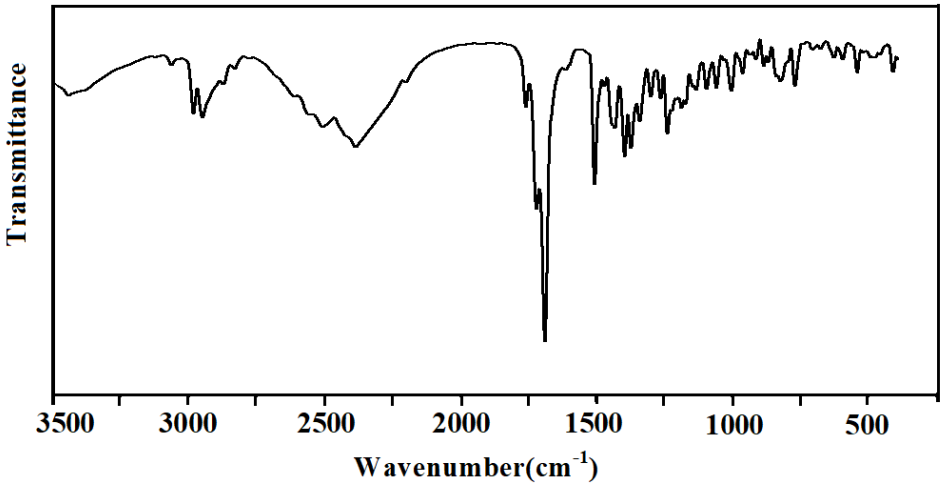

Fig.1 FT-IR spectrum of 1,7,8,9-tetrachloro-10,10-dimethoxy-4-[3-(4-benzylpiperazin-1-yl) propyl]-4-azatricyclo [5.2.1.$0^{2,6}$]dec-8-ene-3,5-dione

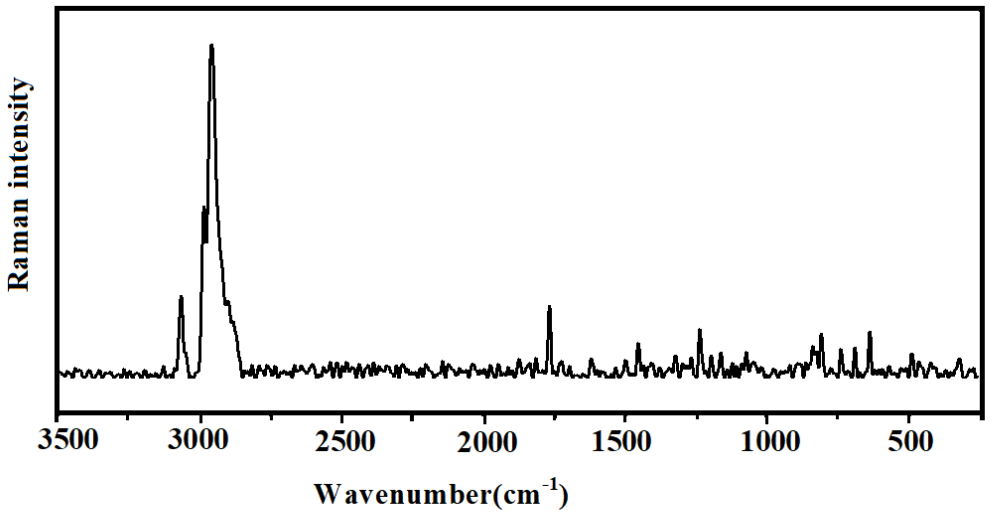

Fig. 2 FT-Raman spectrum of 1,7,8,9-tetrachloro-10,10-dimethoxy-4-[3-(4-benzylpiperazin-1-yl)propyl]-4-azatricyclo [5.2.1.$0^{2,6}$]dec-8-ene-3,5-dione

three C-H bonds extend and contract in phase [35]. For the title compound, corresponding calculated wavenumbers are at 3048, 3035, 3034, 3019 cm^{-1} as $\upsilon_{as}CH_3$ and 2952, 2947, 2941 $cm^{-1}$for $\upsilon_{s}CH_3$ vibrations. Experimentally $\upsilon_{as}CH_3$ band is assigned at 3030 cm^{-1}. With methyl

esters the overlap of the regions in methyl asymmetrical deformations are active (1465 ± 10 and 1460 ± 15 cm^{-1}) and is quite strong, which leads to many coinciding wavenumbers [35]. This is obvious, not only for the asymmetric deformation, but also for the symmetric deformation [35] mostly displayed in the range 1450 ± 20 cm^{-1}. The intensity of these absorptions is only weak to moderate. The DFT calculations give the deformation modes of CH_3 at 1474, 1465, 1459, 1453, 1422 cm^{-1} for the title compound. The bands observed at 1453, 1418 cm^{-1} in the Raman spectrum are assigned as the deformation bands of the methyl group. The methyl rocking vibration [35] are expected at 1190 ± 45 cm^{-1}. The second methyl rock [35] absorb at 1150 ± 30 cm^{-1}. The bands at 1191, 1178, and 1133 cm^{-1} theoretically were assigned as rocking modes of the methyl group. These modes are observed at 1178 cm^{-1} in the IR spectrum. A methoxy group attached to an aromatic ring give CO stretching modes in the range 1200-900 cm^{-1} [36]. The DFT calculation gives CO stretching vibrations at 1167, 1143, 1091, 1031, 1005, 989, 970 and 947 cm^{-1}. The bands observed at 1087, 1004, 969, 943 cm^{-1} in the IR spectrum and at 1088, 997, 973, 948 cm^{-1} in the Raman spectrum are assigned as CO stretching vibrations. Renjith et al. [37] reported the asymmetric and symmetric CO stretching vibrations in the range 1145, 1065 cm^{-1} and 961-947 $cm^{-1.}$ Castaneda et al. reported the methoxy vibrations at 1252, 1190, 1172, 1028 and 1011 cm^{-1} [38]. The C=O stretching frequency appears strongly in the IR spectrum in the range 1600-1700 cm^{-1} because of its large change in dipole moment. The carbonyl group vibrations give rise to characteristics bands in vibration spectra and its characteristic frequency used to study a wide range of compounds. The intensity of these bands can increase owing to conjugation or formation of hydrogen bonds [39, 40]. The carbonyl band of cyclic imides is shifted to higher wavenumber if the ring is strained [40]. The carbonyl groups in the imide fragment give rise to bands [40, 41] in the region of 1720-1790 $cm^{-1.}$ For the title compound, the C=O stretching bands are observed at 1766, 1698 cm^{-1} in the IR spectrum, 1788, 1727 cm^{-1} in the Raman spectrum and at 1786,1728 cm^{-1} theoretically (DFT). The CC vibrations in the Ring I and II are calculated at 1135, 1100 and 1052 cm^{-1} theoretically and in between 1137-1054 cm^{-1}experimentally. Renjith et al. reported these values in between 1093-962 cm^{-1} theoretically, at 1011, 999, 964 cm^{-1} in the Raman spectrum [37]. The CN stretching modes are reported [42] in the range 1100-1300 cm^{-1}. Silverstein et al. assigned CN stretching absorption in the region 1382-1266 cm^{-1} for aromatic amines [43]. In the present case, the υCN stretching modes to C_{13}-N_{15}, C_{16}-N_{15}, C_{19}-N_{15},C_{31}-N_{38} and C_{63}-N_{47} are observed at 1347, 151, 1121 cm^{-1} in the IR spectrum 1340, 1121 cm^{-1} in the Raman spectrum and at 1348, 1339, 1144, 1127, 1107 cm^{-1} theoretically respectively. Kasyan reported the CN stretching in the region 1350-1100 cm^{-1} [44]. For bridging methylene

groups, the CH_2 (at C_{19}, C_{28}, C_{31}, C_{63}) vibrations are observed in the region of 2800-3000, 1200-1400, 875-1150 and 600-850 cm^{-1} [45]. The vibrations of these CH_2 groups (the asymmetric stretch $\upsilon_{as}CH_2$, symmetric stretch $\upsilon_s CH_2$, the scissoring vibration and wagging vibration) appear in the regions of 2940-3005, 2870-2940, 1420-1480 and 1320-1380 cm^{-1}, respectively [35, 36, 46]. These bands are observed at 2989, 2954, 2781 cm^{-1} in the IR spectrum, 3016, 2988, 2961, 2792 cm^{-1} in the Raman spectrum and at 3018, 2991, 2962, 2953, 2947, 2930, 2910, 2782 cm^{-1} theoretically (DFT) for the title compound respectively. According to literature [43] scissoring mode of the CH_2 group give rise to characteristic band near 1465 cm^{-1} in IR and Raman spectra. These modes are unambiguously correlated with the strong bands in the region of 1376-1449 cm^{-1} observed experimentally and theoretically these bands are assigned in between1378-1464 cm^{-1}. The twisting and rocking vibrations of the CH_2 group appear in the region [35] of 1200-1280 and 740-900 cm^{-1}, respectively. These modes are also assigned (Table 2). For the title compound these deformation modes are observed in the range 1298-716 cm^{-1} theoretically and are observed at 845, 799,746 cm^{-1} in the IR spectrum, 1297, 1280, 1235, 835, 754 cm^{-1}in the Raman spectrum. These modes are not pure, but contain significant contributions from other modes also. In the bridging methylene group (C_{19}-C_{28}, C_{28}-C_{31} and C_{63}-C_{52}) CC stretching modes are found at 1169, 1035, 1009 cm^{-1} theoretically and at 1035, 1010 cm^{-1} in the IR spectrum. The CH stretching vibrations occur [36] above 2900 cm^{-1} and CH deformations absorb weakly in the region of 1350–1315 cm^{-1} in the infrared and more distinctive in Raman spectrum. For the title

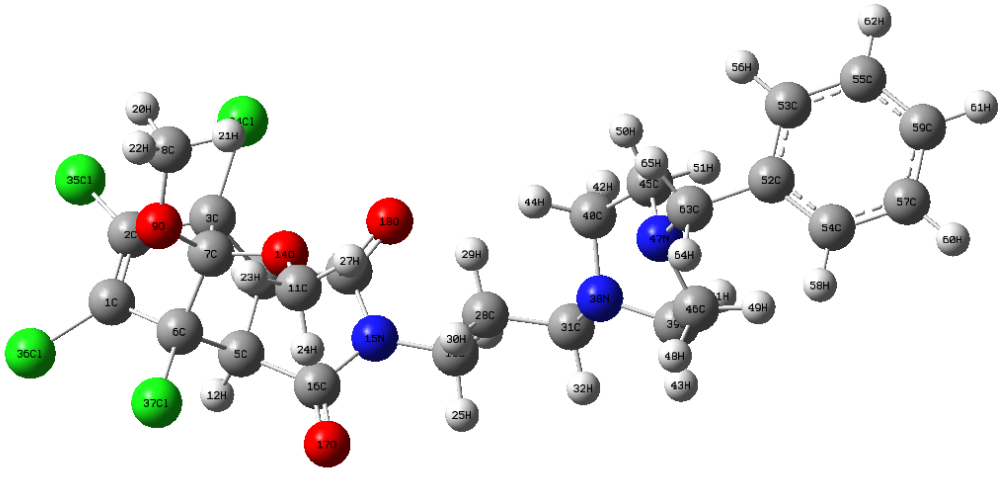

Fig. 3 Optimized geometry of 1,7,8,9-tetrachloro-10,10-dimethoxy-4-[3-(4-benzylpiperazin-1-yl)propyl]-4-azatricyclo [5.2.1.$0^{2,6}$] dec-8-ene-3,5- dione

compound the DFT calculations give the υCH modes in Ring I at 2991 and 2983 cm^{-1}. Kasyan et al. and Tarabara et al. reported the υCH modes at 3080 cm^{-1} and 3070-3050 cm^{-1} for similar derivatives [44, 45]. Most of the bands are not pure, but contains significant contributions from other modes. The C=C stretching mode is expected in the region [46] 1667-1640 cm^{-1}. For the title compound, the C=C stretching mode is assigned at 1595 cm^{-1} in the Raman spectrum and at 1597 cm^{-1} theoretically. For a series of propenoic acid esters, Felfoldi et al. reported the υC=C at 1625 cm^{-1} [47] theoretically. The deformation modes in Ring I is observed at 1270, 1261, 1226, 1192 (DFT), 1270, 1194 cm^{-1}(IR) and at 1265, 1194 cm^{-1}(Raman).The vibrations belonging to the bond between the ring and chlorine atoms are worth to discuss here since mixing of vibrations is possible due to the lowering of the molecular symmetry and the presence of heavy atoms on the periphery of the molecule [48-50]. Mooney assigned vibrations of CCl, Br and I in the wavenumber range of 1129-480 cm^{-1} [49, 50]. The CCl stretching vibrations give generally strong bands in the region 710-505 cm^{-1}. For simple organic chlorine compounds, CCl absorptions are in the region 750-700 $cm^{-1.}$ Sundaraganesan et al. reported CCl stretching at 704 (IR), 705 (Raman), and 715 cm^{-1} (DFT) and the deformation bands at 250 and 160 cm^{-1} [51]. The aliphatic CCl bands absorb [35] at 830-560 cm^{-1} and putting more than one chlorine on a carbon atom raises the CCl wavenumber. The CCl stretching mode is reported at around 738 cm^{-1} for dichloromethane and scissoring mode δCCl at around 284 cm^{-1} [52,36]. Pazdera et al. reported the CCl stretching mode at 890 cm^{-1} [53]. For 2-cyanophenylisocyanide dichloride, the CCl stretching mode is reported at 870 (IR), 877 cm^{-1} (Raman), and 882 cm^{-1} theoretically [54]. Arslan et al. reported the CCl stretching mode at 683 (experimental) and at 736,711, 697 and 687 cm^{-1} theoretically [55]. The deformation bands of CCl are reported [54] at 441, 435 and 431 cm^{-1}. For the title compound the bands at 668, 616 cm^{-1} in Raman and 700, 657 and 610 (DFT) are assigned as CCl stretching modes. The asymmetric stretching CH_2 vibrations in the piperazine ring is reported in the range 3033-2966 cm^{-1}, while the symmetric vibrations lying in the range 2874-2834 cm^{-1} [56]. For the title compound, the bands observed at 2963, 2958, 2935, 2917, 2857, 2837, 2817, 2804 cm^{-1} (DFT) are assigned for CH_2 stretching modes. These bands are observed at 2878, 2837 cm^{-1}in the IR spectrum and 2959, 2832, 2817, 2805 cm^{-1}in the Raman spectrum. In a study on the determination of piperazine rings in ethylene amines, poly (ethyleneamine) and polyethylenimine by infrared spectrometry, Spell reported that the piperazine ring was found to be associated with sharp, well defined absorptions at 1300-1345 cm^{-1}, 1125-1170 cm^{-1}, 1010-1025 cm^{-1} and 915-940 cm^{-1} regions of the IR spectrum [57]. El-Emam et al. reported the vibrations of CH_2 groups in the piperazine ring (the asymmetric stretch υasCH_2, symmetric

stretch $\upsilon_s CH_2$, the scissoring vibration and wagging vibration) in the range 3033-2966, 2874-2834, 1457-1422 and 1379-1344 cm^{-1}respectively [56]. As stated by Spell, this is one of the most useful bands for detecting the presence of di-substituted piperazines [57]. The twisting and rocking vibrations of the CH_2 group appear in the region [35] of 1200-1280 and 740-900 cm^{-1}, respectively. These modes are also assigned (Table 2) For the title compound the deformation modes are observed at in the range 1473-860 cm^{-1} theoretically, at 1229, 1212 cm^{-1}(IR) and at 1473, 1357, 1211, 860 cm^{-1}(Raman). These modes are not pure, but contain significant contributions from other modes also. El-Emam et al. reported the CN stretching vibrations in the region 1154-756 cm^{-1} [56]. For the title compound (C_{40}-N_{38}, C_{39}-N_{39}, C_{45}-N_{47},C_{46}-N_{47}) CN stretching vibrations (in Ring III) are found at 1188, 1116, 954, 764 cm^{-1} theoretically. The shift in the wavenumber may be attributed to the bulky groups attached to the piperazine ring. The CC stretching vibrations for the title compound (in Ring III) are observed at 986, 960, 895 cm^{-1} theoretically, and at 987 cm^{-1} experimentally. These vibrations in the piperazine ring were reported at 972, 903 cm^{-1} [56].

6.4.3 Frontier Molecular Orbital

Frontier molecular study is used to explain the chemical behaviour and stability of molecular system. The atomic orbital components of the frontier molecular orbital are shown in Fig. 4. The delocalization of HOMO and LUMO over the molecular system shows the charge transfer with in the molecular system. The HOMO-LUMO gap is found to be 3.144 eV. The chemical description can be evaluated by using HOMO-LUMO orbital energies, E_{HOMO} and E_{LUMO} as: ionisation energy I = -E_{HOMO}, electron affinity A = -E_{LUMO}, chemical hardness η = (I-A)/2, chemical potential μ = -(I+A)/2 and electrophilicity index ($\omega = \mu 2/2\eta$) [58]. For the title compound I = 8.087, A = 4.943, η = 1.572, μ = -6.515, ω = 13.500 eV (Table. 3). For the title compound, HOMO is delocalized over cyclohexene ring, partially over imido fragment while the LUMO is delocalized strongly over the phenyl ring and partially over the piperazine ring. For fluorine substitution HOMO is delocalized strongly over cyclohexene, piperazine rings and partially over the bridge CH_2 while LUMO is deeply over phenyl ring and N_{47} atom of piperazine ring. For halogen bromine substitution HOMO is delocalized strongly over cyclohexene ring while LUMO is delocalized strongly over phenyl ring. The chemical potential decreases for halogen substitution in the order of bromine substitution< fluorine substitution< parent molecule. The electrophilicity index decreases for halogen substitution in the order fluorine substitution < parent molecule < bromine substitution.

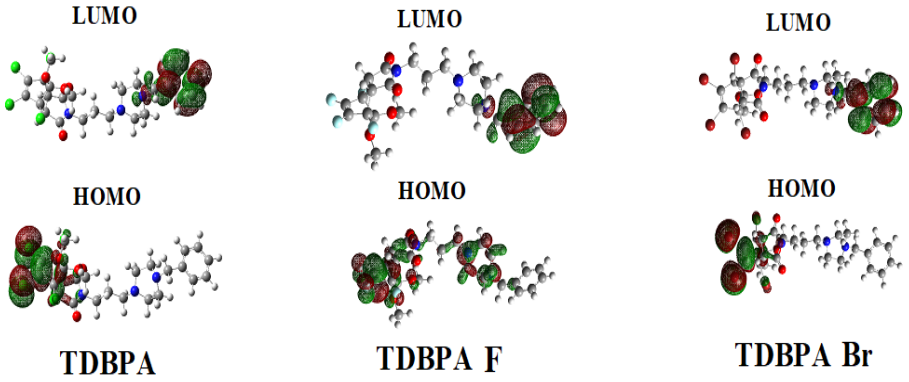

Fig. 4 HOMO-LUMO Plots of TDBPA with halogen substitutions

6.4.5 Molecular Electrostatic Potential Map

Molecular electrostatic potential and electron density are associated to each other to find the reactive sites for electrophilic and nucleophilic sites [59, 60]. For the parent molecule most electrophilic (red and yellow) regions of MEP map (Fig.5) were related electrophilic reactivity while positive blue regions to nucleophilic reactivity. For the parent molecule the electrophilic regions are deeply over N_{38} atom of piperazine ring, slightly over the phenyl ring, marginally over the carbon atoms of cyclohexene ring, slightly over oxygen atoms of imido fragment. The nucleophilic region (blue) is deeply over the hydrogen atoms in the phenyl ring and strongly over methoxy group of cyclohexene ring and deeply over the chlorine atoms of parent molecule.

For fluorine substitution electrophilic region is deeply over the N_{38} atom in the piperazine ring, very slightly over carbon atoms in the phenyl ring (C_{55}, C_{59}). The electrophilic region of carbon atoms in the cyclohexene ring is slightly greater than parent molecule. The nucleophilic region of fluorine substitution is deeply over fluorine atoms and CH_2 groups of propyl part of the molecule. The other part of nucleophilic region of TDBPA fluorine is almost same as that of parent molecule. For halogen substitution bromine atom the electrophilic region is strongly over the N_{38} atom in the piperazine ring, slightly over carbon atoms in the cyclohexene ring but greater than that of TDBPA fluorine. Nucleophilic region is maximum pronounced over the methoxy group, bromine atoms and phenyl ring. Electrophilic region of phenyl ring of parent molecule >TDBPA fluorine >TDBPA bromine. Nucleophilic region is same for halogen

atoms in parent molecule and fluorine substitutions but greater than bromine substitutions. The electrophilic region in the piperazine ring is same for three halogen substitutions. The electrophilic region of cyclohexene ring is more pronounced in bromine substitution than parent molecule and fluorine substitutions.

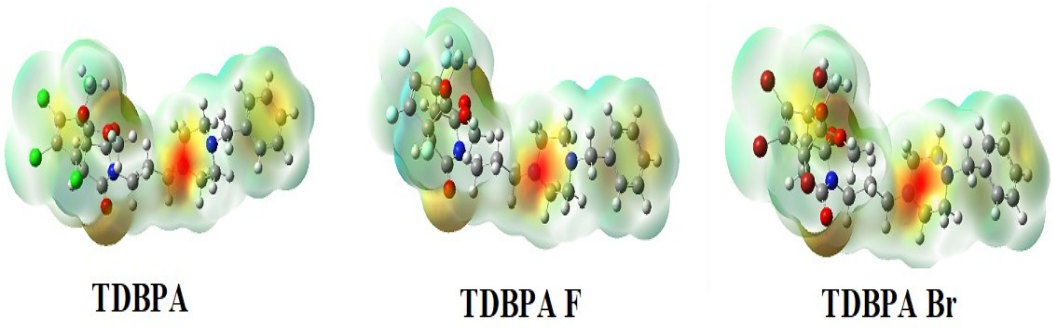

Fig. 5 MEP Plots of TDBPA with halogen substitutions

6.4.6 Natural Bond Orbital Analysis

The natural bond orbitals (NBO) calculations were performed using NBO 3.1 program [61] and the important interactions are presented in Tables 4 and 5. The strong interactions are: C_{13}-O_{16} from N_{11} of n_1 (N_{11})/-π^*(C_{13}-O_{16}), C_2-C_3 from N_{11}/ π^* of n_1 (N_{11})/(C_2-C_3), N_{11}-C_{13} from O_{16} of n_2 (O_{16})/σ^*(N_{11}-C_{13}), C_{13}-$C_{15}$from O_{16} of n_2(O_{16})/σ^*(C_{13}-C_{15}), C_{14}-C_{15} from O_{17} of n_1(O_{17})/π^*(C_{14}-C_{15}), C_{19}-O_{21} from O_{20} of n_2(O_{20})/σ^*(C_{19}-O_{21}). These interactions have high stabilization energies and electron densities, which are respectively, (0.00890, 0.45862, 0.08085, 0.06141, 0.35631, 0.07395 and 53.53, 45.39, 25.06, 18.29, 45.86, 23.37 kJ/mol. The natural orbitals with low and high occupation numbers are: n_2(O_{16}), n_2(O_{17}), n_3(O_{20}), n_2(O_21) and n_1(O_{16}), n_1(O_{17}), n_1(O_{20}), n_1(O_{21}). The orbital with low occupation numbers have higher energies, 0.23464, 0.31867, 0.27482, 0.31862 a.u with considerable p-characters around 100.0% with low occupation numbers, 1.86676, 1.77071, 1.56926 and 1.75646. The orbital have high occupation numbers have low energies, 0.67847, 0.56174, and 0.67554, 0.54974 a.u with p characters, 36.14, 59.46, 41.58, 59.44% and high occupation numbers, 1.97777,

1.97148, 1.95846, 1.96237. Thus a very close to pure p-type lone pair orbital participates in the electron donation to the σ* (C_{19}-O_{21}) orbital for n_2 (O_{20})/σ*(c_{19}-O_{21}), π*(C_{14}-C_{15}) orbital for n_2 (O_{17})/π*(C_{14}-C_{15}) and σ*(N_{11}-C_{13}) orbital for n_2(O_{16})/s*(N_{11}-C_{13}) interaction in the compound.

6.4.7 First Hyper Polarizability

Organic molecules able to control photonic signals efficiently and are of importance in technologies such as optical communication, optical computing, and dynamic image processing. The calculated first hyper polarizability of the 1,7,8,9 - Tetrachloro-10,10-dimethoxy-4-[3-(4-benzylpiperazin-1-yl)propyl]-4-azatricyclo[5.2.1.$0^{2.6}$] dec-8-ene-3,5-dione is 1.66 X 10^{-30} esu which is 12.84 times that of the standard NLO material urea (0.13 x 10^{-30} esu) [62]. Which is comparable with the reported values of similar derivatives (11.77 times that of urea) [63]. From this value we can say that the title compound is an attractive object for future nonlinear studies. In the halogen substituted NLO study of the title compound showed that the hyper polarizability increases to 2.411 x 10-30 esu for fluorine substitution and 1.669 x 10-30 esu for bromine substitution in the place of chlorine atoms in the title compound (Table 6).

6.4.8 Molecular Docking

Molecular docking was employed to recognize the active site of the receptor and acquire the best geometry of ligand-receptor complex. Based on the structure of the title compound, we find the activity of non-basic fXa inhibitors with excellent potency in anti-fXa and anticoagulant assays. Among the many enzymes in the coagulation cascade, factor fXa is one particularly attractive target [64]. Cardiovascular and cerebrovascular diseases, such as deep venous thrombosis (DVT), myocardial infarction (MI), pulmonary embolism (PE), and ischemic stroke, are now and may continue to be leading causes of morbidity and mortality around the world. [64]. Factor Xa (PDB ID: 1wu1) was downloaded from the RCSB protein data bank website. Although thrombin is one of the adequate targets for anticoagulation, there are a few reports in which direct factor Xa (fXa) inhibitors decrease the likelihood of bleeding tendency compared with direct thrombin inhibitors. [65-67]. The structure of a large molecular fragment of factor Xa that lacks only a gladomain has been solved by x-ray crystallography and refined at 2.2A resolution of crystallographic R value of 0.168 [68] .Among several approaches to address the unmet needs, the inhibition of factor Xa (fXa) is known as one of the most popular. This is mainly because fXa inhibitors seemed to have a lower risk of bleeding than heparin and warfarin. The reason would be attributed to the inhibition position in the coagulation cascade. As is well-known, fXa catalyzes thrombin production and is situated at

the confluence of the intrinsic and extrinsic pathways. Thus, fXa inhibitors do not block thrombin directly rather, they block the confluent position of the coagulation cascade [69]. Thus we choose title compound as ligand and Factor Xa receptor as target for docking study. All molecular docking calculations were performed on AutoDock 4.2 [70] and Auto Dock-Vina software [71].The original ligand as well as water molecules were removed from the crystal structure, and polar hydrogens and united atom Kollman charges were assigned for the receptor using the graphical user interface Auto Dock Tools (ADT). The Lammarckian Genetic Algorithm (LGA) [72] was employed to calculate the energy between ligand and receptor. The compound docked the active site of receptors with the grid centre dimension 40×40×40. The conformations with the lowest binding energy is extracted and analysed for detailed interactions in Discovery Studio Visualizer 4.0 software. The ligand binds at the active site of the substrates by weak non-covalent interactions. The amino acids Gly216 forms H-bond with carbonyl group while Gln 192 has an H-bond with methoxy group. Glu97 having an H-bond with CH_2 and electrostatic interactions are detailed in Fig. 6. The docked ligand forms a stable complex with Factor Xa receptor as depicted in Fig. 7 and the binding free energy value is -8.68 kcal/mol. These preliminary results suggest that the compound having inhibitory activity against the coagulation cascade. Thus the title compound can be developed as drug used for the treatment of Cardiovascular and Cerebrovascular diseases.

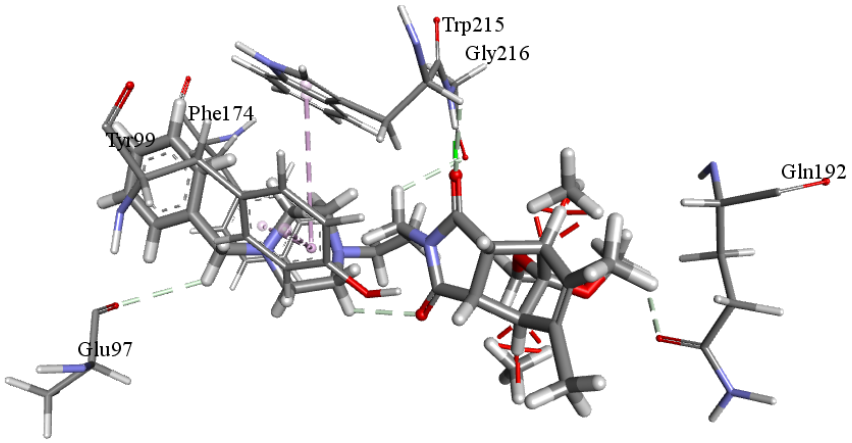

Fig. 6 Ligand interactions TDBPA with the amino acids of factor Xa (fXa) inhibitors

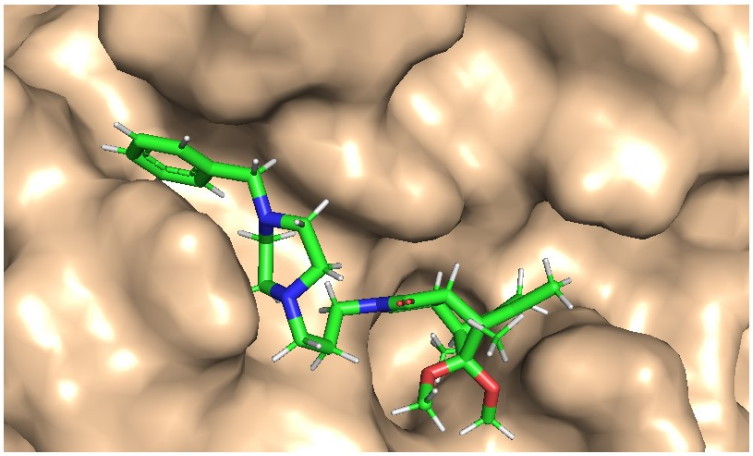

Fig. 7 The docked ligand TDBPA at the active site of the receptor

6.5 Conclusions

In the present study, the molecular structure and vibrational frequencies of 1,7,8,9 - tetrachloro-10,10-dimethoxy-4-[3-(4-benzylpiperazin-1-yl) propyl]-4-azatricyclo [5.2.1.02,6] dec-8-ene-3,5-dione have been studied theoretically and experimentally. The calculated geometrical parameters of the title compound are in good agreement with experimental values. The small difference between experimental and calculated vibrational wavenumbers was that, the experimental results belong to solid phase and the theoretical calculations belong to gaseous phase. For the title compound HOMO is delocalized over cyclohexene ring and LUMO is delocalized at phenyl ring. HOMO-LUMO band gap of the title compound is found to be 3.144 eV and shows the stability of the molecule. From NBO analysis strong interactions are C_{13}-O_{16} from N_{11}, C_2-C_3 from N_{11}, N_{11}-C_{13} from O_{16},C_{13}-C_{15} from O_{16} and C_{14}-C_{15} from O_{11}.The MEP studies shows that the title compound and halogen substitution the electrophilic region is strongly over N_{38} of piperazine ring and nucleophilic region is maximum pronounced over the methoxy group.

Table 1. Optimized geometrical parameters of TDBPA

Bond length(Å)		Bond angle(^{0})		Dihedral angle(^{0})	
C_1-C_2	1.3421	C_2-C_1-C_6	107.9	C_6-C_1-C_2-C_3	0.6
C_1-C_6	1.5304	C_2-C_1-Cl_{36}	127.6	C_6-C_1-C_2-Cl_{35}	173.4
C_1-Cl_{36}	1.7185	C_6-C_1-Cl_{36}	124.2	Cl_{36}-C_1-C_2-C_3	-172.9
C_2-C_3	1.5265	C_1-C_2-C_3	107.3	Cl_{36}-C_1-C_2-Cl_{35}	-0.2
C_2-Cl_{35}	1.7193	C_1-C_2-Cl_{35}	127.9	C_2-C_1-C_5-C_5	-70.8

Bond length(Å)		Bond angle(^{0})		Dihedral angle(^{0})	
C_3-C_4	1.5711	C_1-C_6-C_5	105.7	C_2-C_1-C_6-C_7	34.9
C_3-C_7	1.5854	C_1-C_6-C_7	99.5	C_2-C_1-C_6-Cl_{37}	160.2
C_3-Cl_{34}	1.7837	C_1-C_6-Cl_{37}	114.6	Cl_{36}-C_1-C_6-C_5	103.0
C_4-C_5	1.5534	C_3-C_2-Cl_{35}	124.4	Cl_{36}-C_1-C_6-C_7	-151.2
C_4-H_{10}	1.0945	C_2-C_3-C_4	104.7	Cl_{36}-C_1-C_6-Cl_{37}	-26.0
C_4-C_{13}	1.5337	C_2-C_3-C_7	99.6	C_1-C_2-C_3-C_4	70.2
C_5-C_6	1.5638	C_2-C_3-Cl_{34}	115.9	C_1-C_2-C_3-C_7	-35.9
C_5-H_{12}	1.0948	C_4-C_3-C_7	102.8	C_1-C_2-C_3-Cl_{34}	-162.9
C_5-C_{16}	1.5373	C_4-C_3-Cl_{34}	114.3	Cl_{35}-C_2-C_3-C_4	-102.9
C_6-C_7	1.5810	C_3-C_4-C_5	103.1	Cl_{35}-C_2-C_3-C_7	151.1
C_6-Cl_{37}	1.7826	C_3-C_4-H_{10}	108.6	Cl_{35}-C_2-C_3-Cl_{34}	24.1
C_7-O_9	1.3823	C_3-C_4-C_{13}	118.8	C_2-C_3-C_4-C_5	-69.3
C_7-O_{14}	1.3903	C_7-C_3-Cl_{34}	117.4	C_2-C_3-C_4-C_{13}	175.2
O_8-C_9	1.4342	C_3-C_7-C_6	91.4	C_7-C_3-C_4-C_5	34.4
C_8-H_{20}	1.0957	C_3-C_7-O_9	118.3	C_7-C_3-C_4-C_{13}	-81.1
C_8-H_{21}	1.0953	C_3-C_7-O_{14}	107.8	Cl_{34}-C_3-C_4-C_5	162.8
C_8-H_{22}	1.0938	C_5-C_4-H_{10}	114.2	Cl_{34}-C_3-C_4-C_{10}	-75.7
C_{11}-O_{14}	1.4421	C_5-C_4-C_{13}	105.0	Cl_{34}-C_3-C_4-C_{13}	47.3
C_{11}-H_{23}	1.0935	C_4-C_5-C_6	103.1	C_2-C_3-C_7-C_6	52.6
C_{11}-H_{24}	1.0949	C_4-C_5-H_{12}	114.1	C_2-C_3-C_7-O_9	-58.6
C_{11}-H_{27}	1.0931	C_4-C_5-H_{16}	104.5	C_2-C_3-C_7-O_{14}	171.0
C_{13}-N_{15}	1.3933	H_{10}-C_4-C_13	107.3	C_4-C_3-C_7-C_6	-55.1
C_{13}-O_{18}	1.2077	C_4-C_{13}-N_{15}	107.9	C_4-C_3-C_7-O_9	-166.3
C_{16}-N_{15}	1.3917	C_4-C_{13}-O_{18}	127.4	C_4-C_3-C_7-O_{14}	63.4
C_{19}-N_{15}	1.4617	C_6-C_5-H_{12}	109.4	Cl_{34}-C_3-C_7-C_6	178.5
C_{16}-O_{17}	1.2095	C_6-C_5-C_{16}	118.2	Cl_{34}-C_3-C_7-O_9	67.3
C_{19}-H_{25}	1.0950	C_5-C_6-C_7	102.3	Cl_{34}-C_3-C_7-O_{14}	-63.0
C_{19}-H_{26}	1.0959	C_5-C_6-Cl_{37}	115.9	C_3-C_4-C_5-C_6	2.2
C_{19}-C_{28}	1.5340	H_{12}-C_5-C_{16}	107.6	C_3-C_4-C_5-C_{16}	-122.0
C_{28}-H_{29}	1.0966	C_5-C_{16}-N_{15}	107.9	C_{13}-C_4-C_5-C_6	127.3
C_{28}-H_{30}	1.0969	C_5-C_{16}-O_{17}	127.3	C_13-C_4-C_5-C_{16}	3.1

Bond length(Å)		Bond angle(^{0})		Dihedral angle(^{0})	
C_{28}-C_{31}	1.5342	C_7-C_6-Cl_{37}	116.6	C_3-C_4-C_{13}-N_{15}	116.2
C_{31}-H_{32}	1.0997	C_6-C_7-O_9	107.9	C_3-C_4-C_{13}-O_{18}	-67.9
C_{31}-H_{33}	1.1126	C_6-C_7-O_{14}	116.5	C_5-C_4-C_{13}-N_{15}	1.7
C_{31}-N_{38}	1.4566	O_9-C_7-O_{14}	113.4	C_5-C_4-C_{13}-O_{18}	177.6
N_{38}-C_{39}	1.4574	C_7-O_9-C_8	118.2	C_4-C_5-C_6-C_1	65.4
C_{40}-N_{38}	1.4714	C_7-O_{14}-C_{11}	117.8	C_4-C_5-C_6-C_7	-38.3
C_{39}-H_{41}	1.1096	O_9-C_8-H_{20}	110.7	C_{16}-C_5-C_6-C_1	-179.9
C_{39}-H_{43}	1.0971	O_9-C_8-H_{21}	111.5	C_{16}-C_5-C_6-C_7	76.3
C_{39}-C_{46}	1.5400	O_9-C_8-H_{22}	105.6	C_{16}-C_5-C_6-Cl_{37}	-51.7
C_{40}-H_{42}	1.1089	H_{20}-C_8-H_{21}	109.4	C_4-C_5-C_{16}-N_{15}	-7.0
C_{40}-H_{44}	1.0979	H_{20}-C_8-H_{22}	109.6	C_4-C_5-C_{16}-O_{17}	176.5
C_{40}-C_{45}	1.5438	H_{21}-C_8-H_{22}	109.9	C_6-C_5-C_{16}-N_{15}	-120.8
C_{45}-N_{47}	1.4540	O_{14}-C_{11}-H_{23}	110.9	C_6-C_5-C_{16}-O_{17}	62.6
C_{45}-H_{50}	1.0977	O_{14}-C_{11}-H_{24}	110.5	C_1-C_6-C_7-C_3	-52.0
C_{45}-H_{51}	1.1073	O_{14}-C_{11}-H_{27}	105.6	C_1-C_6-C_7-O_9	68.4
C_{46}-N_{47}	1.4646	H_{23}-C_{11}-H_{24}	109.7	C_1-C_6-C_7-O_{14}	-162.7
C_{46}-H_{48}	1.1005	H_{23}-C_{11}-H_{27}	110.2	C_5-C_6-C_7-C_3	56.6
C_{46}-H_{49}	1.1055	H_{24}-C_{11}-H_{27}	109.9	C_5-C_6-C_7-O_9	176.9
N_{47}-C_{63}	1.4638	N_{15}-C_{13}-O_{18}	124.6	C_5-C_6-C_7-O_{14}	-54.2
C_{52}-C_{53}	1.4032	C_{13}-N_{15}-C_{16}	114.0	Cl_{37}-C_6-C_7-C_3	-175.8
C_{52}-C_{54}	1.4026	C_{13}-N_{15}-C_{19}	122.4	Cl_{37}-C_6-C_7-O_9	-55.4
C_{52}-C_{63}	1.5255	C_{16}-N_{15}-C_{19}	123.3	Cl_{37}-C_6-C_7-O_{14}	73.4
C_{53}-C_{55}	1.3962	N_{15}-C_{16}-O_{17}	124.7	C_3-C_7-O_9-C_8	-68.2
C_{53}-H_{56}	1.0893	N_{15}-C_{19}-H_{25}	106.7	C_6-C_7-O_9-C_8	-169.9
C_{54}-C_{57}	1.3973	N_{15}-C_{19}-H_{26}	106.7	O_{14}-C_7-O_9-C_8	59.5
C_{54}-H_{58}	1.0895	N_{15}-C_{19}-C_{28}	113.0	C_6-C_7-O_{14}-C_{11}	-76.2
C_{55}-C_{59}	1.3975	H_{25}-C_{19}-H_{26}	108.9	C_9-C_7-O_{14}-C_{11}	49.9
C_{55}-H_{62}	1.0885	H_{25}-C_{19}-C_{28}	110.9	C_4-C_{13}-N_{15}-C_{16}	-6.7
C_{57}-C_{59}	1.3965	H_{26}-C_{19}-C_{28}	110.5	C_4-C_{13}-N15-C_{19}	179.2
C_{57}-H_{60}	1.0884	C_{19}-C_{28}-H_{29}	108.5	O_{18}-C_{13}-N_{15}-C_{16}	177.3
C_{59}-H_{61}	1.0882	C_{19}-C_{28}-H_{30}	109.7	C_{13}-N_{15}-C_{16}-C_5	8.8

Bond length(Å)		Bond angle(^{0})		Dihedral angle(^{0})	
C_{63}-H_{64}	1.0998	C_{19}-C_{28}-C_{31}	111.4	C_{13}-N_{15}-C_{16}-O_{17}	-174.6
C_{63}-H_{65}	1.0993	C_{29}-C_{28}-H_{30}	107.8	C_{13}-N_{15}-C_{19}-C_{28}	81.5
		H_{29}-C_{28}-C_{31}	110.6	C_{19}-N_{15}-C_{16}-C_5	-177.1
		H_{30}-C_{28}-C_{31}	108.8	C_{19}-N_{15}-C_{16}-O_{17}	-0.5
		C_{28}-C_{31}-H_{32}	108.8	C_{16}-N_{15}-C_{19}-C_{28}	-92.2
		C_{28}-C_{31}-H_{33}	109.2	N_{15}-C_{19}-C_{28}-C_{31}	-175.9
		H_{28}-C_{31}-H_{38}	112.6	C_{19}-C_{28}-C_{31}-N_{38}	-173.7
		H_{32}-C_{31}-H_{33}	106.6	C_{28}-C_{31}-N_{38}-C_{40}	-65.1
		H_{32}-C_{31}-H_{38}	107.6	C_{31}-N_{38}-C_{39}-C_{46}	-166.1
		H_{33}-C_{31}-H_{38}	111.9	C_{40}-N_{38}-C_{39}-C_{46}	65.5
		C_{31}-H_{38}-C_{39}	113.3	N_{40}-C_{38}-C_{45}-N_{47}	-34.1
		C_{31}-H_{38}-C_{40}	113.0	C_{40}-C_{45}-N_{47}-C_{46}	65.2
		C_{39}-H_{38}-C_{40}	111.0	C_{40}-C_{45}-N_{47}-C_{63}	-159.9
		N_{38}-C_{39}-H_{41}	112.2	C_{39}-C_{46}-N_{47}-C_{45}	-29.0
		N_{38}-C_{39}-H_{43}	108.9	C_{39}-C_{46}-N_{47}-C_{63}	-164.8
		N_{38}-C_{39}-C_{46}	110.2	C_{54}-C_{52}-C_{53}-C_{55}	0.7
		N_{38}-C_{40}-H_{42}	111.4	C_{63}-C_{52}-C_{53}-C_{55}	-178.2
		N_{38}-C_{40}-H_{44}	108.6	C_{53}-C_{52}-C_{54}-C_{57}	-0.7
		N_{38}-C_{40}-C_{45}	111.6	C_{63}-C_{52}-C_{54}-C_{57}	178.2
		H_{41}-C_{39}-H_{43}	106.3	C_{52}-C_{54}-C_{57}-C_{59}	0.2
		H_{41}-C_{39}-C_{46}	110.1	C_{53}-C_{55}-C_{59}-C_{57}	-0.3
		H_{43}-C_{39}-C_{46}	109.0	C_{54}-C_{57}-C_{59}-C_{55}	0.3
		C_{39}-C_{46}-N_{47}	110.8		
		C_{39}-C_{46}-H_{48}	110.0		
		C_{39}-C_{46}-H_{49}	107.9		
		H_{42}-C_{40}-H_{44}	107.2		
		H_{42}-C_{40}-C_{45}	108.4		
		H_{44}-C_{40}-C_{45}	109.5		
		C_{40}-C_{45}-N_{47}	109.5		
		C_{40}-C_{45}-H_{50}	108.8		
		C_{40}-C_{45}-H_{51}	110.3		

Bond length(Å)		Bond angle(^{0})		Dihedral angle(^{0})	
		N_{47}-C_{45}-H_{50}	108.8		
		N_{47}-C_{45}-H_{51}	113.1		
		C_{45}-N_{47}-C_{46}	112.3		
		C_{45}-N_{47}-C_{63}	116.5		
		H_{50}-C_{45}-H_{51}	106.2		
		N_{47}-C_{46}-H_{48}	108.0		
		N_{47}-C_{46}-H_{49}	112.6		
		N_{46}-C_{47}-C_{63}	114.6		
		H_{48}-C_{46}-H_{49}	107.4		
		N_{47}-C_{63}-C_{52}	116.9		
		N_{47}-C_{63}-H_{64}	107.0		
		N_{47}-C_{63}-H_{65}	107.2		
		C_{53}-C_{52}-C_{54}	118.2		
		C_{53}-C_{52}-C_{63}	120.8		
		C_{52}-C_{53}-C_{55}	121.0		
		C_{52}-C_{53}-H_{56}	119.4		
		C_{54}-C_{52}-C_{63}	121.0		
		C_{52}-C_{54}-C_{57}	121.1		
		C_{52}-C_{54}-H_{58}	119.3		
		C_{52}-C_{63}-H_{64}	109.1		
		C_{52}-C_{63}-H_{65}	109.3		
		C_{55}-C_{53}-H_{56}	119.5		
		C_{53}-C_{55}-C_{59}	120.1		
		C_{53}-C_{55}-H_{62}	119.8		
		C_{57}-C_{54}-H_{58}	119.6		
		C_{54}-C_{57}-C_{59}	120.1		
		C_{54}-C_{57}-H_{60}	119.8		
		C_{59}-C_{55}-H_{62}	120.1		
		C_{55}-C_{59}-C_{57}	119.6		
		C_{55}-C_{59}-H_{61}	120.2		
		C_{59}-C_{57}-H_{60}	120.1		

Bond length(Å)		Bond angle(^{0})		Dihedral angle(^{0})	
		C_{57}-H_{59}-C_{61}	120.2		
		C_{64}-H_{63}-H_{65}	106.9		

Table 2 Calculated Scaled wavenumbers, observed IR, Raman bands and vibrational assignments of TDBPA

B3LYP/6-311++G(d,p)			IR	Raman	Assignments
ν(cm^{-1})	IR_I	R_A	ν(cm^{-1})	ν(cm^{-1})	
3078	23.96	310.05	-	-	νCH IV(93)
3066	40.52	47.84	3069	3068	νCH IV(99)
3058	8.36	103.41	-	3053	νCH IV(99)
3048	13.01	62.12	-	-	νCH_3(99)
3046	4.39	76.61	-	-	νCH IV(95)
3044	9.20	14.74	-	-	νCH IV(98)
3035	7.15	45.53	-	-	νCH_3(99)
3034	21.89	73.57	-	3030	νCH_3(97)
3019	19.57	26.71	-	-	νCH_3(99)
3018	9.03	16.53	-	3016	νCH_2(98)
2991	7.27	32.67	2989	2988	νCH_2(97)
2991	2.68	120.67	-	-	νCHI(99)
2983	1.83	36.40	-	-	νCHI(100)
2963	34.25	134.84	-	-	νCH_2III(86)
2962	41.70	12.00	-	2961	νCH_2(91)
2958	58.22	85.08	-	2959	νCH_2III(82)
2953	11.53	37.31	2954	-	νCH_2(86)
2952	25.00	116.70	-	-	νCH_3(95)
2947	6.77	46.87	-	-	νCH_2(85)
2941	31.86	80.31	-	-	νCH_3(100)
2935	28.31	54.94	-	-	νCH_2III(87)
2930	16.25	43.30	-	-	νCH_2(88)
2917	50.99	64.85	-	-	νCH_2III(95)
2910	32.61	86.16	-	-	νCH_2(97)
2857	75.87	121.35	2878	-	νCH_2III(92)
2837	104.79	73.05	2837	2832	νCH_2III(97)

B3LYP/6-311++G(d,p)			IR	Raman	Assignments
$\nu(cm^{-1})$	IR_I	R_A	$\nu(cm^{-1})$	$\nu(cm^{-1})$	
2817	32.46	28.02	-	2817	$\nu CH_2III(98)$
2804	45.84	36.22	-	2805	$\nu CH_2III(93)$
2782	56.58	46.66	2781	2792	$\nu CH_2(94)$
1786	36.63	16.33	1766	1788	νC=O(82)
1728	498.50	0.30	1698	1727	νC=O(83)
1598	1.51	36.61	1621	1610	νIV(62), δCHIV(12)
1597	57.17	31.74	-	1595	νC=C(76)
1579	0.87	9.16	-	1573	νIV(70)
1493	3.20	9.83	1513	1497	$\delta CH_2III(61)$
1479	6.17	1.46	1477	-	νIV(64), δCHIV(26)
1475	4.49	6.75	-	-	$\delta CH_2III(53)$, $\delta CH_2(29)$
1474	11.89	10.37	-	-	$\delta CH_3(83)$
1473	2.47	7.24	-	1473	$\delta CH_2III(79)$
1466	0.84	14.26	-	-	$\delta CH_2III(83)$
1465	14.85	2.64	-	-	$\delta CH_3(90)$
1464	5.67	14.78	-	-	$\delta CH_2(44)$, $\delta CH_2III(27)$
1459	1.13	13.97	-	-	$\delta CH_3(83)$
1453	7.84	1.86	-	1453	$\delta CH_3(67)$, $\delta CH_2(13)$
1450	4.08	18.84	1449	-	$\delta CH_2(70)$, $\delta CH_3(11)$
1437	5.13	0.76	1438	-	νIV(45), δCHIV(43)
1437	1.45	3.58	-	-	νIV(25), $\delta CH_3(46)$
1432	10.05	15.88	-	1434	$\delta CH_2(89)$
1431	19.96	27.39	-	-	$\delta CH_2(88)$
1422	1.98	10.59	-	1418	$\delta CH_3(91)$
1396	2.30	3.66	1402	1402	$\delta CH_2(45)$, $\delta CH_2III(21)$
1382	8.86	4.40	-	-	$\delta CH_2III(67)$
1378	12.28	1.45	1378	1376	$\delta CH_2(46)$, δCH2III(30)
1372	49.41	4.91	-	-	$\delta CH_2III(31)$, $\delta CH_2(25)$
1357	91.58	4.26	-	1357	$\delta CH_2III(30)$, $\delta CH_2(23)$
1348	210.27	6.10	1347	-	νCNII(39), $\delta CH_2(32)$
1339	98.34	8.44	-	1340	νCNII(49), $\delta CH_2(39)$
1331	38.55	13.16	-	-	$\delta CH_2(68)$
1327	24.43	0.65	-	-	$\delta CH_2III(61)$, δCN(18)

B3LYP/6-311++G(d,p)			IR	Raman	Assignments
$\nu(cm^{-1})$	IR_I	R_A	$\nu(cm^{-1})$	$\nu(cm^{-1})$	
1321	8.24	3.19	-	1321	$\delta CH_2III(30)$, $\delta CN(20)$
1309	0.12	0.70	1307	-	$\nu IV(59)$, $\delta CHIV(39)$
1298	11.36	6.96	-	1297	$\delta CH_2(48)$, $\delta CH_2III(14)$
1287	12.69	10.74	-	-	$\delta CH_2(45)$, $\nu IV(14)$, $\delta CH_2III(10)$
1280	9.84	5.58	-	1280	$\delta CH_2(48)$
1274	4.21	8.35	-	-	$\delta CH_2III(61)$
1270	1.08	3.42	1270	-	$\delta CHI(68)$
1261	12.84	5.56	-	1265	$\delta CHI(73)$
1248	18.75	2.29	1246	1252	$\delta CH2III(29)$, $\delta CH_2(37)$
1236	17.49	7.87	-	1235	$\delta CH_2(44)$, $\delta CH_2III(23)$
1229	7.58	10.86	1229	-	$\delta CH_2III(48)$
1226	1.52	2.95	-	-	$\delta CHI(76)$
1212	8.43	9.31	1212	1211	$\delta CH_2III(77)$
1192	23.15	2.46	1194	1194	$\delta CHI(34)$
1191	99.24	1.95	-	-	$\delta CH_3(52)$, $\nu CO(23)$, $\delta CO(15)$
1188	62.08	8.23	-	-	$\nu CNIII(25)$
1178	3.09	2.48	1178	-	$\delta CH_3(53)$, $\upsilon CO(47)$
1169	21.40	20.92	-	-	$\nu CC(33)$, $\delta IV(11)$
1167	119.31	6.12	-	-	$\nu CO(31)$, $\delta CO(19)$
1164	3.91	5.74	-	-	$\delta CHIV(54)$
1161	9.41	7.51	-	1161	$\delta CHIV(27)$
1144	15.50	7.51	1151	-	$\nu CNII(17)$
1143	15.92	3.68	-	-	$\upsilon CO(66)$
1140	0.11	4.72	1140	-	$\delta CHIV(78)$
1135	63.05	2.47	-	1137	$\nu I(46)$, $\nu CCl(12)$, $\delta I(15)$
1133	51.01	5.26	-	-	$\delta CH_3(62)$
1127	33.47	15.10	1121	1121	$\nu CNII(26)$, $\delta CH_2(13)$
1116	12.55	2.78	-	-	$\nu CNIII(30)$, $\nu CCIII(12)$
1107	34.56	2.59	-	-	$\nu CNII(28)$, $\delta CH_2(13)$
1100	129.37	3.74	1100	1106	$\nu I(24)$, $\delta CC(20)$, $\nu CO(16)$
1091	87.04	6.05	1087	1088	$\nu CO(37)$, $\nu I(17)$
1073	75.09	2.11	-	1071	$\delta CH_2III(39)$, $\nu CNIII(20)$
1068	15.04	0.66	1065	-	$\delta CHIV(59)$, $\nu IV(36)$

B3LYP/6-311++G(d,p)			IR	Raman	Assignments
$\nu(cm^{-1})$	IR_I	R_A	$\nu(cm^{-1})$	$\nu(cm^{-1})$	
1058	37.80	1.84	-	-	νCCI(21), δI(12), νI(10)
1052	25.18	5.33	-	1054	νI(43), νCCII(18), νCN(14)
1047	5.19	18.85	-	1044	$\delta CH_2III(60)$
1035	4.21	5.10	1035	-	νCC(45), $\delta CH_2(20)$
1031	7.75	5.57	-	-	νCO(62), δCC(13), νI(11)
1016	2.53	13.45	-	1014	δCHIV(42), νIV(27)
1009	6.17	1.89	1010	-	νCC(41), νI(10)
1005	20.26	4.73	1004	-	νCO(28), νI(12)
989	15.15	3.72	-	997	νCO(46), νCCIII(17)
986	15.20	9.07	987	-	νCCIII(22), νCO(21)
979	1.50	25.76	-	-	νIV(54), δIV(36)
970	19.63	5.12	969	973	νCO(143), νI(35)
967	3.73	1.00	-	-	νI(33)
960	2.75	1.85	-	-	νCCIII(18), υCNIII(8), $\delta CH_2(20)$
954	10.21	1.66	-	-	υCNIII(22), $\delta CH_2III(17)$
950	1.12	0.16	-	-	γCHIV(84), τIV(14)
947	25.49	3.53	943	948	νCO(42), νI(21), νCCl(11)
924	0.05	0.14	921	930	γCHIV(92)
895	2.92	1.95	-	-	νCCIII(30), γCHIV(21), δCN(23)
893	2.36	0.61	891	893	γCHIV(64)
890	12.25	4.69	-	-	τI(14), νCCI(10), νI(10)
881	7.68	4.77	872	887	τI(21), νCCI(10)
860	7.48	0.35	-	860	$\delta CH_2III(64)$
832	3.22	0.38	845	835	$\delta CH_2(49)$
828	0.01	4.64	828	824	γCHIV(100)
819	49.53	1.52	-	-	δI(12)
804	11.98	1.54	-	805	νCNIII(10)
797	3.76	9.48	799	-	$\delta CH_2(42)$, τIV(11), νCC(10), γCHIV(10)
788	16.75	0.62	778	785	νCNIII(12)
764	14.63	10.95	-	771	νCNIII(51)
747	36.05	0.87	746	754	$\delta CH_2(35)$
731	14.72	19.43	-	735	γCHIV(44), γIV(21)
716	3.70	2.52	-	-	$\delta CH_2(36)$

B3LYP/6-311++G(d,p)			IR	Raman	Assignments
$\nu(cm^{-1})$	IR_I	R_A	$\nu(cm^{-1})$	$\nu(cm^{-1})$	
713	4.53	4.70	713	711	γC=O(17), τII(12)
700	18.35	2.22	-	-	νCCl(14), νCO(18)
690	30.46	2.72	684	687	τIV(48), γCHIV(35)
690	6.53	0.83	-	-	τI(13)
657	41.63	1.67	-	668	νCCl(43), δII(35)
646	10.28	3.35	-	648	τIV(24), δIII(19)
632	5.82	3.13	633	634	δCO(24)
610	0.06	4.06	-	616	νCCl(45), δIV(36)
610	8.49	0.27	-	-	δCCl(41)
598	4.30	3.79	602	588	δII(36), νCNII(11)
578	6.39	2.46	-	566	δIV(18), τIV(12), δCH_2(11)
545	0.08	1.38	547	546	γCCl(29), τI(23), δC=O(11)
526	18.93	4.85	527	524	δCH_2(13)
509	4.08	3.02	-	505	δIII(53)
494	0.38	0.61	496	488	νCC(17), γC=O((17)
492	8.67	3.24	483	-	δIV(26), δIII(16)
456	3.19	1.50	461	462	τIV(34), γCC(15)
444	9.01	0.41	-	447	δI(18), τIV(17)
405	8.27	0.50	412	-	δIII(14), τIV(11), δCN(10)
404	0.07	0.04	-	403	τIV(81)
390	8.20	0.26	399	384	δCN(23), δCC(10)
377	7.29	3.95	-	-	δCC(22), δC=O(16)
366	9.96	6.82	-	366	νCCl(20)
351	4.18	0.62	-	-	γCN(33), δIII(15), τIII(13)
346	1.06	1.88	-	348	νCCl(41), δI(22)
340	3.12	4.89	-	-	δCO(32), νCCl(31)
332	6.71	1.94	-	-	δCO(43)
331	5.77	0.58	-	331	γCN(32), τIII(15), δIII(13)
323	2.94	3.12	-	-	δCO(21), γCN(15)
312	8.12	3.49	-	317	δCO(24), γCN(10)
283	2.75	3.46	-	281	δCN(30), δC=O(15)
273	2.75	1.41	-	-	δCN(26)
265	3.51	2.99	-	267	δCC(17), τII(14)

B3LYP/6-311++G(d,p)			IR	Raman	Assignments
$\nu(cm^{-1})$	IR_I	R_A	$\nu(cm^{-1})$	$\nu(cm^{-1})$	
259	2.43	2.03	-	254	τIV(13), τIII(11)
244	2.75	0.57	-	232	δCN(20), δCC(17)
218	3.96	0.58	-	219	τIII(39), γCN(19)
203	2.48	0.46	-	-	τCO(36), τCH_3(15), δCCl(10)
197	0.14	0.78	-	196	τCH_3(44), δCCl(14)
187	2.24	0.37	-	-	δCCl(28), τCO(21)
184	0.79	1.13	-	-	τIII(10), τII(10), τCO(10)
172	0.09	2.48	-	171	τIII(16), γCN(21)
168	0.16	0.75	-	-	τIII(36), δCCl(17)
164	0.19	1.62	-	-	δCCl(79)
162	0.28	0.66	-	-	δCCl(35), τCH_3(12)
160	1.02	0.79	-	-	τCO(35), δCCl(22), τCH_3(13)
149	1.47	0.30	-	150	τCO(44)
146	2.05	1.00	-	-	δCCl(22), δCC(16)
133	0.96	0.94	-	-	τCO(35)
127	1.79	1.22	-	128	δCC(17), τII(12)
123	1.46	0.63	-	-	τII(26), γCN(19), τCO(14)
115	0.44	0.19	-	-	τCH_2(33), τCN(33)
107	1.60	0.47	-	110	τIII(41), τII(24)
94	1.68	0.42	-	89	τCO(21)
84	0.29	0.57	-	83	τI(25), τCH_2(18), γCC(10)
78	0.79	2.63	-	-	τCO(17), τI(14)
72	0.15	1.98	-	-	γCCl(27), τCH_2(11)
59	0.10	3.75	-	65	τII(31), τI(22), τCC(13), τCH_2(12)
54	0.11	1.32	-	-	τII(14), γCCl(20)
52	0.24	2.99	-	-	τCC(28), τII(18), τI(14), τCN(10)
39	0.11	0.79	-	-	τCH_2(27), τCN(17)
26	0.03	1.55	-	-	τIII(70)
21	0.08	0.94	-	-	τCN(31), τCH_2(16)
11	0.02	0.21	-	-	τCH_2(43), γCN(12)
10	0.01	0.42	-	-	τIII(29), τCH_2(22), γCN(13), δCH_2(12)

Table.3. Chemical descriptors of TDBPA and halogen substitutions

	HOMO	LUMO	$I = -E_{HOMO}$	$A = -E_{LUMO}$	ΔE	$\eta = (I-A)/2$	$\mu = -(I+A)/2$	$\omega = \mu^2/2\eta$
TDBPA	-8.087	-4.943	8.087	4.943	3.144	1.572	-6.515	13.500
TDBPA Br	-7.750	-4.945	7.750	4.945	2.805	1.403	-6.347	14.357
TDBPA F	-8.069	-4.944	8.069	4.944	3.425	1.713	-6.507	12.359

Table 4. NBO results showing the formation of Lewis and non-Lewis orbitals

Bond(A-B)	ED/e[a]	EDA%	EDB%	NBO	s%	p%
σC_1-C_2	1.97824	49.97	50.03	$0.7069(sp^{1.53})C$	39.53	60.47
-	-0.79537	-	-	$+0.7074(sp^{1.52})C$	39.63	60.37
πC_1-C_2	1.93817	49.60	50.40	$0.7043(sp^{99.99})C$	0.78	99.22
-	-0.35716	-	-	$+0.7099(sp^{99.99})C$	0.71	99.29
σC_1-C_6	1.95491	49.52	50.48	$0.7037(sp^{1.85})C$	35.04	64.96
-	-0.68814	-	-	$+0.7105(sp^{2.64})C$	27.45	72.55
σC_1-Cl_{36}	1.98385	45.17	54.83	$0.6721(sp^{3.13})C$	24.18	75.82
-	-0.75533			$+ 0.7405(sp^{4.94})Cl$	16.83	83.17
σC_2-C_3	1.95585	49.62	50.38	$0.7044(sp^{1.85})C$	35.06	64.94
-	-0.68912	-	-	$+0.7098(sp^{2.67)}C$	27.27	72.73
σC_1-Cl_{35}	1.98368	45.11	54.89	$0.6716(sp^{3.14})C$	24.15	75.85
-	-0.75561	-	-	$+0.7409(sp^{4.95})Cl$	16.82	83.18
σC_3-C_4	1.95171	50.86	49.14	$0.7132(sp^{2.63})C$	27.54	72.46
-	-0.64730	-	-	$+0.7010(sp^{2.76})C$	26.58	73.42
σC_3-C_7	1.93894	52.00	48.00	$0.7211(sp^{2.70}\}C$	26.99	73.01
-	-0.64999	-	-	$+0.6928(sp^{2.69})C$	27.12	72.88
σC_3-Cl_{34}	1.97855	44.74	55.26	$0.6689(sp^{4.66})C$	17.66	82.34
-	-0.71092	-	-	$+0.7434(sp^{5.15})Cl$	16.26	83.74
σC_4-C_5	1.94613	49.96	50.94	$0.7068(sp^{3.05})C$	24.68	75.32
-	-0.61944	-	-	$+0.7074(sp^{3.06})C$	24.66	75.34
σC_4-C_{13}	1.96505	52.36	47.64	$0.7236(sp^{2.98})C$	25.15	74.85

Bond(A-B)	ED/e[a]	EDA%	EDB%	NBO	s%	p%
-	-0.66159	-	-	$+0.6902(sp^{1.78})C$	35.91	64.09
σC_5-C_6	1.95457	49.37	50.63	$0.7026(sp^{2.72})C$	26.86	73.14
-	-0.64979			$+0.7115(sp^{2.64})C$	27.45	72.55
σC_5-C_{16}	1.96469	52.21	47.79	$0.7225(sp^{3.02})C$	24.90	75.10
-	-0.66084			$+0.6913(sp^{1.78})C$	35.94	64.06
σC_6-C_7	1.93690	51.96	48.04	$0.7208(sp^{2.74})C$	26.77	73.23
-	-0.64931	-	-	$+0.6931(sp^{2.73})C$	26.84	73.16
σC_6-Cl_{37}	1.97833	44.94	55.06	$0.6704(sp^{4.62})C$	17.80	82.20
-	-0.70912	-	-	$+0.7420(sp^{5.15})Cl$	16.25	83.75
σC_7-O_9	1.98700	31.75	68.25	$0.5635(sp^{3.30})C$	23.27	76.73
-	-0.89584	-	-	$+0.8261(sp^{2.12})O$	32.03	67.97
σC_7-O_{14}	1.98639	31.24	68.76	$0.5589(sp^{3.45})C$	22.48	77.52
-	-0.89089	-	-	$+0.8292(sp^{2.14})O$	31.89	68.11
σC_8-O_9	1.98644	30.69	69.31	$0.5540(sp^{4.14})C$	19.58	80.42
-	-0.77372	-	-	$+0.8325(sp^{3.97})O$	24.57	75.43
σC_{11}-O_{14}	1.98578	30.16	69.84	$0.5492(sp^{4.24})C$	19.09	80.91
-	-0.77265	-	-	$+0.8357(sp^{3.03})O$	24.79	75.21
σC_{13}-N_{15}	1.98295	35.62	64.38	$0.5968(sp^{2.28})C$	30.44	69.56
-	-0.82322	-	-	$+0.8024(sp^{2.05})N$	32.82	67.18
σC_{13}-O_{18}	1.99057	33.96	66.04	$0.5828(sp^{1.98})C$	33.54	66.46
-	-1.05921	-	-	$+0.8126(sp^{1.66})O$	37.66	62.34
πC_{13}-O_{18}	1.98302	32.18	67.82	$0.5672(sp^{99.99})C$	0.30	99.70
-	-0.39914	-	-	$+0.8236(sp^{99.99})O$	0.54	99.46
σN_{15}-C_{16}	1.98320	64.28	35.72	$0.8018(sp^{2.02})N$	33.14	66.86
-	-0.82758	-	-	$+0.5976(sp^{2.27})C$	30.59	69.41
σN_{15}-C_{19}	1.98111	64.94	35.06	$0.8059(sp^{1.96})N$	33.83	66.17
-	-0.75184	-	-	$+0.5921(sp^{3.59})C$	21.77	78.23
σC_{16}-O_{17}	1.99064	33.94	66.06	$0.5826(sp^{2.00})C$	33.28	66.72
-	-1.06019	-	-	$+0.8128(sp^{1.66})O$	37.62	62.38
πC_{16}-O_{17}	1.98338	31.96	68.04	$0.5653(sp^{99.99})C$	0.41	99.59
-	-0.40345	-	-	$+0.8249(sp^{99.99})O$	0.63	99.37
σC_{19}-C_{28}	1.97279	51.12	48.88	$0.7150(sp^{2.38})C$	29.59	70.41

Bond(A-B)	ED/e[a]	EDA%	EDB%	NBO	s%	p%
-	-0.59967	-	-	+0.6991($sp^{2.81}$)C	26.27	73.73
σC_{28}-C_{31}	1.97392	50.19	49.81	0.7084($sp^{2.64}$)C	27.47	72.53
-	-0.58756	-	-	+0.7058($sp^{2.54}$)C	28.23	71.77
σC_{31}-N_{38}	1.97944	39.01	60.99	0.6246($sp^{3.02}$)C	24.86	75.14
-	-0.68825	-	-	+0.7810($sp^{2.31}$)N	30.20	69.80
σN_{38}-C_{39}	1.98175	61.09	38.91	0.7816($sp^{2.37}$)N	29.69	70.31
-	-0.68402	-	-	+0.6238(sp3.12)C	24.30	75.70
σN_{38}-C_{40}	1.98249	61.20	38.80	0.7823($sp^{2.46)}$N	28.87	71.13
-	-0.67074	-	-	+0.6229($sp^{3.17}$)C	23.96	76.04
σC_{39}-C_{46}	1.97836	50.24	49.76	0.7088($sp^{2.59}$)C	27.87	72.13
-	-0.58690	-	-	+0.7054($sp^{2.57}$)C	27.98	72.02
σC_{40}-C_{45}	1.97839	49.82	50.18	0.7058($sp^{2.54}$)C	28.26	71.74
-	-0.58765	-	-	+0.7084($sp^{2.59}$)C	27.88	72.12
σC_{45}-N_{47}	1.98384	38.98	61.02	0.6244($sp^{3.13}$)C	24.23	75.77
-	-0.68989	-	-	+0.7811($sp^{2.27}$)N	30.59	69.41
σC_{46}-N_{47}	1.9827-	38.63	61.37	0.6215($sp^{3.17}$)C	23.98	76.02
-	0.676059	-	-	+0.7834($sp^{2.35)}$N	29.85	70.15
σN_{47}-C_{63}	1.97644	61.02	38.98	0.7811($sp^{2.28}$)N	30.52	69.48
-	-0.68315	-	-	+0.6244($sp^{3.15}$)C	24.08	75.92
σC_{52}-C_{53}	1.97418	50.03	49.97	0.7073($sp^{1.92}$)C	34.19	65.81
-	-0.67898	-	-	+0.7069($sp^{1.76}$)C	36.20	63.80
σC_{42}-C_{54}	1.97438	50.06	49.94	0.7076($sp^{1.91}$)C	34.34	65.66
-	-0.68015			+0.7067($sp^{1.76}$)C	36.27	63.73
πC_{52}-C_{54}	1.65132	49.48	50.52	0.7034($sp^{99.99}$)C	0.01	99.99
-	-0.24136	-	-	+0.7108($sp^{100.00}$)C	0.00	100.00
σC_{52}-C_{63}	1.97587	50.93	49.07	0.7136($sp^{2.18}$)C	31.46	68.54
-	-0.60545	-	-	+0.7005($sp^{2.36}$)C	29.77	70.23
σC_{53}-C_{55}	1.97948	50.31	49.69	0.7093($sp^{1.83}$)C	35.31	64.69
-	-0.68226	-	-	+0.7049($sp^{1.80}$)C	35.76	64.24
πC_{53}-C_{55}	1.66968	50.31	49.69	0.7093($sp^{1.00}$)C	0.00	100.00
-	-0.24544	-	-	+0.7049($sp^{1.00}$)C	0.00	100.00
σC_{54}-C_{57}	1.97936	50.29	49.71	0.7092($sp^{1.84}$)C	35.22	64.78

Bond(A-B)	ED/e[a]	EDA%	EDB%	NBO	s%	p%
-	-0.68122	-	-	+0.7050($sp^{1.80}$)C	35.72	64.28
σC_{55}-C_{59}	1.98096	50.06	49.94	0.7075($sp^{1.83}$)C	35.34	64.66
-	-0.68066	-	-	+0.7067($sp^{1.83}$)C	35.38	64.62
σC_{57}-C_{59}	1.98105	50.06	49.94	0.7075($sp^{1.83}$)C	35.38	64.62
-	-0.68145	-	-	+0.7067($sp^{1.82}$)C	35.42	64.58
πC_{57}-C_{59}	1.66603-	49.63	50.37	0.7045($sp^{1.00}$)C	0.00	100.00
-	0.24475	-	-	+0.7097($sp^{1.00}$)C	0.00	100.00
n_1O_9	1.95633	-	-	$sp^{1.32}$	43.17	56.83
-	-0.55802	-	-	-	-	-
n_2O_9	1.90856	-	-	$sp^{99.99}$	0.24	99.76
-	-0.32359	-	-	-	-	-
n_1O_{14}	1.95235	-	-	$sp^{1.31}$	43.32	56.68
-	-0.56939	-	-	-	-	-
n_2O_{14}	1.90829	-	-	$sp^{1.00}$	0.00	100.00
-	-0.32907	-	-	-	-	-
n_2N_{15}	1.58281	-	-	$sp^{99.99}$	0.20	99.80
-	-0.28576	-	-	-	-	-
n_1O_{17}	1.97276	-	-	$sp^{0.62}$	61.76	38.24
-	-0.69378	-	-	-	-	-
n_2O_{17}	1.86985	-	-	$sp^{99.99}$	0.03	99.97
-	-0.28049	-	-	-	-	-
n_1O_{18}	1.97322	-	-	$sp^{0.62}$	61.81	38.19
-	0.69164	-	-	-	-	-
n_2O_{18}	1.86933	-	-	$sp^{99.99}$	0.03	99.97
-	-0.27815	-	-	-	-	-
n_1Cl_{34}	1.98558	-	-	$sp^{0.19}$	83.74	16.26
-	-0.96771	-	-	-	-	-
n_2Cl_{34}	1.96397	-	-	$sp^{99.99}$	0.02	99.98
-	-0.32341	-	-	-	-	-
n_3Cl_{34}	1.95935	-	-	$sp^{1.00}$	0.00	100.00
-	-0.32502	-		-	-	-
n_1Cl_{35}	1.98646	-	-	$sp^{0.21}$	82.80	17.20

Bond(A-B)	ED/e[a]	EDA%	EDB%	NBO	s%	p%
-	-0.95952		-	-	-	-
n_2Cl_{35}	1.96514	-	-	$sp^{99.99}$	0.38	99.62
-	-0.34298	-	-	-	-	
n_3Cl_{35}	1.91874	-	-	$sp^{1.00}$	0.00	100.00
-	-0.33999	-	-	-	-	-
n_1Cl_{36}	1.98623	-	-	$sp^{0.21}$	82.73	17.27
-	-0.95771	-	-	-	-	-
n_2Cl_{36}	1.96474	-	-	$sp^{99.99}$	0.44	99.56
-	-0.34179	-	-	-	-	-
n_3Cl_{36}	1.91620	-	-	$sp^{1.00}$	0.00	100.00
-	-0.33782	-	-	-	-	-
n_1Cl_{37}	1.98572	-	-	$sp^{0.20}$	83.63	16.37
-	-0.96332	-	-	-	-	-
n_2Cl_{37}	1.96375	-	-	$sp^{99.99}$	0.14	99.86
-	-0.31995	-	-	-	-	-
n_3Cl_{37}	1.95864	-	-	$sp^{1.00}$	0.00	100.00
-	-0.32218	-	-	-	-	-
n_1N_{38}	1.88515	-	-	$sp^{7.90}$	11.24	88.76
-	-0.23865	-	-	-	-	-
n_1N_{47}	1.87222	-	-	$Sp^{10.06}$	9.04	90.96
-	-0.22884	-	-	-	-	-

Table 5 Second-order perturbation theory analysis of Fock matrix in NBO basis corresponding to the intramolecular bonds of TDBPA

Donor(i)	Type	ED/e	Acceptor(j)	Type	ED/e	E(2)a	E(j)-E(i)b	F(i,j)c
C_{52}-C_{54}	π	-	C_{53}-C_{55}	π*	0.32725	20.57	0.28	0.068
C_{52}-C_{54}	π	-	C_{57}-C_{59}	π*	0.33212	22.42	0.28	0.071
C_{53}-C_{55}	π	1.66968	C_{52}-C_{54}	π*	0.34688	21.93	0.29	0.071
C_{53}-C_{55}	π	-	C_{57}-C_{59}	π*	0.33212	20.86	0.28	0.068
C_{57}-C_{59}	π	1.66603	C_{52}-C_{54}	π*	0.34688	20.35	0.29	0.068
C_{57}-C_{59}	π		C_{53}-C_{55}	π*	0.32725	21.54	0.28	0.070

Donor(i)	Type	ED/e	Acceptor(j)	Type	ED/e	E(2)a	E(j)-E(i)b	F(i,j)c
LPN_{15}	σ	1.58281	C_{13}-O_{18}	π*	0.23191	50.47	0.26	0.108
LPN_{15}	σ	-	C_{16}-O_{17}	π*	0.24272	51.78	0.26	0.108
LPO_{17}	π	1.86985	C_5-C_{16}	σ*	0.07452	20.16	0.59	0.099
LPO_{17}	π	-	N_{15}-C_{16}	σ*	0.08987	25.63	0.63	0.115
LPO_{18}	π	1.86933	C_4-C_{13}	σ*	0.07415	20.01	0.60	0.099
LPO_{18}	π	-	C_{13}-N_{15}	σ*	0.09077	25.99	0.63	0.115
$LPCl_{35}$	n	-	C_2-C_3	σ*	0.05851	14.68	0.33	0.064
$LPCl_{36}$	n	1.91620	C_1-C_2	π*	0.19750	14.97	0.33	0.064

Table 6 Polarizability values of TDBPA and halogen substitutions

	μ	$\alpha \times 10^{-23}$	$\beta \times 10^{-30}$	$\gamma \times 10^{-37}$	MR=1.333παN=25.21 α
TDBPA	-6.515	4.7836	1.6690	-73.528	120.595
TDBPA Br	-6.347	5.1027	1.7503	-82.795	128.639
TDBPA F	-6.507	4.1196	2.4111	-61.574	103.855

6.6. References

[1] L. H. Atherden, Bentley and Driver's Text Book of Pharmaceutical Chemistry, eighth ed., Oxford Medicinal Publication, (2004) 372-377, 204-205.

[2] A. H. Beckett, J. B. Stenlake, Practical Pharmaceutical Chemistry, fourth ed., CBS Publishers and Distributors, (2003).

[3] C. C. J. Carpenter, M. A. Fischl, S. M. Hammer, M. S. Hirsch, D. M. Jacobsen, D. A. Katzenstein, J. S. G. Montaner, D. D. Richman, M. S. Saag, R. T. Schooley, M. A. Thompson, S. Vella, P. G. Yeni, P. A. Volberding, Antiretroviral Therapy for HIV infection in 1998 updated recommendations of the international AIDS society-USA panel, J. Am. Med. Assoc. 280 (1998) 78-86.

[4] M. Bartok, K. Felfoldi, E. Karpati, A. Molnar, L. Szporny, 3-[4-(2'-Pyridyl)-piperazin-1-yl]-1-(3,4,5-trimethoxybenzoyloxy)-propane or a pharmaceutically acceptable acid-addition salt thereof in a composition with anti-arrhythmic activity. U.S. Pat. US4196206, (1980).

[5] R. Mlynárová, D. Tazká, E. Racanská, J. Kyselovic, P. Svec, Effects of a fluorophenyl) piperazine derivative (substance IIIv) on cardiovascular function. Ceska Slov. Farm. 49
(2000) 177-180.

[6] R. Filosa, A. Peduto, P. de Caprariis, C. Saturnino, M. Festa, A. Petrella, A. Pau, G. A. Pinna, P. La Colla, B. Busonera, R. Loddo, Synthesis and antiproliferative properties of N3/8-disubstituted 3,8-diazabicyclo[3.2.1]octane analogues of 3,8-bis[2-(3,4,5-trimethoxyphenyl)-pyridin-4-yl]methyl-piperazine, Eur. J. Med. Chem. 42 (2007) 293-306.

[7] Y. J. Shaw, Y. T. Yang, J. B. Garrison, N. Kyprianou, C. S. Chen, Pharmacological exploitation of the alpha1-adrenoreceptor antagonist doxazosin to develop a novel class of antitumor agents that block intracellular protein kinase B/Akt activation, J. Med. Chem. 47 (2004) 4453-4462.

[8] S. Richter, C. Parolin, M. Palumbo, G. Palu, Antiviral properties of quinolone-based drugs. Curr. Drug. Targets Infect. Disord. 4 (2004) 111-116.

[9] T. M. Chan, K. Cox, W. Feng, M. W. Miller, D. Weston, S. W. McCombie, Piperidinyl piperazine derivatives useful as inhibitors of chemokine receptors. U.S. Pat. 2006223821, (2006).

[10] M. Kimura, T. Masuda, K. Yamada, N. Kawakatsu, N. Kubota, M. Mitani, K. Kishii, M. Inazu, Y. Kiuchi, K. Oguchi, T. Namiki, Antioxidative activities of novel diphenylalkyl piperazine derivatives with high affinities for the dopamine transporter, Bioorg. Med. Chem. Lett. 14 (2004) 4287-4290.

[11] A. Foroumadi, S. Emami, A. Hassanzadeh, M. Rajaee, K. Sokhanvar, M. H. Moshafi, A. Shafiee, Synthesis and antibacterial activity of N-(5-benzylthio-1,3,4-thiadiazol-2-yl) and N-(5-benzylsulfonyl-1,3,4-thiadiazol-2-yl)piperazinyl quinolone derivatives. Bioorg. Med. Chem. Lett. 15 (2005) 4488-4492.

[12] A. K. Dutta, S. K. Venkataraman, X. S. Fei, R. Kolhatkar, S. Zhang, M. E. Reith, Synthesis and biological characterization of novel hybrid 7-[[2-(4-phenyl-piperazin-1-yl)-ethyl]-propyl-amino]-5,6,7,8-tetrahydro-naphthalen-2-ol and their heterocyclic bioisosteric analogues for dopamine D2 and D3 receptors, Bioorg. Med. Chem. 12 (2004) 4361-4373.

[13] V. Cecchetti, F. Schiaffella, O. Tabarrini, A. Fravolini, (1,4-Benzothiazinyloxy) alkylpiperazine derivatives as potential antihypertensive agents, Bioorg. Med. Chem. Lett. 10 (2000) 465-468.

[14] L. Betti, M. Zanelli, G. Giannaccini, F. Manetti, S. Schenone, G. Strappaghetti, Synthesis of new piperazine-pyridazinone derivatives and their binding affinity toward alpha1-, alpha2-adrenergic and 5-HT1A serotoninergic receptors. Bioorg. Med. Chem. 14 (2006) 2828-2836.

[15] J. Obniska, M. Kołaczkowski, A. J. Bojarski, B. Duszyńska, Synthesis, anticonvulsant activity and 5-HT1A, 5-HT2A receptor affinity of new N-[(4-arylpiperazin-1-yl)-alkyl] derivatives of 2-azaspiro[4.4]nonane and [4.5]decane-1,3-dione,. Eur. J. Med. Chem. 41 (2006) 874-88.

[16] J. Kossakowski, M. Pakosinska-Parys, M. Struga, I. Dybala, A. E. Koziol, P. La Colla, L. E. Marongiu, C. Ibba, D. Collu, R. Loddo, Synthesis and Evaluation of in Vitro Biological Activity of 4-Substituted Arylpiperazine Derivatives of 1,7,8,9-Tetrachloro-10,10-dimethoxy-4-azatricyclo[5.2.1.$0^{2,6}$]dec-8-ene-3,5-dione, Molecules 14 (2009) 5189-5202.

[17] M. Rani, P. Parthiban, R. Ramachandran, S. Kabilan, Design and synthesis of novel piperazine unit condensed 2, 6-diarylpiperidin-4-one derivatives as antituberculosis and antimicrobial agents, Med. Chem. Res. 21 (2012) 653-662.

[18] C.A. Peri, New polychlorinated derivatives containing the ring of 1,4-endomethylenecyclohexane, Gazz. Chim. Ital. 85 (1955) 1118-1140.

[19] J. Kossakowski, M. Pakosinska-Parys, M. Struga, I. Dybala, A. E. Koziol, P. LaColla, L. E. Marongiu, C. Ibba, D. Collu, R. Loddo, Synthesis and Evaluation of in Vitro Biological Activity of 4-Substituted Arylpiperazine Derivatives of 1,7,8,9-Tetrachloro10,10-dimethoxy-4-azatricyclo[5.2.1.$0^{2,6}$]dec-8-ene-3,5-dione, Molecules 14 (2009) 5189-5202.

[20] M. J. Frisch, G. W. Trucks, H. B. Schlegel, G. E. Scuseria, M. A. Robb, J. R. Cheeseman,

G. Scalmani, V. Barone, B. Mennucci, G. A. Petersson, H. Nakatsuji, M. Caricato, X. Li, H. P. Hratchian, A. F. Izmaylov, J. Bloino, G. Zheng, J. L. Sonnenberg, M. Hada, M. Ehara, K. Toyota, R. Fukuda, J. Hasegawa, M. Ishida, T. Nakajima, Y. Honda, O. Kitao, H. Nakai, T. Vreven, J. A. Montgomery Jr., J. E. Peralta, F. Ogliaro, M. Bearpark, J. J. Heyd, E. Brothers, K. N. Kudin, V. N. Staroverov, T. Keith, R. Kobayashi, J. Normand, K. Raghavachari, A. Rendell, J. C. Burant, S. S. Iyengar, J. Tomasi, M. Cossi, N. Rega, J. M. Millam, M. Klene, J. E. Knox, J. B. Cross, V. Bakken,

C. Adamo, J. Jaramillo, R. Gomperts, R. E. Stratmann, O. Yazyev, A. J. Austin, R. Cammi, C. Pomelli, J. W. Ochterski, R. L. Martin, K. Morokuma, V. G. Zakrzewski, G. A. Voth, P. Salvador, J. J. Dannenberg, S. Dapprich, A. D. Daniels, O. Farkas, J. B.

Foresman, J. V. Ortiz, J. Cioslowski, D. J. Fox, Gaussian 09, Revision B.01, Gaussian Inc, Wallingford CT, 2010.

[21] J. B. Foresman, in: E. Frisch (Ed.), Exploring Chemistry with Electronic Structure Methods: A Guide to Using Gaussian, Gaussian Inc., Pittsburg, PA, 1996.

[22] J. M. L. Martin, C. V. Alsenoy, GAR2PED, A Program to Obtain a Potential Energy Distribution from a Gaussian Archive Record, University of Antwerp, Belgium, 2007.

[23] R. Dennington, T. Keith, J. Millam, GaussView, Version 5, Semichem Inc., Shawnee Mission KS, 2009.

[24] N. R. Conley, R. J. Hung, C. G. Willson, , A New Synthetic Route to Authentic N-Substituted Aminomaleimides, J. Org. Chem. 70 (2005) 4553-4555.

[25] T. M. V. D. Pinho e Melo, A. M. T. D. P. Cabral, A. M. R. Gonsalves, A. M. Beja, J. A. Paixao, M. R. Silva, L. A. daVeiga, A New Route to Cross-Conjugated Bis(enamines) and an Unusual Reaction with DDQ, J. Org. Chem. 64 (1999) 7229-7232.

[26] D. Lee, T. M. Swager, Toward Isolated Molecular Wires: A pH-Responsive Canopied Polypyrrole, Chem. Mater. 17 (2005) 4622-4629.

[27] B. Bartkowska, F. M. Bohnen, C. Kruger, W. F. Maier, 4-(1,7,8,9,10,10-Hexachloro-3,5-dioxo-4-aza- tricyclo[5.2.1.0 ^{2,6}]dec-8-en-4-yl) butyric Acid Toluene Solvate, Acta Cryst. C53 (1997) 521-522.

[28] I. N. Tarabara, Y. S. Bondarenko, A. A. Zhurakovskii, L. I. Kas'yan, New derivatives of 2-(3,5-Dioxo-4-azatricyclo [5.2.1.0^{2,6}-endo] dec-8-en-4-yl) acetic acid. Synthesis and reactivity, Russ. J. Org. Chem. 43 (2007) 1297-1304.

[29] H. B. Burgi, J. D. Dunitz, Structure Correlation, vol. 2, VCH, Weinheim (1994) 741-784.

[30] R. Manohar, M. Harikrishna, C. R. Ramanathan, M. S. Kumar, K. Gunasekaran, 1,7,8,9,10,10-Hexachloro-4-(thiophen-2-ylmethyl)-4-azatricyclo[5.2.1.0^{2,6}]dec-8-ene-3,5-dione, Acta Crystallogr. E67 (2011) 2391.

[31] L. I. Kas'yan, V. A. Palchikov, A. V. Turov, S. A. Pridma, A. V. Tokar, Cage-like amines in the synthesis and oxidation of camphor-10-sulfonic acid amides, Russ. J. Org. Chem. 45 (2009) 1007-1017.

[32] L. I. Kasyan, S. V. Sereda, K. A. Poteknin, A. O. Kasyan, Azabrendanes. I. Synthesis, structure and spectral parameters of N-(arylsulfonyl)-exo-2-hydroxy-4-azatricyclo[4.2.1.0^{3,7}] nonanes Heteroatom Chem. 8 (1997) 177-184.

[33] A. A. El-Emam, A. M.S. Al-Tamimi, K. A. Al-Rashood, H. N. Misra, V. Narayan, O. Prasad, L. Sinha, Structural and spectroscopic characterization of a novel potential chemotherapeutic agent 3-(1-adamantyl)-1-{[4-(2-methoxyphenyl) piperazin-1-yl] methyl}-4-methyl-1H-1, 2, 4-triazole-5(4H)-thione by first principle calculations, J. Mol. Struct. 1022 (2012) 49-60.

[34] Z. Karczmarzyk, W. Malinka, Crystal Structure of 4,6-Dimethyl-2-[4-(2,3-dichlorophenyl)piperazin-1-ylmethyl]isothiazolo[5,4-b]pyridin-3(2H)-one, X-ray Structure Analysis Online, Anal. Sci. 23 (2007) 151-152.

[35] N. P. G.Roeges, A Guide to the Complete Interpretation of the Infrared Spectra of Organic Structures Wiley, New York, (1994).

[36] N. B. Colthup, L.H. Daly S.E. Wiberly , Introduction to Infrared and Raman Spectroscopy Academic Press, New York, (1990).

[37] R. Renjith, Y. S. Mary, C. Y. Panicker, H. T. Varghese, M. P. Parys, C. V. Alsenoy, T. K. Manojkumar, Spectrochim. Acta 124 (2014) 500-513.

[38] I. C. H. Castaneda, J. L. Jios, O. E. Piro, G. E. Tobon, C. O. D. Vedova, Conformational and vibrational analysis of S-(2-methoxyphenyl)-4substituted-benzenecarbothioates, using X-ray, infrared and Raman spectroscopy and theoretical calculations J. Mol. Struct. 842 (2007) 46-54.

[39] R. Zhang, X. Li, X. Zhang, Molecular structure and vibrational spectra of phenobaraitone by functional theory and ab initio Hartree Fock calculations Front. Chem. China 6 (2011) 358-366.

[40] G. Socrates, Infrared Characteristic Group Frequencies John Wiley and Sons, New York, (1981).

[41] K. Nakanishi, Infrared Absorption Spectroscopy Practical Holden Day, San Francisco, (1962).

[42] S. Kundoo, A. N. Banerjee, P. Saha, K. K. Chattophyay, Synthesis of crystalline carbon nitride thin films by electrolysis of methanol-urea solution Mater. Lett. 57 (2003) 2193-2197.

[43] M. Silverstein, G. C. Basseler, C. Morill, Spectrometric Identification of Organic Compounds, John Wiley and Sons Inc. Singapore (1991).

[44] L. I. Kasyan, A. V. Serbin, A. O. Kasyan, D. V. Karpenko, E. A. Golodaeva, Reactions of Bi-, Tri-, and tetracyclic amines with succinic anhydride Russ. J. Org. Chem. 44 (2008) 340-347.

[45] I. N. Tarabara, Y. S. Bondarenko, A. A. Zhurakovskii, L. I. Kasyan, New derivatives of 2- (3, 5-Dioxo-4-azatricyclo [5.2.1.$0^{2,6}$-endo]dec-8-en4-yl) acetic acid. Synthesis and
reactivity, Russ. J. Org. Chem. 43 (2007) 1297-1304.

[46] L. H. Daly, S. E. Wiberly, Introduction to Infrared and Raman Spectroscopy Ed. 3, academic Press, Boston (1990).

[47] K. Felfoldi, M. Sutyinszky, N. Nagy, I. Palinko, Synthesis of E- and Z-o-methoxy-substituted 2, 3-diphenylpropenoic acids and its methyl esters Synth. Commun. 30 (2000) 1543-1553.

[48] C. Lee, W. Yang, R. G. Parr, Development of the Colle-Salvetti correlation-energy formula into a functional of the electron density Phys. Rev. 37B (1998) 785-789.

[49] E. F. Mooney, The infra-red spectra of chloro-and bromobenzene derivatives-II. Nitrobenzenes Spectrochim. Acta 20 (1964) 1021-1032.

[50] E. F. Mooney, The infrared spectra of chloro- and bromobenzene derivatives-I: Anisoles and phenetoles, Spectrochim. Acta 19 (1963) 877-887.

[51] N. Sundaraganesan, C. Meganathan, B. D. Joshua, P. Mani, A. Jayaprakash, Molecular structure and vibrational spectra of 3chloro-4-fluorobenzonitrile by ab initio HF and density functional method Spectrochim. Acta 71A (2008) 1134-1139.

[52] G. Varsanyi, Assignments of Vibrational Spectra of Seven Hundred Benzene Derivatives Wiley: New York, (1974).

[53] P. Pazdera, H. Divisova, H. Havilsova, P. Borek, Synthesis of N-(2 Cyanophenyl) chloromethanimidoyl Chloride Molecules 5 (2000) 189-194.

[54] H. T. Varghese, C. Y. Panicker, D. Philip, P. Pazdera, Vibrational spectroscopic studies and ab initio calculations of 2-cyanophenyl isocyanid dichloride, Spectrochim. Acta 67A (2007) 1055-1059.

[55] H. Arslan, U. Florke, N. Kulcu, G. Binzet, The molecular structure and vibrational spectra of 2-chloro-N-(diethylcarbamothioyl)benzamide by Hartree-Fock and density functional methods Spectrochim. Acta 68A (2007) 1347-1355.

[56] A. A. El-Emam, A. S. A. Tamimi, K. A. A. Rashood, H. N. Misra, V. Narayan, O. Prasad, L. Sinha, Structural and spectroscopic characterization of a novel potential chemotherapeutic agent 3-(1adamantyl)-1-{[4-(2-methoxyphenyl) piperazine-1-yl]methyl}-4-methyl -1H-1,2,4-triazole-5(4H)-thione by first principle calculations, J. Mol. Struct. 1022 (2012) 49-60.

[57] H. L. Spell, Determination of piperazine rings in ethyleneamines, poly (ethyleneamine), and polyethylenimine by infrared spectrometry Anal. Chem. 41 (1969) 902-905.

[58] A. S. El-Azab, Y. S. Mary, C. Y. Panicker, A. A.-M A-Aziz, A. Magda, El-Sherbeny, C. V. Alsenoy, DFT and experimental (FT-IR and FT-Raman) investigation of vibrational spectroscopy and molecular docking studies of 2-(4-oxo-3-phenyl-3,4-dihydroquinazolin-2-ylthio)-N-(3,4,5 trimethoxyphenyl) acetamide, J. Mol Struct. 1113 (2016) 133-145.

[59] F. J. Luque, J. M. Lopez, M. Orozco, Perspective on electrostatic interactions of a solute with a continuum, a direct utilization of ab initio molecular potentials for the prevision of solvent effects, Theor. Chem. Acc. 103 (2000) 343-345.

[60] P. Politzer, J. S. Murray, in: D. L. Beveridge, R. Lavery, (Eds.), Theoretical Biochemistry and Molecular Biophysics, Springer, Berlin, 1991.

[61] E. D. Glendening, A. E. Reed, J. E. Carpenter, F. Weinhold, NBO Version 3.1, Gaussian Inc., Pittsburgh, PA, 2003

[62] M. Adant, M. Dupuis, J. L. Bredas, Ab initio study of the nonlinear optical properties of urea: Electron correlation and dispersion effects, Int. J. Quantum. Chem. 56 (1995) 497-507.

[63] R. Renjith, Y. Sheena Mary, C. Yohannan Panicker, Hema Tresa Varghese, Magdalena Pakosin´ ska-Parys, C. Van Alsenoy, T. K. Manojkumar, Vibrational spectroscopic and computational study of 1,7,8,9-Tetrachloro-4-(4-bromo-butyl)-10,10-dimethoxy-4-aza-tricyclo[5.2.1.$0^{2,6}$] dec-8-ene-3,5-dione, Spectrochim. Acta Part A: 124 (2014) 480-491.

[64] Y. K. Lee, M. R. Player Developments in Factor Xa Inhibitors for the Treatment of Thromboembolic Disorders Medicinal Research Reviews, 31 (2011) 202-283.

[65] E. M. Antman, Circulation Hirudin in Acute Myocardial Infarction Safety Report From the Thrombolysis and Thrombin Inhibition in Myocardial Infarction (TIMI) 9A Trial 90 (1994) 1624-1630.

[66] Randomized Trial of Intravenous Heparin Versus Recombinant Hirudin for Acute Coronary Syndromes The Global Use of Strategies to Open Occluded Coronary Arteries GUSTO IIa Investigators Circulation 90 (1994) 1631-1637.

[67] S. Komoriya, N. Haginoya, S. Kobayashi, T. Nagata, A. Mochizuki, M. Suzuki, T. Yoshino, H. Horino, T. Nagahara, M. Suzuki, Y. Isobe , T. Furugoori, Design, synthesis, and biological activity of non-basic compounds as factor Xa inhibitors: SAR study of S1 and aryl binding sites, Bioorganic & Medicinal Chemistry 13 (2005) 3927-3954.

[68] K. Padmanabhan, K. P. Padmanabhan, C. H. Park, W. Bode, R. Huber. D. T Blankenship. A. D. Cardin, W. Kisiel, Structure of human Des (1-45) Factor Xa at 2.2A resolution J. Mol. Biol. 232 (1993) 947-966.

[69] N. Haginoya, S. Kobayashi, S. Komoriya, T. Yoshino, M. Suzuki, T. Shimada, K. Watanabe, Y. Hirokawa, T. Furugori, T. Nagahara, Synthesis and Conformational Analysis of a Non-Amidine Factor Xa Inhibitor That Incorporates 5-Methyl-4,5,6,7-tetrahydrothiazolo [5, 4-c] pyridine as S4 Binding Element J. Med. Chem. 47 (2004) 5167-5182.

[70] G. M. Morris, R. Huey, W. Lindstrom, M. F. Sanner, R. K. Belew, D. S. Goodsell, A. J. Olson, Auto dock 4 and Auto Dock Tools 4: automated docking with selective receptor flexibility, J. Comput. Chem. 16 (2009) 2785-91.

[71] O. Trott, A. J. Olson, AutoDock Vina: Improving the speed and accuracy of docking

with a new scoring function, efficient optimization and multi-threading J. Comput. Chem. 31 (2010) 455-461.

[72] G. M. Morris, D. S. Goodsell, R. S. Halliday, R. Huey, W. E. Hart, R. Belew, A. J. Olson, Automated docking using a Lamarckian genetic algorithm and an empirical binding free energy function, J. Comput. Chem. 19 (1998) 1639-1662.

CHAPTER VII

SUMMARY AND CONCLUSION

7.1 Conclusion

The study presented in this thesis focused on quantum chemical and spectroscopic investigation of five pharmaceutically relevant compounds of two quinolone derivative (EHODQC, CCHODC), two pyrazine carboxamide derivative (NIMPC, CIMPC) and one azatricyclo derivative (TDBPA). Experimental studies using FT-IR and FT-Raman spectroscopy and theoretical studies using Density functional theory of the five organic compounds are conducted. Using GAR2PED software package all the wave numbers are assigned for the different normal mode vibrations of the compounds. The experimental and computationally obtained wave numbers are in good agreement with that of the similar derivatives.

The chemical reactivity and electronic energetic properties of quinolone, pyrazine carboxamide and azatricyclo derivatives were analysed. Among the quinolone derivatives EHODQC has highest HOMO-LUMO gap and in pyrazine derivatives highest for NIMPC. The highest electronegativity out of all the five compound is for EHODQC and the elctrophilicity index for CIMPC.

Molecular electrostatic potential study gave the reactive regions with in the molecule. In EHODQC O16 is the most reactive part for the electrophilic attack. For NIMPC electrophilic regions are oxygen O11, hydrogen atom H17 and iodine atom I27. Also the average local ionisation energy showed the almost same result of that of MEP study for these two compounds. In the other three compounds we conducted halogen substituted studies by replacing either the hydrogen attached with the carbon atom or the existing halogen atom.

The hyper polarizability study conducted using DFT calculations demonstrates that the five compounds may be considered as materials for nonlinear optical (NLO) applications. The highest hyper polarizability for the pyrazine carboxamide derivatives with value 13×10^{-30} e.s.u which is 100 times that of the standard nonlinear material urea.

Natural bond orbital analysis (NBO) is carried out for the title compounds and measured the strong interaction between the electron acceptor and electron donor with in the molecule. Interaction energies with solvent and RDF's, obtained after molecular dynamics (MD)

simulation, indicates that the EHODQC and NIMPC have pronounced interaction with molecules. Also the BDE values of these compounds showed the sensitive towards autoxidation mechanism.

Molecular docking studies of the five organic compound showed that the quinolone derivative EHODQC and CCHODC may be a lead compound for anti-tubercular and anti - malarial. The pyrazine carboxamide derivatives NIMPC and CIMPC may be used as drugs for neurological and psychiatric disorders such as Alzheimer's disease, Parkinson's disease, anxiety, depression, and schizophrenia and anti-inflammatory. The aza tricyclo derivative TDBPA exhibit inhibitory action against anti-coagulant diseases.

.

LIST OF PUBLICATIONS

1. P.K. Ranjith , Y. Sheena Mary , C. Yohannan Panicker , P.L. Anto , Stevan Armakovi, Sanja J. Armakovi, Robert Musiol f, Josef Jampilek , C. Van Alsenoy, New quinolone derivative: Spectroscopic characterization and reactivity study by DFT and MD approaches.(*Journal of Molecular Structure, Volume 1135, 5 May 2017, Pages 1-14*)

2. P.K. Ranjith , Ebtehal S. Al-Abdullah , Fatmah A.M. Al-Omary , Ali A. El-Emam , P.L. Anto , Mary Y. Sheena, Stevan Armakovi, Sanja J. Armakovi, Jan Zitko , Martin Dolezal , C. Van Alsenoy, FT-IR and FT-Raman characterization and investigation of reactive properties of N-(3iodo-4-methylphenyl)pyrazine-2-carboxamide by molecular dynamics simulations and DFT calculations.(Journal of Molecular Structure Volume 1136, Pages 14-24 (15 May 2017))